MONASH University

The mechanistic underpinnings of postprandial thermogenesis in brown fat – the role of glucose-sensing POMC neurons

Paul Nicholas Mirabella

BSc (ScSchProg) (Hons)

A thesis submitted for the degree of

Doctor of Philosophy

at Monash University

June 2020

Department of Physiology

Biomedicine Discovery Institute

Faculty of Medicine, Nursing and Health Sciences

Copyright notice

Some figures in this thesis were created with assistance from BioRender.com.

Abstract

The balance between caloric intake and energy expenditure is maintained by key interoceptive neuronal populations within the hypothalamus that sense internal cues associated with energetic state. The nature of the recruitment of brown adipose tissue (BAT) thermogenesis has captured the imagination of metabolic neuroscientists for the last 40 years; ultimately in pursuit of a means by which to harness its therapeutic potential for the treatment of metabolic disorders. Despite extensive research in this field, the central determinants of meal-activated (postprandial) sympathetic outflow to brown fat remain poorly defined. In this thesis, the overarching aim was to investigate the role of hypothalamic glucose-sensing neurons in transducing postprandial cues into BAT-directed sympathetic drive.

The works presented here utilise a number of pivotal experimental strategies that have been used individually and in combination, including transsynaptic retrograde viral tracing, patch-clamp electrophysiology and *in vivo* loss-of-function or chemogenetic manipulation studies. First, we demonstrate that hypothalamic pre-autonomic and arcuate nucleus (ARC) neurons, that have a defined multi-synaptic trajectory to brown fat, are responsive to fluctuations in extracellular glucose concentration. Dissection of the axonal trajectory of BAT-projecting neurons in the ARC revealed the existence of parallel circuits with indications of redundancy relating to their glucose-sensing capacity. Importantly, we found that proopiomelanocortin (POMC)-expressing neurons comprise the vast majority of BAT-directed neurons that are activated by elevated glucose in both the ARC and the adjacent retrochiasmatic area, providing a candidate neuronal population that could orchestrate the postprandial activation of BAT thermogenesis.

In support of this premise, we demonstrate that chemogenetic stimulation of POMC neurons is sufficient to rapidly activate brown fat thermogenesis via a melanocortin-3/4 receptor-dependent mechanism. We extend this finding to reveal that meal-induced activation of POMC neurons contributes to postprandial thermogenesis in BAT by combining acute pharmacological/chemogenetic loss-of-function strategies with a fast-refeed paradigm. These findings were further substantiated by the permanent ablation of hypothalamic POMC neurons, which produced similar defects in diet-induced thermogenic responses.

In view of accumulating evidence for an intermediary role played by astrocytes in neuronal glucose-sensing, we sought to investigate the mechanism of glucose-induced changes to POMC neuron activity. Here, we reveal a novel adenosine A1 receptor-dependent mechanism that mediates the glucose-induced excitation of POMC cells. Crucially, we establish that astrocyte-dependent metabolism of glucose leads to increased local adenosine production, which in turn acts in a paracrine manner to activate POMC neurons. The role of astrocyte-derived adenosine in this pathway was confirmed by studies involving the chemogenetic stimulation of mediobasal hypothalamic astrocytes, also revealing changes to brown fat thermogenesis *in vivo* that are similar to that arising from POMC neuron activation.

The findings presented in this thesis advance our understanding of how hypothalamic POMC neuron activity is regulated in the postprandial state, and therefore how this neuronal population

contributes to the regulation of meal-induced thermogenesis in brown fat. These data have implications for future investigations relating to the neural control of metabolism, and may inform the development of novel therapies for obesity and associated disorders.

Declaration

This thesis is an original work of my research and contains no material which has been accepted for the award of any other degree or diploma at any university or equivalent institution and that, to the best of my knowledge and belief, this thesis contains no material previously published or written by another person, except where due reference is made in the text of the thesis.

Signature:

Print Name: Paul Nicholas Mirabella

Date: 5th June, 2020

Acknowledgements

I would like to extend my deepest gratitude to everyone who has taught me, supported me and lifted me over the last four years during my PhD studies. This work could not have been possible without your unfailing encouragement, counsel and guidance.

Brian “BJO, but not BO or BJ” Oldfield, you have been truly instrumental in almost every aspect of my growth over the past years. I want to start by saying that I do not take for granted how rare it is to find a supervisor that always has their office door literally and metaphorically open for the most minor to the most serious of experimental (and other) setbacks. Thank you for all of the opportunities that you allowed me along this journey; it’s crazy to think how much has happened between our two (quite literally) “Keystone” experiences together – the first *before* my PhD in Snowbird, to the most recent in Banff – which, each in their own right, will be forever memorable. Know that, despite your scepticism to the claim or to accept it as a compliment, you have instilled in me some of the most important qualities that define a “neuroanatomist” (i.e. a “dinosaur neuroscientist”), and I will value these for (hopefully) the rest of my career as a neuroscientist.

Dave “Mate” Spanswick, the real-life caricature of an eccentric electrophysiologist who wants nothing more than to be left alone at his rig (but instead finds himself more in the air than on ground). While I had no concept of it at the time, it’s really a miracle that you made that commitment to help me make something of what should have been a doomed-to-fail Honours project, all those years ago. Instead, it blossomed into what now constitutes my PhD, and I am forever grateful to you, not only for giving me the opportunity to learn how to patch-clamp, but for cultivating in me a passion for the complexities of neural activity and signalling that makes neuroscience so wonderful; especially to the eye of an electrophysiologist.

To Claire “Bro” Foldi, my officially-unofficial supervisor and mentor; who would have known that you would come to be one of the most influential people for both my professional and personal development over these years. Almost every facet of who I am today has been, knowingly or unknowingly to us both, chiselled and polished by your exceptionally brilliant mind (and sense of humour to boot). More than just being an ever-present support, you have taught me one of the most valuable lessons: that unwavering dedication to your work and... “having a good time” are not mutually exclusive feats. Rather, commitment and hard work inevitably makes the other only more enjoyable. I haven’t quite grasped why this means so much to me, but I’m sure with your guidance, we’ll uncover that. I’m excited for what lies ahead for us both in our careers, and I look forward to continuing to grow through my learning from you.

To the remaining members of the Oldfield and Spanswick labs: Erika “Kika/Parce” Greaves, Aneta Stefanidis, Jess “Huddo” Hudson, Greg Conductier, Laura Milton and other students that have come and gone through the years; thank you so much for your unwavering support and for making every day in the lab something to look forward to. Individually, you have each played an incredibly important role in my growth and for maintaining my (apparent) sanity during my PhD.

Thank you to the undergraduate students, Tom McCord, Eliza O'Shea and Marie Herrnhold who assisted me at different points through the years with the successful completion of a number of experiments; some of which are included in this thesis, and others which are produced elsewhere.

To other members of the Department of Physiology, particularly those in Zane Andrews' Lab, it has been a pleasure to unofficially collaborate and nurture our passion for (neuro)science together.

To my dearest friends Rebecca Harvey, Ashleigh Mosele, Rachael Massarotti and Deana Moltisanti; where would I be without you? Not only did you help me survive the inevitable lows throughout my candidature, you were by my side for each and every monumental high, propelling me along the way to help me arrive at this point. THANK YOU my darlings, I am forever thankful.

To my amazing family: Mum, Dad, Lisa, Michael and Meg. Where do I begin? It's particularly difficult to put into words how eternally grateful I am to you all. To say that I am lucky/fortunate/blessed to have you behind me – to help me get through what felt like most impossible of times – is an understatement. You are all so effortlessly selfless, and you have each contributed, in unique ways, to my progress and growth during my PhD. I will never take for granted how much you gave, without ever asking nor expecting anything in return, over these years. I know we don't have long until I leave you, but I promise to make the most of this "downtime" over the next couple of months… especially to spend time with my darling angel, Frankie.

Lastly, to my "hubby", Mark. Wowee – it's been a hell of a ride. Your stability (despite of my incessant *volatility*) during these years is truly remarkable. I cannot begin to thank you enough for getting me through what has been one of the most difficult periods of my life. You have been exceptionally generous and forgiving, and it's hard to imagine a life without you. It's also extremely strange to think that you don't know me in any form other than being a stressed and broke PhD student. It's can only get better… right? Well, here's to hoping anyway; bring on our new chapter together in Germany!

Table of Contents

List of Figures

List of Tables

Abbreviations

^{18}FDG	[^{18}F]-2-fluoro-D-2-deoxy-D-glucose
α-MSH	α-melanocyte stimulating hormone
β-MSH	β-melanocyte stimulating hormone
γ-MSH	γ-melanocyte stimulating hormone
A_1R	Adenosine A_1 receptor
$A_{2A}R$	Adenosine A_{2A} receptor
$A_{2B}R$	Adenosine A_{2B} receptor
A_3R	Adenosine A_3 receptor
AAV	Adeno-associated virus
aCSF	Artificial cerebrospinal fluid
ADP	Adenosine diphosphate
AgRP	Agouti-related peptide
AMP	Adenosine monophosphate
AP	Action potential
AR	Adenosine receptor
ARC	Arcuate nucleus
ATP	Adenosine triphosphate
AUC	Area under the curve
BAT	Brown adipose tissue
BMI	Body mass index
C57Bl/6^{WT}	Wild-type C57Bl/6 (mice)
CART	Cocaine- and amphetamine-regulated transcript
CD73	Ecto-5'-nucleotidease
CNO	Clozapine-*N*-oxide
CNS	Central nervous system
CSF	Cerebrospinal fluid
Cx43	Connexin43
DIO	Double-floxed inverted orientation
DIO2	Type II iodothyronine deiodinase
DMH	Dorsomedial hypothalamus
DMSO	Dimethyl sulfoxide
DREADD	Designer receptors exclusively activated by designer drugs
ECF	Extracellular fluid
eGFP	Enhanced green fluorescent protein
FGF21	Fibroblast growth factor 21
GABA	γ-aminobutyric acid
GE	Glucose-excited
GFAP	Glial fibrillary acidic protein
GI	Glucose-inhibited
GLP-1	Glucagon-like peptide-1
GLUT1	Glucose transporter-1
GLUT2	Glucose transporter-2
GPCR	G protein-coupled receptor

i.c.v.	Intracerebroventricular
i.p.	Intraperitoneal
iBAT	Interscapular brown adipose tissue
I_H	Cyclic nucleotide-gated hyperpolarisation-activated non-selective cation current
IML	Interomediolateral nucleus
I_T	T-type calcium current
IV	Current-voltage
K_{ATP} channel	ATP-sensitive potassium channel
K_{IR}	Instantaneous inwardly-rectifying potassium currents
LepR	Leptin receptor
LHA	Lateral hypothalamus
M2	Alternatively-activated macrophages
MBH	Mediobasal hypothalamus
MC3R	Melanocortin-3 receptor
MC4R	Melanocortin-4 receptor
MCH	Melanin-concentrating hormone
MTII	Melanotan II
Myf5	Myogenic factor 5
NHS	Normal horse serum
NPY	Neuropeptide Y
NR	Non-responsive
NTS	Nucleus of the solitary tract
PB	Phosphate buffer
PBT	Triton X-100 phosphate buffer
PCR	Polymerase chain reaction
PET/CT	Positron emission topography and computed tomography
PFA	Paraformaldehyde
POA	Preoptic area
POMC	Proopiomelanocortin
PRV	Pseudorabies virus
PVN	Paraventricular nucleus
Rb	Retrobeads
RCA	Retrochiasmatic area
RMP	Resting membrane potential
RVLM	Rostral ventrolateral medulla
Sim1	Single-minded 1
SNA	Sympathetic nerve activity
SNS	Sympathetic nervous system
T2DM	Type 2 diabetes mellitus
TRPC	Transient receptor potential channel
TTX	Tetrodotoxin
UCP1	Uncoupling protein-1
VMH	Ventromedial hypothalamus
VO_2	Oxygen consumption
WAT	White adipose tissue

Chapter 1

General Introduction

1.1 When obesity blows out of proportion

Obesity is a well-established "epidemic", with 67% of Australian adults currently overweight or obese (Australian Bureau of Statistics, 2018), and projections indicating the continued growth of Australian waistlines beyond 2025 (Hayes *et al.*, 2017). Unsurprisingly, this unprecedented incidence of obesity entails a significant financial burden to the Australian economy. In the year of 2005 alone, it was estimated that the direct costs of overweight/obesity summed to $21 billion ($AUD), plus an additional indirect costing of $35.6 billion derived from loss of productivity, early retirement, premature death and carer wages (Colagiuri *et al.*, 2010). Ominously, the deleterious health and quality-of-life effects of obesity are only worsened by its associated comorbidities, including, but not limited to, type 2 diabetes mellitus (T2DM), coronary artery disease, hypertension and many forms of cancer (Khaodhiar *et al.*, 1999; Calle *et al.*, 2003). However, in spite of the clear health and economic burdens posed by overweight/obesity and its associated conditions, and even with intensive research spanning over a quarter of a century, we are still yet to yield an adequate long-term treatment (Li & Cheung, 2011). This failure to combat the "growing" trend is supported by the tendency toward an increasing rather than decreasing prevalence of obesity/overweight in Australia (Australian Bureau of Statistics, 2015) (**Figure 1.1**). In consideration of this, it is critical that we continue to pursue novel therapies that change the paradigm in which obesity treatment is approached.

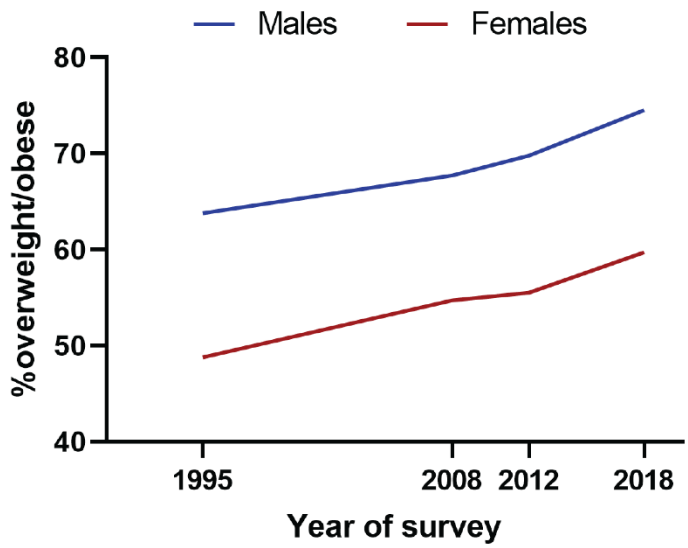

Figure 1.1 | Prevalence of overweight and obesity in Australian adults over the last ~25 years

Continuing upward trajectory of overweight/obesity (body mass index (BMI)>25) in both male and female adults in Australia. Data was collected from federal health surveys from 1995 to 2018. Data adapted and graphed from Australian Bureau of Statistics (2018).

1.2 The rise and fall of obesity pharmacotherapies

The aetiology of obesity is a frequently explored question that has come to be accepted as a complex interaction between environment and genetics (Bell *et al.*, 2005). Industrialisation has moulded the developed world into one with decreasingly labour-intensive workplaces and increasingly sedentary lifestyles. This, in adjunct to unprecedented food access and processing practices, has resulted in an "obesogenic" environment, scored by excess caloric intake and reduced energy expenditure (Butler *et al.*, 2001). Energy homeostasis is defined by the balance of energy intake and energy expenditure. As such, obesity arises from sustained positive energy balance, which is the mathematical imbalance of 'energy in' over 'energy out'. Regardless of the cause of obesity, most, if not all, pharmacotherapies have aimed to reduce the 'energy in' side of the equation by suppression of feeding or decreasing nutrient absorption (Melnikova & Wages, 2006; Dietrich & Horvath, 2012). Given the enduring prevalence of obesity, it is no surprise that these therapies are largely ineffective. Notwithstanding their lack of substantial efficacy, there are also serious safety concerns posed by the vast majority of identified potential anti-obesity drugs. The growing list of medications withdrawn from the market is a testament to this, with the most common adverse effects posing serious health threats being related to cardiotoxicity and psychiatric alterations (Onakpoya et al., 2016).

Presently, there are five approved anti-obesity medications for use, with four of those prescribed on- or off-label in Australia; namely, phentermine, orlistat, bupropion/naltrexone and liraglutide (Khera *et al.*, 2016). It is worth noting that the latter, liraglutide, is a glucagon-like peptide-1 (GLP-1) agonist on which the Australian Therapeutic Goods Administration has recently extended its indications to incorporate the treatment of obesity (3mg daily) (NPS MedicineWise, 2017a), as well as its initial use for T2DM (0.6-1.8mg) (NPS MedicineWise, 2017b). The potential for this single drug to treat two distinct metabolic conditions only further strengthens the relationship between the physiological pathogenesis of the diseases. Outside of pharmacotherapy and traditional diet/exercise recommendations, bariatric surgery represents the final resort for obesity treatment. Currently, surgery remains the only effective long-term treatment for obesity, with most procedures capable of producing in excess of 50% excess weight loss (O'Brien *et al.*, 2005). However, it is critical to acknowledge that while bariatric surgery presents an attractive solution for extreme obesity, it is not an economically viable option to address the needs of the broader overweight/obese community (Melnikova & Wages, 2006). Instead, it is clear that novel means of treating obesity via traditional drug-based approaches are necessary, which are more accessible and cost-effective for large-scale implementation.

1.3 Brown adipose tissue: a new hope for obesity?

In contrast to concerted efforts for the development of therapeutics which reduce energy intake, the focus of a considerable amount of research has recently switched to increasing energy expenditure in the individual via thermogenic pathways in brown adipose tissue (BAT). BAT plays a significant contribution to energy expenditure via two physiological, homeostatic processes: it is recruited to regulate body weight during overfeeding, which is often referred to as "diet-induced thermogenesis", or to maintain body temperature in the cold, which is termed "cold-induced thermogenesis". Thermogenesis within the adipocyte results from the break-down of chemical energy stored in nutrients (fats, carbohydrates), followed by its conversion into heat energy (Cannon & Nedergaard, 2004).

1.3.1 The beginnings of a new era

In the late 1970s, a study by Rothwell and Stock first gave rise to the notion that BAT is able to expend excess consumed calories via diet-induced thermogenesis (Rothwell & Stock, 1979). This process was distinct from the "obligatory" component of postprandial thermogenesis, which occurs as a (necessary) product of the digestion and storage of nutrients following meal-consumption (Himms-Hagen, 1989). Instead, brown fat activity constitutes "facultative" thermogenesis which refers specifically to adaptive heat production that can be rapidly evoked (or suppressed) by the nervous system (Lowell & Spiegelman, 2000). Interest in brown fat as a potential therapeutic target was propelled by the subsequent discovery of uncoupling protein-1 (UCP1), the mitochondrial protein essential for thermogenesis (described in *Section 1.4*), in brown fat obtained from adult humans (Bouillaud *et al.*, 1983). Yet, by the late 1980s, difficulty in identifying the large, circumscribed depots of brown fat in adults, that are otherwise present in infants, drove a scepticism related to its significance in adult human physiology (Maxwell *et al.*, 1987; Ma *et al.*, 1988). However, interest in brown fat was re-ignited following the advent of metabolic imaging studies traditionally utilised for the diagnosis of tumours in cancer patients - namely the co-registering of a radiolabelled glucose analogue, [^{18}F]-2-fluoro-D-2-deoxy-D-glucose (^{18}FDG), with positron emission topography and computed tomography (PET/CT) - which led to the identification of unusually symmetrical regions of high glucose uptake (Barrington & Maisey, 1996; Engel *et al.*, 1996).

The current resurgence of research into brown fat was championed by Nedergaard *et al.* (2007) who published the first retrospective analysis of ^{18}FDG PET/CT scans which highlighted the presence of symmetrical, metabolically-active regions in the upper body consistent with active brown fat in adult humans. Since this revelation, PET/CT and ^{18}FDG studies unequivocally demonstrate active BAT in adult humans that is classically distributed in supraclavicular, abdominal, cervical and paraspinal regions (Hany *et al.*, 2002; Leitner *et al.*, 2017), and with only minor apparent sexual dimorphisms (Fletcher *et al.*, 2020) (**Figure 1.2**).

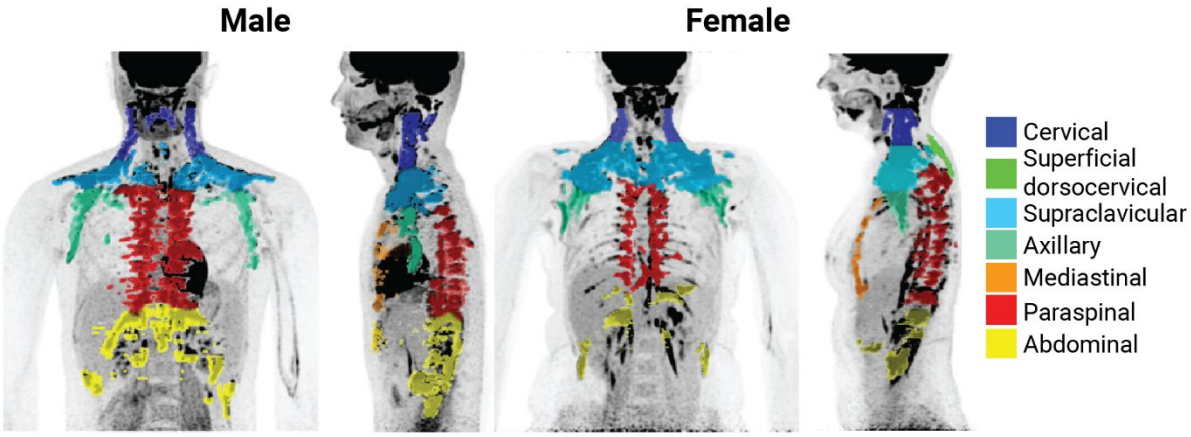

Figure 1.2 | Representative regional distribution of brown fat in adult humans

Using the glucose analogue ^{18}FDG as a tracer, metabolically active BAT depots were identified using combined positron emission tomography and computed tomography (PET/CT). Individualised cold-exposure regimes were utilised to evoke optimal BAT activity. Figure adapted from Fletcher et al. (2020).

1.3.2 BAT biology: A renaissance

The landmark paper by Nedergaard *et al.* (2007) was closely followed by publication of a suite of high-impact articles in the New England Journal of Medicine. In this series, a second retrospective study of ^{18}FDG PET/CT scans revealed that the probability of detection of BAT was inversely correlated with age and BMI amongst older populations, suggesting that brown fat activity may be defective in the obese state (Cypess *et al.*, 2009). Furthermore, it was demonstrated that cold exposure increased detectable BAT activity (i.e. ^{18}FDG uptake) which could be positively correlated to whole body energy expenditure, substantiating that cold exposure could activate brown fat activity in adult humans (van Marken Lichtenbelt *et al.*, 2009). Furthermore, exposure of human subjects to varying ambient temperatures revealed that BAT activity was on average 15 times greater after exposure to cold than warm conditions, and that tissue biopsies from the areas of high glucose uptake expressed classical metabolic markers consistent with active brown fat; in particular the mitochondrial protonophore, UCP1 (Virtanen *et al.*, 2009).

A critical finding from these studies was that BAT function was deemed inversely proportional to body fat percentage, suggesting "room-to-grow" for increasing the metabolic rate of overweight/obese subjects by re-igniting dormant brown fat. Publication of these articles heralded the "explosion" of research into the biochemistry and regulation of brown fat activity that is only still gaining further momentum today.

1.4 BAT structure, biochemistry and innervation

1.4.1 How is brown fat different?

Brown adipose tissue, a site for high metabolic flux, is both functionally and morphologically different to white adipose tissue (WAT), which is primarily a site for energy storage. Brown adipocytes are distinguished microscopically from their white counterparts by their multilocular phenotype, whereas WAT cells are typically unilocular (**Figure 1.3**). The characteristic brown colour of BAT adipocytes is a result of the high mitochondrial density and vascularisation (Cinti, 2007). Furthermore, brown adipocytes are derived from a myogenic factor 5 (Myf5)-expressing cell lineage, whereas white adipocytes are from a separate, Myf5-negative progenitor (Shan *et al.*, 2013). An adipocyte intermediate between brown and white fat has been identified, termed "brite" or "beige" fat, which exhibits the unique functional characteristics of brown adipocytes but whose cells are situated in fat depots traditionally containing white adipocytes (Wu *et al.*, 2012). These metabolically-active adipocytes present an attractive therapeutic target given their established potential to be recruited with cold-exposure and pharmaceutical treatment (Vitali *et al.*, 2012; Dodd *et al.*, 2015).

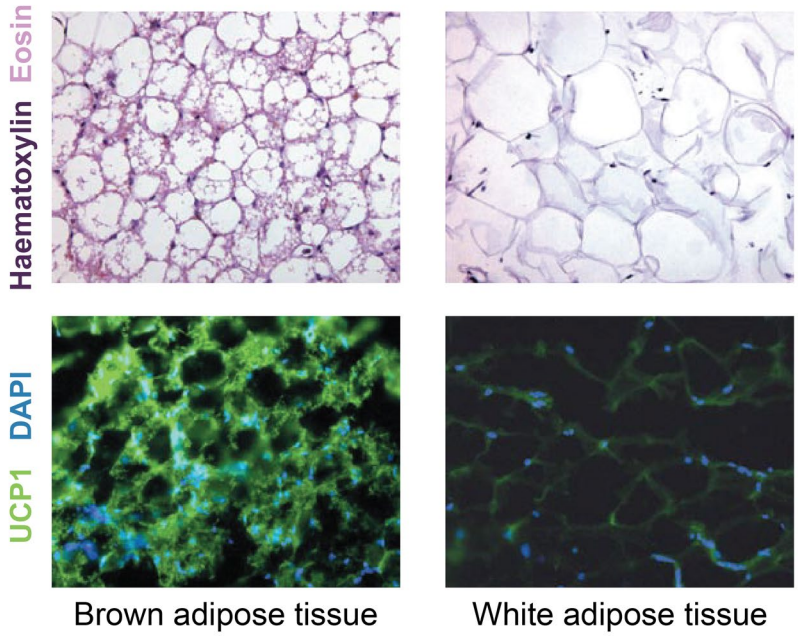

Figure 1.3 | Morphological and UCP1 expression differences in human brown and white fat histological specimens

Haematoxylin and eosin counterstains reveal the relatively small and numerous fat vacuoles characteristic of brown fat relative to white, reflective of multilocular and unilocular phenotypes, respectively. Immunohistochemistry against UCP1 demonstrates expression of the protein in brown adipocyte (green), but not in white adipocytes taken from the same subject. Images taken and adapted from van Marken Lichtenbelt et al. (2009).

1.4.2 The biochemistry of thermogenesis in brown fat

The process of generating heat energy - “thermogenesis” - occurs primarily within the mitochondria of brown adipocytes. Similar to other cell types, brown fat metabolises nutrients into pyruvate in the cytoplasm, which then feed into the tricarboxylic acid cycle within the mitochondria. Following cycling, a proton concentration gradient is generated across the inner mitochondrial membrane, which adenosine triphosphate (ATP) synthase then utilises to drive the (otherwise unfavourable) reaction to generate ATP from adenosine diphosphate (ADP) and inorganic phosphate. However, in brown adipocytes, this ATP-generating reaction is uncoupled, as UCP1 acts to dissipate the proton electrochemical gradient, resulting in a futile cycle in which chemical energy from nutrient metabolism is released, instead, as heat (Rousset *et al.*, 2004). In broad terms, whereas in most cells the metabolism of nutrients results in subsequent production of ATP molecules (chemical energy to chemical energy), respiration in brown adipocytes leads to the production of heat following UCP1-mediated uncoupling (chemical energy to heat energy) (Nicholls & Locke, 1984).

1.4.3 The adrenergic control of thermogenic processes in brown fat

There is dense innervation of the sympathetic nervous system (SNS) to the brown adipocyte itself, as well as to the blood vessels and parenchyma of the pad (Lever *et al.*, 1986; Mukherjee *et al.*, 1989). Importantly, thermogenic activity does not appear to be constitutively active within brown adipocytes of neither humans nor rodents (Cannon & Nedergaard, 2004). Instead, cold exposure (cold-induced thermogenesis) and dietary challenges (diet-induced thermogenesis) are considered the two primary stimuli that lead to the stimulation of sympathetic outflow to BAT which permits activation of UCP1 activity and hence thermogenesis (Golozoubova *et al.*, 2001; Feldmann *et al.*, 2009).

Upon sensory detection of diet or cold within the central nervous system (CNS), the activity of post-ganglionic sympathetic neurons innervating BAT is increased, causing the release of noradrenaline which binds to β3-adrenoreceptors expressed on the brown adipocyte membrane (see **Figure 1.4**) (Chaudhry & Granneman, 1999). Downstream intracellular signalling pathways lead to the induction of lipolysis of triglyceride stored within lipid droplets, which liberates free fatty acids into the cytosol of the cell. In the absence of β3-adrenoreceptor activity, UCP1 is tonically inhibited by purine nucleotides (primarily ATP), which bind to UCP1 and block the translocation pathway (Klingenberg, 2010). It is believed that long-chain free fatty acids, generated within the inner mitochondrial membrane subsequent to lipolysis, bind to and disinhibit UCP1, which initiates the symport of H^+ across the mitochondrial membrane via UCP1 (Fedorenko *et al.*, 2012). Overall, activation of the β3-adrenoreceptor instigates nutrient metabolism as well as disinhibits UCP1 activity, ultimately controlling thermogenic function in brown fat.

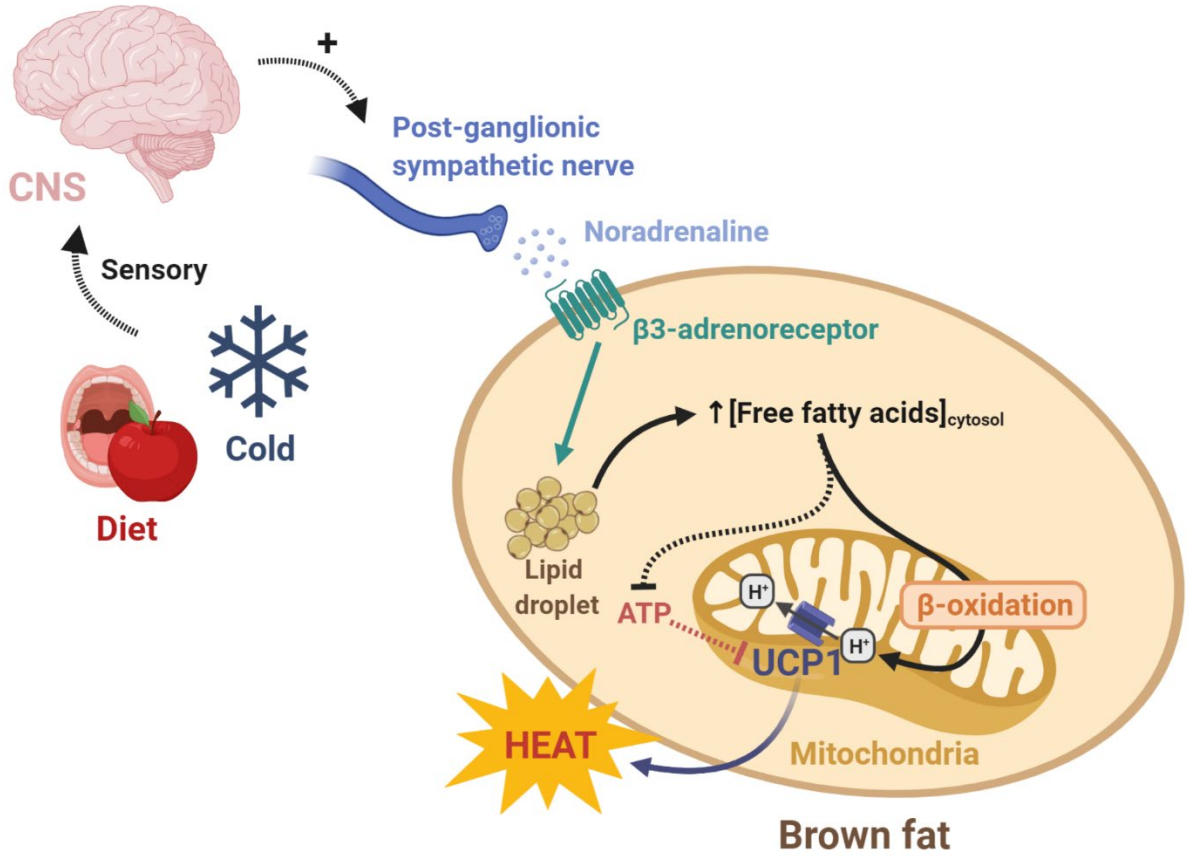

Figure 1.4 | The intracellular mechanisms underlying uncoupled respiration following adrenergic stimulation of the brown adipocyte

Cold exposure or a dietary stimulus signal through the central nervous system to lead to the activation of post-ganglionic sympathetic nerves innervating brown fat. Noradrenaline released binds to β3-adrenoceptors on the brown adipocyte, leading to the mobilisation of free fatty acids from intracellular triglyceride stores. Free fatty acids then disinhibit UCP1 (through release of the tonic ATP-mediated inhibition), and also undergo mitochondrial β-oxidation to lead to the generation of protons in the outer mitochondrial membrane. The proton gradient generated via fatty acid metabolism is dissipated by UCP1, ultimately releasing chemical energy as heat.

1.5 How does BAT weigh up as a target for obesity treatment?

While the existence of BAT in adult humans has been well established, its actual therapeutic viability to combat obesity should be deemed significant to warrant its continued investigation. In order to achieve negative energy balance, BAT must be able to significantly augment energy expenditure in the face of the excessive energy intake characteristic of obese individuals. In their landmark study for the relevance diet-induced activation of energy expenditure in BAT, Rothwell and Stock (1979) demonstrated that when rats were fed a palatable and energy dense "cafeteria" diet, the energy efficiency of the weight gain was ~40% lower than control-fed rats. Excess weight gain was found to be partially offset in the cafeteria diet-fed group due to an adaptive elevation in resting oxygen consumption (VO_2) and body temperature; a direct result of diet-induced thermogenesis in brown fat. Moreover, cafeteria diet-fed rats exhibited enhanced sensitivity to the metabolism-augmenting effects of noradrenaline, while administration of the non-selective β-blocker, propranolol, abolished the elevated resting VO_2, underscoring the importance for the SNS in the depletion of excess energy via BAT thermogenesis.

1.5.1 A debunked "myth"

It is worthy to note that since the publication of the Rothwell and Stock (1979) study, the importance of BAT-mediated thermogenesis, in particular diet-induced thermogenesis, in the maintenance of body weight was the subject of some contention (Maxwell *et al.*, 1987; Kozak, 2010). The first *Ucp1* knockout mouse model failed to exhibit an obese phenotype, despite a blunted increase in VO_2 following β3-agonist administration and marked intolerance to cold (Enerback *et al.*, 1997). Findings that *Ucp1* null mice were not predisposed to obesity were subsequently supported by other studies, with some even proposing that *Ucp1* knockouts are more *resistant* to diet-induced obesity (Liu *et al.*, 2003b; Anunciado-Koza *et al.*, 2008). However, it was found that when *Ucp1* knockout animals are housed at thermoneutral temperatures of 29-30°C, they display the expected obese phenotype which was even further exacerbated when fed a high-fat diet (Feldmann *et al.*, 2009). From this, it was concluded that cold stress in the absence of active brown fat engages compensatory thermogenic mechanisms in order to maintain core temperature that are less efficient than UCP1-dependent thermogenesis. As such, increased metabolic demand to defend body temperature obviated the expected effects of *Ucp1* deletion. The findings presented by Feldmann *et al.* (2009) were crucial in ending the debate of the metabolic relevance of diet- (and cold-) induced thermogenesis in BAT, which has since been substantiated by numerous animal studies (Ueta *et al.*, 2012; Rowland *et al.*, 2016; von Essen *et al.*, 2017; Fischer *et al.*, 2019). Importantly, there is also a growing bank of clinical evidence that reflects, in humans, the functional relevance of brown fat and hence its potential to combat obesity.

1.5.2 Clinical evidence for the metabolic benefits of brown fat activity

Acute or chronic cold exposure have been consistently shown in humans to stimulate the uptake of glucose (^{18}FDG) into BAT (van Marken Lichtenbelt *et al.*, 2009; Cypess *et al.*, 2012; Chen *et al.*, 2013), indicative of increased metabolic demand by the tissue upon cold exposure. Increased metabolic activity in brown fat does appear to translate to increased energy expenditure, where a number of clinical studies have also shown that extended bouts of cold exposure lead to increased BAT quantity/activity as well as energy expenditure post-cold acclimatisation (van der Lans *et al.*, 2013; Yoneshiro *et al.*, 2013; Blondin *et al.*, 2014), even in the obese state or individuals with T2DM (Hanssen *et al.*, 2015; Hanssen *et al.*, 2016). Alternatively, there is rather limited clinical research exploring BAT thermogenic activity specifically stimulated by diet. This is largely due to inherent methodological limitations of techniques available for use in the clinic, whereby BAT temperature is typically not directly measured, but rather inferred from energy expenditure measurements or the BAT-specific uptake of radio-labelled nutrients. Nevertheless, blockade of β-adrenoreceptors significantly reduced thermogenesis associated with intravenous infusion of glucose (Acheson *et al.*, 1983), while treatment with a centrally-acting inhibitor of SNS outflow (clonidine) was shown to significantly blunt postprandial energy expenditure (Schwartz *et al.*, 1988). Furthermore, a genetic polymorphism which lowers UCP1 expression was associated with a lower postprandial thermogenesis response, despite no difference in sympathetic activity (Nagai *et al.*, 2003). These findings indicate a role for meal-activated sympathetic activity in driving energy expenditure, potentially through the recruitment of brown fat thermogenesis. More recently, indirect calorimetry combined with PET/CT confirm that whole-body and BAT thermogenesis (oxygen consumption) is increased after the ingestion of a mixed carbohydrate-rich meal, to the same extent as occurs during cold stress (U Din *et al.*, 2018). It was also shown that subjects who had PET/CT-detectable BAT activity had a larger postprandial thermogenic response and enhanced fatty acid utilisation than those who did not have detectable BAT (Hibi *et al.*, 2016).

These findings provide weight to the notion that diet, as well as cold, is able to induce expenditure of substantial energy through BAT thermogenesis. By one estimate, subjects with active BAT under cold conditions could expend 200-400kcal of energy per day attributed to BAT-mediated processes (Kajimura & Saito, 2014). Moreover, in addition to the increased energy expenditure offered by BAT thermogenesis, it has become increasingly evident that BAT may be “worth more than its weight” in the treatment of other metabolic pathologies. Strikingly, despite the fact that BAT accounts for only 5% of total tissue weight, under conditions of cold exposure (when BAT is highly active) nearly half of total triglyceride and over 75% of glucose from a meal is disposed and metabolised by brown fat (Bartelt *et al.*, 2011). Indeed, acclimation to mild cold in humans has been demonstrated to increase diet-induced thermogenesis and improve postprandial whole-body insulin sensitivity (Lee *et al.*, 2014), in addition to cold exposure leading to enhanced non-esterified fatty acid uptake and the oxidative activity in BAT (Ouellet *et al.*, 2012; Blondin *et al.*, 2014). These studies neatly demonstrate the ability of BAT to rapidly sequester and combust circulating nutrients following a meal, extending the potential therapeutic benefits of BAT recruitment to include not only weight loss, but also to treat hyperglycaemia (as in T2DM) and hyperlipidaemia (Nedergaard *et al.*, 2011). Taken together, brown fat is a *bona fide* therapeutic target in the fight against obesity and associated dysregulated metabolic processes.

1.6 Peripheral factors in the regulation of adaptive BAT thermogenesis

The essential role of sympathetic activity in the regulation of thermogenesis has influenced the development of pharmaceutical sympathomimetics with the aim to induce weight loss through increased energy expenditure in BAT (Carey *et al.*, 2013; Cypess *et al.*, 2015). However, deleterious side-effects associated with non-specific adrenergic activation ignited interest in peripherally-active factors which bypass the SNS. A high-profile *Nature* publication reported a non-neuronal source of noradrenaline, released from alternatively-activated macrophages (M2), which contributed to BAT-mediated adaptive thermogenesis in response to cold (Nguyen *et al.*, 2011). Subsequent to this finding, a series of other studies supported the role of M2 immune cells to promote thermogenesis following activation from circulating hormones or other immune cells (Rao *et al.*, 2014; Hui *et al.*, 2015; Fabbiano *et al.*, 2016). However, in spite of convincing evidence for M2-mediated thermogenic activation, another paper more recently demonstrated that deletion of the enzyme necessary for the biosynthesis of noradrenaline (tyrosine hydroxylase) from haematopoietic cells had no effect on energy expenditure, thermogenesis or WAT browning in response to cold challenge (Fischer *et al.*, 2017). In view of the conflicting findings, the most rational conclusion to be drawn was that macrophages at least do not generate noradrenaline *de novo*, dampening the prospects of an immune system-mediated activation of brown fat.

There have also been reports of peripherally-derived hormones that can promote energy expenditure by signalling directly through brown adipocytes. Recently, the gut-derived hormone, secretin, was reported to be involved in the postprandial recruitment of brown fat thermogenesis via a mechanism that may be independent of the SNS (Li *et al.*, 2018). Notably, though, there is evidence that the sufficiency to regulate intracellular signalling in brown fat by peripheral hormones does not negate the necessity of interaction with the SNS in order to produce thermogenesis. For example, global knockout of Type II iodothyronine deiodinase (DIO2), the enzyme which catalyses the conversion of thyroxine to the more potent triiodothyronine, induced a severe blunting of the thermogenic response to cold exposure and noradrenaline infusion, implicating a role for thyroid signalling in the control of BAT activity (de Jesus *et al.*, 2001). However, while DIO2 is expressed within brown adipocytes, the activity of the enzyme depends on β3-adrenoceptor activation (Silva & Larsen, 1983), and there is other convincing evidence that thyroid hormone signals through the CNS to promote energy expenditure via activation of brown fat thermogenesis (Coppola *et al.*, 2007; Lopez *et al.*, 2010). In this vein, while Fibroblast growth factor 21 (FGF21) can act directly on the brown adipocyte to induce insulin-sensitising effects, its energy expenditure-promoting and weight loss effects rely on centrally-mediated signalling, and hence the activation of sympathetic outflow to brown fat (Owen *et al.*, 2014; BonDurant *et al.*, 2017).

Despite the attractive therapeutic potential of peripherally-active factors, their relative contribution to brown fat thermogenesis is not clearly defined, and in some cases require synergy with activation of adrenergic receptors on the tissue. Indeed, denervation of BAT sympathetic nerves reduces UCP1 expression and mitochondrial uncoupling (Desautels *et al.*, 1986; Gong *et al.*, 1990), and molecular adaptations leading to increased thermogenesis following both dietary or thermal challenges require in-tact sympathetic innervation (Rothwell & Stock, 1984a; Geloen *et al.*, 1992; Fischer *et al.*, 2019). These taken into consideration, it is clear that the nervous system remains unparalleled in its necessity and sufficiency to regulate brown fat thermogenesis.

1.7 The origins of brown fat-directed sympathetic outflow

Advances in the ability to trace synaptically-connected neural circuits pioneered a methodological paradigm shift for the investigation of the central determinants controlling sympathetic outflow to brown fat. Even though there was clear evidence for strong sympathetic innervation to brown fat, the localisation of CNS neurons that modulate peripheral nerve activity was not possible until the development of a virulence-attenuated form of pseudorabies virus (PRV), a transsynaptic retrograde virus, which could be utilised in animal models as a neural tracer. Injection of PRV directly into the interscapular brown fat depots enabled an elucidation of the neuroanatomical blueprint of neurons projecting via multiple synapses to BAT (Bamshad *et al.*, 1999; Oldfield *et al.*, 2002; Cano *et al.*, 2003; François *et al.*, 2019). The virus was initially transported to the post-ganglionic sympathetic neurons within the upper thoracic sympathetic chain ganglia (first-order neurons), and then to the pre-ganglionic sympathetic neurons of the intermediolateral nucleus (IML) of the spinal cord (second-order). From here, virus subsequently passed to third-order (or "premotor") neuronal populations in the brain stem, such as the raphe pallidus and rostral ventrolateral medulla, in addition to those in the hypothalamus, such as the paraventricular nucleus, dorsomedial hypothalamus, retrochiasmatic area and lateral hypothalamus. Further increasing the survival time post-inoculation allowed the identification of fourth-order neurons within other key nuclei of the brain stem and hypothalamus, including the arcuate nucleus, nucleus of the solitary tract and the broader region that comprises the preoptic area. These projections to brown fat, including select inter-nucleus connections, are depicted in **Figure 1.5** below.

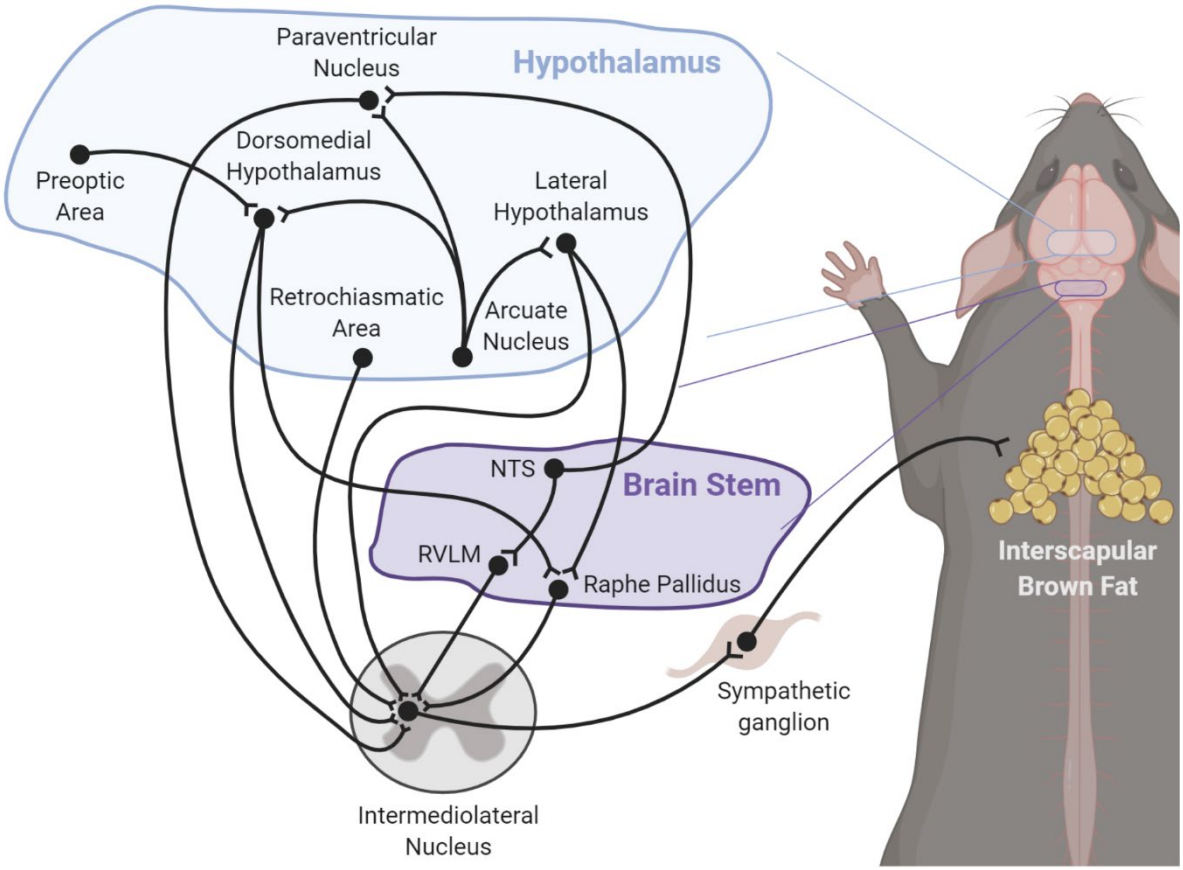

(legend on next page)

Figure 1.5 | A schematic stencilling part of the neurocircuitry involved in the regulation of BAT-directed sympathetic outflow

Key brain regions that have been implicated in the control of BAT sympathetic outflow are indicated as black circles in a sagittal schematic of the hypothalamus and brain stem. Anatomical connections between regions ultimately projecting to brown fat have been established through a combination of mono- and trans-synaptic retrograde tracing, as well as more recent circuit-specific optogenetic functional manipulations or circuit mapping. NTS, nucleus of the solitary tract; RVLM, rostral ventrolateral medulla.

With the appreciation that BAT thermogenesis is activated following meal ingestion or by cold exposure, it is unsurprising that PRV-labelled brain regions overlap with those renowned for their involvement in the homeostatic control of energy balance and body temperature (Cano *et al.*, 2003; Morton *et al.*, 2006; Morrison, 2016). Notably, only few labelled hypothalamic regions are implicit in the control of both energy balance (appetite) and thermoregulation, suggestive of a divergence in the higher-order neuronal populations that detect or receive sensory signals associated with each stimulus (i.e. meal ingestion or cold). The development of therapeutics that could augment cold- or diet-induced thermogenesis would benefit from sophisticated and intricate understandings of the nature of the central regulation of sympathetic tone to brown fat. Indeed, rational drug design, based on the comprehensive delineation of hypothalamic circuits which regulate appetite and energy expenditure, led to the development of the currently approved anti-obesity pharmaceutical, Contrave (Greenway *et al.*, 2009; Sherman *et al.*, 2016). The specific question to be answered, then, is: how and where in the CNS are the sensory signals associated with thermal and dietary challenges integrated to compute adaptations in sympathetic tone to brown fat?

1.7.1 Cold-induced thermogenesis

Significant headway has been made regarding the delineation of a synaptically-defined circuit that connects cold exposure with the activation of sympathetic nerves directed to brown fat. In its most simplistic form, this circuit involves thermal afferent pathways, which are activated (in the skin) by reduced ambient temperature, and relay an excitatory signal (via the brain stem) to the hypothalamus where it is integrated, leading to the co-ordinated activation of descending efferent pathways to the sympathetic pre-ganglionic neurons in the IML (Morrison *et al.*, 2014). This circuit was elucidated from over a decade of research involving a variety of techniques, including PRV viral tracing (Bamshad *et al.*, 1999; Oldfield *et al.*, 2002), cold-induced Fos activation studies (Baffi & Palkovits, 2000; Cano *et al.*, 2003), modulation of cold sensory receptors (Steiner *et al.*, 2007; Ono *et al.*, 2011) and *in vivo* electrophysiology combined with stereotaxic delivery of pharmacological agents (Madden & Morrison, 2006, 2010; Madden *et al.*, 2013).

More recently, the development of novel biotechnologies has enabled further characterisation of temperature-sensitive circuits by the identification of molecular markers that define cold (and warm)-responsive neurons, particularly within the dorsomedial hypothalamus (DMH) and preoptic area (POA)

(Zhang *et al.*, 2011; Rezai-Zadeh *et al.*, 2014; Tan *et al.*, 2016; Yu *et al.*, 2016; Zhao *et al.*, 2017). In a number of these studies, the thermoregulatory and/or metabolic outcomes associated with the activity of these genetically-defined neurons was achieved through the use of neuronal manipulation technologies like optogenetics (light-sensitive ion channels) or "DREADDs" (Designer Receptors Exclusively Activated by Designer Drugs) (Armbruster *et al.*, 2007; Deisseroth, 2011). While outside the focus of this thesis, these studies, so far, describe a delicate balance of excitatory and inhibition neurotransmission that occurs between cold- and warm-responsive neurons in the higher-order "command" centres in the DMH and POA, which ultimately orchestrate thermoregulation through autonomic modulation of both BAT thermogenesis and tail vasodilation (which enables heat dissipation) (see recent review, Morrison and Nakamura (2019)).

1.7.2 Diet-induced thermogenesis: elusive central determinants

In stark contrast to the thermoregulatory circuit projecting to brown fat, the exact central origin(s) of **diet-induced** sympathetic outflow to BAT remain poorly understood. While the sensory detection of cold is almost entirely restricted to activity of cutaneous temperature-sensitive afferents, the "sensing" of meal-consumption is an inherently more complex phenomenon. There is evidence to indicate that diet-induced (or "postprandial") thermogenesis may be regulated not only by pre-absorptive sensory cues like taste perception or activation of chemo-sensors in the gastrointestinal tract (LeBlanc *et al.*, 1984; Blouet & Schwartz, 2012), but also through post-absorptive signals including the activity of circulating nutrients or peripherally-derived hormones (Lockie *et al.*, 2012; Tovar *et al.*, 2013; Rezai-Zadeh *et al.*, 2014; Li *et al.*, 2018). That being said, regarding the postprandial regulation of autonomic flow to brown fat, we believe that the "light shines brightest" on brain regions which rely on the detection of meal-related cues in order to maintain energy homeostasis by modulating appetite and energy expenditure.

The hypothalamus plays a crucial role for the sensing and integration of metabolic signals, effecting not only physiological but also behavioural changes to sustain basic homeostatic needs (Morrison *et al.*, 2012; Coll & Yeo, 2013). Hypothalamic neuronal populations are uniquely positioned to access humoral signals given that the blood-brain barrier at the median eminence, which is positioned at the base of the hypothalamus and third ventricle, is comprised of fenestrated capillaries which are permeable to circulating nutrients and hormones (Cheunsuang *et al.*, 2006; Ciofi, 2011). Most hypothalamic nuclei contain neurons that have been implicated in either (or both of) the regulation of brown fat thermogenesis, or in the sensing of meal-related signals, including circulating hormones and nutrients (Labbé *et al.*, 2015). The **"master"** regulator of postprandial thermogenesis, though, may originate at the most ventromedial portion of the hypothalamus, the arcuate nucleus, the centre of the melanocortin system, which is poised to afford the most likely conduit between meal consumption and sympathetic output to BAT.

1.8 The melanocortin system: a primary regulator of energy balance

1.8.1 Melanocortin signal transduction

The melanocortin system comprises two antagonistic neuronal populations, namely proopiomelanocortin (POMC)-expressing and agouti-related peptide (AgRP)-expressing neurons, the latter of which largely co-express neuropeptide Y (NPY) and γ-aminobutyric acid (GABA). POMC neurons are largely anorexigenic in their action, signalling satiety during caloric surplus, in addition to promoting energy expenditure and weight loss (Atasoy *et al.*, 2012; Zhan *et al.*, 2013; Dodd *et al.*, 2015). Conversely, AgRP neurons represent the anabolic arm of the melanocortin pathway, and as such are activated by caloric deprivation to drive energy conservation by increasing feeding and reducing energy expenditure (Aponte *et al.*, 2011; Krashes *et al.*, 2011; Atasoy *et al.*, 2012). The activity of these two populations according to energy availability is regulated (typically in an inverse manner) by "sensing" changes in circulating nutrients (Fioramonti *et al.*, 2007; Parton *et al.*, 2007), or hormones like leptin, insulin and gut-derived peptides (Cowley *et al.*, 2001; van den Top *et al.*, 2004; Acuna-Goycolea *et al.*, 2005; Secher *et al.*, 2014; Dodd *et al.*, 2018). The cleavage products of POMC, α-melanocyte stimulating hormone (α-MSH), β-MSH and γ-MSH bind to downstream melanocortin-3 or -4 receptors (MC3R or MC4R) to effect changes in neuronal activity (Cone, 2005); notably, it is the action of α-MSH on MC4R that is attributed to majority of catabolic effects associated with POMC neuron activity (Krashes *et al.*, 2016). On the contrary, AgRP activity opposes that of POMC-derived peptides by acting as an antagonist or inverse agonist at MC4Rs, and hence mediating anabolic functions (Ollmann *et al.*, 1997; Haskell-Luevano & Monck, 2001).

1.8.2 Location of hypothalamic POMC and AgRP/NPY neurons

In the hypothalamus, POMC and AgRP/NPY neurons are typically regarded to be located solely within the arcuate nucleus (ARC), however both neuronal populations are **also** expressed in the adjacent retrochiasmatic area (RCA). Astonishingly, the RCA is consistently either "ignored" or simply conflated with the rostral part of the ARC, presumably because it is located in confluence with the rostral boundary of the ARC under the third ventricle, as well as wrapping laterally around the outer boundary of the rostral-mid ARC (see **Figure 1.6** on next page) (Swanson & Kuypers, 1980b; Paxinos & Watson, 1998). In fact, only few published studies accurately distinguish POMC and AgRP/NPY neurons between these two nuclei; and in almost all cases, this is due to the fact that these studies involve a comprehensive analysis of the cytoarchitectonic divisions that exist through the rostro-caudal extent of the nuclei (Elias *et al.*, 1999; Williams *et al.*, 2010; He *et al.*, 2018). In support of the need to distinguish the two regions, there is evidence of genetic and/or functional divergence that is particularly evident for POMC-expressing neurons (Elias *et al.*, 1998; Münzberg *et al.*, 2003; Jarvie & Hentges, 2012). Critically for this thesis, there is also evidence for differing anatomical connectivity of neurons between each nucleus. POMC neurons in the RCA connect to brown fat directly through pre-ganglionic sympathetic neurons in the spinal cord (third-order), while those in the ARC categorically do not project to the spinal cord, and hence project via other pre-autonomic regions *en route* to brown fat (Oldfield *et al.*, 2002) (see **Chapter 3**).

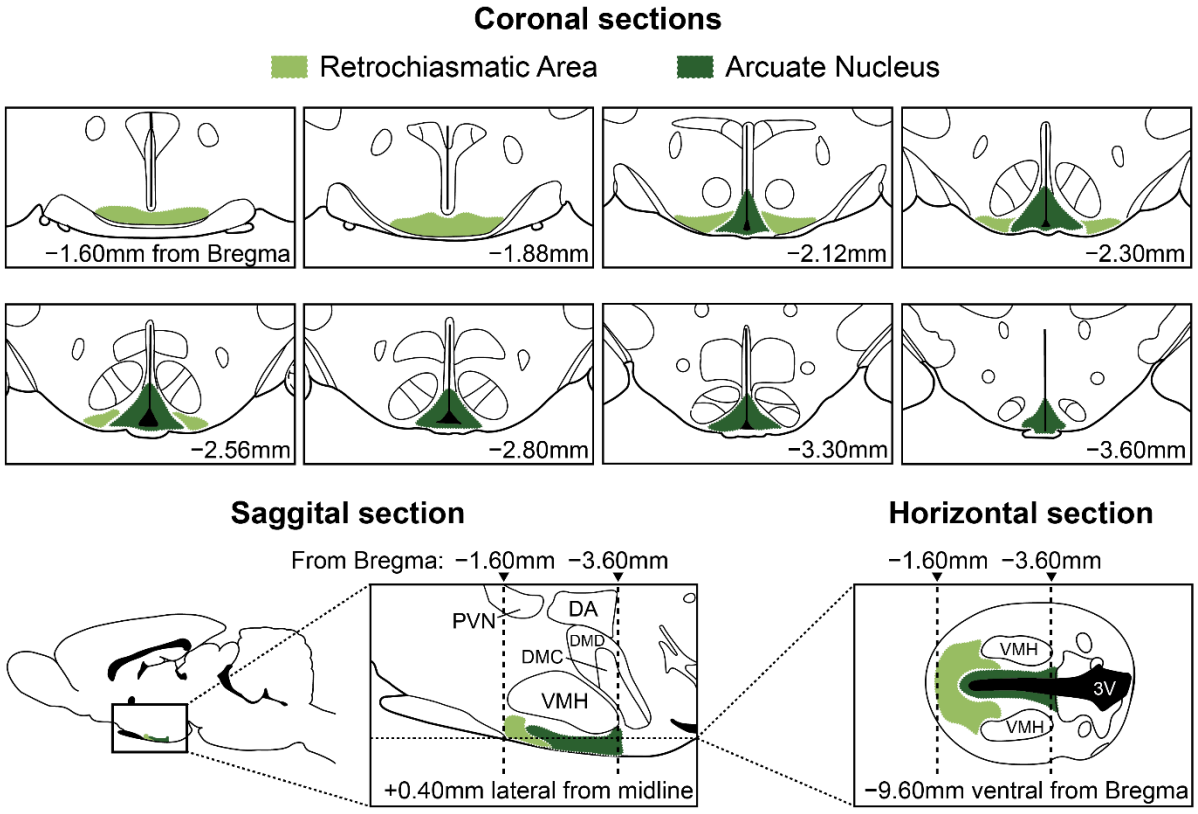

Figure 1.6 | Demarcation of the boundaries of the ARC and RCA in the rat hypothalamus

Line drawing of eight coronal sections of rostral to caudal levels (distance from Bregma in bottom right) of the rat hypothalamus illustrating the boundaries of the retrochiasmatic area (light green) and arcuate nucleus (dark green). Sagittal and transverse sections of the hypothalamus are also included for a three-dimensional representation of the boundaries of each nucleus. Dotted lines on the sagittal and transverse representations refer to the first and last coronal sections presented. 3V, third ventricle; DA, dorsal hypothalamic area; DMC, dorsomedial hypothalamus, compact; DMD, dorsomedial hypothalamus, dorsal; PVN, paraventricular nucleus; VMH, ventromedial hypothalamus. Boundaries of each nucleus were derived from Paxinos and Watson (1998) and Swanson and Kuypers (1980b).

1.8.3 Melanocortin signalling and BAT thermogenesis

The role of melanocortinergic signalling in the control of energy expenditure has been comprehensively studied. Genetic deletion of *Pomc* or *Mc4r* genes consistently leads to extreme obesity characterised by both increased food intake and reduced energy expenditure (Ste. Marie *et al.*, 2000; Butler *et al.*, 2001; Xu *et al.*, 2005). While there is evidence of reduced locomotor activity in these mutants (Chen *et al.*, 2000; Lam *et al.*, 2015), the hypometabolic phenotype is primarily attributed to reduced brown fat thermogenesis. The MC4R is expressed in a large proportion of BAT-projecting neurons (Voss-Andreae *et al.*, 2007; Song *et al.*, 2008), and the central delivery of MC4R agonists consistently promotes interscapular BAT UCP1 expression, thermogenesis and energy expenditure (Brito *et al.*, 2007; Monge-Roffarello *et al.*, 2014b; Cote *et al.*, 2016). Indeed, recent technological advances have enabled the acute chemogenetic manipulation of hypothalamic POMC neurons using DREADDs, confirming a rapid increase in brown fat temperature subsequent to POMC activation (Fenselau *et al.*, 2017).

Importantly, diet-induced thermogenesis in brown fat appears to be at least partly regulated by MC4R signalling, where *Mc4r* knockout mice display blunted elevations in energy expenditure that usually accompany high-calorie diet feeding (Butler *et al.*, 2001; Albarado *et al.*, 2004). More specifically, it appears that MC4R expression on pre-sympathetic ganglionic neurons in the spinal cord plays a major role in relaying thermogenic signals driven by activation of POMC neuron activity (Rossi *et al.*, 2011; Berglund *et al.*, 2014).

In view of these findings, an important question remains to be answered: **what stimulus (or stimuli) is responsible for driving sympathetic nerve activity that mediates postprandial thermogenesis in brown fat?** By extension of this, does this neural signal begin with POMC neurons at the base of the hypothalamus, where neurons are uniquely positioned to process humoral factors that reflect nutritional status?

It is logical to conceive that a stimulus effecting this process is one which increases in plasma concentration following a meal, and which can be "sensed" by central neurons regulating BAT thermogenesis. One of the most obvious candidates would be the neuronal primary fuel substrate, **glucose**, whose plasma and concomitant cerebrospinal fluid concentration is inextricably linked with the prandial state (Steffens *et al.*, 1988; Geracioti *et al.*, 1995; Silver & Erecinska, 1998).

1.9 Sensing changes in circulating glucose by the brain

Elevations in blood-borne nutrients are considered the primary indicator of the postprandial state. Following meal-consumption, carbohydrates are the most rapidly metabolised and absorbed macronutrient from the gastrointestinal tract (Trout *et al.*, 1977; Goetze *et al.*, 2007). Glucose-sensing neurons in the brain are able to detect changes in blood glucose associated with feeding (or fasting), which induces changes in neuronal activity that regulate both glucose and energy homeostasis (Routh *et al.*, 2014). The first indications of glucose-sensing neurons in the brain were evidenced from *in vivo* electrophysiological extracellular recordings in the mid-20th century, where it was found that neurons in the lateral and ventromedial hypothalamus rapidly adjusted their action potential firing rate according to glucose availability (Anand *et al.*, 1964; Oomura *et al.*, 1969). From these and other experiments, two broad classes of glucose-sensing neurons were established: glucose-excited and glucose-inhibited neurons, which were depolarised and hyperpolarised, respectively, in milieus of increasing glucose (Oomura & Yoshimatsu, 1984).

The cellular mechanisms that mediate glucose-induced changes in membrane potential have been comprehensively examined over the last two decades or so. At the level of an overview, glucose-induced excitations are most commonly recognised to be mediated by the closure of ATP-sensitive potassium (K_{ATP}) channels. Indeed, **hypothalamic POMC neurons are excited by glucose** in a manner that is dependent on the inactivation of K_{ATP} channels (Ibrahim *et al.*, 2003; Parton *et al.*, 2007). In these cells, glucose-induced changes in neuronal excitability are proposed to be transduced in a manner akin to glucose-induced insulin release from pancreatic β-cells (Ashford *et al.*, 1990; Schuit *et al.*, 2001). Specifically, elevations in extracellular glucose lead to increased uptake by the cell through low-affinity, high-capacity glucose transporters. Neuronal metabolism of glucose within mitochondria causes a dose-dependent elevation in cytosolic ATP/ADP ratio, which ultimately induces closure of K_{ATP} channels to block tonic K^+ efflux, and hence depolarise the neuron and increase firing rate (**Figure 1.7**).

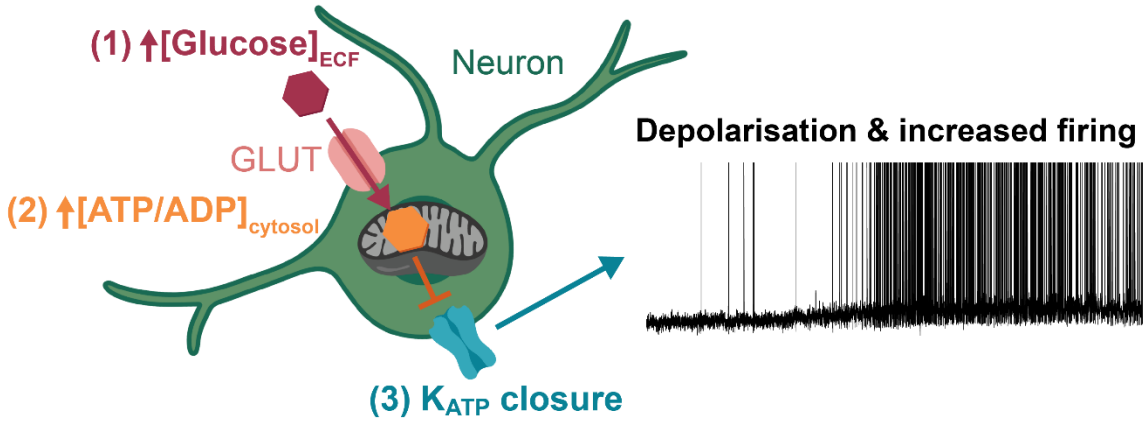

Figure 1.7 | The classical model accepted to mediate neuronal glucose-induced excitations

Elevations in extracellular fluid (ECF) glucose lead to increased entry of glucose into the neuron (1) through glucose transporters (GLUT). Mitochondrial metabolism of glucose into ATP increases the cytosolic ATP/ADP ratio (2), which results in the closure of K_{ATP} channels (3). Cessation of K^+ efflux results in neuronal depolarisation and increased firing rate.

However, there is emerging evidence that glucose-sensing is more complex and heterogenous than once believed (see López-Gambero *et al.* (2019) for recent review). Indeed, glucose-induced inhibitions do not appear to occur uniformly across different neuronal populations. There is evidence for increased neuronal glucose metabolism to lead to activation of chloride or potassium conductances which induce neuronal hyperpolarisation (Murphy *et al.*, 2009; Lamy *et al.*, 2014), or alternatively activation of a potassium conductance through a metabolism-independent mechanism that is yet to be completely elucidated (Burdakov *et al.*, 2006). Importantly, with advances in the understanding of neuronal glucose-sensing, there is now accumulating evidence for a role of other, non-neuronal cell types in the regulation of neuronal activity in face of fluctuating glucose levels.

1.9.1 The role for astrocytes in neuronal glucose-sensing

Astrocytes, a glial cell, have long been assigned a crucial role in fuelling neuronal activity through the delivery, storage and production of energy for neighbouring neurons (Stobart & Anderson, 2013). However, this classical "support-only" dogma of the cells is being increasingly challenged, with recent findings indicating that astrocytes express key glucose-sensing machinery that at the minimum qualify their capacity to regulate glucose uptake and metabolism in proportion to its extracellular availability (Arluison *et al.*, 2004; Millan *et al.*, 2010; Stanley *et al.*, 2013). In support of this notion, re-expression of the glucose transporter-2 (GLUT2) specifically in astrocytes, but not neurons, in *Glut2* global knockouts restores the otherwise defective central detection of glucopenia (Marty *et al.*, 2005). Furthermore, in the nucleus of the solitary tract (NTS), calcium imaging of both neurons and astrocytes revealed that while reduced extracellular glucose led to increased calcium activity in both cell types, the neuronal response seemed to be orchestrated by astrocyte activity, the latter of which began ~40% earlier following glucoprivation (McDougal *et al.*, 2013).

Relevant to this thesis, there is also a growing body of evidence that substantiates astrocyte-regulated glucose-sensing in POMC neurons. The activation of both neurons and astrocytes in the ARC following intracarotid infusion of a glucose bolus was shown to be dependent on astrocyte-mediated metabolism of glucose (Guillod-Maximin *et al.*, 2004). Importantly, deletion of the insulin-receptor in astrocytes induced defective cerebral glucose uptake, as well as causing an attenuation in the glucose-induced activation of POMC neurons and its associated satiety-producing effects (Garcia-Caceres *et al.*, 2016). Furthermore, it was recently shown that glial retraction from POMC neurons in the postprandial state is regulated by fluctuations in extracellular glucose, leading to changes in POMC neuron activity and synaptic input which ultimately modified patterns of meal consumption (Nuzzaci *et al.*, 2020).

The body of evidence implicating astrocytes as the "first step" to sensing fluctuations in extracellular glucose is compelling, including for the regulation of POMC neuron activity. A key question, then, is **what is/are the astrocyte-derived transmitter(s) that mediate this inter-cellular signalling**?

1.9.2 How do astrocytes communicate glucose availability?

An abundance of evidence indicates that astrocytes show a preference for glycolytic (anaerobic) metabolism (Bittar *et al.*, 1996; Bouzier-Sore *et al.*, 2006; Laughton *et al.*, 2007), whereas neurons have been shown to largely perform oxidative respiration (Itoh *et al.*, 2003; Herrero-Mendez *et al.*, 2009). Additionally, neurons show preference in the utilisation of lactate as a substrate for oxidative metabolism, whereas glucose utilisation is more important in astrocytes (Waagepetersen *et al.*, 1998; Bouzier-Sore *et al.*, 2006; O'Brien *et al.*, 2007). These findings together are supportive of a model where astrocytes primarily take up and metabolise (anaerobically) circulating glucose into lactate, which is then utilised by neighbouring neurons as its preferred energy substrate. With these findings in mind, it is possible that glucose-sensing neurons derive signals of glucose availability from glial cell-derived transmitters ("gliotransmitters"), such as lactate, rather than from the autonomous processing of glucose by neurons themselves.

It has been demonstrated that (neurochemically-unidentified) glucose-excited neurons from the mediobasal hypothalamus (MBH) are responsive to lactate in a similar manner to glucose, inducing depolarisation that is mediated by closure of K_{ATP} channels (Ainscow *et al.*, 2002). It is possible that POMC neurons comprise part of this lactate-responsive population, as i.c.v. administration of lactate reduces food intake in a manner that is dependent on its ability to be metabolised intracellularly (Lam *et al.*, 2008). Furthermore, the knockdown of monocarboxylate transporters (through which lactate is trafficked in and out of the cell) in the MBH caused increased food intake and prevented glucose-induced upregulation of *Pomc* expression (Elizondo-Vega *et al.*, 2016).

In addition to lactate, astrocytes are recognised to release a range of other molecules as gliotransmitters, including glutamate (Gordon *et al.*, 2009), D-serine (Henneberger *et al.*, 2010) and ATP (Koizumi *et al.*, 2003; Tan *et al.*, 2017), the latter of which can be dephosphorylated into adenosine by extracellularly-expressed ectonucleotideases, which can then signal to surrounding neurons through adenosine A_1, A_{2A}, A_{2B} and A_3 receptors (Dunwiddie *et al.*, 1997; Fields & Burnstock, 2006). As indicated earlier, neurons in the NTS respond to reductions in extracellular glucose through a mechanism dependent on astrocyte signalling. Importantly, investigators found that astrocyte-derived adenosine (and ATP) signal in a paracrine fashion to neighbouring neurons to mediate glucoprivation-induced excitations (Rogers *et al.*, 2016; Rogers *et al.*, 2018). Furthermore, in the hypothalamus, astrocyte-derived adenosine activates sleep-promoting neurons of the ventrolateral preoptic nucleus in response to elevations in extracellular glucose by activation of adenosine A_{2A} receptors (Scharbarg *et al.*, 2016).

The relevance for astrocyte-derived adenosine signalling in the regulation of POMC neuron activity is scarce. However, recent advances in technology that permit the real-time modulation of gliotransmission have gained traction for notion that astrocytes do contribute to melanocortin-regulated energy homeostasis through adenosinergic signalling.

1.9.3 Adenosine signalling: a link between glucose and the melanocortin system?

Astroglial networks are electrically and chemically coupled by gap-junction channels which enable the inter-cellular passage of ions or small molecules (Giaume *et al.*, 2010). Calcium waves are

known to propagate through astrocytic syncytia in response to external stimuli, resulting in the release of gliotransmitters which thus form the basis of reciprocal communication with adjacent neurons (Scemes & Giaume, 2006). Chemogenetic and optogenetic technologies have been employed to "exogenously" evoke astrocytic calcium waves, which can induce the release of astrocyte-derived purines (ATP and/or adenosine) (Gourine *et al.*, 2010; Savtchouk & Volterra, 2018; Durkee *et al.*, 2019). Critically, activation of calcium-dependent astrocyte signalling in the hypothalamus has been shown reduce food intake in an adenosine A_1 receptor-dependent manner via the dampening of AgRP neuron activity (Yang *et al.*, 2015; Sweeney *et al.*, 2016). However, in conflict with these findings, another study found that chemogenetic activation of astrocytes evoked voracious feeding that was mediated by AgRP neuron *activation* (but the adenosine-dependence of this effect was not examined) (Chen *et al.*, 2016). This discrepancy is likely explained by the topographical location of the astrocytes undergoing chemo- and opto-genetic manipulation, where the former studies appeared to activate astrocytes throughout the *whole* hypothalamus, whereas DREADD labelling in the latter study was largely restricted to the ARC (based on histological sections shown in each paper).

In view of these findings, astrocytes are evidently involved in the detection and signalling of extracellular glucose changes to neighbouring neurons. Considering recent indications of astrocyte-mediated control of neighbouring POMC neurons (Garcia-Caceres *et al.*, 2016; Nuzzaci *et al.*, 2020), we theorise that glucose-derived signals from astrocytes, such as adenosine, contribute to the paracrine regulation of POMC excitability. **What is the evidence, then, that the detection of elevated glucose levels regulates postprandial thermogenesis in brown fat?**

1.9.4 Glucose and POMC neurons: regulators of postprandial thermogenesis?

A series of thermoregulatory studies almost half a century ago demonstrated the central role that glucose plays in body temperature maintenance. Administration of glucoprivic agents both peripherally or centrally was found to induce profound hypothermia (Freinkel *et al.*, 1972; Sun *et al.*, 1979; Shiraishi & Mager, 1980; Penicaud *et al.*, 1986). In the same vein, hypothalamus-specific glucopenia silenced BAT-directed sympathetic outflow and reduced mitochondrial uncoupling (Arase *et al.*, 1987; Egawa *et al.*, 1989a, b), indicative of nutrient-sensing hypothalamic network(s) which facilitate energy conservation by reducing BAT thermogenesis in the face of nutrient depletion.

Importantly, hypothalamic glucose-sensing networks are also sufficient to promote thermogenesis in milieus of caloric repletion, where intra-hypothalamic or third ventricle injections of glucose rapidly activate BAT-directed sympathetic activity (Sakaguchi & Bray, 1987, 1988; Holt & York, 1989). In attempt to define glucose-sensing neuronal population(s) that may promote BAT activity, one group developed a mutant of the archetypal glucose-sensing K_{ATP} channels that was resistant to closure (Tovar *et al.*, 2013). The authors found that K_{ATP}-mediated glucose-sensing in central catecholaminergic neurons, particularly those in the locus coeruleus, was important for the regulation of diet-induced thermogenesis in brown fat. However, while these findings indicate a role for hindbrain glucose-sensors, there is no direct evidence for the identity of the hypothalamic neuronal population(s) that mediate nutrient-induced activation (or glucoprivation-induced inhibition) of sympathetic tone to brown fat.

1.10 Aims and hypotheses of thesis

There is no doubt that the determinants of postprandial thermogenesis in brown fat are multifactorial, particularly in view of the complex nature and range of stimuli associated with meal consumption. However, there is substantial evidence to implicate glucose as a principal meal-associated signal that is sufficient to modulate brown fat thermogenesis. In consideration of findings that POMC neurons are activated by meal-related cues, including glucose, and that signalling at MC4R promotes BAT thermogenic activity and energy expenditure, we hypothesise that:

1) **POMC neurons of the ARC and RCA constitute a hypothalamic glucose-sensing population that contributes to the postprandial recruitment of sympathetic activity to brown fat**

Furthermore, considering the emerging role of astrocytes as a "bridge" between fluctuations in extracellular glucose and adaptations in the excitability of neuronal glucose-sensors, we hypothesise that:

2) **Astrocyte-derived metabolites of glucose modulate POMC neuronal excitability subsequent to extracellular glucose excursions that are associated with the postprandial state**, and in view of our first hypothesis**, that astrocytes of the mediobasal hypothalamus contribute to the postprandial regulation of thermogenesis in brown fat**

These hypotheses are to be interrogated in this thesis under a number of aims which relate to each chapter:

Chapter 3: To investigate the glucose-sensitivity of individual hypothalamic neurons that have a defined polysynaptic trajectory to brown fat and hence modulate BAT-directed sympathetic output.

Chapter 4: To substantiate the sufficiency of POMC signalling to modulate BAT thermogenic activity and its necessity in the meal-induced activation of BAT thermogenesis.

Chapter 5: To investigate the role of astrocyte-derived gliotransmission, particularly adenosine release, in the regulation of POMC neuron excitability following elevations in extracellular glucose. Furthermore, to test the sufficiency of astrocyte-mediated regulation of POMC neurons to modulate BAT thermogenesis.

Chapter 2

General Methods

2.1 Animals, Breeding and Husbandry

All rats and mice used in these experiments were bred on campus at Monash University, Clayton. All experimental procedures were reviewed and approved by the Monash Animal Resource Platform Ethics committee and performed in accordance with the "Australian Code of Practice for the Care and Use of Animals for Scientific Purposes".

2.1.1 Wild-type rats

Male Sprague-Dawley rats were used for experiments described in **Chapter 3** of this thesis. Rats were bred by and obtained from Monash Animal Services (Clayton, Victoria), and were used in experiments from 7-14 weeks of age. Rats were individually housed in a humidity (60 ± 20%) and temperature (22 ± 2°C) controlled room on a standard 12:12h light/dark cycle. Rats received *ad libitum* access to standard laboratory chow (13.2kJ/g digestible energy, 24% digestible energy from lipids, 25% digestible energy from protein, 102119–1070; Barastoc-Ridley, Victoria, Australia) and water, except for the night before electrophysiological recordings when food was removed (~16 hours before euthanasia).

2.1.2 Wild-type and transgenic mice

Wild-type or transgenic male mice were used for experiments described in **Chapter 4** and **Chapter 5**. A mixture of hemi- and homozygous mutant mice was used from all genetically modified strains. Mice were housed in a temperature (24 ± 1°C) controlled room and received *ad libitum* access to standard laboratory chow (13.2kJ/g digestible energy, 24% digestible energy from lipids, 25% digestible energy from protein, 102119–1070; Barastoc-Ridley, Victoria, Australia) and water, except in experiments involving overnight fasts (~16 hours food deprivation).

For food intake, energy expenditure, BAT temperature assays and virus validation studies, singly-housed wild-type C57Bl/6 (C57Bl/6^{WT}) mice were bred by and obtained from Monash Animal Services (Clayton, Victoria) and used for experimentation at 8-18 weeks of age

For patch-clamp electrophysiology, immunohistochemistry and neuronal activation (Fos) studies, singly- or group-housed Pomc^{eGFP} mice maintained on a C57Bl/6 background were used for experimentation at 7-18 weeks of age. Mice were generated as previously described (Cowley *et al.*, 2001), and the colony was founded from donor mice received from Prof Tony Tiganis (Biomedicine Discovery Institute, Monash University), who purchased the mice from Jax (C57BL/6J-Tg(Pomc-EGFP)1Low/J, 009593).

For food intake and BAT temperature assays, singly-housed Agrp$^{IRES\text{-}Cre}$ mice maintained on a C57Bl/6 background were used for experimentation at 8-16 weeks of age. Mice were generated as previously described (Tong *et al.*, 2008), and the colony was founded from donor mice received from A/Prof Zane Andrews (Biomedicine Discovery Institute, Monash University), who purchased the mice from Jax (Agrptm1(cre)Lowl/J, 012899).

For both short- and long-term food intake and BAT temperature assays, body weight and *ex vivo* electrophysiology validation experiments, singly-housed Pomc$^{IRES\text{-}Cre}$ mice maintained on a mixed C57Bl/6 x 129/Sv background were used for experimentation at 8-24 weeks of age. Mice were generated as previously described (Fenselau *et al.*, 2017), and the colony originated from donor mice received directly from the original founder, Bradford B. Lowell (Beth Israel Deaconess Medical Center, Harvard Medical School).

Validation of Cre-mediated recombination was performed by crossing the Cre-reporter mouse strain, Ai14^{tdTomato}, with Pomc$^{IRES\text{-}Cre}$ mice. Reporter mice were generated as previously described (Madisen *et al.*, 2010), and the colony was founded from donor mice received from A/Prof Zane Andrews (Biomedicine Discovery Institute, Monash University), who purchased the mice from Jax (B6.Cg-Gt(ROSA)26Sor$^{tm14(CAG\text{-}tdTomato)Hze}$/J, 007914).

2.1.3 Genotyping

Genotyping of transgenic mouse lines was performed by polymerase chain reaction (PCR) on DNA extracted from tail samples taken 10-11 days postnatally. In some cases, genotype was determined by the extraction and amplification of segments of DNA containing the genetic mutation and internal positive control, followed by gel electrophoresis. In most cases, genotyping was performed by PCR through an external laboratory (Transnetyx, Memphis, USA). The sequences of primers used to generate the amplicon and assign genotype for each transgenic mouseline are provided in **Table 2.1**.

Line name	Primer sequences
Pomc^{eGFP}	1. 5'-AGT GCT TCA GCC GCT ACC (Mutant [eGFP] – forward) 2. 5'-GAA GAT GGT GCG CTC CTG (Mutant [eGFP] – reverse) 3. 5'-CAC GTG GGC TCC AGC ATT (Internal positive control – forward) 4. 5'-TCA CCA GTC ATT TCT GCC TTT G (Internal positive control – reverse)
Agrp$^{IRES\text{-}Cre}$	1. 5'-GCG GTC TGG CAG TAA AAA CTA TC (Mutant [Cre] – forward) 2. 5'-GTG AAA CAG CAT TGC TGT CAC TT (Mutant [Cre] – reverse) 3. 5'-CAC GTG GGC TCC AGC ATT (Internal positive control – forward) 4. 5'-TCA CCA GTC ATT TCT GCC TTT G (Internal positive control – reverse)
Pomc$^{IRES\text{-}Cre}$	1. 5'-TTA ATC CAT ATT GGC AGA ACG AAA ACG (Mutant [Cre] – forward) 2. 5'-CAG GCT AAG TGC CTT CTC TAC A (Mutant [Cre] – reverse) 3. 5'-GAA CGC GCA CAA GAA GGG CCA (Wild type – forward) 4. 5'-GAA GAT CAG AGC CGA CTG TGA AAT CTG A (Wild type – reverse)
Ai14^{tdTomato}	1. 5'-CTG TTC CTG TAC GGC ATG G (Mutant [tdTomato] – forward) 2. 5'-GGC ATT AAA GCA GCG TAT CC (Mutant [WPRE] – reverse) 3. 5'-AAG GGA GCT GCA GTG GAG TA (Wild type – forward) 4. 5'-CCG AAA ATC TGT GGG AAG TC (Wild type – reverse)

Table 2.1 | Transgenic mouse lines used for all studies

Line name refers to name assigned to each transgenic mouse strain in this thesis. Primer sequences 5'-3' are listed with a description in brackets following the sequence

2.2 Surgeries: anaesthesia and analgesia

Surgical procedures requiring anaesthesia in both rats and mice were performed using isoflurane delivered in medical grade oxygen (5% isoflurane for induction of anaesthesia, 1.5-2.5% isoflurane for maintenance). Anaesthesia was ascertained by loss of both pedal and corneal reflexes. Eye lubricant was applied directly onto the eyes of the anaesthetised animal to prevent moisture loss. Animals were maintained under inhalation anaesthesia through a rodent mask, and sufficient depth of anaesthesia was monitored throughout the surgical period by observation of respiratory rate and lack of corneal/pedal reflexes. At the beginning of surgery, animals were injected subcutaneously with meloxicam (1mg/kg in rats, 2mg/kg in mice) as well as with 0.5% bupivacaine locally at the site of skin incision (head or interscapular region). Skin was sterilised with 80%v/v ethanol before incision was made. Wounds were sutured closed using non-absorbable silk thread. At the end of the surgery, animals were removed from the isoflurane mask and placed back into their warmed home cage on heat pad for 20-30 minutes. Animals were monitored daily and received additional subcutaneous injections of meloxicam for 3 days following surgery.

2.3 Interscapular brown fat temperature measurement

To gain real-time interscapular BAT (iBAT) temperature measurements, a temperature-sensitive transponder (IPTT-300, Bio Medic Data Systems) was surgically implanted directly beneath the fat pad (**Figure 2.1A**). This procedure, performed under anaesthesia, involved a midline incision made over the interscapular region of the mouse after which a small pocket was blunt dissected in a caudal-to-rostral direction underneath the overlaying white fat (**Figure 2.1B$_1$**). Using a sterilised delivery trochar, the temperature-sensitive probe was inserted deep into this pocket with the temperature-sensitive end placed directly beneath both iBAT lobes (**Figures 2.1B$_2$ and B$_3$**). Using silk suture, the transponder was secured into place to adjacent muscle and the incised skin was closed (**Figures 2.1B$_4$ and B$_5$**). Animals were allowed at least 1-week recovery following surgery, and at least three days of handling and/or habituation to injection (intraperitoneal, intracerebroventricular) before experiments began. Instantaneous temperature was collected using a handheld reader (DAS-8027IUS Portable Reader, Bio Medic Data Systems) by scanning through the side of the animal's home cage. Scanning of mice was performed discreetly to circumvent disturbances which may confound BAT temperature readings.

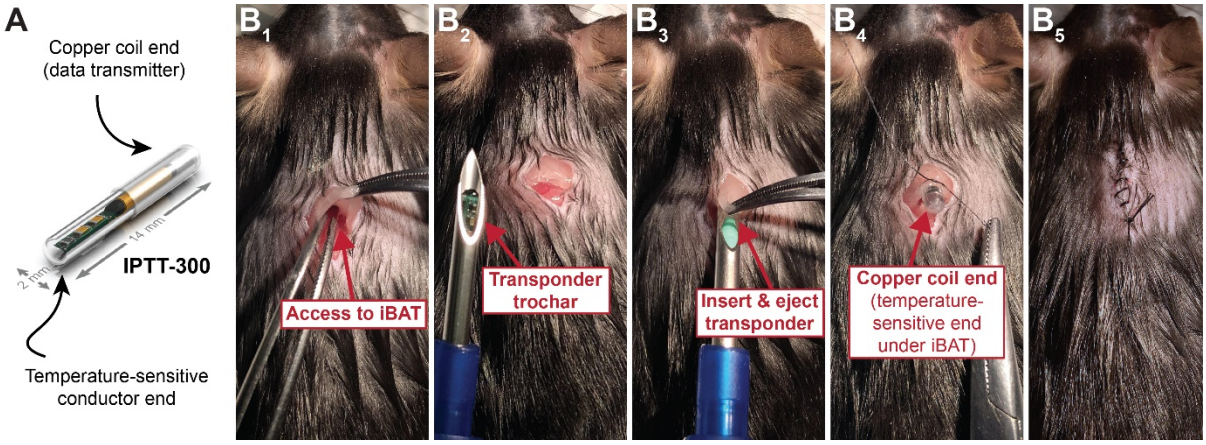

Figure 2.1 | Temperature transponder placement underneath interscapular brown fat

(A) Depiction of the design of the temperature-sensitive IPTT-300 transponder and its dimensions. Image was taken directly from the product website (https://www.bmds.com/products/transponders/iptt-300/specs). **(B_{1-5})** Series of images depicting the blunt dissection deep beneath the overlaying white fat to gain access to the interscapular brown adipose tissue (iBAT, B_1). A trochar loaded with the temperature-sensitive transponder (B_2) is inserted and ejected underneath the iBAT (B_3). The overlying white fat is sutured to secure in place, noting that the temperature-sensitive end is beneath the iBAT and the copper coil transmitter end is exposed (B_4), before skin is sutured closed (B_5).

Chapter 3

Investigation of the glucose-sensitivity of hypothalamic neurons projecting to brown fat

3.1 Introduction

The two classical drivers of sympathetic outflow to BAT are cold exposure and meal consumption, resulting in cold- and diet-induced thermogenesis, respectively (Cannon & Nedergaard, 2004). Significant headway has been made into the delineation of the neural circuitry subserving cold-induced thermogenesis, which originates primarily as the activation of discrete temperature-sensitive sensory fibres in the skin (reviewed by Morrison and Nakamura (2019)). However, the identification of analogous circuitry in the CNS that regulates the meal-induced activation of sympathetic tone to brown fat remains elusive. Efforts to demarcate a neural circuit have been hampered by the complexity and diversity of stimuli that link meal consumption and brown fat activity. Indeed, these processes range from oropharyngeal taste perception and activation of vagal afferents in the gut, to the central detection of factors released or absorbed following food intake (LeBlanc et al., 1984; Blouet & Schwartz, 2012; Lockie et al., 2012; Tovar et al., 2013; Yamazaki et al., 2019).

Homeostatic circuits in the hypothalamus and brain stem fine-tune energy intake and expenditure by sensing and integrating sensory signals that pertain to metabolic status. Energy homeostatic regions that are involved in the detection of energetic surplus (or demand) are polysynaptically linked to brown fat (Bamshad *et al.*, 1999; Oldfield *et al.*, 2002), and may therefore orchestrate the activation of sympathetic outflow to brown fat in the absorptive phase of meal consumption. In support of this hypothesis, the central administration of nutrients such as glucose or leucine (Sakaguchi & Bray, 1987, 1988; Holt & York, 1989; Burke *et al.*, 2017), and hormonal factors like leptin, insulin or gut-derived peptides (Yoshimatsu *et al.*, 1992; Muller *et al.*, 1997; Enriori *et al.*, 2011; Lockie *et al.*, 2012; Beiroa *et al.*, 2014) have been shown to robustly promote brown fat sympathetic nerve activity (SNA) and/or thermogenesis. Importantly, genetic-inactivation of the K_{ATP} channel, a conductance classically associated with glucose-sensing, in catecholaminergic locus coeruleus neurons caused obesity associated with defective glucose-induced activation of BAT SNA (Tovar *et al.*, 2013). While this study suggests a role for hindbrain glucose-sensors in the regulation of BAT thermogenesis, it remains to be determined whether hypothalamic glucose- (or “meal”-) sensing circuitry contribute to the regulation of postprandial thermogenesis.

The hypothalamus contains several glucose-sensing populations that have both anatomical and functional links to the regulation of brown fat SNA. Notably, POMC-expressing neurons in the arcuate nucleus (ARC) and adjacent retrochiasmatic area (RCA) project to brown fat and are reported to depolarise and increase firing in response to elevations in glucose (Oldfield *et al.*, 2002; Ibrahim *et al.*, 2003; Claret *et al.*, 2007) (see also **Chapter 5**). While their glucose-sensing role has not been explicitly linked with the regulation of BAT activity, activation of POMC neurons or their downstream melanocortin receptors rapidly increases oxygen consumption and BAT thermogenesis (Hwa *et al.*, 2001; Song *et al.*, 2008; Fenselau *et al.*, 2017). Furthermore, the paraventricular nucleus (PVN) and lateral hypothalamus (LHA) represent key regulatory nodes for sympathetic outflow to BAT, and are also reported to contain neurons that are sensitive to fluctuations in extracellular glucose (Oldfield *et al.*, 2002; Burdakov *et al.*, 2005; Melnick *et al.*, 2011).

In light of these reports, we hypothesised that hypothalamic neurons with a trajectory to brown fat rapidly detect meal-evoked excursions in cerebrospinal fluid (CSF) glucose. Here, we combine

transsynaptic retrograde tracing and whole-cell patch-clamp technologies to assess the glucose-sensitivity of neurons with an established multi-synaptic projection to BAT. By profiling the responsiveness of BAT-projecting neurons to elevations in extracellular glucose, a surrogate for meal consumption, we aim to advance the understanding of the central determinants of the postprandial activation of BAT sympathetic nerve activity and thermogenesis.

3.2 Experimental Procedures

3.2.1 Tracing BAT-directed neurons using pseudorabies virus

In order to identify neurons with a defined polysynaptic projection to brown fat, the eGFP-expressing transsynaptic retrograde tracer, pseudorabies virus (PRV)-152, was injected into the interscapular brown fat of male Sprague-Dawley rats. Given that PRV is not endemic in Australia, the use of the virus throughout experiments presented in this Chapter was restricted to a quarantine containment (QC3/PC3) facility, as regulated by the *Australian Department of Agriculture and Water Resources*. Using a previously established protocol (Oldfield *et al.*, 2002), under isoflurane anaesthesia the interscapular BAT was exposed via midline incision, and 4 x 1μL injections of PRV-152 were made into each fat lobe (8μL total virus). Care was taken during the surgical procedure to ensure delivery of the virus only to the BAT, and to avoid inadvertent denervation of the pad. Following injection, the area around the lobes was flushed thoroughly with sterile saline. Following surgery, animals received post-operative care as outlined in *Chapter 2: General Methods*.

3.2.2 Preparation of brain slices for patch-clamp recording

Whole-cell patch-clamp recordings were made from PRV-infected neurons in acutely prepared hypothalamic brain slices to test the glucose-sensitivity of BAT-projecting neurons. To induce a physiological state relevant for meal-induced elevations in extracellular glucose, animals underwent an overnight fast (16 hours) prior to brain collection. Specific consideration was given to survival times post-inoculation with PRV-152 to ensure early arrival of the virus at the investigated hypothalamic nuclei, precluding the onset of virally-induced cytopathy. 72-hours (PVN, LHA and RCA recordings) or 96-hours (ARC recordings) following viral injection, animals were deeply anaesthetised with isoflurane (5% in oxygen) and decapitated. Brains were rapidly removed and placed in ice cold, carbogenated (95% O_2/5% CO_2) artificial cerebrospinal fluid (aCSF), whose components were (in mM): 127 NaCl, 1.9 KCl, 1.2 KH_2PO_4, 26 $NaHCO_3$, 2.4 $CaCl_2$, 1.3 $MgCl_2$, 1.0 D-glucose, 9.0 D-mannitol, 0.34 ascorbic acid; osmolarity 300-305mOsm/kg, pH 7.3-7.4. After removing dura and pia mater, the hind brain and excess forebrain were excised. The remaining brain was then mounted with superglue onto a slicing platform with an agar block support to its rear. Using a Leica Series 1000 vibratome (Oxford Instruments), 200μm thick coronal hypothalamic brain slices were made. The slices were incubated at 34-35°C for 20 minutes, then subsequently stored at room temperature (21-23°C) for at least 45 minutes before recording commenced. The glucose concentration was maintained at 1.0mM throughout all brain slicing and incubation protocols to mimic the nutrient environment in the brain following an overnight fast. For testing glucose-responsiveness (see below), the 5.0mM D-glucose aCSF was osmotically balanced by reducing the concentration of D-mannitol to 5.0mM.

3.2.3 Whole-cell patch-clamp recording details

Patch pipettes were pulled from thin-walled borosilicate glass capillaries (GC-150TF-10, Harvard) and had resistances between 4 and 7 MΩ when filled with recording solution. The constituents of the intracellular recording solution were (in mM): 140 KGluconate, 10 KCl, 10 HEPES, 1 Na_2EGTA, 2 Na_2ATP. In some instances, biocytin hydrochloride (5mM, Sigma-Aldrich) was included in the intracellular solution to enable retrospective immunohistochemical probing of neurochemistry. The pH of the solution was adjusted to 7.3 with KOH, and osmolarity to 300-310mOsm/kg with sucrose.

For recording, brain slices were transferred to a recording chamber constantly bathed in carbogenated aCSF (flow rate = 4-6mL/min). BAT-projecting (PRV-infected) neurons were identified using brightfield infrared-differential interference contrast optics with a 40x objective, as well as fluorescence microscopy using a GFP filter (or rhodamine filter for Red Retrobeads, see below) to scan the slice and identify virally infected cells by their eGFP content. Images were captured in real-time using a camera (Hamamatsu) and displayed on a video monitor. Infected cells were visually inspected for health and, thus, viability for electrophysiological recording based upon a clearly identifiable cell body and, in some instances, dendrites. It is likely that the duration of viral infection correlates with more brightly labelled neurons (increased eGFP translation). Therefore, where possible, all efforts were made to record from cells which exhibited the least amount of fluorescence given their probable lower risk of cytopathy. In addition, cells deep in the slice were favoured over superficial cells given their reduced likelihood to have sustained losses to their dendritic arbour during the slicing process which may affect their integrity. A back-filled patch pipette was inserted into an electrode holder where the silver-chloride recording wire contacted the intracellular solution. Offset potentials were negated with the Junction Null function of the Axopatch 1D amplifier in voltage-clamp mode. The current response to a repetitive 3mV x 25ms, 20Hz voltage pulse was observed on a Gould 1602 oscilloscope set at a sweep speed of 5ms/division. With a delicate positive pressure applied from the back of the pipette, the tip of the electrode was lowered through the slice and onto the cell's surface, then gentle negative pressure was applied until >1GΩ seal was made with the tip of the patch pipette and the membrane of the cell. The membrane was subsequently ruptured with brief negative pressure pulses until electrical access to the cell interior was established (whole-cell patch-configuration). Whole-cell capacitance and serial resistance compensation (>70%) were then applied. In current-clamp mode, cells were selected for further investigation provided the action potentials overshot 0mV and they exhibited a stable firing pattern or resting membrane potential that was within physiological range (−35mV to −80mV).

3.2.4 Testing glucose-sensitivity and data handling

In order to ascertain glucose-sensitivity, baseline membrane properties in 1.0mM extracellular glucose were first taken for all cells, including a current-voltage protocol where current was injected in steps of varying amplitude, the largest of which was sufficient to hyperpolarise the cell to approximately -100mV. This protocol allowed identification of sub-threshold active conductances expressed by the cell and to calculate membrane input resistance. Following a gap-free recording period of at least five minutes in basal glucose levels (1.0mM), the slice was exposed to the 5.0mM D-glucose for 5-10

minutes or until a peak response (if present) was established. Neurons were considered to be responsive to glucose if membrane potential changes were ≥2.0mV for a glucose-induced excitation or ≤−2.0mV for a glucose-induced inhibition. Furthermore, changes in membrane potential and/or firing rate were required to be time-locked to the arrival of increased glucose at the brain slice to be considered a true response, and in many cases was confirmed by a reversal of the response upon washout to 1.0mM glucose. Cells with unstable fluctuations in membrane potential were excluded from analysis. Membrane potential and action potential firing rates were quantified from ~30seconds of stable recording just prior to glucose application and at the peak of the response while 5.0mM glucose was present.

Some cells were probed pharmacologically with specific channel blockers to confirm the identity of sub-threshold active conductances revealed during current-voltage protocols. Current and voltage data were displayed on-line with a digital oscilloscope and stored on a personal computer running pCLAMP 9 software (Axon Instruments). Analysis of electrophysiological data was performed offline using Clampex software (Axon Instruments). Membrane potential values were not compensated to account for liquid junction potential (−9 mV).

3.2.5 Tracing monosynaptic axonal trajectory of BAT-projecting neurons

In order to trace monosynaptic projections, Red Retrobeads (LumaFluor) were stereotaxically injected bilaterally into one of four brain or spinal cord regions which are known to relay arcuate nucleus/retrochiasmatic area neuron projections (across multiple synapses) to brown fat. Rats were anaesthetised with isoflurane and placed in a stereotaxic apparatus (Stoelting). For brain injections, after exposing the skull via midline incision, a small hole was drilled for injection of Retrobeads. Injections were made bilaterally via pulled-glass pipettes (tip diameter ≈ 40μm) using a picospritzer (General Valve Corportation, Picospritzer II; 10ms, ~20psi) into one of the following sites: paraventricular nucleus (80nL each side, from bregma: AP: −1.8mm, ML: ±0.4mm, DV: −7.8mm), dorsomedial hypothalamus (80nL each side, from bregma: AP: −2.8mm, ML: ±0.4mm, DV: −7.8mm), lateral hypothalamus (2x 80nL each side, from bregma: AP: −2.6mm & −2.9mm, ML: ±1.5mm, DV: −8.1mm).

For spinal cord injections, the upper thoracic spinal cord was exposed by the blunt dissection of the area between the scapulae, followed by incision of overlying muscle and tendon. The T2 vertebra was used as a landmark as it is easily identifiable as the largest and most dorsally-protruding vertebra (Johnson & Kida, 1995; Johnson *et al.*, 1999). Without removing any bone (i.e. without performing a laminectomy), the spine was placed in a position of light flexion, and the dura between segments T2→T3 and T3→T4 was gently removed to expose the spinal cord. Bilateral injections were made between each of the pairs of segments, aimed for the intermediolateral cell column (ML: ±0.6mm, DV: −1.0mm). Relatively large injection volumes were used (100nL per injection; 400nL total) to ensure substantial dorsal/caudal diffusion of the tracer into the pre-ganglionic sympathetic neurons of the IML along the spinal column, meaning that in most cases the injections were not *specific* to the IML. However, given that the IML is the primary spinal cord site both receiving inputs from RCA neurons and providing input to post-ganglionic sympathetic neurons innervating brown fat (Ribeiro-Barbosa *et al.*,

1999; Cano *et al.*, 2003), this strategy maintains accurate tracing specifically of IML-projecting RCA neurons that also project to brown fat.

Retrobead-injected animals were allowed to recover for at least 3 days following surgery before they were then injected with PRV-152 into the interscapular BAT as outlined above. BAT-projecting neurons that relayed through the injected brain/spinal cord region were identifiable by their colocalization of both eGFP and red Retrobeads (PRV^+Rb^+).

Upon preparation of hypothalamic coronal sections, brains slices were examined extensively for accuracy of stereotaxic hypothalamic Retrobead injections. Recordings were made from PRV^+Rb^+ neurons exclusively from rats that fulfilled the following criteria: a) Retrobead injections fully or partially saturated the targeted nucleus, and; b) that there was no spill-over of injectate into other hypothalamic sites (i.e. medial, lateral or ventral extra-nuclear spread). Note that Retrobeads deposited along the pipette tract (i.e. dorsal to injection site) was considered acceptable given that there are no pre-autonomic sites dorsal to the hypothalamus that could relay PRV transport to the ARC. We did not specifically examine the spinal cords of all IML-injected rats. PRV injected into interscapular BAT is known to exclusively travel through pre-ganglionic sympathetic neurons in the IML to the hypothalamus (Oldfield *et al.*, 2002; Cano *et al.*, 2003), and therefore the presence of PRV^+Rb^+ neurons in these rats confirms accuracy of injection by default.

3.2.6 Immunohistochemistry and microscopy

For processing biocytin-filled cells, brain slices were immediately fixed in 4% paraformaldehyde (PFA)-phosphate buffer (PB) for 2-16 hours, and then stored in PBS with 0.01% sodium azide until immunohistochemical processing was performed (in batches). Slices were washed in PB, then blocked in 10% normal horse serum (NHS) in 0.03% Triton PB (PBT) for 30 minutes. Sections were transferred to 1% NHS-PBT overnight containing primary antiserum at room temperature (rabbit anti-POMC, Phoenix Peptides H-029-30, 1:3000; chicken anti-GFP, Abcam ab13970, 1:3000). The next day, sections were washed in 1%NHS-PB, then incubated at room temperature for 2 hours in secondary antibody (Donkey anti-rabbit Alexa 647 (Abcam), Goat anti-chicken Alexa 488 (Abcam), streptavidin-Alexa 405 (Molecular Probes), all 1:500). Following washes in PB, slices were then mounted onto glass slides and coverslipped with Dako fluorescent mounting medium.

Imaging was conducted using a Leica SP5 5-channel or Zeiss LSM780 FCS confocal microscope (×20 or x40 objective magnification) running LAS AF or Zen 2010 software, respectively. Z-stacked images (~2µm slices) were captured and a max intensity image was generated. Biocytin (Alexa 405), PRV/eGFP (Alexa 488), Red Retrobeads (where applicable) and POMC (Alexa 647) fluorophores were excited by 405nm, 488nm, 561nm and 633nm laser lines, respectively. POMC peptide expression was determined by colocalisation of biocytin (Alexa 405) with POMC immunostaining (Alexa 647)

3.2.7 Drugs

Drugs used to confirm the identity of sub-threshold active conductances and responsiveness to melanocortin agonists were made up as concentrated stocks prior to experiments and diluted in recording aCSF just prior to use. Cs^{2+} (as $CsCl_2$; used at 0.5-5mM), Ni^{2+} (as $NiCl_2$; 0.5-1mM), Ba^{2+} (as $BaCl_2$; 100μM), tetrodotoxin (TTX; as TTX citrate; 1mM) and Melanotan II (MTII; Bachem, H-3902; 500nM) were dissolved in distilled water and stored at either 4°C ($CsCl_2$, $NiCl_2$, $BaCl_2$) or −20°C (TTX, MTII). The application of drugs, or alterations in glucose concentration, was achieved through gravity-driven perfusion from 50mL syringes arranged in series with the main perfusion line.

3.2.8 Statistical analyses

Data was graphed and statistically analysed using GraphPad Prism 8.0 (Graphpad Software; CA, USA); significance for all tests was set at $p<0.05$. Grouped data is presented as mean ± SEM unless otherwise indicated. Individual data points are also presented in most grouped data sets. One-way ANOVA and Holm-Sidak's multiple comparisons was used to compare changes in resting membrane potential and action potential frequency between ARC PRV-/Retrobead-expressing neurons, while unpaired *t* test was used to compare these for RCA neurons. One-way ANOVA was used to compare changes in electrophysiological parameters between POMC-expressing neurons of the ARC and RCA. Chi-squared Test for Independence was used to determine the association of POMC expression with glucose-responsiveness in the ARC. Paired *t* tests were used to compare the membrane potentials of PVN and LHA neurons before and after exposure to Melanotan II.

3.3 Results

3.3.1 PRV-infected neurons are viable for electrophysiological recording

PRV-152 is an attenuated retrograde, transsynaptic tracer that is regularly used to trace the central regulators of sympathetic nerve activity to brown fat (Bamshad *et al.*, 1999; Oldfield *et al.*, 2002; Cano *et al.*, 2003). In line with former reports, injection of PRV-152 into the interscapular BAT yields time-dependent labelling of upstream neurons that typically equates to the number of synapses traversed (**Figure 3.1A**). At 72 hours post-inoculation, PRV infection was restricted primarily to spinally-projecting (third-order) hypothalamic nuclei. Classical pre-autonomic regions like the dorsal and ventral parvicellular divisions of the PVN and caudal aspects of the LHA (including the perifornical area) demonstrated moderate numbers of PRV-infected (PRV^+) neurons (**Figures 3.1B$_1$ and B$_2$**). Furthermore, PRV^+ cells were scattered throughout the RCA, including the area ventral to the third ventricle that is immediately rostral to the median eminence (**Figure 3.1B$_3$**), and in some cases lateral to the anterior ARC (not shown). At this survival time, small numbers of cells were labelled in the dorsal hypothalamic area, which is the dorsal region of the dorsomedial hypothalamus (DMH). Delaying brain collection until ~96 hours post-injection revealed greater labelling in all these nuclei, particularly in the DMH (**Figure 3.1B$_4$**), corresponding with the labelling of fourth-order neurons. PRV labelling in the ARC presented only in rats culled at this longer survival time, indicative of an exclusive fourth-order projection to brown fat from this nucleus (**Figure 3.1B$_5$**).

To verify that neurons infected with PRV-152 remain viable for electrophysiological recordings, we prepared acute *ex vivo* hypothalamic brain slices from rats injected with PRV (72-96 hours prior), and performed whole-cell patch-clamp recordings from PRV^+ neurons throughout the hypothalamus (**Figure 3.1C**). Consistent with previous accounts of undisturbed electrophysiological properties, the resting membrane potentials (RMP) and spontaneous action potential (AP) frequencies of PRV-infected neurons from the PVN (n = 30), LHA (n = 22), RCA (n = 41) and ARC (n = 112) were similar to those reported for uninfected neurons of the same region (Stern, 2001; Li *et al.*, 2002; van den Pol *et al.*, 2004; van den Top *et al.*, 2004; Williams *et al.*, 2010) (see **Table 3.1**). PRV-infected cells also displayed the expected variety of spontaneous electrical events including tonic or burst-firing patterns of activity, or electrical quiescence (**Figure 3.1D**), and synaptic input from upstream neurons remained functional as indicated by the presence of fast excitatory and inhibitory post-synaptic potentials (**Figure 3.1E**).

Injection of transient current-steps into BAT-projecting cells revealed a number of sub-threshold active conductances that were expressed in varying proportions between hypothalamic nuclei. Cyclic nucleotide-gated hyperpolarisation-activated non-selective cation currents, also known as H-currents (I_H), were revealed in the majority of cells in each nucleus (see **Table 3.2**). This current is rapidly activated by hyperpolarisation, leading to a “sag” depolarisation soon after the onset of the negative current step (**Figure 3.1F**). Application of Cs^{2+}, an I_H channel blocker, was used to confirm the identity of the conductance through abolition of the characteristic “sag” (n = 3). The T-type calcium current (I_T) is a conductance activated in response to a depolarising stimulus following hyperpolarisation-induced de-inactivation that was also expressed to a varying degree in PRV-infected cells (**Table 3.2**). We confirmed the expression of Ni^{2+}-sensitive I_T conductance in PRV-expressing neurons by holding the cell close to −80mV, then injecting positive current steps into the cell (n = 3, in the presence of TTX)

(**Figure 3.1G**). The I_T current also often presented as a rebound depolarisation following a hyperpolarising step from resting membrane potentials (not shown). It is likely that the I_H and/or I_T conductances are involved in the generation of burst firing and pacemaker-like patterns of electrical activity (see **Figure 3.1D**), which indicates a functional importance with regards to downstream communication and release of neurotransmitter. Instantaneous inwardly-rectifying potassium currents (K_{IR}) were expressed in a subset of PRV-infected cells across the hypothalamus (**Table 3.2**). This conductance was identified by the instantaneous reduction in neuronal input resistance associated with membrane hyperpolarisation, and confirmed by application of the K_{IR} blocker Ba^{2+} (n = 3) which prevented the attenuation of membrane response to large amplitude hyperpolarising current steps (**Figure 3.1H**).

	Paraventricular Nucleus (n = 30)	Lateral Hypothalamus (n = 22)	Retrochiasmatic Area (n = 41)	Arcuate Nucleus (n = 112)
RMP (mV)	−48.4 ± 5.4	−53.4 ± 10.5	−53.0 ± 7.6	−50.9 ± 7.6
AP frequency (Hz)	0.42 ± 0.75	0.71 ± 0.96	1.14 ± 1.28	1.10 ± 1.54

Table 3.1 | Electrophysiology parameters of PRV-infected (BAT-projecting) hypothalamic neurons

Resting membrane potential (RMP) and spontaneous action potential (AP) firing frequency of PRV-infected (BAT-projecting) neurons. Data are presented as mean ± standard deviation.

	Paraventricular Nucleus (n = 20)	Lateral Hypothalamus (n = 11)	Retrochiasmatic Area (n = 23)	Arcuate Nucleus (n = 71)
H-current (I_H)	18 (90%)	11 (100%)	15 (65%)	51 (72%)
T-type current (I_T)	8 (40%)	7 (64%)	10 (44%)	49 (69%)
Inward-rectifier (K_{IR})	2 (10%)	0 (0%)	8 (35%)	25 (35%)

Table 3.2 | Sub-threshold active conductance expression in BAT-projecting neurons

The number (% of total) of cells expressing the relevant sub-threshold active conductance per hypothalamic nucleus.

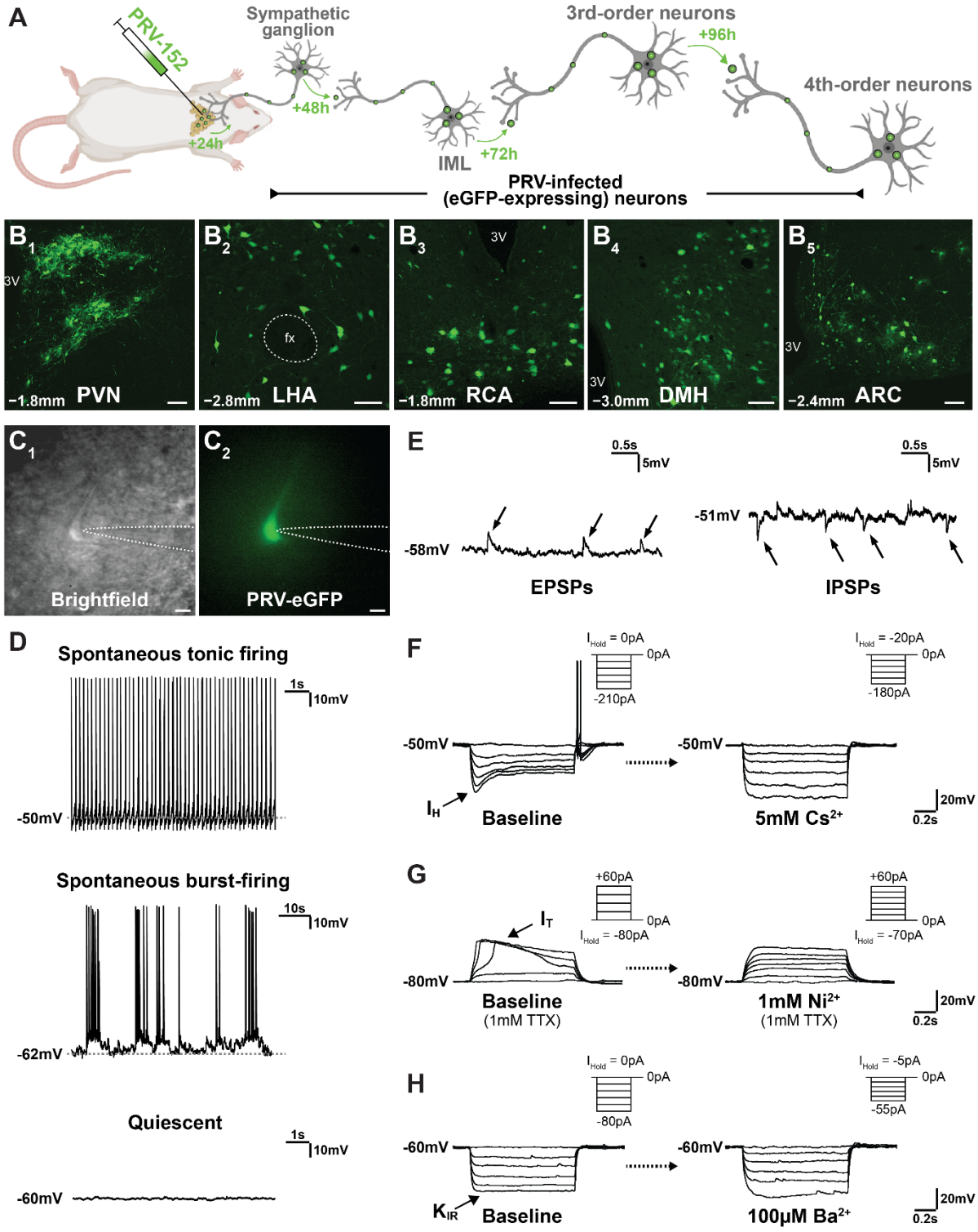

Figure 3.1 | Hypothalamic BAT-projecting neurons defined by PRV-expression remain viable for electrophysiological recording.

(A) Viral-tracing strategy to identify BAT-projecting hypothalamic neurons by injection of retrograde, transsynaptic tracer PRV-152 into interscapular brown fat of Sprague-Dawley rats. Depending on survival time post-inoculation, up to four orders of synaptic connections within the central nervous system may be labelled by eGFP-expressing PRV. **(B_{1-5})** Representative confocal microphotographs showing hypothalamic nuclei labelled by PRV-eGFP approximately 96h following injection into the interscapular brown fat. This includes mixed third- and fourth-order neurons of the PVN (B_1), LHA (B_2), RCA (B_3) and DMH (B_4), and exclusively fourth-order neurons of the ARC (B_5). Rostro-caudal level indicated by distance from bregma in lower left corner. Scale bar, 100µm. 3V, third ventricle; fx, fornix.

(C_1 and C_2) Brightfield (C_1) and eGFP epifluorescence (C_2) images of BAT-projecting (PRV-eGFP infected) ARC neuron during whole-cell patch-clamp recording. Dotted white line is traced around the patch pipette. Scale bar, 20µm. **(D)** Whole-cell current-clamp recordings from different PRV-infected neurons demonstrating a range of spontaneous neuronal activity, consistent with uncompromised electrophysiological features in PRV-infected neurons. **(E)** Whole-cell current-clamp recordings of PRV-infected neurons exhibiting fast excitatory or inhibitory post-synaptic potentials (EPSP/IPSPs), indicative of functional inputs from pre-synaptic neurons. **(F)** Whole-cell current-clamp recording of PRV-infected neuron revealing an H-current (I_H) evoked in response to hyperpolarising current steps (shown superimposed), as indicated by the characteristic "sag" depolarisation shortly after the onset of the current step, as well as rebound discharge following cessation of current injection. This current is blocked by application of the I_H-blocker, Cs^{2+} (5mM). Top right in each set of trace sweeps indicates the magnitude of current injection steps and holding current. **(G)** Whole-cell current-clamp recording of PRV-infected neuron revealing a T-type current (I_T) in response to depolarising current steps (shown superimposed) when held at approximately −80mV. I_T is activated shortly after onset of the second, third and fourth positive steps and becomes inactivated by the end of the current step. I_T is inhibited by the blocker, Ni^{2+} (1mM). The recording was performed in the presence of 1mM TTX to block action potential firing which obfuscates the nature and kinetics of the current. **(H)** Whole-cell current-clamp recording of PRV-infected neuron revealing an instantaneous inwardly rectifying potassium current (K_{IR}) in response to hyperpolarising current steps (shown superimposed) where the magnitude of membrane hyperpolarisation is not linear despite linear changes in negative current injection. K_{IR} is inhibited by the blocker, Ba^{2+} (100µM). In this cell, blockade of K_{IR} with Ba^{2+} revealed the presence of an I_H current also expressed in the cell.

3.3.2 Hypothalamic BAT-projecting neurons sense changes in glucose availability

Having established the feasibility of recording from PRV-infected neurons, we next sought to test our hypothesis that neurons with a defined multi-synaptic projection to brown fat are glucose-sensing. We sampled neurons from all PRV-labelled hypothalamic nuclei except the DMH; guided by those which have previous reports of glucose-sensing capacity. In order to most appropriately reproduce an environment of "meal consumption" in an *ex vivo* context, brain slices were prepared from overnight fasted rats and bathed in a glucose concentration relevant for the nutritional state (1.0mM D-glucose). Current-clamp recordings were made from neurons projecting to brown fat over three (RCA, PVN, LHA) or four (ARC) synapses and their glucose-sensitivity was assessed by bath-application of osmotically-balanced 5.0mM D-glucose-containing aCSF (**Figures 3.2D-G$_1$**). Indeed, a range of responses consistent with glucose-sensitivity were observed in BAT-projecting neurons from all hypothalamic nuclei tested. Neurons that were depolarised with an accompanying increase in action potential firing were considered glucose-excited (GE) neurons (**Figure 3.2A**). Alternatively, neurons exhibiting hyperpolarisation with concomitant reductions in firing rate following the arrival of increased glucose were deemed glucose-inhibited (GI) neurons (**Figure 3.2B**). In most cases, the observed electrophysiological changes were reversible upon washout and return to basal (1.0mM) glucose concentration, substantiating the robust glucose-sensitivity of these cells. Neurons which did not display an enduring change in membrane potential or firing rate were deemed non-responsive (NR) to changes in glucose availability (**Figure 3.2C**).

We found that glucose-sensing was heterogeneously distributed both between and within each hypothalamic nucleus (**Figures 3.2D-G$_2$**). In the present study, sampling of PRV$^+$ neurons of the ARC and the adjacent RCA was prioritised in consideration of the established role of the melanocortin neurons in these regions to sense extracellular glucose as well as regulate BAT thermogenesis (Claret *et al.*, 2007; Krashes *et al.*, 2016; Fenselau *et al.*, 2017). Of the neurons in the ARC treated with 5.0mM glucose, 41% (*n* = 18 of 44) were excited with an average membrane potential change of +5.1 ± 0.6mV from an RMP of −49.5 ± 1.2mV, resulting in an increased firing rate (∆+0.53 ± 0.14Hz). 23% of neurons (*n* = 10 of 44) were hyperpolarised (∆−6.5 ± 1.1mV, RMP = −47.7 ± 0.8mV) and reduced action potential discharge by −0.52 ± 0.15Hz, while the remaining cells did not respond (**Figures 3.2D$_2$ and D$_3$**). Similarly, neurons of the RCA were predominantly glucose-excited (*n* = 9 of 19, 47%), exhibiting depolarisations of +7.5 ± 1.2mV from a baseline RMP of −50.7 ± 1.9mV, also corresponding to increased firing rate (∆+0.73 ± 0.23Hz). Considering its topographical vicinity to the ARC, neurons in the RCA were substantially less likely to be inhibited by glucose (11%, *n* = 2 of 19), and the remaining 42% (*n* = 8 of 19) of neurons were insensitive to changes in glucose (**Figures 3.2E$_2$ and E$_3$**).

In contrast to cells in the mediobasal hypothalamus (MBH), PVN neurons were predominantly glucose-inhibited (*n* = 9 of 20, 45%), exhibiting hyperpolarisations of −7.8 ± 2.0mV from a RMP of −54.9 ± 1.9mV, resulting in a −0.16 ± 0.11Hz reduction in firing rate. Only 10% (*n* = 2 of 20) of PVN neurons demonstrated glucose-induced excitations, indicating that most neurons of the PVN were either inhibited or not responsive to changes in glucose (*n* = 9 of 20, 45%) (**Figures 3.2F$_2$ and F$_3$**). Similarly, BAT-projecting neurons in the LHA exhibited primarily glucose-induced inhibitions (*n* = 7 of 12, 58%) marked by relatively large amplitude hyperpolarisations of −16.7 ± 2.6mV from a resting membrane

potential of −49.7 ± 2.6mV (**Figures 3.2G$_2$ and G$_3$**). Notably, while hyperpolarisation begun shortly after the arrival of high glucose (<2 minutes), the responses consistently did not reverse upon washout to basal glucose concentration (up to 20 minutes of washing). Moreover, while all glucose-inhibited LHA cells were completely silenced by glucose, LHA neurons discharged few spontaneous action potentials at basal glucose levels and therefore the absolute reduction in firing frequency was relatively small (∆−0.06 ± 0.02Hz). The remaining LHA neurons sampled were non-responsive to elevated glucose (*n* = 5 of 12, 42%), with no evidence of any glucose-excited BAT-projecting cells. These findings suggest that subpopulations of neurons with a defined polysynaptic projection to brown fat are capable of glucose-sensing in all hypothalamic nuclei probed, and that the response types within each nucleus are to some extent heterogeneous.

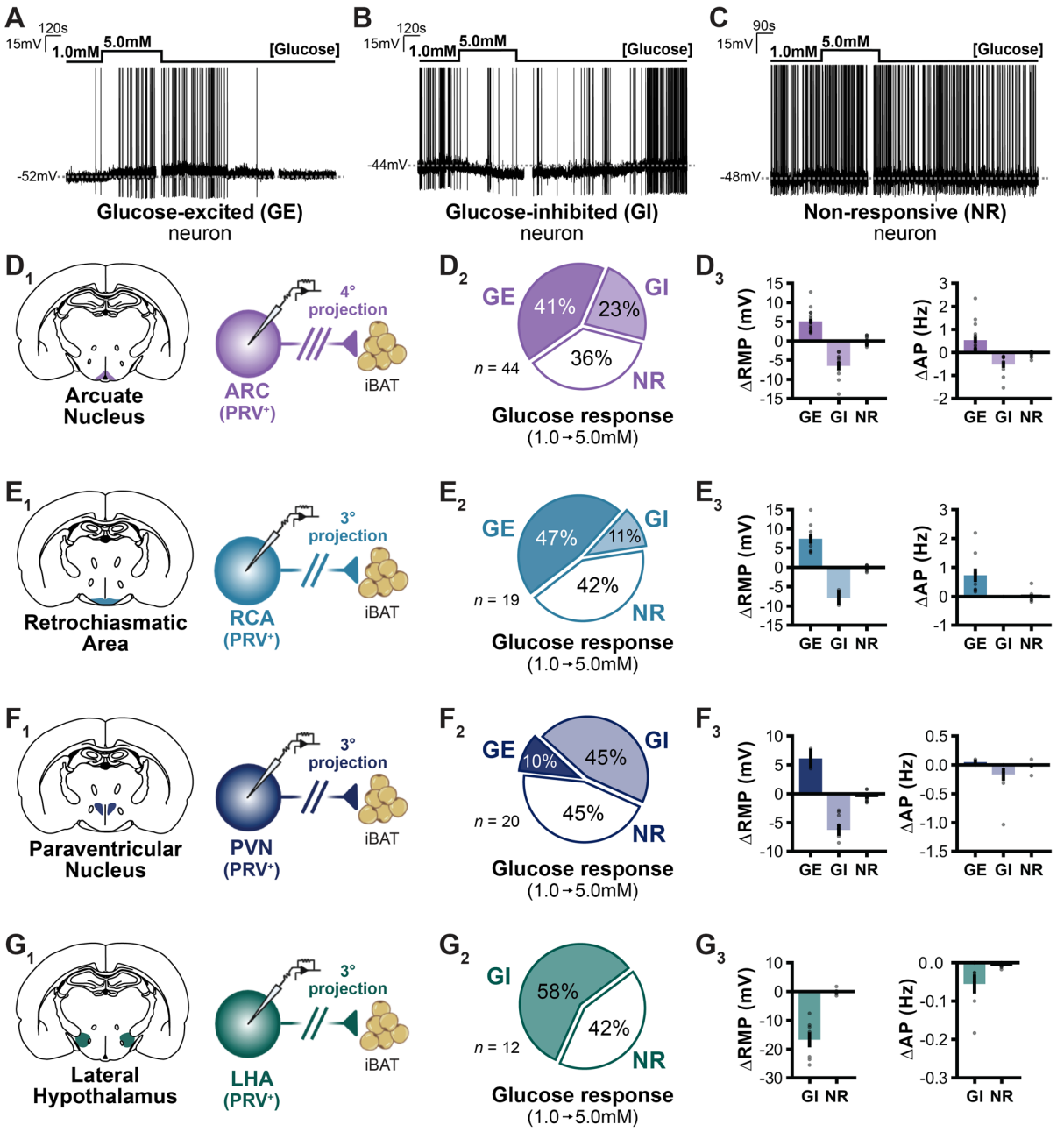

Figure 3.2 | BAT-projecting neurons of the hypothalamus respond to *ex vivo* elevations in CSF glucose

(A-C) Representative whole-cell current-clamp recordings from BAT-projecting neurons in the hypothalamus that were either excited (A), inhibited (B) or not responsive (C) to elevations in extracellular glucose. Note that in responsive neurons, changes in membrane potential and firing rate were time-locked to arrival of 5.0mM glucose to the slice, and in the demonstrated cases were reversible upon washout to baseline glucose levels. **(D_{1-3})** Diagram of recording strategy from ARC neurons fourth-order in their projection to BAT (PRV^+) (D_1). The proportion of the glucose-response types in ARC neurons following increase of extracellular glucose from 1.0 to 5.0mM (D_2) with the corresponding changes in RMP and AP firing rate (D_3). **(E_{1-3})** Diagram of recording strategy from RCA neurons fourth-order in their projection to BAT (PRV^+) (E_1). The proportion of the glucose-response types in RCA neurons following increase of extracellular glucose from 1.0 to 5.0mM (E_2) with the corresponding changes in RMP and AP firing rate (E_3). **(F_{1-3})** Diagram of recording strategy from PVN neurons fourth-order in their projection to BAT (PRV^+) (F_1). The proportion of the glucose-response types in PVN neurons following increase of extracellular glucose from 1.0 to 5.0mM (F_2) with the corresponding changes in RMP and AP firing rate (F_3). **(G_{1-3})** Diagram of recording strategy from LHA

neurons fourth-order in their projection to BAT (PRV^+) (G_1). The proportion of the glucose-response types in LHA neurons following increase of extracellular glucose from 1.0 to 5.0mM (G_2) with the corresponding changes in RMP and AP firing rate (G_3).

Note that breaks in recording (<2 minutes) are indicated by a gap in the trace and are a result of breaking recording to determine current-voltage relationships. Data are represented as mean ± SEM and individual values are labelled by grey circles.

3.3.3 Mediobasal hypothalamus glucose-sensors project to brown fat via multiple relays

Function-specific circuitry has been identified for a number of neuronal populations in the brain, including AgRP neurons in the arcuate nucleus (Betley *et al.*, 2013; Steculorum *et al.*, 2016). We therefore sought to investigate whether the glucose-responsiveness of neurons of the ARC and RCA projecting to brown fat is circuit-specific. To address this question, we implemented a modified tracing strategy: rats first received a bilateral injection of red Retrobeads (Rb) into either the PVN, LHA or DMH in the hypothalamus, or into the IML of the spinal cord. The former regions were anticipated to be relays for fourth order arcuate nucleus neurons, and the latter to be the site downstream of third-order retrochiasmatic area neurons. The interscapular brown fat was then injected with eGFP-expressing PRV-152 as previously described, permitting the multiplexing of retrograde tracers (**Figures 3.3A and B$_1$**). 96-hours following PRV injection into animals that received Retrobead injections into a hypothalamic nucleus, there were substantial numbers of PRV$^+$Rb$^+$ neurons in the arcuate nucleus (**Figure 3.3B$_2$**), but only sparse double-labelling of neurons in the retrochiasmatic area, confirming these downstream sites relay projections to BAT primarily from fourth-order neurons in the ARC. IML-injected animals were sacrificed ~72 hours following inoculation with PRV, revealing considerable numbers of PRV$^+$Rb$^+$ neurons in the RCA (not shown), as well as in other pre-autonomic cells of the PVN and RCA (not shown), but there was complete absence of either retrograde tracer in the ARC, consistent with reports that few (if any) ARC neurons are spinally-projecting (Swanson & Kuypers, 1980a; Cechetto & Saper, 1988). In the present study, recordings were performed specifically from fourth-order ARC and third-order RCA PRV$^+$Rb$^+$ neurons, and the glucose-sensitivity of these neurons, identified on the basis of their monosynaptic trajectory, was determined (**Figures 3.3C-F$_1$**).

Remarkably, we found that there was no overt difference in the glucose-sensitivity of ARC neurons with regard to their axonal trajectory. ARC neurons with diverging trajectories to brown fat through the PVN, LHA or DMH exhibited comparable glucose-induced excitations, in 42% (*n* = 8 of 19), 43% (*n* = 6 of 14) and 40% (*n* = 4 of 10) of cases, respectively (**Figures 3.3C-E$_2$**). Importantly, this proportion of neurons activated by glucose recapitulates those from the original population of ARC PRV$^+$ (only) neurons (41%, see **Figure 3.2D$_2$**). The magnitudes of the glucose-induced depolarisations did not differ between ARC neurons with a defined projection nor to the original PRV$^+$ only population (PVN: Δ+5.6 ± 0.7mV, LHA: Δ+7.3 ± 1.8mV, DMH: Δ+6.2 ± 1.7mV, PRV$^+$ only: Δ+5.1 ± 0.6mV; *p*=0.4803) (**Figure 3.3G**). However, glucose-induced increases in firing frequency were found to differ between ARC subpopulations (*p*=0.0433), with post-hoc statistical analyses revealing LHA-projecting ARC neurons had significantly greater increases in firing rate than ARC PRV$^+$ neurons (*p*=0.0429). In addition, the proportion of neurons that were inhibited by glucose was also comparable between neurons projecting to the PVN (11%), LHA (7%) or DMH (10%), but these were relatively fewer proportion-wise than ARC PRV$^+$ (only) neurons (23%).

In a similar way, the glucose-sensitivity of IML-projecting RCA neurons was remarkably similar to RCA PRV$^+$ (only) neurons, with the majority of cells exhibiting glucose-induced depolarisations (Δ+5.7 ± 0.7mV, *n* = 8 of 18, 44%) but only a small proportion of glucose-induced inhibitions (12%) (**Figures 3.3F$_2$ and F$_3$**). The magnitude of membrane potential and firing changes also did not differ

between RCA cells with and without a defined trajectory to BAT via the IML (RMP, p=0.2574; AP, p=0.1070) (**Figure 3.3H**). These findings suggest that there is no dedicated circuit through which ARC or RCA glucose-sensing neurons project through *en route* to brown fat.

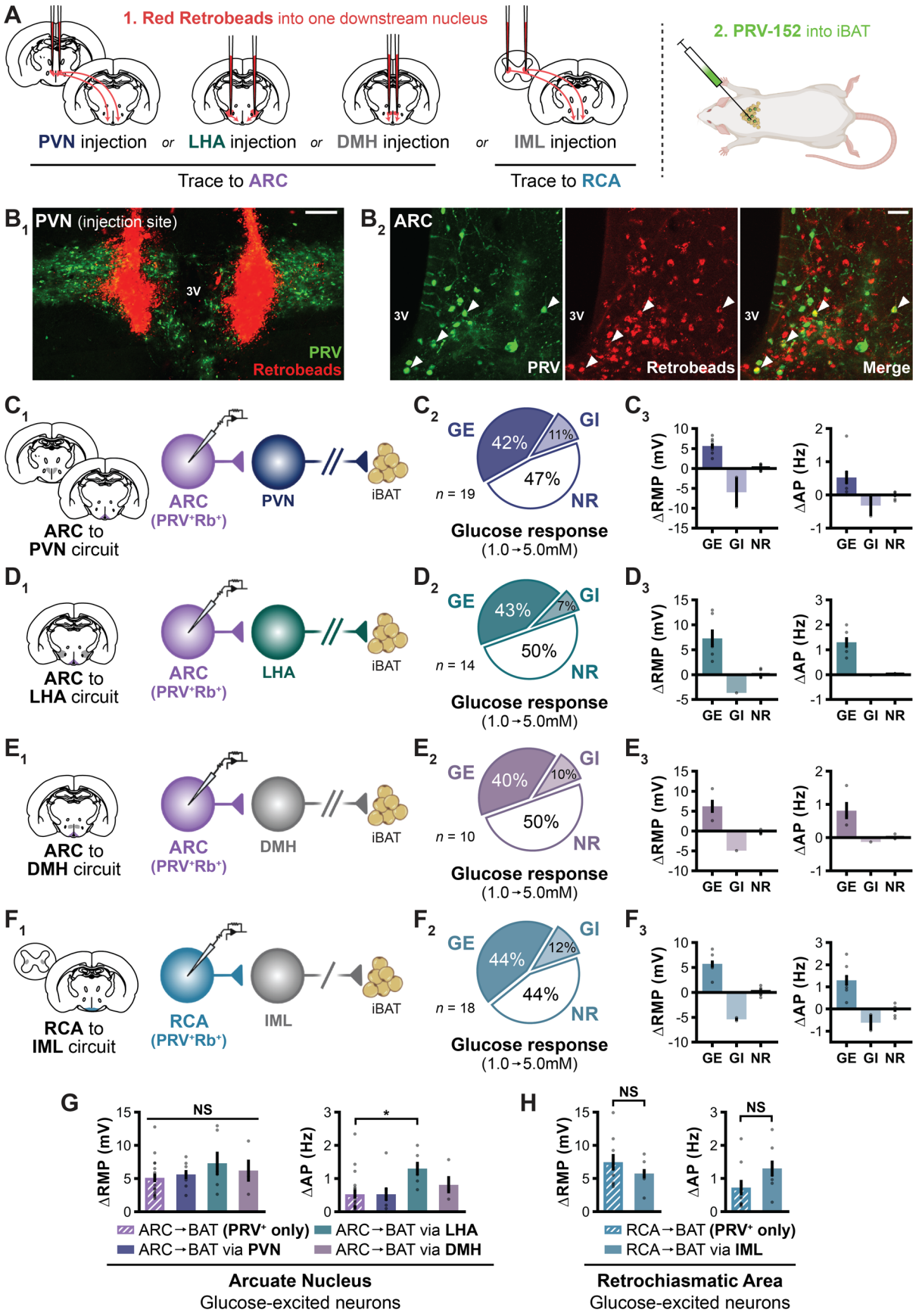

Figure 3.3 | Investigating relevance of axonal trajectory in defining glucose-sensitivity in BAT-projecting neurons

(A) Dual tracer strategy to identify neurons with a defined projection to brown fat with an established relay through a downstream projection region. To trace monosynaptic projections from the arcuate

nucleus, Red Retrobeads were injected bilaterally into third-order neurons in the PVN, LHA or DMH. To trace monosynaptic projections from third-order retrochiasmatic area neurons, Red Retrobeads were injected bilaterally into the IML of the spinal cord. The interscapular brown fat was injected with the transsynaptic retrograde tracer, PRV-152 (eGFP-expressing), which labels synaptically connected neurons that project to brown adipose tissue. **(B_1 and B_2)** Representative confocal microphotographs of a typical bilateral injection site of red Retrobeads into the PVN amongst PRV-labelled (BAT-projecting cells) (B_1), which are both transported to label PVN-projecting neurons of the ARC which also project to brown fat (white arrows). Scale bars: B_1, 200μm; B_2, 50μm. 3V, third ventricle. **(C_{1-3})** Diagram of recording strategy from ARC neurons that project multi-synaptically to brown fat via the PVN (PRV^+Rb^+) (C_1). The proportion of the glucose-response types in PVN-projecting ARC neurons following increase of extracellular glucose from 1.0 to 5.0mM (C_2) with the corresponding changes in RMP and AP firing rate (C_3). **(D_{1-3})** Diagram of recording strategy from ARC neurons that project multi-synaptically to brown fat via the LHA (PRV^+Rb^+) (D_1). The proportion of the glucose-response types in LHA-projecting ARC neurons following increase of extracellular glucose from 1.0 to 5.0mM (D_2) with the corresponding changes in RMP and AP firing rate (D_3). **(E_{1-3})** Diagram of recording strategy from ARC neurons that project multi-synaptically to brown fat via the DMH (PRV^+Rb^+) (E_1). The proportion of the glucose-response types in DMH-projecting ARC neurons following increase of extracellular glucose from 1.0 to 5.0mM (E_2) with the corresponding changes in RMP and AP firing rate (E_3). **(F_{1-3})** Diagram of recording strategy from RCA neurons that project multi-synaptically to brown fat via the IML (PRV^+Rb^+) (F_1). The proportion of the glucose-response types in IML-projecting RCA neurons following increase of extracellular glucose from 1.0 to 5.0mM (F_2) with the corresponding changes in RMP and AP firing rate (F_3). **(G)** Bar charts comparing the RMP and AP firing rate changes between glucose-excited neurons in the ARC that have a defined monosynaptic trajectory *en route* to brown fat compared to ARC cells recorded in the absence of monosynaptic tracing ("PRV^+ only"). Changes in electrophysiological parameters were analysed by one-way ANOVA followed by Holm-Sidak's multiple comparisons test where appropriate (RMP, n = 36 total cells; $F(3, 32) = 0.8433$, p=0.4803 (NS). AP, n = 36 total cells; $F(3, 32) = 3.035$, p=0.0433. ARC to BAT (PRV+ only) vs ARC to BAT with LHA, *p=0.0429; all other comparisons p>0.05). **(H)** Bar charts comparing the RMP and AP firing rate changes between glucose-excited neurons in the RCA that have a defined monosynaptic trajectory *en route* to brown fat compared to RCA cells recorded in the absence of monosynaptic tracing ("PRV^+ only"). Changes in electrophysiological parameters were analysed by unpaired t test (RMP, n = 17 total cells; t = 1.177, df = 15, p=0.2574; AP, n = 17 total cells; t = 1.715, df = 15, p=0.1070).

Data are represented as mean ± SEM and individual values labelled by grey circles.

3.3.4 POMC neurons project to brown fat and constitute most glucose-excited neurons in the ARC and RCA

Considering that POMC neurons are known to project from the ARC and RCA to brown fat (Oldfield *et al.*, 2002), we sought to test the relative glucose-sensitivity of POMC-expressing and non-POMC neurons sampled here. To this end, a subset of recordings from ARC and RCA neurons were made with biocytin, an inert neural tracer, incorporated into the intracellular patch-solution, and brain slices were processed immunohistochemically for expression of POMC peptide. Confocal microscopy revealed that 59% (*n* = 27 of 46) of biocytin-filled ARC neurons were POMC-expressing (ARC^{POMC+}) (**Figures 3.4A$_1$**). These cells were scattered topographically throughout the ventro-dorsal and medio-lateral portions of the nucleus. Consistent with prior reports (Ibrahim *et al.*, 2003; Parton *et al.*, 2007), a large proportion (48%) of ARC^{POMC+} were excited by increased glucose concentration (*n* = 13 of 27), however we did also observe some indication of glucose-inhibited POMC neurons projecting to brown fat (*n* = 2 of 27, 7%) (**Figure 3.4B$_1$**). The remaining ARC cells that did not colocalise with POMC (ARC^{POMC-}) (*n* = 19 of 46) were also distributed throughout the nucleus, however in most cases were located in the inner ventromedial portion of the arcuate nucleus, consistent with the stereotypical location of AgRP/NPY neurons (**Figure 3.4A$_2$**). In comparison to POMC-expressing cells, ARC^{POMC-} cells were predominantly inhibited by glucose (*n* = 8 of 19, 42%) or were non-responsive (*n* = 9 of 19, 47%), with only a small fraction of cells exhibiting glucose-induced excitations (*n* = 2 of 19, 11%) (**Figure 3.4 B$_2$**). Correspondingly, POMC-expression was associated with glucose-response type in BAT-projecting cells of the arcuate nucleus, where ARC^{POMC+} neurons accounted for 87% of glucose-induced excitations but only 20% of glucose-inhibitions ($\chi^2(2) = 11.04$, p=0.0040) (**Figure 3.4B$_3$**).

Remarkably, all biocytin-filled neurons in the retrochiasmatic area expressed POMC peptide (RCA^{POMC+}, *n* = 19 of 19), indicating a particularly significant POMC projection from the RCA to brown fat. A comparable, if not greater, proportion of RCA^{POMC+} cells were excited (53%) or inhibited (16%) by increased glucose compared to the ARC^{POMC+} population (**Figure 3.4C**). There was no significant difference in membrane potential and firing rate changes between the glucose-excited (One-way ANOVA, RMP: $F(2, 22) = 0.04208$, p=0.9589; AP: $F(2, 22) = 0.7105$, p=0.5023) or glucose-inhibited (RMP: $F(2, 10) = 0.5346$, p=0.6017; AP: $F(2, 10) = 0.07113$, p=0.9318) ARC^{POMC+}, ARC^{POMC-} and RCA^{POMC+} neurons, indicating that neither POMC-expression nor the locality of the neuron impact the magnitude of glucose-induced responses.

Importantly, we also determined POMC-expression in a subset of PRV^+Rb^+ neurons; that is, of those projecting to brown fat from the ARC or RCA with defined axonal trajectories. 50% (*n* = 2 of 4) of PVN-projecting, 75% (*n* = 3 of 4) of LHA-projecting and 100% (*n* = 3 of 3) of DMH-projecting glucose-sensing neurons in the ARC immuno-stained positively for POMC peptide (**Figures 3.4D$_{1-3}$**). All glucose-sensitive IML-projecting neurons (*n* = 6 of 6) in the RCA expressed POMC (**Figures 3.4D$_4$**). While sample sizes were too low to make meaningful comparisons of glucose-response types between the projection sites, the majority of glucose-sensitive POMC neurons projecting to each region were also glucose-excited (67-100% of responses).

In view of the findings that ARC^{POMC+} BAT-projecting neurons are largely glucose-excited and projecting via pre-autonomic hypothalamic sites, we sought to determine whether third-order BAT-

directed neurons of the PVN and LHA are responsive to melanocortin agonism. Indeed, bath application of the MC3/4R agonist, MTII, caused marked inhibition of BAT-projecting neurons both in the PVN (*n* = 4 of 7, 57%) and LHA (*n* = 4 of 6, 67%) (**Figures 3.4E$_1$ and F$_1$**). Interestingly, the hyperpolarising effect of MTII on BAT-projecting PVN neurons (∆−6.0 ± 1.1mV, *p*=0.0107) was reversible upon washout (**Figures 3.4E$_1$ and E$_2$**). In contrast, MTII-induced hyperpolarisation of BAT-projecting LHA neurons (∆−10.3 ± 3.2mV, *p*=0.0480) was not reversible (within ~10 minutes), and in some cases the response did not peak until after drug had already washed-out (**Figures 3.4F$_1$ and F$_2$**). Interestingly, the relative reversibility (or irreversibility) of MTII-induced responses for PVN and LHA neurons mirrors the glucose-induced inhibition responses. Consistent with these observations, all PVN neurons that were responsive to MTII were reversibly hyperpolarised in response to application of 5.0mM glucose, while all LHA neurons responsive to MTII were also irreversibly hyperpolarised by glucose (**Figures 3.4E$_1$ and F$_1$**). Furthermore, MTII-unresponsive neurons in both nuclei also did not respond to glucose (not shown). Together, the responsiveness of PVN and LHA neurons to melanocortin agonism and elevated extracellular glucose was identical (PVN, *n* = 4; LHA, *n* = 3). Indeed, biocytin-filling of BAT-projecting cells responsive to glucose and MTII showed evidence of POMC terminal field-reactivity directly apposed to or ontop of the recorded neuron (PVN, *n* = 2; LHA, *n* = 2) (**Figures 3.4E$_3$ and F$_3$**). These findings suggest a role for glucose-excited ARC^{POMC+} neurons to regulate the activity of downstream BAT-projecting cells in (at least) the PVN and LHA.

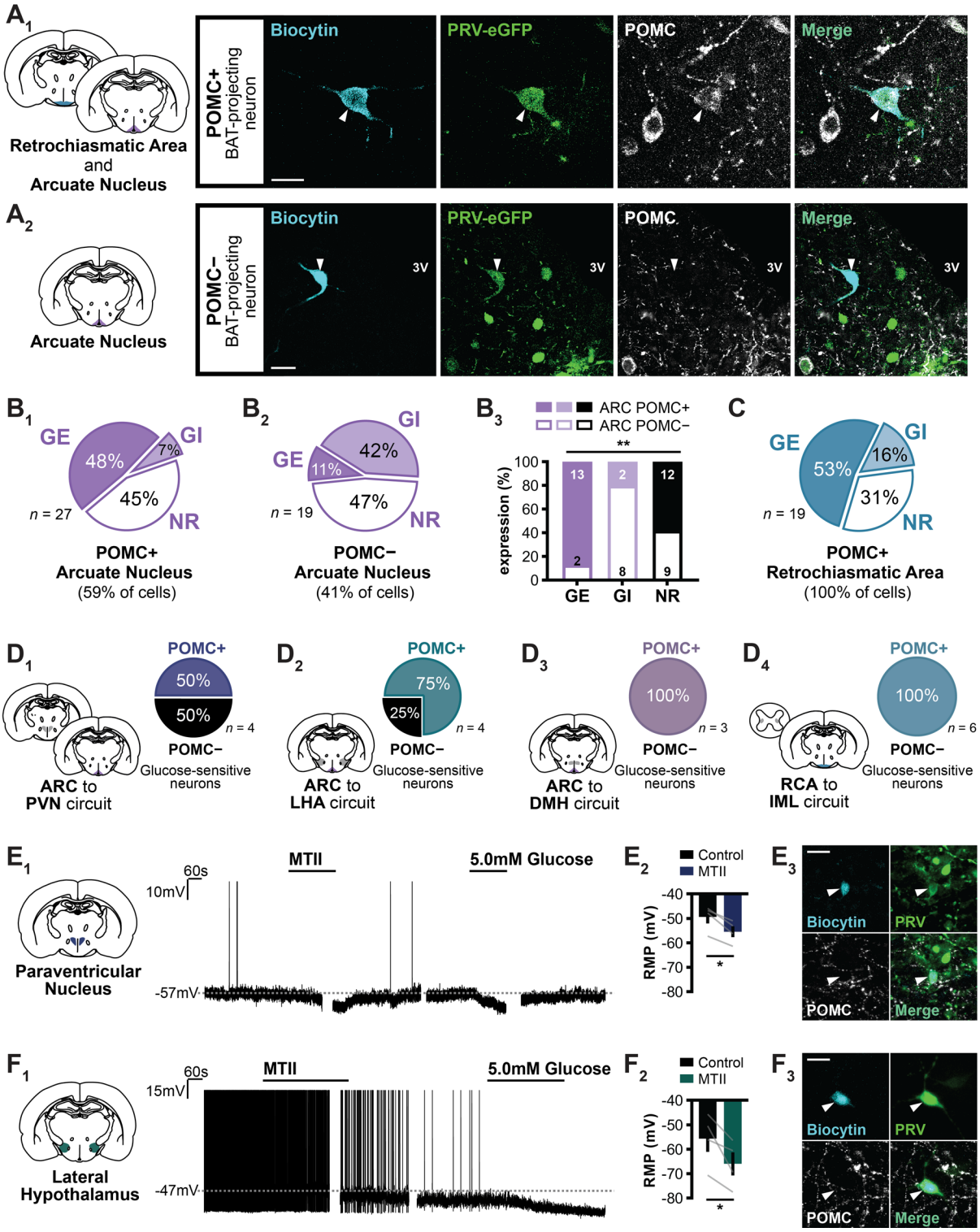

Figure 3.4 | Glucose-sensing POMC neurons in the MBH project to brown fat, and inhibit upstream glucose-inhibited BAT-projecting cells in the PVN and LHA

(A$_1$ and A$_2$) Representative confocal microphotographs of BAT-projecting (PRV-expressing, green) recorded neurons (biocytin filled, cyan) that immuno-stained positively (A$_1$) or negatively (A$_2$) for POMC peptide (grey). POMC+ neurons were found in both the ARC and RCA, while POMC− neurons were found in the ARC only. Scale bars, 20μm. 3V, third ventricle. **(B$_{1-3}$)** Glucose-response distributions of ARC neurons that immuno-stained positively (B$_1$, 59% of recorded cells) or negatively (B$_2$, 41% of recorded cells) for POMC peptide. Contingency plot depicting the proportion of ARC^{POMC+} and ARC^{POMC-} neurons that were found to be GE, GI or NR (B$_3$). The difference in proportions of POMC-expressing cells by glucose-response type was analysed by Chi-squared test of independence (χ^2(2)

= 11.04, ***p*=0.0040). **(C)** Glucose-response distributions of RCA neurons that immuno-stained positively (100% of recorded cells) for POMC peptide. **(D_{1-4})** POMC+ glucose-sensitive neurons project from the ARC and RCA to all downstream regions tested. Pie charts indicating the proportion of POMC+ and POMC− neurons of cells that were responsive (GE or GI) to elevations in extracellular glucose for the ARC to PVN (D_1), ARC to LHA (D_2), ARC to DMH (D_3) and RCA to IML (D_4) circuits with a final trajectory to interscapular BAT. **(E_{1-3})** Whole-cell current-clamp recording from a BAT-projecting PVN neuron testing the responsiveness to the MC3/4R agonist, MTII (500nM), and to increased extracellular D-glucose (E_1). Diagram depicting the membrane potential of PVN BAT-projecting cells before and after application of MTII (E_2). Representative confocal microphotograph of a recorded (biocytin-filled) BAT-projecting (PRV^+) PVN neuron that was inhibited by MTII and glucose application (E_3). POMC-immunoreactive fibres form close appositions with the BAT-projecting PVN neuron. Scale bar, 25μm. MTII-induced change in membrane potential was analysed by paired *t* test (*t* = 5.701, *df* = 3, **p*=0.0107). **(F_{1-3})** Whole-cell current-clamp recording from a BAT-projecting LHA neuron testing the responsiveness to the MC3/4R agonist, MTII (500nM), and to increased extracellular D-glucose (F_1). Diagram depicting the membrane potential of LHA BAT-projecting cells before and after application of MTII (F_2). Representative confocal microphotograph of a recorded (biocytin-filled) BAT-projecting (PRV^+) LHA neuron that was inhibited by MTII and glucose application (F_3). POMC-immunoreactive fibres form close appositions with the BAT-projecting LHA neuron. Scale bar, 25μm. MTII-induced change in membrane potential was analysed by paired *t* test (*t* = 3.237, *df* = 3, **p*=0.0480).

Note that breaks in recording (<2 minutes) are indicated by a gap in the trace and are a result of breaking recording to determine current-voltage relationships. Data are represented as mean ± SEM and individual paired values are labelled by connected grey lines.

3.4 Discussion

We present here the first categorical evidence that elevations in glucose, like those that occur in the postprandial state, are capable of modulating the activity of hypothalamic "command" neurons that regulate sympathetic outflow to brown fat. By combining transsynaptic retrograde tracing and patch-clamp electrophysiology, we investigated the responsiveness of single interscapular BAT-directed neurons to increased glucose availability, where this single nutrient was used as a surrogate for meal consumption. We observed heterogenous glucose-sensing profiles of BAT-directed neurons in each hypothalamic nucleus, including neurons that were either activated or those that were silenced following application of increased glucose, indicative of a system that integrates glucose signals at multiple nodes (nuclei). Furthermore, ARC and RCA glucose-responsive cells project through at least three hypothalamic nuclei and the spinal cord, mounting evidence for redundancy in the glucose-sensing circuitry controlling BAT activity. Importantly, neurochemically-defined POMC neurons constitute the majority of glucose-excited neurons projecting to BAT from the mediobasal hypothalamus. Melanocortin receptor agonism caused hyperpolarisation of BAT-projecting neurons in the PVN and LHA, which were also inhibited by glucose, providing insight into how glucose-excited POMC neurons in the ARC may modulate downstream pre-motor autonomic neuron activity. These findings provide the beginnings of a framework to map the neural circuits in the CNS that collectively regulate sympathetic drive to BAT through a nutrient-sensing mechanism.

3.4.1 Extending the connection between glucose-sensing and brown fat activity

Neurons within hypothalamus were amongst the first indicated to be able to modulate BAT-directed sympathetic outflow in response to both hyperglycaemia or glucopenia over 30 years ago. Administration of glucopenia-inducing substances into the third ventricle or lateral hypothalamus was shown to suppress BAT SNA (Egawa *et al.*, 1989a, b), while injection of glucose (albeit large volumes and concentrations) into the paraventricular or ventromedial nucleus of the hypothalamus induced rapid but transient increases in BAT sympathetic nerve firing rate (Sakaguchi & Bray, 1987, 1988). Little progress has since been made in the way of identifying the exact localisation and neurochemical phenotype of glucose-responsive neuronal population(s) responsible for this effect. Here, we assess the responsiveness of *individual* BAT-directed hypothalamic neurons to elevations in extracellular glucose that are reflective of physiological CSF glucose changes that occur during the transition from the fasted to fed state (Silver & Erecinska, 1994; de Vries *et al.*, 2003; van den Top *et al.*, 2017), hence recapitulating meal-consumption in an *ex vivo* setting.

Our study extends upon previous indications that K_{ATP}-mediated glucose-sensing by catecholaminergic hindbrain neurons contributes to diet-induced thermogenesis in brown fat (Tovar *et al.*, 2013). An important caveat of this study, though, is that K_{ATP} expression appears to be neither necessary nor sufficient to confer neuronal glucose-sensitivity (Levin, 2002; Fioramonti *et al.*, 2004; O'Malley *et al.*, 2006; Melnick *et al.*, 2011), and therefore, at face value, the role of glucose-sensing in brown fat thermogenesis may have been incompletely (or inaccurately) assessed. Here, we overcome

this deficit by assessing, directly, the electrophysiological response to elevated glucose of single neurons with an identified end-point in brown fat through use of the transsynaptic tracer, PRV-152.

A number of published works have employed patch-clamp electrophysiology in conjunction with the virulence-attenuated strain of PRV to trace the central neural regulators of peripheral organ(s). However, we provide the first comprehensive screen of hypothalamic neurons with a defined poly-synaptic projection to brown fat. Importantly, newly-infected neurons exhibited no degradation in membrane or synaptic properties, evidenced by resting membrane potentials and action potential firing rates similar to prior reports from non-infected cells from the same region. The viability of recording from PRV-infected neurons was ensured by carefully timing the arrival of PRV to the sampled hypothalamic nucleus, in accord with previous studies (Smith *et al.*, 2000; Williams & Smith, 2006; Williams *et al.*, 2007; McCarthy *et al.*, 2009). Specifically, most recordings were made ~72-hours post-inoculation for PVN, LHA and RCA neurons, and ~96-hours cells in the ARC, consistent with approximate transport times to these areas (Oldfield *et al.*, 2002; Cano *et al.*, 2003).

The presence of sub-threshold active conductances, including I_H, I_T and K_{IR} in the majority of BAT-projecting neurons is in line with the typical electrophysiological profile of uninfected hypothalamic neurons (Stern, 2001; van den Top *et al.*, 2004; Smith *et al.*, 2007; Jais *et al.*, 2020). In addition to supporting an uncompromised physiological profile, these bioelectrical events serve to code external and intrinsic information to their downstream target(s). The spontaneous burst firing that we observe in BAT-projecting neurons of the mediobasal hypothalamus, not surprisingly, is consistent with the phasic oscillatory events driven by I_T and/or I_H currents in hypothalamic cells (Wagner *et al.*, 2000; van den Top *et al.*, 2004; Chu *et al.*, 2010; Stagkourakis *et al.*, 2016) that favour the release of neuropeptides (Dutton & Dyball, 1979; Bicknell & Leng, 1981; Cazalis *et al.*, 1985). The question then becomes focussed on what is the neurochemical nature of these glucose-responsive neurons, and how do they regulate BAT-directed sympathetic activity?

3.4.2 Rationalising a functional relevance for BAT-directed hypothalamic glucose-sensors

PRV is transported uniquely through synaptically-connected neurons in a retrograde manner (Pickard *et al.*, 2002; Pomeranz *et al.*, 2017). As such, changes in electrical activity are relayed through a chain of neurons (defined here by PRV injection) to ultimately drive *post-ganglionic sympathetic neurons* innervating brown fat. That being said, the post-ganglionic neurons that form the final common outflow to BAT are two to three synapses from the neurons sampled in this study, and therefore represent those that are at or near to the “headwaters” of this pathway. An important consideration, then, is that the output signal is likely to be modified along its route by converging inputs from other regions of the CNS. The simplest schema that could explain the postprandial recruitment of brown fat thermogenesis following the glucose-induced excitation of neurons in the MBH is that this excitation also promotes an increase in the activity of the post-ganglionic neurons innervating BAT. Conversely, glucose-induced inhibitions could relieve sympathoinhibitory tone. The challenge is to incorporate, into a model or overall schema, the heterogeneity that we observed in the glucose-responsiveness of BAT-

projecting neurons both between and within each neurochemically-diverse nucleus. Moreover, it is similarly challenging to assimilate relevant data from other studies where glucose-responsiveness has been evaluated.

3.4.2.1 Paraventricular nucleus

We selected candidate hypothalamic regions to record from on the basis of those previously established to contain glucose-sensitive neurons. The PVN of the hypothalamus is a major pre-autonomic regulatory hub that has foundational links to the control of BAT-directed sympathetic activity (Morrison *et al.*, 2014). Here, we demonstrate that bath-application of elevated glucose induced hyperpolarisation and inhibition of firing in a substantial proportion of BAT-projecting PVN neurons (45%). Congruent with a potential sympathoinhibitory role for these neurons, pharmacological activation of the PVN was shown to rapidly inhibit BAT SNA and thermogenesis (Madden & Morrison, 2009). In a similar vein, the orexigenic peptide NPY, which increases the excitability of PVN neurons by reducing inhibitory input (Cowley *et al.*, 1999; Pronchuk *et al.*, 2002), signals through the PVN to rapidly suppress BAT SNA and thermogenic activity (Egawa *et al.*, 1991; Shi *et al.*, 2013). Therefore, sympathoinhibitory PVN neurons may represent the observed glucose-inhibited neurons in this study, and thus provide a basis for the disinhibition of sympathetic outflow to BAT during the postprandial state.

That being said, in line with exceptionally high neuronal diversity within the nucleus, we also observed the presence of a smaller number of glucose-excited PVN neurons projecting to BAT (10%). This is consistent with reports of the presence of both glucose-induced excitations and inhibitions amongst putative pre-autonomic neurons in the PVN (Melnick *et al.*, 2011). It is possible, or even likely, that the pharmacological study by Madden and Morrison (2009) mentioned above simply demonstrates a more dominant, but not exclusive, sympathoinhibitory role for the nucleus. Perhaps the division in glucose-responsiveness is attributable to distinct subpopulations of neurons which have opposing effects on BAT sympathetic output. Indeed, chemogenetic activation of PVN oxytocin-expressing neurons or agonism of central oxytocin receptors resulted in increased energy expenditure and BAT temperature (Sutton *et al.*, 2014; Roberts *et al.*, 2017). Previous studies indicate that 10-15% of PVN neurons labelled with PRV transported from brown fat colocalise with oxytocin (Oldfield *et al.*, 2002), a number which is consistent with the observed proportion of glucose-excited PVN neurons projecting to BAT; providing weight for the possibility that oxytocinergic neurons represent the small group of glucose-excited BAT-directed neurons in our study.

3.4.2.2 Lateral hypothalamus

The LHA is a highly interconnected brain region that regulates both cognitive and peripheral physiological processes, including regulation of the sympathetic nervous system (Ferguson & Samson, 2003). Neurochemical characterisation of BAT-projecting LHA neurons indicated that substantial proportions (up to 30-50%) express the neuropeptides orexin or melanin-concentrating hormone (MCH) (Oldfield *et al.*, 2002), both of which are established glucose-responsive populations (Burdakov *et al.*, 2005). In our sample, 58% (n = 7 of 12) of BAT-directed LHA neurons exhibited large magnitude

hyperpolarisations in response to application of elevated glucose, with no evidence of any glucose-activated cells. Considering reports that 70-80% of MCH neurons are glucose-excited and >95% of orexin neurons are glucose-inhibited (Burdakov *et al.*, 2005; Kong *et al.*, 2010), the absence of glucose-excited cells would suggest that either the glucose-*insensitive* MCH neurons are concentrated within the BAT-projecting population, or that by chance there was preferential recording from predominantly orexin-expressing neurons; the latter of which is not improbable in light of the modest sample size. In fact, this explanation seems likely given that following hyperpolarising current injection into cells, all LHA neurons sampled here displayed H-current-mediated depolarisation (i.e. I_H), an electrophysiological signature of orexin neurons that is absent in MCH-expressing cells (Burdakov *et al.*, 2005). Therefore, it is most likely that most or all sampled BAT-projecting LHA neurons are orexin-expressing, and that the discrepancy in the proportion of glucose-sensing orexin neurons compared to published data is attributed either to differences in recording conditions or the species from which tissue was collected (mouse vs. rat).

The role of orexin neurons in the regulation of BAT-directed SNA is not entirely clear. Orexin neurons project to brown fat via the IML or through other pre-motor sites like the raphe pallidus (Oldfield *et al.*, 2002; Llewellyn-Smith *et al.*, 2003; Tupone *et al.*, 2011), and in these regions, orexin appears to act to promote neuronal activity and hence increase BAT-directed sympathetic outflow (Antunes *et al.*, 2001; van den Top *et al.*, 2003; Tupone *et al.*, 2011). However, the thermogenic/sympathetic response to central administration of orexin receptor agonists (or antagonists) does not consistently support a pro-thermogenic role for the peptide (Yoshimichi *et al.*, 2001; Monda *et al.*, 2003; Yasuda *et al.*, 2005; Verty *et al.*, 2010). This may be due to confounding arousal-related effects of orexin signalling that also contribute to heat production. Alternatively, it has been suggested that in a connected network, orexin neurons play more of a modulatory role to promote the “gain” of excitatory inputs (Madden *et al.*, 2012). This is supported by the finding that pharmacological activation of neurons in the LHA/perifornical area, or orexin injection directly into the raphe pallidus, potentiates cold-induced SNA to BAT but has no effect in warmer environments when BAT SNA is quiescent (Tupone *et al.*, 2011). Taking all of these issues together and considering differences in approach (*ex vivo* vs. *in vivo*), species (rat vs. mouse) and context (arousal in free-living rodent experiments), it remains unclear how to rationalise the glucose-induced inhibition of putative orexinergic BAT-projecting neurons demonstrated here in the context of glucose-(meal-) induced thermogenesis in brown fat.

In this vein, it is important to acknowledge, however, that in the absence of an in-tact physiological system or of known neurochemical identities of sampled PVN or LHA cells, the rationalisation of the *in vivo* outcome of observed glucose-induced changes in the activity is purely speculative. Furthermore, even though previous studies have demonstrated that glucose-sensing responses in orexin and pre-autonomic PVN neurons persist in synaptic isolation (Burdakov *et al.*, 2005; Melnick *et al.*, 2011), we cannot categorically exclude the contribution of upstream glucose-responsive neurons to the responses observed here considering our studies were not performed in the presence of synaptic blockers. Indeed, we focussed the majority of our glucose-sensing recordings on fourth-order ARC neurons which we hypothesised, and then demonstrated, project to brown fat through these two nuclei and the DMH (discussed in *Section 3.4.3*), making it more than likely that the observed

responses in such nuclei are influenced by inputs from the ARC which are maintained in the slices examined in this study.

3.4.2.3 Arcuate nucleus & Retrochiasmatic area

The ARC and RCA are the home of the melanocortin system, comprising an arrangement of functionally-opposing interoceptive populations, namely the catabolic POMC and anabolic AgRP/NPY neurons, which have been demonstrated to be excited and inhibited by increased glucose, respectively (Ibrahim *et al.*, 2003; Claret *et al.*, 2007; Fioramonti *et al.*, 2007). In this study, we found that, in contrast to cells in the PVN and LHA (review above), BAT-projecting neurons in the ARC and RCA were predominantly *excited* by elevations in glucose (41% and 47%, respectively). Considering that POMC neurons are known to project to BAT from both of these regions (Oldfield *et al.*, 2002), we hypothesised that the glucose-excited responders comprised at least a subset of BAT-projecting POMC neurons. Immunohistochemical analyses of biocytin-filled cells revealed that 59% or 100% of recovered neurons in the ARC or RCA colocalised with POMC peptide, respectively. While it is possible that *all* RCA BAT-projecting neurons express POMC, it is more likely that our findings are a chance/sampling phenomenon given previous reports of high, but not exclusive, expression of POMC/cocaine- and amphetamine-regulated transcript (CART) in BAT-projecting cells in this region (Oldfield *et al.*, 2002). In accordance with previous reports, POMC-expressing neurons corresponded primarily with glucose-induced excitations in both nuclei, while only a small fraction of residual POMC-negative cells were similarly activated by glucose. This indicates that increased extracellular glucose selectively stimulates POMC neurons projecting to brown fat. Considering that activation of POMC neurons and the downstream MC4R reliably stimulates BAT thermogenesis (Brito *et al.*, 2007; Song *et al.*, 2008; Fenselau *et al.*, 2017), our studies elucidate a candidate role for melanocortinergic neurons to activate BAT SNA following postprandial excursions in glycaemia (discussed further in *Section 3.4.4*).

Finally, it is important to acknowledge that we did also observe a small proportion of glucose-inhibited POMC-expressing neurons projecting to BAT (7% in ARC, 16% in RCA). The physiological function of these neurons is unclear; indeed, they are yet to be reported in the literature (see **Chapter 5** for further discussion). In contrast, glucose-inhibited neurons were concentrated within the ARC^{POMC-} population, accounting for 80% of all glucose-induced inhibitions within immunohistochemically-assessed ARC cells. Whilst we cannot be certain of the neurochemical phenotype of the POMC-negative cells, we speculate that at least some of these neurons include the AgRP/NPY neuronal population. Notably, ARC^{POMC-} neurons were frequently localised within the most ventromedial portion of the nucleus where AgRP/NPY neurons are typically located. It has been shown that chemogenetic activation of AgRP/NPY neurons suppresses BAT SNA and thermogenesis (Steculorum *et al.*, 2016; Burke *et al.*, 2017), which is probably mediated by a combination of MC4R antagonism (AgRP) and activation of hypothalamic and medullary sympathoinhibitory Y1 receptors (NPY) (Verty *et al.*, 2010; Shi *et al.*, 2013; Nakamura *et al.*, 2017). One possibility consistent with these observations, then, is that the glucose-induced silencing of BAT-projecting AgRP/NPY neurons could contribute to postprandial thermogenesis by alleviating sympathoinhibitory tone. However, future studies are required to confirm the glucose-responsiveness of genetically-identified AgRP/NPY neurons projecting to BAT.

3.4.3 An evaluation of function-specific glucose-sensing circuitry projecting to BAT

Advancing technologies that permit the identification and manipulation of genetically-defined neuronal populations have generated much interest in recent years. A part of the evolution of viral and opto-/chemo-genetic technologies includes the facility to dissect the contribution of individual axonal projections to the physiological or behavioural phenotype of population-level manipulation (see review, Haery *et al.* (2019)). Using these strategies, function-specific circuitry has been extensively investigated for AgRP neurons of the hypothalamus, resulting in the elucidation of dedicated projections that control hunger and other metabolic processes (Atasoy *et al.*, 2012; Betley *et al.*, 2013; Stachniak *et al.*, 2014; Fu *et al.*, 2019). Importantly, one such study reported circuit-specific control of autonomic outflow to brown fat. Investigators showed that optogenetic activation of AgRP terminals in the LHA and ventrolateral portion of the anterior bed nucleus of the stria terminalis, but not in other sites of projection, induced insulin resistance in brown fat by inhibition of BAT-directed SNA (Steculorum *et al.*, 2016). In light of these reports, and in consideration of the heterogeneity in glucose-responsiveness of ARC and RCA neurons observed here (even within stratified POMC-positive and negative populations), we hypothesised that different glucose-sensitive subpopulations may project through specific downstream relays *en route* to brown fat.

By combining traditional monosynaptic retrograde tracers with transsynaptic PRV transport from BAT, we confirmed that neurons in the ARC project to brown fat (within four synapses) through the PVN, LHA and DMH but not the IML, while the inverse is predominantly true for neurons in RCA. These findings are in line with expected anatomical connectivity based on transport times for the arrival of PRV in each nucleus (Oldfield *et al.*, 2002; Cano *et al.*, 2003). Additionally, monosynaptic retrograde tracing from the upper thoracic spinal cord, where the pre-ganglionic sympathetic neurons innervating BAT (via sympathetic paravertebral ganglia) are located, reveals transport to the RCA which is consistent with the observed RCA to IML circuit defined here, in addition to transport to the PVN, LHA and dorsal hypothalamic area (dorsal part of DMH), sites through which ARC neurons are known to project (Swanson & Kuypers, 1980a; Cechetto & Saper, 1988; Bouret *et al.*, 2004; Wang *et al.*, 2015).

In spite of a function-specific circuit connecting AgRP neurons to brown fat, we found that glucose-responsiveness of BAT-projecting ARC neurons did not differ based on axonal trajectory. In other words, there were similar proportions of glucose-induced excitations (40-43%) between specified relays, and no difference in the magnitude of membrane depolarisation; barring LHA-projecting cells which, on average, exhibited greater increases in firing rate, which may have some functional relevance. Moreover, while we observed that similar proportions of ARC PRV^+Rb^+ were inhibited by glucose (7-11%), this represented less than half of the percentage of glucose-induced inhibitions observed in PRV^+ (only) neurons in the ARC (23%). It is possible that another neural projection relays a separate, predominantly glucose-inhibited subpopulation of ARC neurons; however, it is unclear what this target would be. We found no IML-projecting neurons in the ARC, consistent with previous reports (Cechetto & Saper, 1988), confirming that ARC neurons must project to brown fat via pre-motor region, but there is no substantial projection from the ARC to the remaining pre-motor sites that innervate BAT, such as the raphe pallidus, RVLM and A5 noradrenergic cell group (Sim & Joseph, 1991; Nogueira *et al.*, 2000; Cano *et al.*, 2003; Yeo & Herbison, 2011). While we cannot categorically exclude the possibility of

another ARC-based circuit, we postulate instead that the discrepancy relates to the intrinsic bias that exists in patch-clamp sampling, leading to selection of cells that were more likely to express POMC in these experiments (based on morphology and topographical distribution). Indeed, the proportion of glucose-inhibited POMC-expressing cells (7%) is similar to $PRV^{+}Rb^{+}$ neurons recorded in the ARC (7-11%).

In consideration of the distinctive nature of spinally-projecting RCA neurons, it is perhaps unsurprising that the glucose-sensing profile of BAT-projecting neurons in the RCA (PRV^{+} only) was wholly recapitulated in RCA cells with a defined trajectory through the IML. This suggests that the predominantly glucose-excited RCA neurons project *at least* directly to the IML, but we cannot discount the possibility for fourth-order RCA glucose-sensing circuits that relay elsewhere in the brain.

3.4.4 Glucose-sensing POMC circuits projecting to brown fat: a discussion of the evidence for functional redundancy

The findings presented in this Chapter support the notion of a demarcated neural circuit that is responsive to meal-related stimuli (glucose), and thus may subserve postprandial thermogenesis in brown fat; however, its interpretation is complicated. We demonstrated the existence of glucose-sensing central regulators of BAT SNA in at least four distinct hypothalamic sites, each with a heterogenous set of membrane responses. The glucose-sensitive neurons observed in the PVN, LHA and RCA all project in parallel to brown fat, while glucose-responsive neurons in the ARC reciprocally regulate downstream glucose-sensors in the PVN and LHA, as well as third-order DMH neurons (whose glucose-sensitivity was not investigated here).

On the basis of the functional, anatomical and interoceptive nature of sensory “first-order” melanocortin neurons, we propose that meal-sensing CNS structures that regulate BAT sympathetic outflow may be orchestrated by hypothalamic POMC neurons. Our circuit-specific studies revealed that glucose-sensing neurons project from the ARC and RCA to brown fat through multiple sites in remarkably similar proportions. Furthermore, we determined retrospectively by immunohistochemistry that POMC neurons constituted at least 50% of the glucose-sensing population relaying through each site, and that the majority of these POMC cells were excited by glucose. Therefore, our study builds a compelling case for redundancy in glucose-activated melanocortin circuitry to regulate the meal-induced activation of BAT SNA. However, it is unclear whether this should translate into functional redundancy; that is, whether each glucose-activated melanocortin circuit could theoretically subserve postprandial thermogenesis. By synthesising the cursory indications of melanocortin-responsiveness in BAT-projecting PVN/LHA neurons described here and findings from past studies, we make tentative propositions regarding the potential glucose-induced thermogenic relevance of each circuit below.

3.4.4.1 ARC^{POMC} → PVN circuit

The hypothalamic PVN is the principal region responsible for the MC4R-regulated effects on appetite (Shah *et al.*, 2014; Garfield *et al.*, 2015), however reports are conflicting on its role in the control of MC4R-mediated energy expenditure. The re-expression of MC4R in Single-minded 1 (Sim1)-

expressing neurons (which comprises most PVN neurons) in *Mc4r* knockout mice almost completely normalises food intake, but only reduces excess body weight by ~60%, attributed in part to persistent hypometabolism in the partial *Mc4r* knockout (Balthasar *et al.*, 2005). This finding suggests that MC4R activity at Sim1-expressing PVN neurons regulates appetite but is dispensable for the regulation of energy expenditure and BAT thermogenesis, which has since been supported by a number of other studies (Kublaoui *et al.*, 2006; Shah *et al.*, 2014). However, in contrast to these reports, intra-PVN microinjection of MTII, the MC3/4R agonist, consistently elevates oxygen consumption and increases BAT sympathetic outflow (Cowley *et al.*, 1999; Song *et al.*, 2008; Monge-Roffarello *et al.*, 2014b).

MC3/4R agonism of MC4R-expressing PVN neurons is reported to cause robust depolarisation and increased action potential firing (Ghamari-Langroudi *et al.*, 2011; Garfield *et al.*, 2015; Ghamari-Langroudi *et al.*, 2015). However, we demonstrate that BAT-projecting neurons in the PVN (and LHA) are hyperpolarised by MTII, suggesting, perhaps, that sampled BAT-projecting neurons represent a population that does not express MC4R, but receive input from MC4R-expressing pre-synaptic neurons. Indeed, recordings from unidentified parvocellular PVN neurons have demonstrated that MC3/4R agonism leads to inhibition by potentiating GABAergic input (Cowley *et al.*, 1999). Additionally, we found that all MTII-responsive neurons were also inhibited by glucose, whereas those that did not respond to MC3/4R agonism were glucose-insensitive. Remarkably, this exact phenomenon was observed during *in vivo* extracellular recordings, employing puff-application of both MTII and 5.0mM glucose which rapidly suppressed firing of neurons in the PVN and LHA (Guan *et al.*, 2017), providing further support for the MTII-induced hyperpolarisation observed here.

Considering that the vast majority of MC4R-expressing PVN neurons do not express the vesicular GABA transporter (Xu *et al.*, 2013), it is likely that pre-synaptic, MC4R-expresing GABAergic neurons are located outside of the PVN. This could also explain why Sim1-specific deletion of *Mc4r* or re-expression in global *Mc4r*-knockout models does not evoke changes in MC4R-regulated energy expenditure. While the evidence for MC4R signalling in the PVN to regulate BAT thermogenesis is clearly conflicting, it remains a possibility that elevations in extracellular glucose promote BAT SNA through hyperpolarisation of *sympathoinhibitory* MC4R-negative PVN neurons by two mechanisms: 1) increased α-MSH release from upstream glucose-excited POMC neurons which acts pre-synaptically on Sim1-negative, MC4R-positive GABAergic neurons to potentiate inhibitory tone, and 2) post-synaptic glucose-induced inhibition of the same BAT-projecting PVN neurons (**Figure 3.5**).

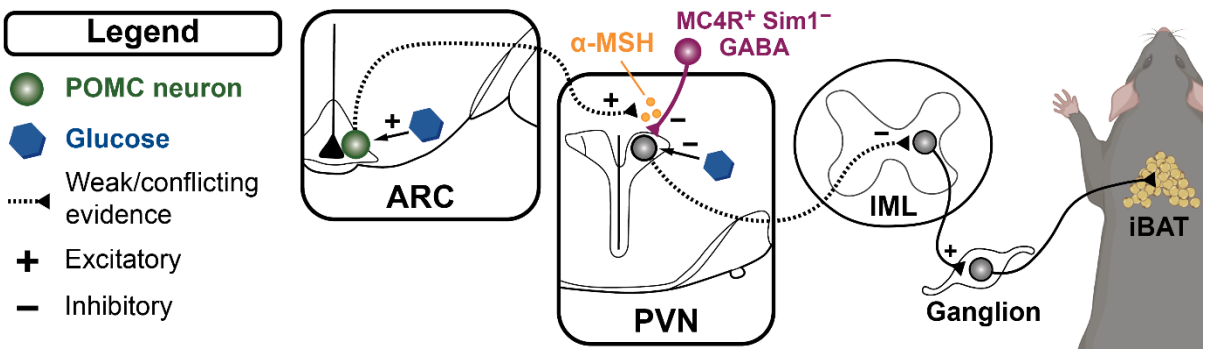

Figure 3.5 | Proposed glucose-regulated effects of ARC^{POMC} → PVN circuit

A tentatively-defined glucose-regulated ARC^{POMC} → PVN circuit that may promote BAT SNA.

3.4.4.2 ARC^{POMC} → LHA circuit

In contrast to the PVN, melanocortin signalling in the LHA is primarily implicated in the control of autonomic tone to BAT but reportedly plays little role in appetite regulation. LHA-specific re-expression of MC4R in Mc4r$^{loxTB/loxTB}$ mice (by stereotaxic virally-mediated delivery of Cre) was shown to have no impact on body weight and food intake, but dramatically improved glucose intolerance which was at least partly due to restoration of BAT-facilitated glucose clearance (Morgan *et al.*, 2015). Indeed, central administration of MTII in these mice rapidly promoted BAT SNA, but had no effect on global *Mc4r* knockouts, indicating the sufficiency of melanocortin signalling in the LHA to promote thermogenesis.

We rationalised in *Section 3.4.2.2* that most if not all LHA neurons sampled here express orexin on the basis of their electrophysiological profile and glucose-responsiveness. Similar to those in the PVN, we found that BAT-projecting neurons in the LHA were inhibited by both MC3/4R agonism and application of high glucose. Remarkably, there are no published reports of membrane responses to MC3/4R agonism in orexin-expressing (or any) LHA neurons, however central infusion of α-MSH downregulates orexin expression (López *et al.*, 2007), suggestive of an inhibitory effect in line with our findings. Considering that few, if any, orexin neurons express the MC4R (Cui *et al.*, 2012; Mickelsen *et al.*, 2017), this would suggest that the observed MTII-induced inhibition of LHA neurons is also mediated pre-synaptically. In support of this model, GABAergic interneurons in the LHA express MC4R and have been shown to densely innervate orexin neurons (Liu *et al.*, 2003a; Ferrari *et al.*, 2018; Pei *et al.*, 2019). On the balance of evidence presented from this and former studies, it appears that elevations in glucose can inhibit BAT-directed putative orexin neurons by: 1) glucose-induced excitation of POMC neurons which increase the activity of pre-synaptic, MC3/4R-expressing GABAergic interneurons, and 2) post-synaptic glucose-induced hyperpolarisation of the same melanocortin-responsive LHA neuron (**Figure 3.6**). However, whether this translates functionally into increased BAT SNA requires further investigation; as it stands in the literature, there are conflicting reports as to whether orexin neurons are sympathoinhibitory or sympathoexcitatory (Verty *et al.*, 2010; Tupone *et al.*, 2011).

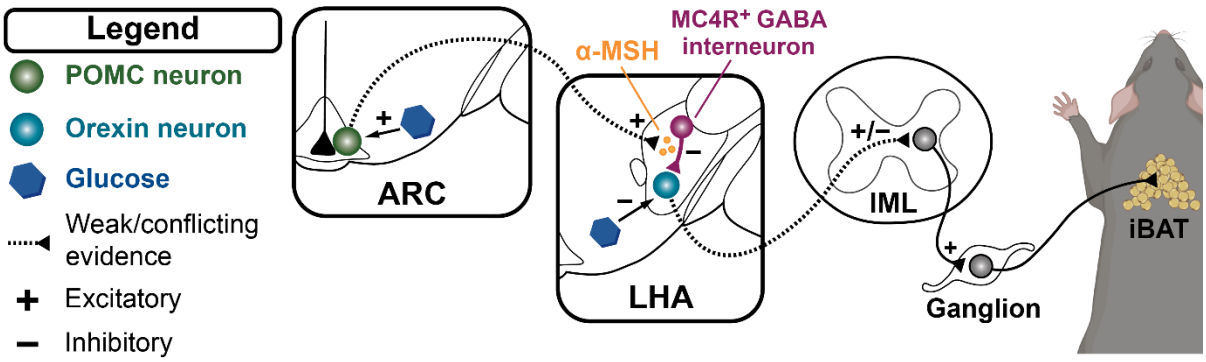

Figure 3.6 | Proposed glucose-regulated effects of ARC^{POMC} → LHA circuit

A tentatively-defined glucose-regulated ARC^{POMC} → LHA circuit involving putative orexin neurons that may promote BAT SNA.

3.4.4.3 ARC^{POMC} → DMH circuit

In this study, we did not record from BAT-projecting neurons in the DMH primarily because there is no evidence (yet) that these neurons are capable of sensing changes in extracellular glucose. Nevertheless, melanocortin activity the DMH is reported to robustly promote energy expenditure through brown fat activity. DMH-specific deficiency of G protein stimulatory alpha subunit ($G_s\alpha$), through which MC4R couples to engage effects on membrane potential and gene transcription (Mountjoy *et al.*, 1994), causes marked obesity that is underscored by both hyperphagia and diminished energy expenditure (Chen *et al.*, 2012; Chen *et al.*, 2017; Chen *et al.*, 2019). Importantly, both DMH-specific $G_s\alpha$ deletion or pharmacological MC3/4R antagonism in the DMH blunts the activation of energy expenditure and BAT thermogenesis following peripheral administration of MTII (Enriori *et al.*, 2011; Chen *et al.*, 2019), confirming the sufficiency of DMH MC4R-activation to promote brown fat thermogenesis. Previous studies show that MTII depolarises MC4R-expressing cells in the DMH (Liu *et al.*, 2003a), however it is not clear whether BAT-projecting DMH neurons, specifically, are excited by MC3/4R agonism (or may actually be inhibited, as we found with PVN neurons). Nevertheless, considering that DMH neurons are considered sympathoexcitatory for BAT SNA (Zaretskaia *et al.*, 2002; Cao *et al.*, 2004), together these reports would suggest that glucose-induced activation of DMH-projecting POMC neurons is a *viable* circuit to contribute to postprandial thermogenesis (**Figure 3.7**).

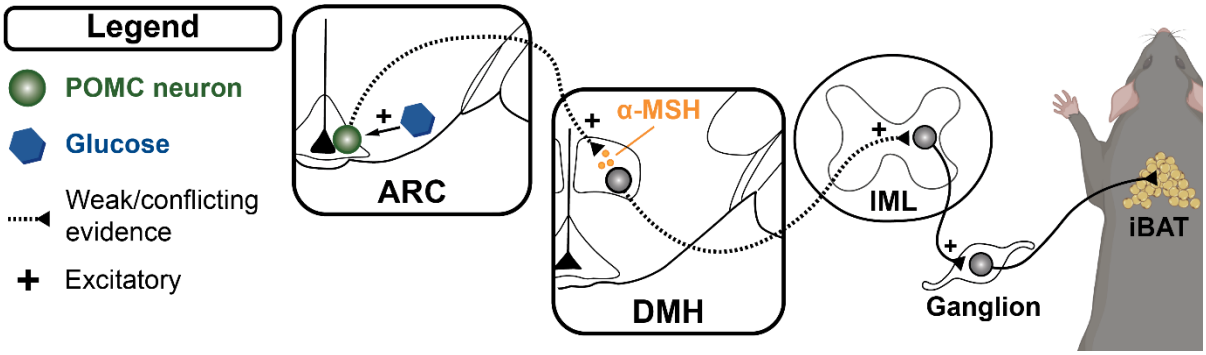

Figure 3.7 | Proposed glucose-regulated effects of ARC^{POMC} → DMH circuit

A tentatively-defined glucose-regulated ARC^{POMC} → DMH circuit that may promote BAT SNA.

3.4.4.4 RCA^{POMC} → IML circuit

Finally, the direct projection of POMC neurons in the RCA to pre-ganglionic sympathetic neurons in the IML is a circuit that has arguably the most definitive link to the regulation of diet-induced thermogenesis, but, unfortunately is largely understudied presumably for its lack of recognition (in comparison to POMC neurons in the ARC). A landmark publication demonstrated that re-expression of MC4R in pre-ganglionic sympathetic (but not parasympathetic) neurons in *Mc4r* mull mice provides modest amelioration of obesity by normalisation of oxygen consumption without affecting the marked hyperphagic phenotype (Rossi *et al.*, 2011), indicating that MC4R-expressing IML neurons specifically regulate energy expenditure and not appetite. Consistent with these findings, deletion of the MC4R specifically in pre-ganglionic sympathetic neurons leads to moderate obesity caused by energy expenditure reduction alone; an effect that is amplified when fed a high-calorie diet (Berglund *et al.*,

2014). These findings suggest that the high-calorie diet-induced thermogenesis, which is absent in global *Mc4r* knockouts (Butler *et al.*, 2001; Albarado *et al.*, 2004), is mediated primarily through increased melanocortin signalling in the spinal cord.

In consideration of these loss-of-function studies, and that intrathecal MTII increases energy expenditure and MC3/4R agonism depolarises and activates cholinergic neurons in the IML (Sohn *et al.*, 2013; Adank *et al.*, 2018), we propose that this circuit most convincingly activates BAT-directed SNA following fluctuations in glucose associated with the postprandial state. This proposal is strengthened by the direct nature of the POMC projection to sympathetic autonomic neurons, which is thus less susceptible to converging neural inputs that may otherwise attenuate the sympathoexcitatory output resulting from glucose-induced excitation of IML-projecting POMC neurons (**Figure 3.8**).

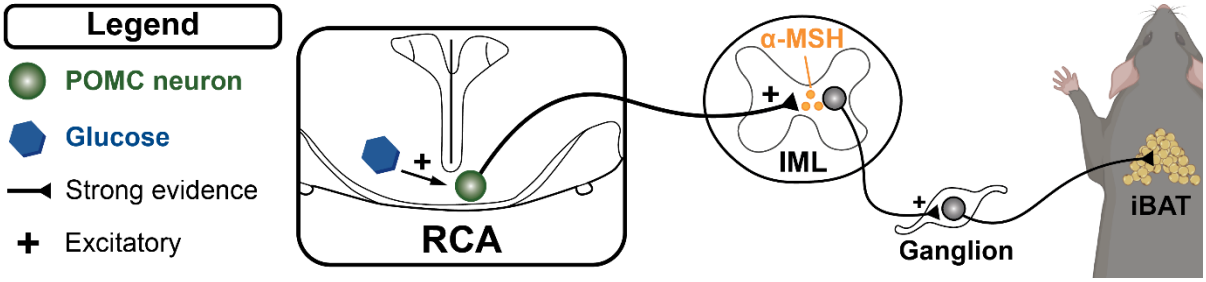

Figure 3.8 | Proposed glucose-regulated effects of RCA^{POMC} → IML circuit

A tentatively-defined glucose-regulated RCA^{POMC} → IML circuit that may promote BAT SNA.

In summary, glucose- and MC4R-regulated control of sympathetic output to BAT in each of these circuits is certainly possible, however there is neither categorical evidence *for* nor *against* the argument of functional (thermogenic) redundancy. It is clear, then, that this question warrants further study. That being said, on the balance of the evidence presently available, our opinion is that the direct RCA^{POMC} → IML circuit is most compelling in its role for glucose (or meal)-regulated postprandial thermogenesis in brown fat and, therefore, should be of particular focus in future studies.

3.4.5 Conclusions

Until now, the central mechanisms subserving the hypothalamic regulation of diet-induced sympathetic activity in brown fat had remained elusive, in contrast to the cold-induced thermogenic circuit which has been better defined. In this Chapter we present data which unequivocally demonstrate the glucose-sensing capacity of subsets of hypothalamic neurons projecting to brown fat within three or four synapses. We demonstrate that POMC-expressing neurons in the ARC and RCA are predominantly activated by elevations in extracellular glucose concentration, and that these glucose-sensitive populations project in equal proportions through hypothalamic pre-autonomic nuclei (from the ARC) and directly to pre-ganglionic sympathetic neurons in the spinal cord (from the RCA). While the physiological output(s) of glucose-induced changes in neuronal activity were outside of the parameters of the current investigations, our studies provide a blueprint for a functional link between elevated glucose levels sensed in the brain and postprandial thermogenesis.

Chapter 4

Hypothalamic POMC neurons in the regulation of postprandial thermogenesis

4.1 Introduction

POMC neurons that encompass both the ARC and RCA form the catabolic arm of the melanocortin system, promoting satiety and energy expenditure. In line with its role in energy regulation, embryonic homozygous deletion of the gene encoding POMC with a variety of techniques has consistently yielded an obese, hyperphagic and hypometabolic phenotype (Yaswen *et al.*, 1999; Challis *et al.*, 2004; Xu *et al.*, 2005). Furthermore, deletion of the MC4R similarly evokes morbid obesity through both increased food intake and reduced energy expenditure (Huszar *et al.*, 1997; Ste. Marie *et al.*, 2000; Butler *et al.*, 2001), outcomes which also present in humans with mutations on either gene (Krude *et al.*, 1998; Vaisse *et al.*, 1998; Yeo *et al.*, 1998; Farooqi *et al.*, 2000; Creemers *et al.*, 2008). While impaired melanocortin signalling mildly reduces locomotor activity (Chen *et al.*, 2000; Lam *et al.*, 2015), there is strong evidence that the hypometabolic phenotype is primarily attributed to blunted BAT thermogenesis. MC4Rs are expressed in BAT-projecting neurons throughout most brain nuclei and the IML (Voss-Andreae *et al.*, 2007), and their pharmacological activation promotes interscapular BAT UCP1 expression, thermogenesis and energy expenditure (Chen *et al.*, 2000; Williams *et al.*, 2003; Enriori *et al.*, 2011; Xu *et al.*, 2013). By comparison, pharmacological inhibition of MC4R reduces energy expenditure and UCP1 expression in BAT (Kooijman *et al.*, 2014), and activation of AgRP neurons, the endogenous melanocortin antagonist, dramatically reduces BAT temperature in mice that do not have access to food (Burke *et al.*, 2017).

Considering that POMC neurons are activated postprandially by hormones and other stimuli related to meal consumption (Elias *et al.*, 1998; Claret *et al.*, 2007; Wu *et al.*, 2014), the melanocortin system is well positioned to mediate the diet-induced activation of sympathetic tone to brown fat. In support of this framework, MC4R knockouts have a blunted increase in energy expenditure when exposed to high-fat diet feeding (Butler *et al.*, 2001; Albarado *et al.*, 2004), an effect which seems to be dependent primarily on MC4R expression on pre-ganglionic sympathetic neurons of the IML (Rossi *et al.*, 2011; Berglund *et al.*, 2014). However, it remains unclear whether transitory signals associated with recent meal consumption activate the melanocortin system *acutely* to modulate BAT thermogenesis, or whether this process occurs on an “adaptive”, longer-term timescale driven by, for example, hormonal factors that reflect energy stores.

In light of findings presented in **Chapter 3***,* namely that BAT-projecting POMC neurons are largely excited by short-term meal-related cues (i.e. glucose), and that chemogenetic activation of POMC neurons rapidly promotes brown fat thermogenesis (Fenselau *et al.*, 2017), we hypothesise that acute activation of POMC neurons following consumption of a standard diet to promote thermogenesis in BAT. Here we aim to confirm, in our hands, that POMC neurons and melanocortin signalling are *sufficient* to promote thermogenesis in brown fat. We will then explore the extent to which hypothalamic POMC neurons are *necessary* to regulate facultative postprandial thermogenesis in BAT by employing acute and chronic loss-of-function models.

4.2 Experimental Procedures

4.2.1 Validation of Pomc$^{IRES\text{-}Cre}$ transgenic mouse

In order to selectively modulate hypothalamic POMC neuron activity, we obtained an established Pomc$^{IRES\text{-}Cre}$ transgenic mouse line (see *Chapter 2: General Methods)* which has been reported to drive Cre expression specifically in hypothalamic POMC neurons with high specificity (Fenselau *et al.*, 2017). The fidelity of Cre expression in POMC-expressing neurons was validated by crossing Pomc$^{IRES\text{-}Cre}$ mice with Ai14^{tdTomato} Cre-reporter mice (Pomc$^{IRES\text{-}Cre}$::Ai14^{tdTomato}), in a similar way to what has been previously reported (Fenselau *et al.*, 2017). Using mice from different litters, the brains of 8-week old male mice were collected and processed (see *Section 4.2.7*) for the specificity and efficiency of Cre-mediated recombination in POMC neurons. High specificity and efficiency of Cre expression was confirmed by performing immunohistochemistry against POMC peptide and counting total tdTomato$^+$, POMC$^+$ and colocalised (tdTomato$^+$POMC$^+$) neurons across the rostro-caudal extent of the arcuate nucleus and retrochiasmatic area. Neuron counts were made using ImageJ software.

4.2.2 Chemogenetic manipulation of POMC neurons

To test the involvement of POMC neuron activity on BAT thermogenesis, the arcuate nucleus and retrochiasmatic area of Pomc$^{IRES\text{-}Cre}$ mice were injected with an adeno-associated virus (AAV) that encoded Cre-dependently for the expression of either the excitatory hM3Dq (Pomc^{hM3Dq}) or inhibitory hM4Di (Pomc^{hM4Di}) DREADD. At least two weeks after transduction, the designer drug clozapine-*N*-oxide (CNO; 1 or 3mg/kg) or vehicle was administered intraperitoneally in order to activate the DREADD receptor and hence modulate POMC neuron activity, and thus determine the physiological effect of POMC neuron modulation on BAT temperature and food intake. Injections were performed in the early phase of the light period in either *ad libitum* fed Pomc^{hM3Dq} or Pomc^{hM4Di} mice, or an hour prior to refeeding overnight fasted Pomc^{hM4Di} mice. BAT temperature and food intake was recorded at the time points indicated. Interscapular brown fat temperature was measured using IPTT-300 temperature-sensitive transponders (Bio Medic Data Systems) and collected using a handheld reader (see *Chapter 2: General Methods*).

4.2.3 Central administration of melanocortin receptor modulators

In order to pharmacologically modulate melanocortin receptors, wild type C57Bl/6 (C57Bl/6^{WT}) or Pomc^{hM3Dq} mice were implanted with an indwelling cannula into the lateral ventricle. To activate central melanocortin receptors, a MC3/4R agonist (MTII) was injected intracerebroventricularly (2nmol in 2uL saline) in C57Bl/6^{WT} mice, and food intake and BAT temperature were measured at regular intervals for up to 24 hours after injection. To inhibit signalling at central melanocortin receptors, a MC3/4R antagonist (SHU9119) was administered intracerebroventricularly in either fasted C57Bl/6^{WT} mice an hour prior to refeeding (1nmol in 1uL saline) or Pomc^{hM3Dq} mice 30 minutes prior to CNO injection (0.5nmol in 1uL saline), and food intake and BAT temperature were measured. In all cases, volume-matched sterile saline was used as control.

4.2.4 POMC neuron ablation strategy

To establish a chronic POMC loss-of-function model, the arcuate nucleus and retrochiasmatic area of $Pomc^{IRES\text{-}Cre}$ mice were injected with an AAV that encoded Cre-dependently for either the modified pro-apoptotic enzyme taCaspase-3 to ablate POMC neurons ($Pomc^{Caspase}$), or to induce expression of eGFP as control ($Pomc^{eGFP}$). Importantly, mice were assigned to each treatment group by matching them on a range of metabolic parameters and hence accounting for inter-animal variability. To this end, $Pomc^{IRES\text{-}Cre}$ mice were implanted with a temperature-sensitive transponder beneath the interscapular BAT two to three weeks prior to virus injection. Twice daily BAT temperature recordings were made in calorically-sated mice; one made in the early light phase (~9-10:00am) and another in the late light phase (~4-5:00pm; lights off 7:00pm). Daily food intake and body weights were also recorded during this period. Furthermore, to assess specifically *postprandial* thermogenesis, BAT temperature (and food intake) was recorded following the refeeding of overnight-fasted mice on two occasions, approximately one week apart. The recorded values of postprandial food intake and BAT temperature were averaged to ascertain a "baseline" refeeding response.

Following injection of viruses, the effect of POMC neuron ablation on food intake (excluding week 1), body weight and daily BAT temperature was monitored for 6 weeks. At the end of this period, mice were subjected to another fast-refeed paradigm to compare postprandial thermogenesis and food intake between ($Pomc^{Caspase}$ vs. $Pomc^{eGFP}$) and within (pre-surgery vs. post-surgery) treatment.

4.2.5 Electrophysiological validation of DREADD function in *ex vivo* brain slices

POMC neuron modulation with DREADD activation was validated using whole-cell patch clamp electrophysiology. To prepare brain slices, $Pomc^{hM3Dq}$ or $Pomc^{hM4Di}$ mice were anaesthetised and decapitated, and brains were rapidly collected into oxygenated ice-cold sucrose-modified aCSF (in mM, 200 Sucrose, 1.9 KCl, 1.2 NaH_2PO_4, 26 $NaHCO_3$, 5.0 D-glucose, 5.0 D-mannitol, 0.5 ascorbic acid, 10 $MgCl_2$), and were cut into 250-300µm coronal sections of the arcuate nucleus and retrochiasmatic area using a vibratome (VT1000S; Leica, Cambridge, UK). Slices were transferred to recording aCSF (in mM, 127 NaCl, 1.9 KCl, 1.2 KH_2PO_4, 26 $NaHCO_3$, 5.0 D-glucose, 5.0 D-mannitol, 1.3 $MgCl_2$, 2.4 $CaCl_2$, 0.34 ascorbic acid; equilibrated with 95% O_2 and 5% CO_2, pH 7.3-7.4, 300-305mOsm/L) at 34-35°C for 25 mins, and then left to rest at room temperature for >45 minutes before electrophysiological recordings were conducted.

For recordings, hypothalamic brain slices were transferred to a recording chamber and constantly bathed in aCSF (flow rate = 3-5mL/min). DREADD-expressing neurons were identified by mCherry epifluorescence, then with differential interference contrast microscopy neurons were selected for recording using a Multiclamp 700A amplifier (Axon Instruments, Foster City, CA, USA). Patch-pipettes were pulled using a horizontal puller (Sutter Instruments, USA; P1000 model) from thin-walled borosilicate glass (Harvard Apparatus; GC150-TF10) to resistances between 6 and 9MΩ when filled with intracellular recording solution (in mM, 140 K-gluconate, 10 HEPES, 10 KCl, 1.0 EGTA and 2.0 Na_2ATP, 0.3 Na_2GTP; pH adjusted to 7.35 with KOH, osmolarity adjusted to ~305mOsm/L with sucrose). In current clamp mode, baseline recordings were taken until membrane potential was stable

(~5 minutes), then CNO was bath-applied to the brain slice for 2-4 minutes. Baseline membrane potential was taken when stable just prior the application of CNO, and then at the peak of the CNO response. Firing frequency was determined by measuring the number of action potentials fired in a 30-second period at baseline and at the peak CNO response. For data analysis, the signal was digitised at 10kHz and analysed utilising a computer running pClamp10 (Axon Instruments). Membrane potential values were not compensated to account for liquid junction potential (−9 mV).

4.2.6 Stereotaxic cannulation and virus injection

$Pomc^{IRES\text{-}Cre}$ or $C57Bl/6^{WT}$ mice were anaesthetised and placed in a stereotaxic apparatus (mouse adaptor 51625, Stoelting, Wood Dale IL). After exposing the skull via midline incision, a small hole was drilled for cannulation through which there was subsequent delivery of pharmacological agents, or for injection of AAVs encoding DREADDs, Caspase or control fluorophores. For cannulation, a 26-gauge guide cannula (InVivo1, Roanoke, WA) was inserted into the brain just above the lateral ventricle (coordinates from bregma: AP: -0.5mm, ML: 1.0mm, DV: −1.7mm) and held in place by light-cured bond and dental cement. A dummy cannula was inserted into the guide when not in use to keep the cannula patent and free from contaminant. For injection of MTII and SHU9119 (or saline), a custom-designed 33-gauge injector was attached to PE tubing connected to a 10µL syringe (Hamilton Company, USA) and inserted into the guide cannula extending 0.5mm past the tip, into the lateral ventricle. Pharmacological agents were delivered at approximately 2µL/min.

Bilateral AAV injections were made stereotaxically into the mediobasal hypothalamus of $Pomc^{IRES\text{-}Cre}$ mice to encompass both the ARC and RCA (250nL per side, coordinates from bregma: AP: −1.3mm, ML: ±0.3mm, DV: −5.8mm) via pulled-glass pipettes (tip diameter ≈ 40µm) using a pressure-injection system. Viruses were delivered over 5 minutes, and pipettes left in place for a further 5 minutes before removal from the brain to minimise efflux of the injectate. The viruses injected were either AAV-hSyn-DIO-hM3Dq-mCherry (Addgene viral prep #44361-AAV5, titre ≥ 7×10^{12} vg/mL; $Pomc^{hM3Dq}$), AAV-hSyn-DIO-hM4Di-mCherry (Addgene viral prep #44362-AAV5, titre ≥ 7×10^{12} vg/mL; $Pomc^{hM4Di}$), AAV-hEF1α-flex-(pro)taCasp3-TEVp (University Zurich Viral Vector Facility v185-AAV5, titre 4.7×10^{12} vg/mL from Addgene plasmid #45580; $Pomc^{Caspase}$) or AAV-synP-DIO-EGFP-WPRE-hGH (Addgene viral prep #100043-AAV9, titre ≥ 1×10^{13} vg/mL; $Pomc^{eGFP}$). The plasmids used for virus manufacture were a gift from Brian Roth (DREADDs), Nirao Shah & Jim Wells (Caspase) and Ian Wickersham (eGFP).

At the conclusion of experiments, all virally-transfected mice were perfused and brains were processed (see *Section 4.2.7*) for accuracy and efficiency of viral-transfection. For DREADD experiments, only mice which exhibited substantial bilateral expression of mCherry that was wholly contained within the boundaries of the rostro-caudal extent of the ARC and RCA were used for analysis. For Caspase experiments, the degree of POMC neuron deletion in $Pomc^{Caspase}$ mice was determined by the immunohistochemical processing of hypothalamic brain slices for POMC peptide, which stains cell bodies (and axons) in the ARC and RCA. Mice that showed an overall reduction in POMC cell body number greater than 50% relative to control ($POMC^{eGFP}$) mice were included in analyses. In total, 6 of

16 $Pomc^{Caspase}$ mice were excluded from analysis due to insufficient bilateral POMC ablation most often explained by misplaced, unilateral injections of virus into the third ventricle.

4.2.7 Brain tissue preparation & immunohistochemistry

To examine the brain for accuracy of virus injection or validation of Cre-recombination, mice were terminally anaesthetised with i.p. sodium pentobarbitone (>100mg/kg) and perfused transcardially first with phosphate-buffered saline (pH = 7.4) and then 4% PFA solution in PB. The brains were stored in the same fixative overnight at 4°C, and then transferred into 30% sucrose PB solution at 4°C for at least 24 hours. Using a cryostat (Leica), 35µm coronal sections of the brain were collected into four equal series and stored at −20°C in cryoprotectant until processing.

Brain sections were washed in 0.1M PB, and then blocked in 10% NHS and 0.3% Triton X-100 in PB (PBT) for at least 30 minutes. Sections were then incubated overnight at room temperature in 1% NHS PBT containing primary antisera (rabbit anti-DsRed, Living Colours 632496, 1:2000; rabbit anti-POMC, Phoenix Pharmaceuticals H-029-30, 1:2000). The next morning sections were washed in 1%NHS PB and then incubated for 2h at room temperature in PB with Alexa-fluorophore conjugated secondary antibodies (Donkey anti-rabbit Alexa488, Abcam 1:500; Donkey anti-rabbit Alexa594, Abcam, 1:500). After several washes in PB, sections were mounted onto glass slides and coverslipped with VECTASHIELD® HardSet™ with DAPI or Dako Fluorescence Mounting Medium. Fluorescence images were captured using a Leica SP5 5-channel confocal microscope using a 10x dry objective or 20-40x oil-immersion objective.

4.2.8 Drugs

The peptides MTII (Bachem; used at 2nmol/2µL for i.c.v) and SHU9119 (Bachem; 0.5 or 1nmol/µL) were dissolved in sterile saline and stored at -20°C. Clozapine-*N*-oxide (CNO, Carbosynth; used at 1 or 10µM for electrophysiology, 1 or 3mg/kg i.p.) was made up as a stock solution in DMSO and stored at -20°C. On the day of use, CNO was diluted in either recording aCSF for electrophysiology (maximum 0.01% DMSO), or in saline (5% DMSO) for intraperitoneal injection. For intracerebroventricular injections, volumes of either 1 or 2µL were delivered, depending on the drug administered. Intraperitoneal injection volumes were performed at 3mL/kg body weight.

4.2.9 Statistical analyses

Data was graphed and statistically analysed using GraphPad Prism 8.0 (Graphpad Software; CA, USA); significance for all tests was set at $p<0.05$. Grouped data is presented as mean ± SEM unless otherwise indicated. Individual data points (paired and unpaired) are also presented in some grouped data sets. Repeated measures two-way ANOVA with Sidak's multiple comparisons was used to compare changes in BAT temperature, food intake body weight and feed efficiency over time between treatment groups, as well as comparing area under the curve (AUC) changes in BAT temperature

between $Pomc^{Caspase}$ and $Pomc^{eGFP}$ mice pre- and post-surgery. Repeated measures three-way ANOVA with Tukey's multiple comparisons was used to compare changes in refeed-induced BAT temperature and food intake in $Pomc^{Caspase}$ and $Pomc^{eGFP}$ mice across time (refeed) and time (surgery). Paired *t* tests were used to compare changes in BAT temperature AUC and electrophysiological parameters. Note that in all experiments measuring the effect of an acute intervention (e.g. injection of drug, refeeding), baseline "pre-intervention" time point(s) were excluded from statistical analysis so not to confound the analysis of intervention. Full statistical reports are stated either in the body text or in the figure legends.

4.3 Results

4.3.1 Hypothalamic POMC neurons are sufficient to drive brown fat thermogenesis

To confirm the fidelity of Cre-expression in Pomc$^{IRES\text{-}Cre}$ mice, we crossed Cre-expressing males with female Ai14^{tdTomato} Cre-reporter mice (Pomc$^{IRES\text{-}Cre}$::Ai14^{tdTomato}), and processed brains of offspring immunohistochemically for expression of tdTomato and POMC peptide. In keeping with previous reports (Fenselau *et al.*, 2017), the Cre-mediated expression of tdTomato was isolated to the arcuate nucleus and retrochiasmatic area (**Figure 4.1A$_1$**), with negligible expression in the cortex, hippocampus, midbrain, cerebellum, pons and medulla. Colocalisation of endogenous tdTomato with immunohistochemically-labelled POMC peptide revealed Cre-expression with excellent efficiency, where 95.7 ± 0.7% of POMC-immunoreactive neurons throughout the ARC and RCA colocalised with endogenous tdTomato fluorescence (1930 tdTomato$^+$POMC$^+$/2017 POMC$^+$ cells, from n = 2 animals). Furthermore, Cre-expression was highly specific to POMC-expressing neurons, where 86.8 ± 0.1% of tdTomato neurons colocalised with POMC immunoreactive cell bodies (1930 tdTomato$^+$POMC$^+$/2223 tdTomato$^+$ cells, from n = 2 animals). This figure is likely an underestimate of true specificity given the limitations of antibody penetration and binding to epitopes in fixed material combined with the relatively low sensitivity of fluorescence immunohistochemistry. Importantly, the efficiency and specificity of Cre expression remained relatively constant throughout the rostro-caudal extent of the RCA (−0.94 to −1.06mm from Bregma) and ARC (rostral: −1.22 to −1.34mm; mid: −1.46 to −1.94mm; caudal: −2.18 to −2.30mm from Bregma) (**Figure 4.1A$_2$**). These data in combination validate the adequacy of this transgenic strain for the targeting of hypothalamic POMC neurons using the Cre-Lox recombination strategies.

In order to investigate the sufficiency of hypothalamic POMC neurons to activate BAT thermogenesis, expression of the excitatory (hM3Dq) DREADD was induced in ARC and RCA POMC neurons (Pomc^{hM3Dq}). This was achieved by bilateral injection of a Cre-dependent AAV containing a double-floxed inverted orientation (DIO) sequence for the mCherry-tagged receptor into the mediobasal hypothalamus of Pomc$^{IRES\text{-}Cre}$ mice (**Figure 4.1B**). To first validate that exposure of hM3Dq-expressing POMC neurons to the designer ligand, clozapine-*N*-oxide (CNO), increases neuronal activity, whole-cell patch-clamp recordings were made from mCherry- (hM3Dq-) expressing POMC neurons in acutely prepared *ex vivo* brain slices. Bath-application of CNO (1μM) caused a reversible 12.0 ± 1.5mV depolarisation in membrane potential (n = 11, p<0.0001) as well as a 1.51 ± 0.24Hz increase in action potential frequency (p<0.0001) (**Figure 4.1C**), validating that activation of the hM3Dq receptor increases POMC neuron activity.

We sought to test whether acute activation of POMC neurons in *ad libitum* fed mice was able to modulate BAT-directed sympathetic outflow, and hence thermogenesis (**Figure 4.1D$_1$**). Brown fat thermogenesis was measured by surgically implanting temperature-sensitive transponders beneath the interscapular brown fat, and evaluating changes in temperature over time. A single intraperitoneal injection of CNO (1mg/kg) in Pomc^{hM3Dq} mice significantly elevated BAT temperature for at least four hours post-injection, with a peak increase of above vehicle of 0.99 ± 0.13°C (1h, n = 11, p<0.0001; $p_{treatment}$=0.0086, $p_{interaction}$<0.0001) (**Figure 4.1D$_2$**). Food intake was also significantly supressed by hM3Dq-activation, where mice ate 7.9 ± 5.0% less food in the 24 hours subsequent to injection (24h,

p=0.0040; $p_{treatment}$=0.0083) (**Figure 4.1D$_3$**), in line with previous reports that POMC neuron activity promotes long-term satiety (Aponte *et al.*, 2011; Zhan *et al.*, 2013).

To establish whether increased downstream α-MSH release, as opposed to the release of other neurotransmitter(s), formed the basis for elevated thermogenesis following POMC neuron activation, a cohort of Pomc^{hM3Dq} mice were implanted with an indwelling lateral ventricle cannula (**Figure 4.1E$_1$**). Intracerebroventricular pre-treatment with the MC3/4R antagonist, SHU9119 (0.5nmol), 30 minutes prior to intraperitoneal injection effectively blocked CNO-induced BAT thermogenesis in SHU9119-treated but not saline-treated Pomc^{hM3Dq} mice, with a peak BAT temperature difference of 1.00 ± 0.35°C (1.5h, n = 6, p=0.0008; $p_{treatment}$=0.0126, $p_{interaction}$=0.0334) (**Figure 4.1E$_2$**). SHU9119 administration combined with intraperitoneal vehicle treatment did not significantly affect BAT temperature compared with saline-treated controls ($p_{treatment}$=0.7965, $p_{interaction}$=0.1487), indicating that, at least during the light cycle, central MC3/4Rs do not constitutively promote BAT thermogenesis (**Figure 4.1E$_3$**).

To further establish the role of melanocortin receptors in the regulation of sympathetic flow to BAT, we centrally administered the MC3/4R agonist, MTII (2nmol), to calorically replete C57Bl/6^{WT} mice in the early light phase (**Figure 4.1F$_1$**). Similar to DREADD-mediated activation of hypothalamic POMC neurons, central melanocortin agonism significantly increased BAT temperature compared to saline-treated controls (0.74 ± 0.21°C greater than saline at 1h, n = 9, p<0.0001; $p_{treatment}$=0.0026, $p_{interaction}$<0.0001) (**Figure 4.1F$_2$**). The satiety-inducing effect of central melanocortin receptor agonism appeared to be more potent than DREADD-mediated activation of POMC neurons, where overnight food intake was reduced by 25.8 ± 12.0% compared to vehicle treated mice (24h, p<0.0001; $p_{treatment}$=0.0342, $p_{interaction}$=0.0017) (**Figure 4.1F$_3$**), although we recognise this may be due to the supra-effective dose of the agonist used. Our findings corroborate thermogenic effects related to MC3/4R activation, and, hence, that hypothalamic POMC neurons are sufficient to drive thermogenesis through melanocortin signalling.

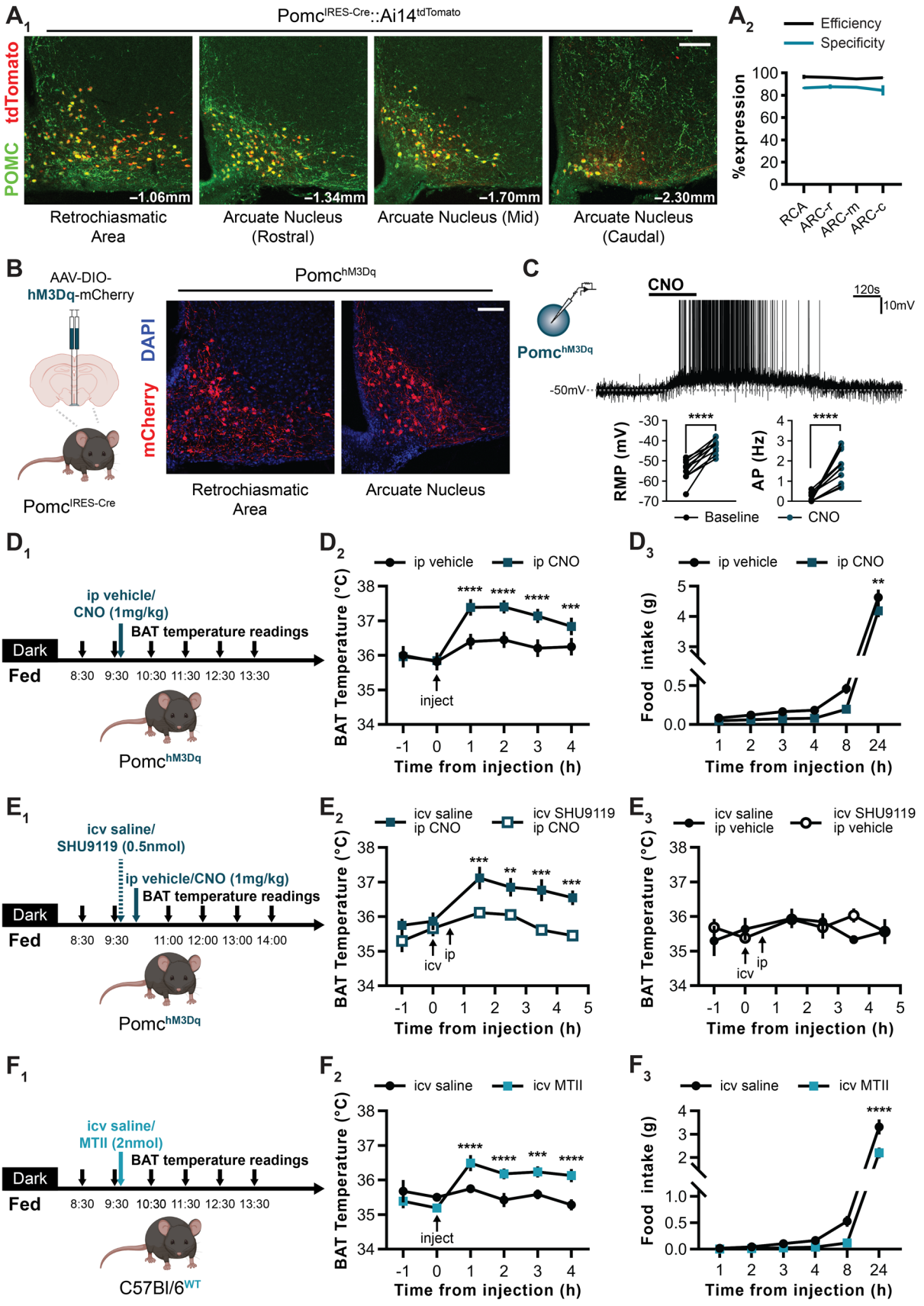

Figure 4.1 | POMC neuron and melanocortin receptor activation drive BAT thermogenesis and reduce feeding

(A_1 and A_2) Representative confocal microphotographs of $Pomc^{IRES\text{-}Cre}$::$Ai14^{tdTomato}$ reporter mice confirmed recombination (tdTomato expression, red) primarily within POMC neurons (identified

immunohistochemically, green) of the retrochiasmatic area and all levels of the arcuate nucleus (colocalised expression appears as yellow) (A_1). Diagram for quantification of the percentage efficiency (double labelled/all POMC+) and specificity (double labelled/all tdTomato+) of Cre-expression in POMC neurons in $Pomc^{IRES\text{-}Cre}$ transgenic mice, n = 2. Rostro-caudal distance from Bregma in bottom right corner. RCA, retrochiasmatic area. ARC-r, ARC-m and ARC-c, rostral mid and caudal arcuate nucleus. Scale bar, 100µm. **(B)** POMC-activation strategy: $Pomc^{IRES\text{-}Cre}$ mice injected bilaterally with Cre-dependent AAV to induce expression of excitatory DREADD receptor, hM3Dq, in POMC neurons in the mediobasal hypothalamus ($Pomc^{hM3Dq}$). Representative confocal microphotographs revealing expression of mCherry-tagged DREADD in the arcuate nucleus and retrochiasmatic area, with DAPI counterstain. Scale bar, 100µm. **(C)** Representative trace of *ex vivo* whole-cell patch-clamp recording from $Pomc^{hM3Dq}$ neuron that is depolarised and increases action potential firing rate in response to bath application of 1µM CNO. Grouped data depicts the increase in resting membrane potential (RMP) and action potential (AP) frequency for all recorded $Pomc^{hM3Dq}$ cells. Changes in electrophysiological parameters were analysed by paired t test (RMP, n = 11 cells; t = 8.249, df = 10, ****p<0.0001. AP, n = 11 cells; t = 6.280, df = 10, ****p<0.0001). **($D_{1\text{-}3}$)** Experimental timeline for acute activation of POMC neurons by injection of hM3Dq agonist, CNO (1mg/kg), in fed $Pomc^{hM3Dq}$ mice in the early phase of the light cycle (D_1). Diagrams indicate the effect on BAT temperature (D_2) and food intake (D_3) in the indicated hours subsequent to injection. BAT temperature and food intake were analysed by repeated measures (both factors) two-way ANOVA followed by Sidak's multiple comparisons test (D_2, n = 11 animals; treatment F(1, 10) = 40.33, p<0.0001; time F(4, 40) = 31.16, p<0.0001; interaction F(4, 40) = 11.41, p<0.0001. 0h, p=0.9999; 1h, ****p<0.0001; 2h, ****p<0.0001; 3h, ****p<0.0001; 4h, ***p=0.0001. D_3, n = 11 animals; treatment F(1, 10) = 10.77, p=0.0083; time F(5, 50) =552.2, p<0.0001; interaction F(5, 50) = 1.664, p=0.1607. 1h, p=0.9999; 2h, p=0.9971; 3h, p=0.9768; 4h, p=0.9548; 8h, p=0.2002; 24h, **p=0.0040). **($E_{1\text{-}3}$)** Experimental timeline for acute activation of POMC neurons with CNO (1mg/kg) in fed $Pomc^{hM3Dq}$ mice pre-treated with intracerebroventricular injection of MC3/4R antagonist, SHU9119 (0.5nmol) (E_1). Diagrams indicate BAT temperature in CNO-injected (E_2) or vehicle-injected (E_3) mice that received injection of 0.5nmol SHU9119 or saline 30 minutes prior. BAT temperature was analysed by repeated measures (both factors) two-way ANOVA followed by Sidak's multiple comparisons test (I, n = 6 animals; treatment F(1, 5) = 14.45, p=0.0126; time F(4, 20) = 8.796, p=0.0003; interaction F(4, 20) = 3.240, p=0.0334. 0h, p=0.8957; 1h, ***p=0.0008; 2h, **p=0.0068; 3h, ***p=0.0002; 4h, ***p=0.0003. J, n = 6 animals; treatment F(1, 5) = 0.07395, p=0.7965; time F(4, 20) = 8.279, p=0.5230; interaction F(4, 20) = 1.907, p=0.1487. 0-4h, p>0.05). **($F_{1\text{-}3}$)** Experimental timeline for acute activation of melanocortin receptors by intracerebroventricular injection of M3/4R agonist, MTII (2nmol), in fed wild-type C57Bl/6 mice in the early phase of the light cycle (K). Diagrams indicate the effect on BAT temperature (L) and food intake at varying time intervals in the 24h subsequent to injection (M). BAT temperature and food intake was analysed by repeated measures (both factors) two-way ANOVA followed by Sidak's multiple comparisons test (L, n = 9 animals; treatment F(1, 8) = 18.62, p=0.0026; time F(4, 32) = 9.465, p<0.0001; interaction F(4, 32) = 12.91, p<0.0001. 0h, p=0.1193; 1h, ****p<0.0001; 2h, ****p<0.0001; 3h, ***p=0.0002; 4h, ****p<0.0001. M, n = 9 animals; treatment F(1, 8) = 6.502, p=0.0342; time F(5, 40) = 360.4, p<0.0001; interaction F(5, 40) = 4.765, p=0.0017. 1h, p>0.9999; 2h, p>0.9999; 3h, p=0.9991; 8h, p=0.2381; 24h, ****p<0.0001).

Data are represented as mean ± SEM for figures A_2, D_2, D_3, E_2, E_3, F_2 and F_3 and as individual paired values in C.

4.3.2 Postprandial BAT thermogenesis is partially attributed to POMC neuron activity

To address our primary hypothesis that POMC neurons are acutely activated by food intake to subsequently promote BAT-directed sympathetic activity and diet-induced thermogenesis, we sought to acutely inactivate POMC neurons prior to meal consumption. To this end, $Pomc^{IRES\text{-}Cre}$ mice were injected bilaterally with a Cre-dependent AAV that induced expression of the inhibitory DREADD receptor, hM4Di, in POMC neurons of the mediobasal hypothalamus ($Pomc^{hM4Di}$) (**Figure 4.2A**). To validate functionality of the receptor, whole-cell recordings were from $POMC^{hM4Di}$ neurons in *ex vivo* brain slices. Bath-applied CNO (10μM) caused a reversible hyperpolarisation (−6.2 ± 1.1mV; n = 16, p<0.0001) and reduction in firing frequency (−0.51 ± 0.14Hz, p=0.0025), including the complete silencing of 7 of 16 (44%) neurons (**Figure 4.2B**), substantiating the effectiveness of the hM4Di DREADD to acutely reduce neuronal activity.

We found that intraperitoneal injection of CNO (3mg/kg) in *ad libitum* fed $Pomc^{hM4Di}$ mice had no effect on brown fat temperature relative to vehicle-injected mice (n = 9, $p_{treatment}$=0.2445, $p_{interaction}$=0.5455) (**Figure 4.2C**), in support of our previous findings that melanocortin antagonism did not affect BAT temperature in fed mice. In order to test the involvement of POMC neurons to regulate thermogenesis following an acute, temporally-defined meal bout, overnight-fasted $Pomc^{hM4Di}$ mice received a CNO injection one hour prior to refeeding (**Figure 4.2D$_1$**). DREADD-mediated pre-inhibition of POMC neurons caused a significant attenuation, but not elimination, of the postprandial elevation in brown fat temperature (n = 11, $p_{treatment}$=0.0046) and the associated AUC of BAT temperature across time (−5.0 ± 1.4%, p=0.0043) (**Figure 4.2D$_2$**). This finding demonstrates a role for the meal-induced activation of POMC neurons in regulating, at least partially, the postprandial recruitment of BAT thermogenesis. Inhibition of POMC neurons had no effect on food intake in the first four hours of refeeding following overnight fasting (1-4h, p>0.05), but caused a small increase in 24h food intake (8.6 ± 5.7%, p=0.0232), suggesting that POMC neuron activity regulates long-term satiety even in overnight fasted mice (**Figure 4.2D$_3$**).

To further substantiate these findings using a pharmacological approach, we also administered the MC3/4R antagonist, SHU9119 (1nmol), intracerebroventricularly into overnight fasted $C57Bl/6^{WT}$ mice an hour prior to refeeding (**Figure 4.2E$_1$**). Indeed, antagonism of central MC3/4Rs significantly reduced postprandial thermogenesis in BAT (n = 9, $p_{treatment}$=0.0100) and associated AUC following refeeding (−6.4 ± 2.2%, p=0.0194) relative to controls pre-treated with saline (**Figure 4.2E$_2$**). Similar to DREADD-mediated inhibition of hypothalamic POMC neurons, pre-treatment with SHU9119 had no short-term effect food intake (1-4h, p>0.05) but significantly increased overnight food intake by 7.3 ± 4.8% (24h, p=0.0305) (**Figure 4.2E$_3$**).

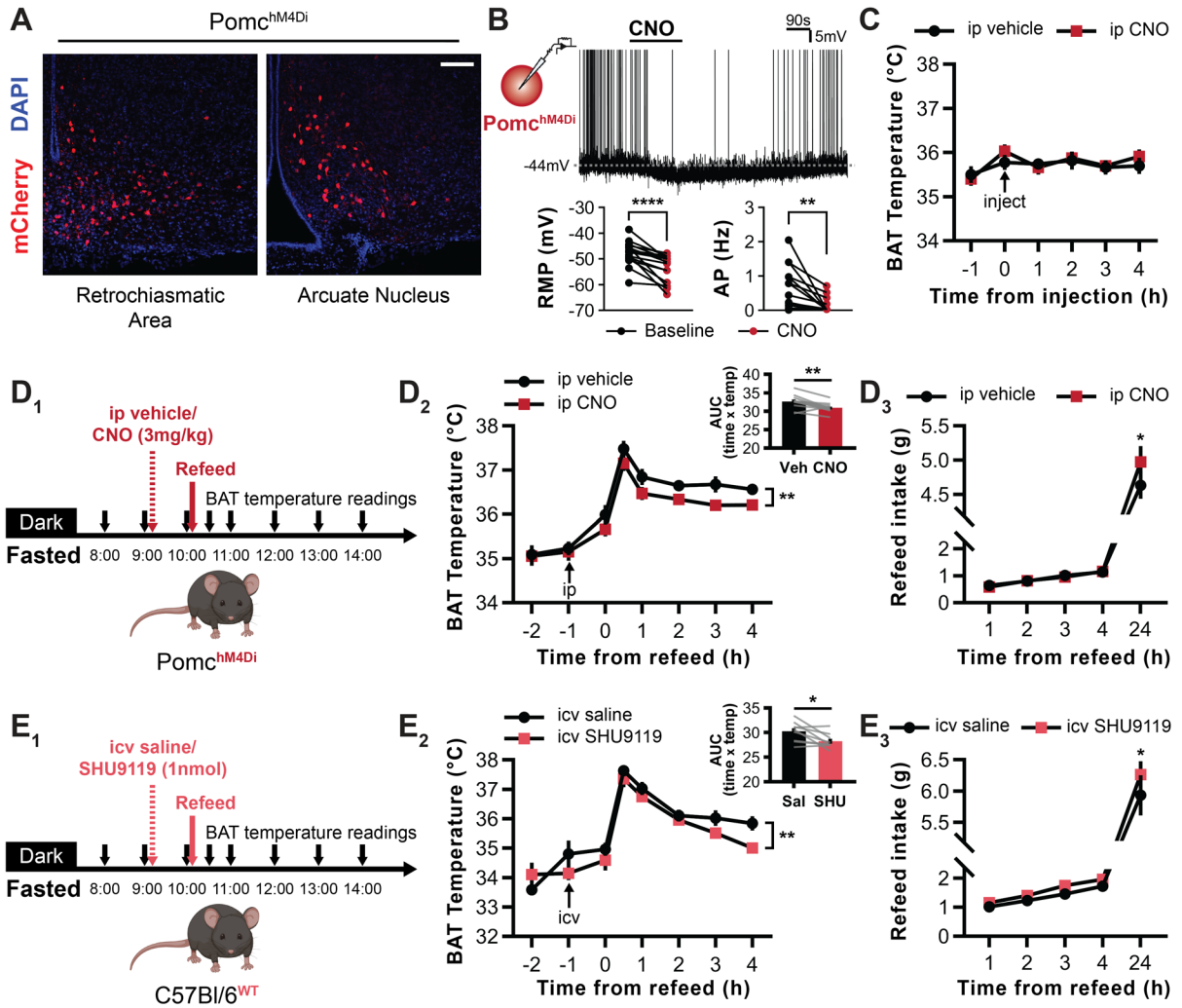

Figure 4.2 | POMC neuron and melanocortin receptor inhibition reduce postprandial thermogenesis and increase fasting-induced refeeding

(A) A Cre-dependent AAV was injected bilaterally into the mediobasal hypothalamus of Pomc$^{IRES-Cre}$ mice, inducing expression of the inhibitory DREADD receptor, hM4Di, in POMC neurons in the mediobasal hypothalamus (Pomc^{hM4Di}). Representative confocal microphotographs revealing expression of mCherry-tagged DREADD in the arcuate nucleus and retrochiasmatic area, with DAPI counterstain. Scale bar, 100µm. **(B)** Representative trace of *ex vivo* whole-cell patch-clamp recording from Pomc^{hM4Di} neuron that is hyperpolarised and decreases action potential firing rate in response to bath application of 10µM CNO. Grouped data depicts the decrease in resting membrane potential (RMP) and firing rate for all recorded POMC^{hM4Di} cells. Changes in electrophysiological parameters were analysed by paired *t* test (RMP, n = 16 cells; t = 5.421, df = 15, ****p<0.0001. AP, n = 16 cells; t = 3,625, df = 15 **p=0.0025). **(C)** Diagram depicting BAT temperature in response to acute inhibition of POMC neurons by injection of hM4Di agonist, CNO (3mg/kg), in *ad libitum* fed POMC^{hM4Di} mice in the early phase of the light cycle. BAT temperature was analysed by repeated measures (both factors) two-way ANOVA (n = 9 animals; treatment F(1, 8) = 1.578, p=0.2445; time F(4, 32) = 0.7817, p=0.5455; interaction F(4, 32) = 0.4180, p=0.7944). **(D$_{1-3}$)** Experimental timeline for acute inhibition of POMC neurons by injection of CNO (3mg/kg) in the early phase of the light cycle prior to refeeding overnight fasted POMC^{hM4Di} mice (D$_1$). Diagrams indicate the effect on BAT temperature with AUC analysis (y=30) (D$_2$) and food intake at varying time intervals in the 24h subsequent to refeeding (D$_3$). BAT temperature and refeed food intake was analysed by repeated measures (both factors) two-way ANOVA followed by Sidak's multiple comparisons test (D$_2$, n = 11 animals; treatment F(1, 10) = 13.23, **p=0.0046; time F(6, 60) = 40.46, p<0.0001; interaction F(6, 60) = 0.4824, p=0.8189. -1h, 0h, 0.5h, 1h, 2h, 4h, p>0.05; 3h, p=0.0509. D$_3$, n = 11 animals; treatment F(1, 10) = 0.3595, p=0.5621; time F(4,

40) = 513.2, p<0.0001; interaction $F(4, 40) = 2.122$, p=0.0959. 1h, p=0.9958; 2h, p>0.9999; 3h, p=0.9888; 4h, p>0.9999; 24h, *p=0.0232) and AUC by paired t test (n = 11 animals; t = 3.666, df = 10, **p=0.0043). **(E_{1-3})** Experimental timeline for acute inhibition of melanocortin receptors by intracerebroventricular injection of M3/4R antagonist, SHU9119 (1nmol), in the early phase of the light cycle prior to refeeding overnight fasted wild-type C57Bl/6 mice. (E_1). Diagrams indicate the effect on BAT temperature with AUC analysis (y=30) (E_2) and food intake at varying time intervals in the 24h subsequent to refeeding (E_3). BAT temperature and refeed food intake was analysed by repeated measures (both factors) two-way ANOVA followed by Sidak's multiple comparisons test (E_2, n = 9 animals; treatment $F(1, 8) = 11.26$, **p=0.0100; time $F(6, 48) = 62.60$, p<0.0001; interaction $F(6, 48) = 0.4008$, p=0.8749. -1h, 0h, 0.5h, 1h, 2h, 3h, 4h, p>0.05. E_3, n = 9 animals; treatment $F(1, 8) = 3.075$, p=0.1176; time $F(4, 32) = 582.4$, p<0.0001; interaction $F(4, 32) = 0.4903$, p=0.7428. 1h, p=0.6993; 2h, p=0.5765; 3h, p=0.0804; 4h, p=0.2223; 24h, *p=0.0305) and AUC by paired t test (n = 9 animals; t = 2.917, df = 8, *p=0.0194).

Data are represented as mean ± SEM for figures C, D_2, D_3, E_2 and E_3 and as individual paired values in B, D_2 and E_2.

4.3.3 Hypothalamic POMC neuron deletion reduces postprandial BAT thermogenesis

We next sought to generate a chronic POMC loss-of-function model to further corroborate findings that inactivation of the melanocortin system reduces postprandial thermogenesis in brown fat. To this end, we induced apoptosis of hypothalamic POMC neurons by employing an established cell-type specific model involving the pro-apoptotic enzyme, pro-taCasp3, and its activator, tobacco etch virus protease (TEVp) (Yang *et al.*, 2013). Delivery of this construct was achieved by bilateral injection of AAVs encoding Cre-dependently either pro-taCasp3-TEVp to ablate POMC neurons ($Pomc^{Caspase}$) or eGFP as control ($Pomc^{eGFP}$) in adult mice (**Figure 4.3A**). This strategy enabled ablation specific to hypothalamic POMC neurons and circumvented potential confounding adaptations associated with embryonic deletion. Inclusion criteria for $Pomc^{Caspase}$ animals required at least a 50% reduction in POMC cell number compared to $Pomc^{eGFP}$ controls determined by port-mortem immunohistochemical evaluation of the number of POMC-expressing neurons across the ARC and RCA. In 10 of 16 animals, we observed moderate to extensive ablation of POMC neurons across both nuclei, where in many cases there were few, if any, cells remaining in each slice (**Figure 4.3A**). It is noteworthy that, despite substantial or complete ablation of POMC neuronal cell bodies in sections from some mice, there remained residual POMC-immunoreactive fibres. It is likely that the latter are derived from POMC neurons in the nucleus of the solitary tract which are known to have substantial projections to the ARC and RCA (Wang *et al.*, 2015).

In line with the established role of hypothalamic POMC neurons in body weight regulation, $Pomc^{Caspase}$ mice gained significantly more weight than $Pomc^{eGFP}$ controls in the weeks subsequent to virus injection. While mice were matched for body weight before assignment to receive Caspase or eGFP, the subsequent exclusion of six $Pomc^{Caspase}$ mice with insufficient neuronal ablation reduced the average starting body weight of mice receiving Caspase virus, however this was not statistically significant (0w, p=0.7285) (**Figure 4.3B, left**). Nonetheless, there was significant interaction of body weight over time, where $Pomc^{Caspase}$ gained weight more rapidly than $Pomc^{eGFP}$ controls ($p_{interaction}$<0.0001). Expressed as a percentage from body weight at surgery, POMC-ablated mice gained dramatically more than control animals, increasing body weight by 47.4 ± 6.5% at six weeks post-surgery compared to 22.9 ± 2.9% gain in controls (n = 10, n = 12, respectively; 6w, p<0.0001; $p_{treatment}$=0.0016, $p_{interaction}$<0.0001) (**Figure 4.3B, right**). Furthermore, ablation of hypothalamic POMC neurons resulted in marked increases in food intake, with $Pomc^{Caspase}$ mice eating on average 41% more than controls six weeks after virus injection (6w, p=0.0081; $p_{treatment}$=0.0274, $p_{interaction}$<0.0001) (**Figure 4.3C**). When standardised to body weight, food intake in $Pomc^{Caspase}$ mice peaked two weeks following surgery (36% greater than $Pomc^{eGFP}$, p=0.0034) but remained consistently higher than control for the entire post-operative period ($p_{treatment}$=0.0199, $p_{interaction}$=0.0031) (**Figure 4.3D**).

Considering that a role for brown fat in diet-induced thermogenesis was discovered by demonstrating changes in feed efficiency (Rothwell & Stock, 1979), we calculated the weight gain of mice as a proportion of their caloric intake to obtain a crude estimate of energy expenditure. We found that change in feed efficiency in $Pomc^{Caspase}$ mice was significantly elevated within two weeks of surgery (2w, p<0.0001), however the effect appeared to diminish across the six-week experimental period ($p_{treatment}$=0.0019, $p_{interaction}$=0.0001) (**Figure 4.3E**). This indicates that POMC neuron ablation may

reduce energy expenditure, albeit temporarily, potentially by means of reducing thermogenesis in brown fat. Indeed, we observed that POMC-ablation gradually reduced brown fat temperature in the calorically-sated state as recorded during the light cycle (6w, p=0.0210; $p_{treatment}$=0.0398) (**Figure 4.3F**).

Six weeks following virus injection, we investigated BAT thermogenesis in overnight fasted mice following refeeding in Pomc^{Caspase} and Pomc^{eGFP} mice, and compared these to baseline measurements that were made prior to virus injection, to account for inter-subject variability and order effects. We found that while refeed-induced BAT thermogenesis appeared to be blunted in both groups following surgery, this reduction was significantly greater in Pomc^{Caspase} mice ($p_{time(refeed)\ x\ time(surgery)\ x\ virus}$=0.0020) (**Figure 4.3G$_1$**). This effect was also reflected by a significantly reduced AUC in POMC-deficient mice compared to baseline postprandial thermogenesis (9.2 ± 2.4%, p=0.0003), while a smaller reduction that did not meet statistical significance was observed in Pomc^{eGFP} mice (3.9 ± 1.4%, p=0.0806) (**Figure 4.3G$_1$, inset**). These studies indicate that permanent loss-of-function of hypothalamic POMC neurons also attenuates the engagement of brown fat thermogenesis in the postprandial state.

Intriguingly, hypothalamic POMC deletion reduced postprandial thermogenesis in spite of dramatic increases in food intake from baseline compared to control-injected mice ($p_{time(refeed)\ x\ time(surgery)\ x\ virus}$=0.0002) (**Figure 4.3G$_2$**). Compared to pre-surgery refeed food intake, GFP-injected mice showed no significant change in food intake at any time point (1-24h, p>0.05). In contrast, hypothalamic POMC ablation evoked a marked increase in food intake where mice consumed 98.2 ± 31.5% and 61.2 ± 14.9% more food at 8 and 24 hours, respectively, compared to pre-surgery refeeding (8h, p=0.0005; 24h, p<0.0001). Furthermore, comparison of food intake between virus-treatment groups indicated a 33.9% increase after 24 hours (p<0.0001), highlighting the long-term satiety role driven by hypothalamic POMC neurons.

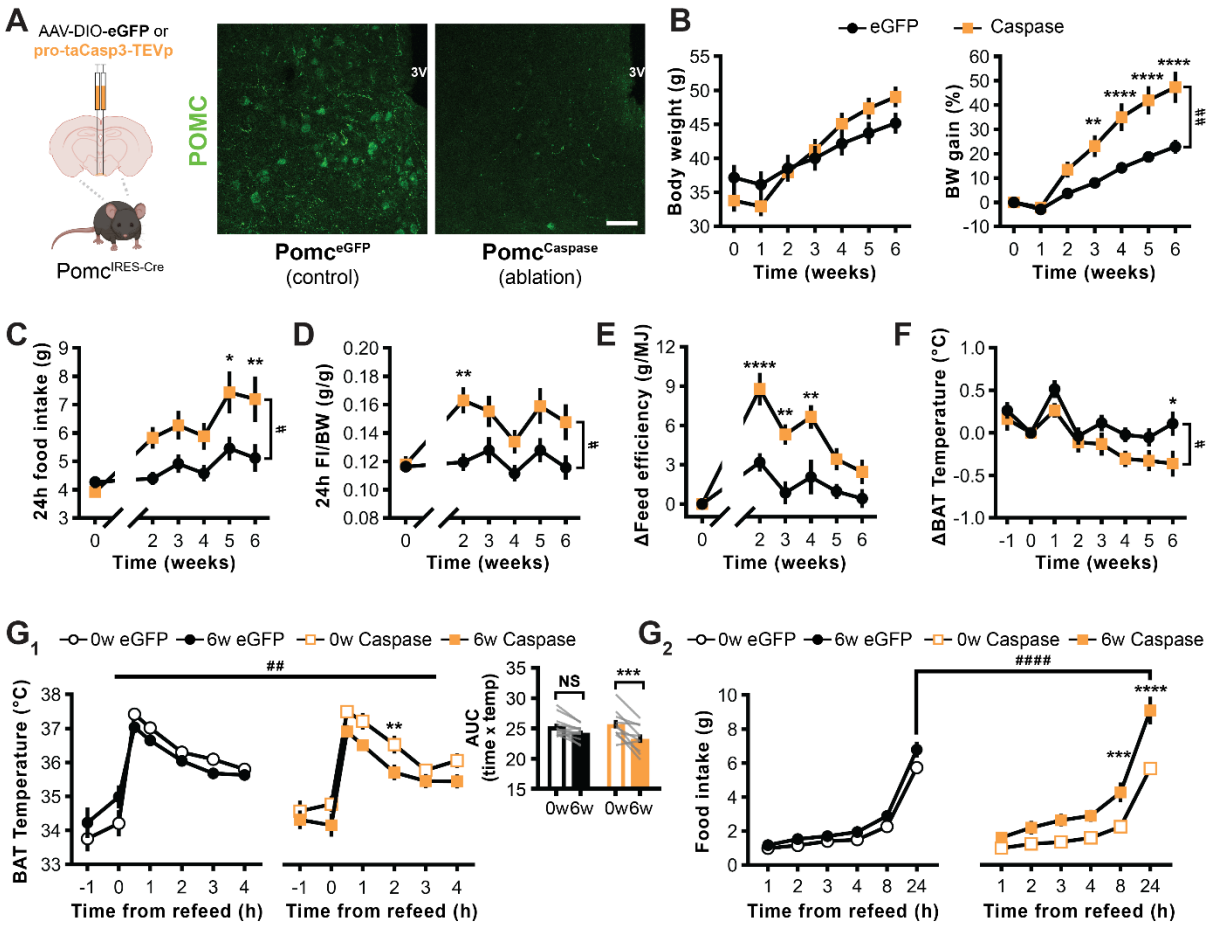

Figure 4.3 | Ablation of hypothalamic POMC neurons attenuates fast-refeeding thermogenesis in brown fat

(A) A Cre-dependent AAV was injected bilaterally into the mediobasal hypothalamus of Pomc$^{IRES\text{-}Cre}$ mice, encoding for pro-taCasp3-TEVp ("Caspase"), a pro-apoptotic enzyme to ablate POMC neurons, or eGFP as control (Pomc^{Caspase} and Pomc^{eGFP}, respectively). Representative confocal microphotographs revealing immunoreactive POMC cell bodies are dramatically reduced in POMC^{Caspase} mice compared to control POMC^{eGFP} mice. Scale bar, 50µm. 3V, third ventricle. **(B)** Diagram depicting body weight (left) and body weight gain as a percentage of body weight at surgery (right) of Pomc^{Caspase} and Pomc^{eGFP} mice. Changes in body weight were analysed by repeated measures (time factor) two-way ANOVA followed by Sidak's multiple comparisons test (absolute BW, n = 12 (eGFP) and n = 10 (Caspase) animals; treatment $F(1, 20) = 0.07339$, p=0.7892; time $F(6, 120) = 187.5$, p<0.0001; interaction $F(6, 120) = 18.60$, p<0.0001. 0-6w, all p>0.05. BW gain (%), n = 12 (eGFP) and n = 10 (Caspase) animals; treatment $F(1, 20) = 13.25$, $^{\#\#}p$=0.0016; time $F(6, 120) = 114.7$, p<0.0001; interaction $F(6, 120) = 13.97$, p<0.0001. 0w, 1w, p>0.9999; 2w, p=0.2137; 3w, $^{**}p$=0.0067; 4w, 5w, 6w, $^{****}p$<0.0001). **(C)** Diagram depicting daily food intake following virus injection averaged across the span of week. Food intake was not measured in the week immediately after surgery (week 1). Changes in food intake were analysed by repeated measures (time factor) two-way ANOVA followed by Sidak's multiple comparisons test (n = 12 (eGFP) and n = 10 (Caspase) animals; treatment $F(1, 20) = 5.660$, $^{\#}p$=0.0274; time $F(5, 100) = 22.83$, p<0.0001; interaction $F(5, 100) = 6.169$, p<0.0001. 0w, p=0.9953; 2w, p=0.1423; 3w, p=0.1890; 4w, p=0.2237; 5w, $^{*}p$=0.0137; 6w, $^{**}p$=0.0081). **(D)** Diagram depicting daily food intake relative to daily body weight following virus injection averaged across the span of week. Food intake was not measured in the week immediately after surgery (week 1). Changes in food intake were analysed by repeated measures (time factor) two-way ANOVA followed by Sidak's multiple comparisons test (n = 12 (eGFP) and n = 10 (Caspase) animals; treatment $F(1, 20) = 6.399$, $^{\#}p$=0.0199; time $F(5, 100) = 9.632$, p<0.0001; interaction $F(5, 100) = 3.852$, p=0.0031. 0w, p>0.9999; 2w, $^{**}p$=0.0034; 3w, p=0.1497; 4w, p=0.3614; 5w, p=0.0727; 6w,

p=0.0603). **(E)** Diagram depicting the change in feed efficiency of mice from virus injection, as calculated by their weekly weight gain as a proportion of weekly energy consumption from food. Food intake was not measured in the week immediately after surgery (week 1), and hence feed efficiency could not be calculated in this week. Changes in feed efficiency were analysed by repeated measures (time factor) two-way ANOVA followed by Sidak's multiple comparisons test (*n* = 12 (eGFP) and *n* = 10 (Caspase) animals; treatment $F(1, 20) = 12.72$, $^{\#\#}p=0.0019$; time $F(5, 100) = 23.76$, $p<0.0001$; interaction $F(5, 100) = 5.619$, $p=0.0001$. 0w, $p>0.9999$; 2w, $^{****}p<0.0001$; 3w, $^{**}p=0.0019$; 4w, $^{**}p=0.0012$; 5w, $p=0.2179$; 6w, $p=0.4484$). **(F)** Diagram depicting the change in BAT temperature (averaged across the span of a week) relative to week 0 when viruses were injected. Changes in BAT temperature were analysed by repeated measures (time factor) two-way ANOVA followed by Sidak's multiple comparisons test (*n* = 12 (eGFP) and *n* = 10 (Caspase) animals; treatment $F(1, 20) = 4.835$, $^{\#}p=0.0398$; time $F(7, 140) = 9.672$, $p<0.0001$; interaction $F(7, 140) = 1.341$, $p=0.2357$. -1w, $p=0.9969$; 0w, $p>0.9999$; 1w, $p=0.5805$ 2w, $p=0.9997$; 3w, $p=0.6138$; 4w, $p=0.4394$; 5w, $p=0.4836$; 6w, $^{*}p=0.0210$). **(G_1 and G_2)** Diagrams depicting the BAT temperature with AUC (G_1) and food intake (G_2) following the refeeding of overnight fasted mice as either the average of two pre-surgery fast-refeeds (0w, week zero; open circles/squares) or six weeks following virus injection (6w; closed circles/squares). G_1; changes in BAT temperature were analysed by repeated measures ($time_{refeed}$ and $time_{surgery}$ factors) three-way ANOVA followed by Tukey's multiple comparisons test (*n* = 12 (eGFP) and *n* = 10 (Caspase) animals; $time_{refeed}$ $F(5, 100) = 99.70$, $p<0.0001$; $time_{surgery}$ $F(1, 20) = 19.46$, $p=0.0003$; virus $F(1, 20) = 0.006719$, $p=0.7981$; interaction: $time_{refeed}$ x $time_{surgery}$ $F(5, 100) = 3.880$, $p=0.0030$; interaction: $time_{refeed}$ x virus $F(5, 100) = 0.2221$, $p=0.9522$; interaction: $time_{surgery}$ x virus $F(1, 20) = 8.037$, $p=0.0102$; interaction: $time_{refeed}$ x $time_{surgery}$ x virus $F(5, 100) = 4.106$, $^{\#\#}p=0.0020$. *Within-group 0w to 6w multiple comparisons:* eGFP: 0h, $p=0.0181$; other time points, $p>0.05$. Caspase: 2h, $^{**}p=0.0098$; other time points, $p>0.05$) and AUC by repeated measures (time factor) two-way ANOVA followed by Sidak's multiple comparisons test (*n* = 12 (eGFP) and *n* = 10 (Caspase) animals; virus $F(1, 20) = 0.1635$, $p=0.6902$; $time_{surgery}$ $F(1, 20) = 24.61$, $p<0.0001$; interaction $F(1, 20) = 4.069$, $p=0.0573$. eGFP: $p=0.0806$ (NS); Caspase: $^{***}p=0.0003$). G_2; changes in refeed food intake were analysed by repeated measures ($time_{refeed}$ and $time_{surgery}$ factors) three-way ANOVA followed by Tukey's multiple comparisons test (*n* = 12 (eGFP) and *n* = 10 (Caspase) animals; $time_{refeed}$ $F(5, 100) = 844.3$, $p<0.0001$; $time_{surgery}$ $F(1, 20) = 19.71$, $p=0.0003$; virus $F(1, 20) = 4.306$, $p=0.0511$; interaction: $time_{refeed}$ x $time_{surgery}$ $F(5, 100) = 18.36$, $p<0.0001$; interaction: $time_{refeed}$ x virus $F(5, 100) = 4.861$, $p=0.0005$; interaction: $time_{surgery}$ x virus $F(1, 20) = 5.452$, $p=0.0301$; interaction: $time_{refeed}$ x $time_{surgery}$ x virus $F(5, 100) = 5.281$, $p=0.0002$. *Within-group 0w to 6w multiple comparisons:* eGFP: all time points, $p>0.05$. Caspase: 8h, $^{***}p=0.0005$; 24h, $^{****}p<0.0001$; other time points, $p>0.05$. *Between-group multiple comparisons:* 24h, $^{\#\#\#\#}p<0.0001$. All other time points, $p>0.05$).

Data are represented as mean ± SEM in all diagrams and individual values labelled by paired lines in G_1.

4.4 Discussion

Hypothalamic POMC neurons and associated MC3/4R have a well-established role in the control of energy homeostasis, however it is not presently understood whether POMC neurons play an acute role in the modulation of BAT thermogenesis immediately following meal consumption. This is an essential piece of information if we are to better understand the nature of the central neural control of postprandial thermogenesis. Here we present data to corroborate the sufficiency of (chemogenetically-mediated) POMC neuron activation to increase brown fat temperature specifically through the engagement of downstream MC3/4Rs. In addition, we demonstrate through acute loss-of-function studies that hypothalamic POMC neurons and central MC3/4R signalling contribute to postprandial thermogenesis in brown fat, indicating that prandial stimuli rapidly activate uncoupled respiration through the central melanocortin system. Moreover, the chronic disruption (caspase-mediated ablation) of hypothalamic POMC signalling recapitulated the reduced postprandial thermogenesis seen with acute inactivation of POMC cells, as well as evoking enduring reductions in BAT temperature throughout the periprandial period. Our findings endorse a schema whereby the postprandial activation of hypothalamic POMC neurons is necessary to recruit the complete facultative component of diet-induced thermogenesis in brown fat.

4.4.1 Rationale

These studies were undertaken primarily to extend the findings presented in **Chapter 3**, that hypothalamic POMC neurons with a defined polysynaptic projection to brown fat are largely excited by elevations in extracellular glucose, where glucose was used as an experimentally convenient and appropriate surrogate of a meal. To reproduce the studies in an *in vivo* context, the experiments here were originally carried out with intention to verify the contribution of POMC neurons to *glucose*-induced thermogenesis in brown fat. However, we experienced difficulties related to evoking robust BAT thermogenic responses to peripheral or central administration of a glucose bolus. Irrespective of the dose of glucose administered and metabolic state of the animal (i.e. fasted or calorically sated), the enduring hyperthermia associated with the stress of experimenter-handling obfuscated any such response above control injection (data not presented). Despite extensive efforts, these experimental "complications" consistently yielded unreliable data. This outcome may seem at odds with reports that intracerebroventricular and intra-hypothalamic infusions of glucose stimulate BAT SNA (Sakaguchi & Bray, 1987, 1988; Holt & York, 1989; Tovar *et al.*, 2013), however in each of the preceding cases, electrophysiological recordings from BAT sympathetic nerves were necessarily performed in anaesthetised animals. Nevertheless, in hindsight the experimental challenges are unsurprising considering psychosocial stress is known to engage sympathetic nerves innervating brown fat via cortical and hypothalamic circuitry (Kataoka *et al.*, 2014; Kataoka *et al.*, 2020).

While the original intention was to create consistency between the *ex vivo* (i.e. data presented in **Chapter 3**) and *in vivo* approaches, the fact remains that glucose was used primarily surrogate for a meal. In reality, the fast-refeed paradigm utilised in the experiments described here is a more appropriate representation of the postprandial state and has previously been shown to rapidly promote

heat production and increase UCP1 expression in interscapular brown fat (Mounien *et al.*, 2010; Lockie *et al.*, 2012; Li *et al.*, 2018). This approach not only guarantees the temporal precision of onset of meal consumption, which is requisite for measurement of transitory changes in temperature, but still encapsulates the energetically deplete-to-replete environment fashioned during *ex vivo* glucose-sensing studies.

4.4.2 Validation of melanocortin-driven thermogenesis

The sufficiency and necessity of the melanocortin system to influence BAT thermogenesis was explored here using modern chemogenetic and Cre-lox recombination technologies (Armbruster *et al.*, 2007; Tsien, 2016). In light of reports that Pomc-Cre BAC transgenic mice show embryonic expression of Cre in neuronal progenitor cells that do not express POMC in adulthood (Padilla *et al.*, 2012), we adopted the use of the $Pomc^{IRES\text{-}Cre}$ transgenic strain to circumvent potential confounds associated with non-specific recombination. Consistent with the original publication (Fenselau *et al.*, 2017), we demonstrate that $Pomc^{IRES\text{-}Cre}$ mice exhibit excellent efficiency and specificity of Cre expression within POMC neurons in the ARC and RCA, and hence can verify their adequacy to specifically modulate melanocortin activity. Importantly, we confirmed through current-clamp recordings of DREADD-transfected POMC cells that the CNO-induced activation of Gq (via hM3Dq) signalling depolarises and promotes action potential firing, while Gi (via hM4Di) signalling leads to hyperpolarisation and suppression of neuronal activity, consistent with previous studies implementing similar strategies (Atasoy *et al.*, 2012; Zhan *et al.*, 2013).

The view that melanocortin signalling increases energy expenditure, particularly by means of SNS activation, has been extensively examined (see review Krashes *et al.* (2016)). Using DREADDs, we confirmed the sufficiency of hypothalamic POMC neuron activity to acutely evoke BAT thermogenesis. This dramatic thermogenic response occurs even during the early light-period and calorically-sated state, when POMC neuron activity is typically at its maximum (Mandelblat-Cerf *et al.*, 2015). BAT temperature peaked within less than an hour of CNO injection, recapitulating the rapid response observed using the Pomc-Cre BAC transgenic mouseline (Fenselau *et al.*, 2017).

The heterogeneity of hypothalamic POMC neurons is often underappreciated; for example *Pomc* mRNA transcripts colocalise with other neuropeptides like CART and nociceptin (Adam *et al.*, 2002; Jais *et al.*, 2020), and CRACM studies reveal the existence of functional both GABAergic and glutamatergic POMC synapses (Dicken *et al.*, 2012; Jarvie & Hentges, 2012; Wittmann *et al.*, 2013; Atasoy *et al.*, 2014). In consideration of this, we extended our observations to investigate the contribution made specifically by α-MSH (rather than other transmitters) by pre-treating mice centrally with a MC3/4R antagonist. Indeed, the BAT temperature changes following activation of hypothalamic POMC cells were completely abolished by SHU9119, indicative of an melanocortin-dependent mechanism. In favour of this, we and others demonstrate that central (or peripheral) administration of MTII, the MC3/4R agonist, recapitulates the thermogenic response in brown fat (Williams *et al.*, 2003; Yasuda *et al.*, 2004; Song *et al.*, 2008; Enriori *et al.*, 2011). As such, we contend that the melanocortin

system is sufficient to drive thermogenesis in BAT and moreover is central to the coordination of postprandial thermogenesis given that POMC neurons are readily activated by meal-related stimuli.

4.4.3 Evidence for the involvement of the melanocortin system in the regulation of postprandial thermogenesis

Our primary aim was to delineate the contribution of meal-activated POMC neurons to the facultative component of postprandial thermogenesis in BAT. We demonstrated that chemogenetic inhibition of POMC cells had no effect on BAT temperature in energy-replete mice. However, both inhibition of hypothalamic POMC neurons or central MC3/4R antagonism prior to refeeding overnight-fasted mice significantly attenuated subsequent BAT temperature excursions. To our knowledge, this is the first direct evidence, using an acute loss-of-function model, that increased central melanocortin signalling promotes thermogenesis in brown fat directly subsequent to meal consumption. Other studies may have alluded to this fact, finding that infusion of a MC3/4R antagonist into the fourth ventricle just prior to the dark period (when rodents are active and food consummatory behaviour typically occurs) caused a reduction in core body temperature (Zheng *et al.*, 2005). However, it is unclear whether the change in core temperature was a consequence of reduced meal-induced thermogenesis in BAT.

We then extended our studies into a chronic loss-of-function setting by ablating hypothalamic POMC neurons using an established model to trigger Caspase-3-mediated apoptosis in a cell-specific manner (Yang *et al.*, 2013). Consistent with former studies of adult-onset ablation of POMC neurons, mice rapidly developed obesity gaining significantly more weight than controls over the experimental period (Zhan *et al.*, 2013). We observed that feed efficiency (weight gain relative to food intake) dramatically increased following POMC ablation, but the difference compared to controls tapered off by the end of the six-week experimental period. This measure is a crude indication that energy expenditure was reduced (albeit temporarily with a peak at approximately 2 weeks post-lesion) in POMC deficient mice, however we cannot categorically exclude other forms of inefficient weight gain like nutrient malabsorption or excretion, considering that a genetic model of hypothalamic POMC deficiency promotes increased urinary glucose excretion (Chhabra *et al.*, 2016; Chhabra *et al.*, 2017).

Nevertheless, BAT temperature during the light phase and calorically-replete state progressively decreased after virus injection (maximally reduced 6 weeks post-lesion), supportive of a “constitutive” role of melanocortin-induced thermogenesis outside of the acute postprandial period. The discrepancy in the timeline between changes in feed efficiency and (periprandial) BAT temperature (see **Figures 4.3E and F**) may be explained by a progressive worsening of the thermogenic capacity of BAT which, when combined with sub-thermoneutral housing (24-25°C) that was employed here, caused mice to adopt less metabolically-efficient thermogenic processes to maintain core body temperature. This type of compensation has been demonstrated to occur in a different context in which *Ucp1* knockout mice exhibited increased energy expenditure when housed at standard animal house conditions (18-22°C); an effect that is reversed to an obesity-promoting hypometabolism when *Ucp1* knockouts are housed at thermoneutrality (~30°C) (Enerback *et al.*, 1997; Liu *et al.*, 2003b; Feldmann *et al.*, 2009). Thus, paradoxically, POMC deletion may acutely reduce energy expenditure by blunting

diet-induced thermogenesis in BAT, but then the reliance on inefficient heat-production mechanisms reverses this change in expenditure, reflected by the return of feed efficiency to levels similar to GFP-injected controls. In support of maintained disruption to BAT thermogenesis (in spite of diminished feed efficiency), refeeding following an overnight-fast at the end of the six-week period revealed a remarkable attenuation in postprandial thermogenesis in POMC-ablated mice but not controls, consistent with our hypothesis that POMC neurons contribute to postprandial thermogenesis in BAT.

4.4.4 Melanocortin-independent regulators of postprandial thermogenesis?

It is worth noting that while both acute and chronic disruptions in hypothalamic POMC neuron signalling provided statistically significant reductions in postprandial brown fat temperature, these were only *partial* effects; far from a complete abolition of the thermogenic response. Notably, the residual thermogenic response was not due to an incomplete deactivation/ablation of hypothalamic POMC neurons, considering that a robust postprandial thermogenic response remained even in mice in which retrospective immunohistochemical analyses revealed a near complete (~95-99%) deletion of POMC neurons (data not shown). Instead, we propose that there are at least two other likely physiological explanations for this outcome.

4.4.4.1 Other, non-POMC central regulators

The first is that there are POMC-independent central pathways that are also recruited postprandially to activate BAT-directed SNA which contribute to the response. Indeed, there is evidence that other appropriately-positioned neuronal populations which access peripheral indicators of meal-consumption may contribute to the regulation of BAT thermogenesis. For example, also located within the arcuate nucleus, anabolic AgRP/NPY neurons are typically inhibited by signals related to energy-repletion such as glucose, insulin and leptin (van den Top *et al.*, 2004; Fioramonti *et al.*, 2007; Könner *et al.*, 2007; Mountjoy *et al.*, 2007). The postprandial reduction of central release of NPY, an established suppressor of sympathetic outflow to BAT (Egawa *et al.*, 1991; Nakamura *et al.*, 2017), may therefore relieve tonic sympathoinhibition and promote increased thermogenesis in brown fat. Furthermore, glucose-sensitive orexin and melanin-concentrating hormone (MCH) neurons of the lateral hypothalamus are implicated in the control of BAT-directed sympathetic output (Oldfield *et al.*, 2002; Burdakov *et al.*, 2006; Kong *et al.*, 2010). Indeed, infusion of MCH and/or orexin receptor agonists or antagonists into the lateral ventricle or directly into raphe pallidus modulates brown fat temperature and sympathetic tone (Verty *et al.*, 2010; Tupone *et al.*, 2011). Further experiments are required, then, to determine the involvement of other central neural circuits in mediating postprandial thermogenesis.

4.4.4.2 Peripherally-derived factors

An alternative explanation is the involvement of peripheral factor(s) which either directly or indirectly (through the CNS) recruit BAT thermogenesis in the postprandial state. In this vein, a recent publication reported the gut-derived hormone, secretin, is responsible for mediating thermogenesis in

brown fat upon refeeding (Li *et al.*, 2018). The authors demonstrate that elevations in circulating secretin following meal consumption drove BAT thermogenesis independently of β-adrenergic signalling, and that inactivation of secretin signalling (using a polyclonal antibody) completely abolished the thermogenic response to feeding overnight-fasted mice. However, these findings are difficult to reconcile with our current view of postprandial thermogenesis for a number of reasons: a) the authors report the complete absence of *any* thermogenic response, even obligatory thermogenesis, and; b) the secretin-dependent component of thermogenesis reported are within 60 minutes of meal consumption, which corresponds to the cephalic phase of postprandial thermogenesis in both rats and humans (Rothwell & Stock, 1984b; LeBlanc & Cabanac, 1989). This period is largely preabsorptive meaning the physiological response primarily occurs as a result of sensory cues or food anticipation (Henry *et al.*, 2010; Smeets *et al.*, 2010), and thus it is unclear how a gut-derived peptide mediates the *entire* thermogenic effect within this timeframe. Nonetheless, we agree with the authors that the SNS appears to contribute to facultative postprandial thermogenesis primarily during the absorptive phase (1-4 hours), and this has been corroborated in human studies using β-blockers (De Jonge & Garrel, 1997; Pezeshki *et al.*, 2016; Limberg *et al.*, 2017). This period of SNS engagement is largely temporally consistent with the attenuated BAT thermogenesis effects we observed following inactivation of melanocortin signalling and subsequent refeeding (see **Figures 4.2D$_2$ and E$_2$, 4.3G$_1$**).

There is also substantial evidence to suggest that meal-induced secretion of leptin could mediate changes in BAT-directed sympathetic outflow. Leptin has been shown to activate hypothalamic POMC neurons and thus promote BAT SNA (Elias *et al.*, 1998; Ste. Marie *et al.*, 2000; Cowley *et al.*, 2001), however this would not explain residual thermogenic responses observed here in POMC-ablated mice. Indeed, there are studies that demonstrate that leptin-induced activation of BAT SNA occurs independently of MC4R signalling (Haynes *et al.*, 1999; Enriori *et al.*, 2011). It is possible, instead, that BAT-projecting circuits in the POA and DMH are responsible for the sympathoexcitatory effects of leptin. Leptin receptor (LepR)-expressing neurons in these nuclei have been demonstrated to project multi-synaptically to brown fat (Zhang *et al.*, 2011). In this vein, leptin signalling in the DMH regulates energy expenditure in part by activation of BAT thermogenesis, and deletion of the LepR in the POA impairs HFD-induced elevations in energy expenditure (Rezai-Zadeh *et al.*, 2014; Yu *et al.*, 2018).

As an alternative to a centrally-mediated effect, it was recently indicated that postprandial elevations in *core* temperature are dependent, at least in part, on leptin-induced activation of brown fat thermogenesis, in a manner that is *independent* of the SNS (Perry *et al.*, 2020). The reports relating to leptin-regulated BAT thermogenesis are only further confounded by another study which concluded that leptin is *not* thermogenic (i.e. it does not stimulate the production of heat), but instead is *pyrexic* (i.e. it increases body temperature) (Fischer *et al.*, 2016). The authors demonstrated through infrared thermography that temperature of the tail, a major thermoregulatory organ in mice, dramatically reduces in response to leptin treatment (in *ob*/*ob* mice). This suggests that leptin functions to induce tail vasoconstriction which resultantly reduces thermal conductance (heat loss); thus, increasing core temperature without altering energy expenditure. This assertion is supported by another study that demonstrated that, under sub-thermoneutral conditions, leptin signalling maintains core body temperature in a manner that is not dependent on BAT thermogenesis, but instead through reducing

thermal conductance (heat loss) (Kaiyala *et al.*, 2016). In view of these reports, it remains to be determined, then, whether leptin signalling contributes to postprandial thermogenesis in brown fat.

4.4.4.3 Other technical considerations

We draw attention to the possibility of another, *technical*, consideration which may underestimate the true impact of melanocortin inactivation on postprandial thermogenesis in BAT. While telemetric recordings of brown fat temperature have been a mainstay in this field for over a decade and are assumed to be an accurate measure of BAT activity (Verty *et al.*, 2009; Meyer *et al.*, 2017), including the IPTT-300 transponder (Bio Medic Data Systems) employed here especially for measurements in mice (Kong *et al.*, 2012; Tan *et al.*, 2016), there is the possibility that these devices also measure, in some part, changes in *core* temperature particularly considering the very small volume of interscapular BAT in a mouse. Indeed, some studies concurrently record core and BAT temperature to gain an index of thermogenesis specifically attributed to BAT activity (Almeida *et al.*, 2012; Mohammed *et al.*, 2014). Moreover, there is a potential for BAT temperature measurements to be "contaminated" by heat produced from nearby skeletal muscle during the basic rest-activity cycles that accompany food-seeking behaviour (see Blessing (2018) for review). In light of these technical considerations, a thermogenic component (of unknown size) unrelated to sympathetically-mediated uncoupled respiration in BAT may influence our readings, obfuscating and diminishing the true effect size of hypothalamic POMC neuron inactivation/deletion on postprandial thermogenesis.

Nevertheless, we reconcile our findings with others presented in the literature and the potential of technical impediments by acknowledging that the central melanocortin system likely only contributes in part to facultative meal-induced thermogenesis in brown fat, and that future studies are needed to determine the relative contributions of other meal-related factors, or meal-responsive circuits, to the process.

4.4.5 Commentary on manipulations of food intake

While ancillary to the primary aims of this chapter, we also measured ingestive behaviour in mice following acute and chronic manipulations to central melanocortin circuitry. In addition to energy expenditure regulation. Opto- or chemo-genetic activation of hypothalamic POMC neurons is known to induce hypophagia, however, intriguing in relation to this phenomenon are reports that suppression of food intake only manifests on a long-term (~24 hour) timescale (Aponte *et al.*, 2011; Zhan *et al.*, 2013; Fenselau *et al.*, 2017), which contrasts dramatically with the rapidly-evoked voracious feeding observed following AgRP neuron stimulation (Aponte *et al.*, 2011; Krashes *et al.*, 2011). We observed that the DREADD-mediated activation of POMC neurons, as well as the central administration of a MC3/4R agonist, recapitulated published findings of suppressed 24-hour food intake, with the exception that we also observed indications of more rapidly-induced satiety. While not presented in the Results of this chapter, statistical analysis of (specifically) the four-hour feeding window subsequent to CNO injection revealed a significantly reduced intake for both chemogenetic and pharmacological activation of melanocortin signalling, a finding that is directly at odds with a recent report (Fenselau *et al.*, 2017).

One possible explanation for this deviation is that our experiments were performed during the early phase of the light period when drive to eat (i.e. AgRP neuron activity) is low, while Fenselau and colleagues measured food intake following POMC neuron stimulation at the onset of the dark cycle. Perhaps the depletion of energy stores fomented over the course of the light cycle (i.e. increasing AgRP neuron activation) resulted in the overriding of a rapidly-driven POMC satiety signal in their study, which otherwise, manifested under our experimental conditions of caloric repletion. This hypothesis is supported by the finding that concurrent optogenetic activation of both AgRP and POMC neurons produces a robust feeding response and rapid latency to eat, identical to that which occurs with activation of AgRP neurons alone (Atasoy *et al.*, 2012).

We also demonstrate that DREADD-mediated POMC inhibition or central MC3/4R antagonism in energy-deplete (overnight-fasted) caused overnight, but not short-term, increases in food intake; indicating that the presence of an orexigenic homeostatic signal at the time of POMC neuron or MC3/4R inhibition does not preclude long-term reductions in satiety. This finding extends previous indications that chemogenetic inhibition of hypothalamic POMC neurons induces an equivalently slow-to-mount hyperphagia in calorically-*replete* mice (Atasoy *et al.*, 2012; Üner *et al.*, 2019). Furthermore, a role for MC4R-regulated long-term satiety in energy-deplete mice was further corroborated by the deletion of hypothalamic POMC neurons. POMC-ablated mice consumed significantly more food over the 24-hour refeed period compared to controls, with no statistically significant change in short-term refeeding food intake. Moreover, daily food intake was increased in these mice, even when accounting for successive increases in body weight, substantiate a role for hypothalamic POMC neurons in the regulation of long-term satiety.

4.4.6 Conclusions

The central melanocortin system has an established role to promote adaptive thermogenesis in brown fat in periods of caloric excess, however direct evidence is lacking for its recruitment and associated thermogenesis following *acute* dietary intake. Here we affirm that DREADD-evoked activity of hypothalamic POMC neurons is sufficient to promote BAT thermogenesis through activation of downstream MC3/4R, ruling out the involvement of other neurotransmitters released by this neurochemically-heterogenous population in the mediation of POMC-driven thermogenesis. We demonstrate unambiguously, through both acute and chronic inactivation of central melanocortin signalling, that a temporally-defined dietary intervention invokes hypothalamic POMC activity to drive thermogenesis in brown fat. Collectively these studies substantiate the necessity of POMC neurons in the mediobasal hypothalamus to orchestrate adaptive energy-expending processes following acute bouts of feeding. These data thus extend the comprehensive body of literature which implicates hypothalamic POMC neurons as an integral processor of episodic signals relating to energetic status, and contributing to the acute recruitment of BAT activity in the postprandial state.

Chapter 5

The regulation of POMC neuron glucose-sensing by astrocyte-derived signals

5.1 Introduction

The physiological function of hypothalamic POMC neurons is largely attributed to their capacity to detect and integrate humoral signals relating to energy status. In view of the complexity associated with signalling in the hypothalamus, responsiveness to these sensory signals is unlikely to be homogeneous across all POMC neurons. Indeed, two topographically-segregated subpopulations of POMC neurons have been identified to respond to either, but not both, of the peripherally-derived hormones, leptin and insulin (Williams *et al.*, 2010). Furthermore, single-cell RNA sequencing technology revealed significant genetic variation between POMC-expressing neurons, leading to the identification of (at least) three genetically-distinct clusters (Campbell *et al.*, 2017; Lam *et al.*, 2017). POMC neurons are widely accepted to respond to elevations in extracellular glucose by depolarisation and concomitant increased action potential firing. The mechanism mediating this response has been primarily attributed to inactivation of K_{ATP} channels, which is proposed to occur following the neuron-autonomous intracellular metabolism of glucose into ATP (Ibrahim *et al.*, 2003; Parton *et al.*, 2007). However, in consideration of their functional and genetic heterogeneity, including our observations of formerly unidentified glucose-*inhibited* POMC neurons (see **Chapter 3**), the mechanisms regulating POMC neuronal glucose-sensing require further investigation.

There is mounting evidence that astroglial networks in the hypothalamus and brain stem can be instrumental in the neuronal detection of glucose availability. Glucose entry into the brain from the periphery is primarily facilitated by diffusion through glucose transporter-1 (GLUT1) which is expressed on astrocytic endfeet that ensheath cerebral vasculature (Kacem *et al.*, 1998; Devraj *et al.*, 2011). Disruption of brain glucose uptake by the deletion of astrocytic insulin receptors was shown to cause defects in glucose-induced satiety and peripheral glucose tolerance, likely as a result of disturbances to POMC neuron glucose-sensing (Garcia-Caceres *et al.*, 2016). Astroglial cells form large interconnected networks adjoined by gap-junction channels that permit their electrical and chemical coupling. Connexin 43 (Cx43) is one of three connexin proteins that mediate the formation of astrocytic syncytia by facilitating the passage of ions, or small molecules like glucose-derived metabolites, between astrocytes (through gap-junctions) or from astrocytes into the extracellular space (through hemi-channels) (see Giaume *et al.* (2010)). Orexin neurons in the lateral hypothalamus were demonstrated to require astrocyte-derived lactate (a glucose metabolite) to sustain their tonic firing, and the transduction of this signal is at least partially dependent on astrocytic Cx43 (Parsons & Hirasawa, 2010; Clasadonte *et al.*, 2017). Moreover, astrocyte-dependent metabolism of glucose in proportion to its extracellular availability can facilitate the *neuronal* sensing of glucose via the paracrine action of released metabolites. For example, the glucose-dependent release of astrocyte-derived purines (ATP and adenosine) can act on neuronally-expressed G-protein coupled receptors (GPCRs) to mediate glucose-induced changes in neuronal activity in the nucleus of the solitary tract and ventrolateral pre-optic area (McDougal *et al.*, 2013; Rogers *et al.*, 2016; Scharbarg *et al.*, 2016; Rogers *et al.*, 2018). A role for astrocyte-derived transmitters (gliotransmitters) in hypothalamic POMC neuron glucose-sensing is yet to be determined.

The propagation of calcium waves through connected astroglial networks (via gap-junctions) is considered to be a specific form of astrocyte “excitability” that can promote, or be the result of, reciprocal

communication between astrocytes and neurons (Scemes & Giaume, 2006). The calcium-dependent liberation of ATP from astrocytes can act on P2X/P2Y receptors expressed on adjacent neurons, or alternatively can be degraded into adenosine by extracellularly-expressed ectonucleotideases and signal through pre- and/or post-synaptic adenosine receptors (Fields & Burnstock, 2006; Garré *et al.*, 2010). Recently, chemogenetic and optogenetic technologies have been employed to "artificially" evoke astrocytic calcium waves, demonstrating the capacity for astrocyte-derived purines to modulate the activity of neighbouring neuronal populations (Gourine *et al.*, 2010; Savtchouk & Volterra, 2018; Durkee *et al.*, 2019). Within the hypothalamus, optogenetic activation of astrocytes was found to increase local adenosine production which signalled via the adenosine A_1 receptor (A_1R) to decrease food intake (Sweeney *et al.*, 2016). Similarly, chemogenetic activation of hypothalamic astrocytes reduced dark cycle food intake by inhibiting AgRP neurons through A_1R-dependent signalling (Yang *et al.*, 2015). However, these findings are in conflict with another study, which demonstrated that chemogenetic activation of astrocytes specifically within the ARC (not whole hypothalamus) evokes voracious feeding characteristic of AgRP neuron activation, but not did examine the mechanism responsible for astrocyte-regulated neuronal activation (Chen *et al.*, 2016).

Here, we aim to comprehensively investigate the heterogeneity associated with glucose-sensing POMC neurons in the ARC and RCA, with a focus on identifying previously unknown mechanism(s) that facilitate glucose-induced changes in neuronal activity. In light of the demonstrable role for gliotransmitters to regulate neuronal activity in the ARC and mediate neuronal glucose-sensing elsewhere in the brain, we hypothesised that astrocyte-derived adenosine communicates changes in extracellular glucose to neighbouring POMC neurons through a paracrine signalling mechanism.

5.2 Experimental Procedures

5.2.1 Preparation of brain slices for *ex vivo* recording

Acute hypothalamic brain slices from $Pomc^{eGFP}$ mice were prepared for subsequent whole-cell patch clamp electrophysiology. Overnight-fasted mice were anaesthetised with isoflurane and decapitated. Brains were rapidly collected into oxygenated ice-cold sucrose-modified aCSF (in mM, 200 sucrose, 1.9 KCl, 1.2 NaH_2PO_4, 26 $NaHCO_3$, 2.0 D-glucose, 8.0 D-mannitol, 0.5 ascorbic acid, 10 $MgCl_2$), and were cut into 250-300μm coronal sections encompassing the ARC and RCA using a vibratome (VT1000S; Leica, Cambridge, UK). Slices were transferred to recording aCSF (in mM, 127 NaCl, 1.9 KCl, 1.2 KH_2PO_4, 26 $NaHCO_3$, 1.0 D-glucose, 9.0 D-mannitol, 1.3 $MgCl_2$, 2.4 $CaCl_2$, 0.34 ascorbic acid; equilibrated with 95% O_2 and 5% CO_2, pH 7.3-7.4, 300-305mOsm/L) at 34-35°C for 25 mins, and then left to recover at room temperature for >45 minutes before electrophysiological recordings were conducted. For a subset of experiments, brain slices were prepared from *ad libitum* fed $Pomc^{eGFP}$ mice using the same method, with the exception that both cutting and recording solutions contained 5.0 D-glucose and 5.0 D-mannitol (mM).

5.2.2 Electrophysiology: Investigating POMC glucose-sensing mechanism

For recording, brain slices were transferred to a recording chamber and constantly bathed in aCSF (flow rate = 3-6mL/min). GFP-expressing POMC neurons in the ARC and RCA were identified using epifluorescence and differential interference contrast microscopy, and whole-cell patch clamp recordings were made using a Multiclamp 700A amplifier (Axon Instruments, Foster City, CA, USA). Patch-pipettes were pulled using a horizontal puller (Sutter Instruments, USA; P1000 model) from thin-walled borosilicate glass (Harvard Apparatus; GC150-TF10) to resistances between 6 and 10MΩ when filled with intracellular recording solution (in mM, 140 K-gluconate, 10 HEPES, 10 KCl, 1.0 Na_2EGTA and 1.0 or 2.0 Na_2ATP; pH adjusted to 7.35 with KOH, osmolarity adjusted to ~305mOsm/L with sucrose).

In order to investigate the mechanism of glucose-sensing in POMC neurons, glucose-responsive cells were first identified by increasing extracellular D-glucose from 1.0mM to 5.0mM. Neurons were considered glucose-sensing if membrane potential changes were ≥2.0mV for a glucose-induced excitation or ≤−2.0mV for a glucose-induced inhibition. Furthermore, changes in membrane potential and/or firing rate were required to be time-locked to the arrival of increased glucose at the brain slice to be considered a true response, and to exhibit a complete or partial reversal of the response upon washout to 1.0mM glucose. To test the involvement of adenosine receptors, transporter channels or astrocyte metabolism in POMC neuron glucose-sensing, the relevant inhibitor was bath-applied: a) in most cases, following washout of glucose and subsequent reversal of the response for at least 5 minutes before high glucose was re-applied, or b) in a few cases, while the high glucose was still present to determine the potential for reversal of the response by a pharmacological agent. Glucose-induced changes in membrane potential and/or firing rate in the presence of the inhibitor were quantified and compared to the baseline response. For data analysis, the signal was digitised at 2-10 kHz and

analysed utilising a computer running pClamp10 (Axon Instruments). Membrane potential values were not compensated to account for liquid junction potential (−9 mV).

5.2.3 Adenosine receptor antagonism food intake and energy expenditure studies

C57Bl/6^{WT} mice were used to investigate how central antagonism of A_1R affects food intake and energy expenditure during the dark cycle (feeding phase). In order to deliver drugs centrally, C57Bl/6^{WT} mice were implanted with an indwelling cannula into the lateral ventricle. The A_1R antagonist, DPCPX, was injected intracerebroventricularly (300ng, in 2uL 20% DMSO in saline) in the half-hour preceding the dark cycle, and food intake and energy expenditure were measured at regular intervals in a cross-over design. A separate cohort of mice were injected with antagonists of the remaining adenosine receptors, A_{2A}R (SCH442416), A_{2B}R (PSB603) and A_3R (MRS1523) to determine their involvement in food intake regulation. In all experiments, volume-matched vehicle was used as control.

To measure energy expenditure, mice were individually housed in an indirect calorimeter (LabMaster; TSE-systems, Bad Homburg, Germany) which measured consumption and production of oxygen and carbon dioxide, respectively, to indirectly calculate energy expenditure. Airflow was set at 0.5L/min, and gas was sampled from each cage for 3.75 minutes at 30-minute intervals. After 48 hr acclimatisation, mice were injected with an adenosine receptor antagonist or vehicle immediately before the onset of the dark period. The experiment was crossed-over following a 48-hour washout period. Data was analysed as half-hourly readings and presented relative to animal body weight.

5.2.4 Electrophysiology: Investigating astrocyte communication to POMC neurons

In order to determine how the activity of MBH astrocytes affects POMC neurons, we transfected astrocytes to express the Gq-coupled DREADD, hM3Dq. To achieve DREADD expression specifically in astrocytes surrounding POMC neurons, an AAV encoding the receptor with a GFAP promoter was injected into the ARC and RCA. Specificity of DREADD expression in astrocytes was first confirmed by AAV injection into C57Bl/6^{WT} mice (C57Bl/6^{WT}::GFAP^{hM3Dq}), whose brains were collected two weeks later and processed immunohistochemically for GFAP, NeuN (neuronal marker) and mCherry (see *Section 5.2.8*).

Following confirmation of astrocyte-specific expression, AAV was injected bilaterally into Pomc^{eGFP} mice (Pomc^{eGFP}::GFAP^{hM3Dq}). At least two weeks later, hypothalamic brain slices for electrophysiology were prepared (see *Preparation of brain slices for ex vivo recording* above) and whole-cell current-clamp recordings were made from GFP-expressing POMC neurons in the field of mCherry-expressing astrocytes. Following stabilisation of POMC neuron membrane potential and firing, the hM3Dq-receptor agonist, CNO (1μM), was briefly bath applied (3-5 minutes) to activate astrocytes and promote gliotransmission, and the subsequent change in POMC neuron membrane potential and firing rate was quantified. In a subset of cells, CNO was washed off and then re-applied in the presence of a non-selective adenosine receptor antagonist (CGS15943) and ectonucleotidease inhibitor (PSB12379) to test the contribution of astrocyte-derived nucleosides to POMC neuron responses.

5.2.5 Fos analysis

In a separate set of experiments, POMC neuron activation was assessed *in vivo* following CNO-induced activation of MBH astrocytes. At least two weeks after virus injection and four consecutive days of handling, $Pomc^{eGFP}$::$GFAP^{hM3Dq}$ mice received i.p. injection of vehicle (5% DMSO in saline) or CNO (1mg/kg). Mice were perfused 90 minutes following injection, and brain tissue was collected and processed immunohistochemically for Fos protein (see *Section 5.2.8*), a marker of recent neuronal activation. Quantification of Fos expression in POMC neurons was performed by counts made of colocalised Fos-related immunofluorescence with antibody-amplified GFP expression in POMC neurons. 10 x 1.0µm z-stack sections were taken of one hemisphere of the RCA and rostral, mid and caudal ARC in each animal, and counts were made from the maximum intensity projection images using ImageJ software. Data are reported as total Fos numbers per hemisphere or as the proportion of activated relative to total POMC neurons.

5.2.6 Astrocyte activation food intake and brown adipose tissue temperature studies

To test the hypothesis that astrocyte activation recruits both POMC and AgRP neurons, $Agrp^{IRES\text{-}Cre}$ mice received bilateral injections of AAV-GFAP-hM3Dq-mCherry into the MBH, in conjunction with a second virus that Cre-dependently encoded either mCherry as control ($GFAP^{hM3Dq}$::$Agrp^{mCherry}$) or the inhibitory Gi-coupled hM4Di DREADD receptor ($GFAP^{hM3Dq}$::$Agrp^{hM4Di}$) under a human synapsin (neuron-specific) promoter. With this design, administration of the DREADD ligand, CNO, only activates astrocytes in $GFAP^{hM3Dq}$::$Agrp^{mCherry}$ mice, or concurrently activates and inhibits astrocytes and AgRP neurons, respectively, in $GFAP^{hM3Dq}$::$Agrp^{hM4Di}$ mice. Food intake and brown adipose tissue (BAT) temperature, which are both influenced by POMC and AgRP neuron activity, were monitored in the hours subsequent to intraperitoneal injection of vehicle or CNO (3mg/kg). To control for the effect of AgRP neuron inhibition, a third group of $Agrp^{IRES\text{-}Cre}$ mice injected only with the AAV encoding hM4Di ($Agrp^{hM4Di}$) were included in experiments. Interscapular brown fat temperature was measured using IPTT-300 temperature-sensitive transponders (Bio Medic Data Systems) and collected using a handheld reader (see *Chapter 2: General Methods*).

5.2.7 Stereotaxic cannulation and virus injection

Mice were anaesthetised and placed in a stereotaxic apparatus (mouse adaptor 51625, Stoelting, Wood Dale IL). After exposing the skull via midline incision, a small hole was drilled for cannulation through which there was subsequent delivery of pharmacological agents, or for injection of AAVs encoding DREADDs. For cannulation, a 26-gauge guide cannula (InVivo1, Roanoke, WA) was inserted into the brain just above the lateral ventricle (coordinates from bregma: AP: -0.5mm, ML: 1.0mm, DV: −1.7mm) and held in place by light-cured bond and dental cement. A dummy cannula was inserted into the guide when not in use to keep the cannula patent and free from contaminant. For injection of adenosine receptor antagonists, a custom-designed 33-gauge injector was attached to PE tubing connected to a 10µL syringe (Hamilton Company, USA) and inserted into the guide cannula

extending 0.5mm past the tip, into the lateral ventricle. Pharmacological agents were delivered at approximately 2µL/min.

Bilateral AAV injections were made stereotaxically into the mediobasal hypothalamus of C57Bl/6^{WT}, Pomc^{eGFP} and Agrp$^{IRES\text{-}Cre}$ mice to encompass both the ARC and RCA (60nL per side, coordinates from bregma: AP: −1.3mm, ML: ±0.3mm, DV: −5.8mm) via pulled-glass pipettes (tip diameter ≈ 40µm) using a pressure-injection system. Viruses were delivered over 5 minutes, and pipettes left in place for a further 5 minutes before removal from the brain to minimise efflux of the injectate. C57Bl/6^{WT} (for virus validation) and Pomc^{eGFP} (for electrophysiology and Fos experiments) mice were injected with AAV-GFAP-hM3Dq-mCherry (Addgene viral prep #50478-AAV5, titre ≥ 7×10^{12} vg/mL) diluted 1:3 in sterile PBS. For food intake and BAT temperature experiments, Agrp$^{IRES\text{-}Cre}$ mice were injected with a 1:3 mixture of AAV-GFAP-hM3Dq-mCherry and either AAV-hSyn-DIO-mCherry (Addgene viral prep #50459-AAV5, titre ≥ 7×10^{12} vg/mL; GFAP^{hM3Dq}::Agrp^{mCherry}) or AAV-hSyn-DIO-hM4Di-mCherry (Addgene viral prep #44362-AAV5, titre ≥ 7×10^{12} vg/mL; GFAP^{hM3Dq}::Agrp^{hM4Di}), or with only AAV-hSyn-DIO-hM4Di-mCherry (Agrp^{hM4Di}). The plasmids used for virus manufacture were a gift from Brian Roth (DREADDs and mCherry control).

At the conclusion of experiments, all virally-transfected mice were perfused and brains were processed (see *Section 5.2.8*) for accuracy and efficiency of viral-transfection. For experiments involving astrocyte-specific expression of hM3Dq DREADD, only mice which exhibited substantial bilateral expression of the mCherry reporter that was wholly or predominantly contained within the rostro-caudal extent of the RCA and ARC were used for analysis. For experiments involving AgRP neuron-specific expression of hM4Di DREADD, only mice which exhibited substantial bilateral expression of mCherry that was wholly contained within the boundaries of the rostro-caudal extent of the ARC and RCA were used for analysis.

5.2.8 Brain tissue preparation & immunohistochemistry

To examine the brain for accuracy of virus injection or for Fos expression, mice were terminally anaesthetised with i.p. sodium pentobarbitone (>100mg/kg) and perfused transcardially first with phosphate-buffered saline (pH = 7.4) and then 4% PFA solution in PB. The brains were stored in the same fixative overnight at 4°C, and then transferred into 30% sucrose PB solution at 4°C for at least 24 hours. Using a cryostat (Leica), 35µm coronal sections of the brain were collected into four equal series and stored at −20°C in cryoprotectant until processing.

Brain sections were washed in 0.1M PB, and then blocked in 10% NHS and 0.3% PBT for at least 30 minutes. Sections were then incubated overnight at room temperature in 1% NHS PBT containing primary antisera (chicken anti-GFP, Abcam 13970, 1:2000; rabbit anti-DsRed, Living Colours 632496, 1:2000; goat anti-GFAP, Abcam ab53554, 1:1000; rabbit anti-NeuN, Merck Millipore ABN78, 1:500; rabbit anti-Fos, Santa Cruz sc-52, 1:350; rabbit anti-Adenosine A_1 receptor, Abcam ab82477, 1:200; rabbit anti-Adenosine A_{2A} receptor, Abcam ab3461, 1:50; rabbit anti-Adenosine A_3 receptor, Santa Cruz sc-13938, 1:20). The next morning sections were washed in 1% NHS PB and then incubated for 2h at room temperature in PB with Alexa-fluorophore conjugated secondary antibodies (Donkey anti-chicken Alexa488, Jackson Laboratories 1:500; Donkey anti-rabbit Alexa594, Abcam,

1:400; Donkey anti-rabbit Alexa647, Abcam 1:400; Donkey anti-goat Alexa647, Abcam 1:400). After several washes in PB, sections were mounted onto glass slides and coverslipped with VECTASHIELD® HardSet™ with DAPI mounting medium. Fluorescence images were captured using a Leica SP5 5-channel confocal microscope using a 10x dry objective or 20-40x immersion objective with 6-10x 1.0-1.5µm Z-stacks.

5.2.9 Drugs

For electrophysiological and *in vivo* experiments, drugs were made up as concentrated stocks prior to experiments and diluted in recording aCSF (electrophysiology) or vehicle (*in vivo*) just prior to use, with the exception of Gap26 (AusPep; used at 200µM) which was dissolved in aCSF from solid on the day of recording. DPCPX (Tocris; used at 100nM or 300ng/2µL for i.c.v.), SCH442416 (Tocris; 300ng/2µL for i.c.v.), PSB603 (Tocris; 300ng/2µL for i.c.v.), MRS1523 (Santa Cruz; 300nM or 100ng/2µL for i.c.v.), CGS15943 (Tocris; 1µM), Gabazine (Tocris; 10µM), SDZ WAG 994 (Tocris; 500nM), BAY876 (Tocris; 1µM) and clozapine-*N*-oxide (CNO, Carbosynth; 1µM or 3mg/kg for i.p.) were dissolved in DMSO and stored at −20°C. Carbenoxolone (Sigma-Aldrich; used at 100-200µM), PSB12379 (Tocris; 1µM) and fluorocitrate (Sigma-Aldrich, 50µM) were dissolved in distilled water and stored at −20°C. The fluorocitrate stock was prepared by dissolving DL-Fluorocitric acid barium salt (Sigma-Aldrich, F9634) in 1.5M HCl, and then adding equimolar sulfate (as Na_2SO_4) to precipitate the barium out of solution as $BaSO_4$. The pH of the supernatant solution was then neutralised to ≈ 7.4 by dropwise addition of 5M NaOH.

The final concentration of DMSO when drugs were dissolved in aCSF for electrophysiological recordings did not exceed 0.05%. For intracerebroventricular injection, the final concentration of DMSO was 10% (MRS1523 and vehicle) or 20% (DPCPX, SCH442416, PSB603 and vehicle) diluted in sterile saline. For intraperitoneal injection of CNO, the injected concentration of DMSO was 5% in saline. For intracerebroventricular injections, a volume of 2µL solution was delivered over approximately one minute. Intraperitoneal injection volumes were performed at 3mL/kg body weight.

5.2.10 Statistical analyses

Data was graphed and statistically analysed using GraphPad Prism 8.0 (Graphpad Software; CA, USA); significance for all tests was set at $p < 0.05$. Grouped data is presented as mean ± SEM unless otherwise indicated. Individual data points (paired and unpaired) are also presented in some grouped data sets. Chi-squared Test for Independence was used to determine differences in glucose-responsiveness of POMC neurons in the ARC compared to RCA. Paired *t* tests were used to compare changes in membrane potential and action potential firing rate in glucose-responsive neurons at baseline and in the presence of a pharmacological inhibitor. Repeated measures two-way ANOVA with Sidak's multiple comparisons was used to compare changes in food intake and energy expenditure following central administration of adenosine receptor antagonists as well as changes in Fos expression across rostro-caudal levels of the ARC and RCA following chemogenetic activation of astrocytes. One sample *t* tests were used to measure change in membrane potential and action potential frequency of

POMC neurons following chemogenetic activation of astrocytes, while paired *t* test was used to compare electrophysiological parameter changes induced by CNO in the presence and absence of pharmacological inhibitors. Changes in food intake (1-8h) and BAT temperature following *in vivo* chemogenetic activation of astrocytes were analysed using repeated measures two-way ANOVA with Sidak's multiple comparisons, while the 24h food intake interval was analysed using paired *t* test. Note that for energy expenditure and BAT temperature experiments, baseline “pre-intervention” time point(s) were excluded from statistical analysis so not to confound the analysis of intervention. Full statistical reports are stated either in the body text or in the figure legends.

5.3 Results

5.3.1 POMC neuron glucose-responsiveness is heterogeneous

We prepared acute *ex vivo* hypothalamic brain slices from overnight fasted Pomc^{eGFP} mice, and made whole-cell current clamp recordings from POMC neurons throughout the rostro-caudal extent of the ARC and RCA. We increased the extracellular glucose concentration from 1.0 to 5.0mM and noted changes in membrane potential and firing activity indicative of glucose-sensitivity. We recorded from a total of 452 POMC neurons in the mediobasal hypothalamus (RCA, *n* = 195; ARC, *n* = 257) and observed a range of glucose-induced changes in electrical activity; including those that have been previously reported and some not yet described in POMC neurons (**Figures 5.1A$_1$ and A$_2$**). Most POMC neurons in the RCA (46%) and ARC (55%) were not responsive to increased glucose, displaying no sustained change in membrane potential or firing rate when D-glucose levels increased to 5.0mM (**Figure 5.1B$_1$**). Current injection steps at baseline and during 5.0mM glucose application reveal similar current-voltage (IV) relationships in non-responsive (NR) POMC neurons, consistent with a lack of change in neuronal conductance (**Figure 5.1B$_2$**). The most prevalent responses were glucose-induced excitations (GE; 39% RCA, 33% ARC), characterised by depolarisation and increased spontaneous firing rate following the glucose excursion (**Figure 5.1C$_1$**). In approximately 70% of GE cells, the response reversed following washout of glucose (within 20 minutes). The change in IV relationship revealed in most, but not all, glucose-excited POMC neurons, the closure of one or more potassium conductances indicated by increased input resistance and the intersection of the IV curves near the reversal potential for potassium ions (≈ −90mV) (**Figure 5.1C$_2$**). It is likely that closure of the K_{ATP} channel is responsible for reduced potassium conductance and hence depolarisation of POMC cells, in line with previous reports (Ibrahim *et al.*, 2003; Parton *et al.*, 2007). It is worthy of note that some glucose-induced excitations evoked changes in IV relationships consistent with the opening of one or more non-selective cation conductances (reduced input resistance, reversal potential ≈ −40mV), suggestive of other conductances which may regulate depolarisation following exposure to high glucose (data not shown).

We observed a relatively small population of glucose-inhibited (GI) POMC neurons that, remarkably, has not yet been reported despite many published glucose-sensing works on these cells. These neurons (7% RCA, 8% ARC) were hyperpolarised and silenced by the presence of high glucose (**Figure 5.1D$_1$**). Most IV curves of glucose-inhibited POMC neurons revealed a reduction in input resistance with a reversal potential around that of potassium, indicating the opening of one or more potassium channels (**Figure 5.1D$_2$**). We also observed a number of glucose-induced inhibitions associated with reduced input resistance with a reversal potential ≈ −65mV, suggestive of activation of chloride conductance(s) (data not shown).

Intriguingly, a small fraction of POMC neurons (8% RCA, 4% ARC) displayed a unique glucose-induced burst-firing response that has not yet been reported (**Figures 5.1E$_{1-4}$**). This response was characterised by spontaneous oscillations in membrane potential with superimposed bursts of action potentials at the peak of the depolarising phase, followed by hyperpolarisation and cessation of activity preceding the onset of the subsequent regenerative cycle of activity. This pattern of activity persisted well after returning glucose to baseline levels (in some cells for over an hour). The frequency and

magnitude of the oscillations varied considerably between cells, but remained relatively consistent within cells once rhythmic behaviour was established. Due to the dynamic nature of the oscillations, it was difficult to ascertain reliable IV relationships for most glucose-induced burst-firing cells, barring one with a particularly slow and large magnitude oscillation (**Figure 5.1E$_1$**). Determination of IV relationships during the "down", "mid" (between) and "up" oscillation state revealed the unambiguous opening/closure of an inwardly-rectifying potassium channel (**Figure 5.1E$_2$**). Notably, glucose-induced burst-firing was evoked in POMC neurons regardless of baseline neuronal activity (i.e. quiescent, irregularly firing, tonic firing; see **Figures 5.1E$_1$, E$_3$ and E$_4$**), and was unaffected by repeated exposure to 5.0mM glucose (*n* = 5) (**Figure 5.1E$_3$**). Another feature of these cells was the expression of a hyperpolarisation-activated non-selective cation conductance (I_H). This conductance is observed as a depolarising sag at the peak of the membrane response to hyperpolarising current injection and as a rebound excitation at the termination of hyperpolarising current injection (see **Figures 5.1D$_2$ and E$_2$**). This is a known "pacemaker activity-driving" conductance described extensively in the nervous system and heart (McCormick & Pape, 1990; Brãuer *et al.*, 2001; Herrmann *et al.*, 2015), and may contribute to the burst-firing patterns of activity described here. Application of the $GABA_A$ receptor antagonist, Gabazine, was able to reversibly and repeatedly block action potential trains during the "up" state of the burst, but did not completely prevent underlying oscillation in membrane potential (**Figure 5.1E$_4$**), indicating that pre-synaptic GABAergic neurons are important for co-ordinating and initiating burst-firing, but do not impact the opening/closure of potassium channels mediating oscillations.

The proportions of glucose-induced responses of POMC-expressing neurons trended to be dependent on whether neurons were located in the ARC or the RCA (Chi-squared Test of Independence, $\chi^2(3) = 6.972$, p=0.0728). While we did not specifically aim to correlate topographical location of glucose-induced responses within each nucleus, there was no overt distribution across the medio-lateral or dorso-ventral bounds of the nuclei. However, glucose-induced burst-firing POMC neurons were distributed more rostrally in the hypothalamus, with a greater proportion of these neurons found in the RCA than ARC (8.2% versus 3.9%), and those in the ARC were located only in the rostral or middle region of the nucleus.

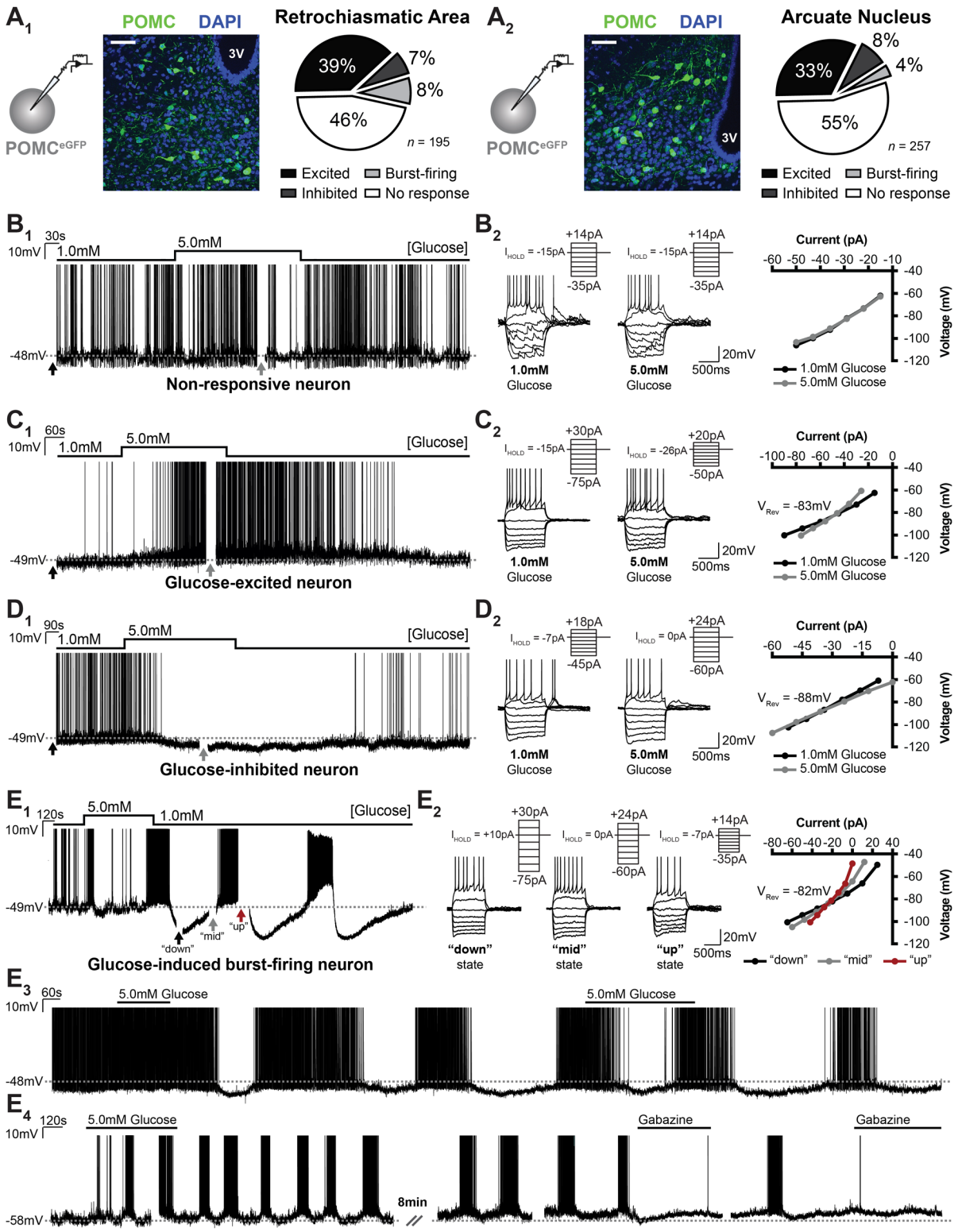

Figure 5.1 | RCA and ARC POMC neurons sense increases in extracellular glucose, evoking burst-firing in a subset of these cells

(A_1 and A_2) Whole-cell patch clamp recordings were made from GFP-expressing POMC neurons in *ex vivo* brain slices from $Pomc^{eGFP}$ mice in the retrochiasmatic area (A_1) and arcuate nucleus (A_2). The proportion of responses to elevated extracellular D-glucose in each nucleus is depicted as a pie chart. Confocal microphotographs of coronal sections from $Pomc^{eGFP}$ mice demonstrating POMC neuron expression in the RCA (A_1) and ARC (A_2), with DAPI counterstain. 3V, third ventricle. Scale bars, 50µm. **(B_1 and B_2)** Representative whole-cell recording from a POMC neuron that is not responsive to elevation in extracellular D-glucose concentration from 1.0 to 5.0mM (B_1). Current-voltage (IV)

relationship curves are plotted for the cell's response to hyperpolarising and depolarising current steps (shown superimposed) at baseline (1.0mM G, black) and in elevated glucose (5.0mM G, grey), indicating no change in conductance or resting membrane potential for the cell (B_2). Top right in each set of trace sweeps indicates the magnitude of current injection steps and holding current (I_{HOLD}). **(C_1 and C_2)** Representative whole-cell recording from a POMC neuron that is excited by elevation in extracellular D-glucose concentration from 1.0 to 5.0mM (C_1). IV relationship curves are plotted for the cell's response to hyperpolarising and depolarising current steps (shown superimposed) at baseline (1.0mM G, black) and in elevated glucose (5.0mM G, grey), indicating increased resistance (slope) and resting membrane potential for the cell (C_2). IV curves intersect at approximately −83mV, which approximates the reversal potential of K^+ under our recording conditions, indicating the glucose-induced excitation was a result of closure of one or more K^+ conductances. Top right in each set of trace sweeps indicates the magnitude of current injection steps and holding current (I_{HOLD}). **(D_1 and D_2)** Representative whole-cell recording from a POMC neuron that is inhibited by elevation in extracellular D-glucose concentration from 1.0 to 5.0mM (D_1). IV relationship curves are plotted for the cell's response to hyperpolarising and depolarising current steps (shown superimposed) at baseline (1.0mM G, black) and in elevated glucose (5.0mM G, grey), indicating decreased resistance (slope) and resting membrane potential for the cell (D_2). IV curves intersect at approximately −88mV, indicating the glucose-induced inhibition was a result of opening of one or more K^+ conductances. Top right in each set of trace sweeps indicates the magnitude of current injection steps and holding current (I_{HOLD}). **(E_{1-4})** Representative whole-cell recording from POMC neurons which elicit spontaneous burst-firing and oscillations in membrane potential in response to changes in extracellular D-glucose concentration from 1.0 to 5.0mM (E_1, E_3 and E_4). IV relationship curves are plotted for the cell's (E_1) response to hyperpolarising and depolarising current steps (shown superimposed) at baseline at the bottom ("down" state, black), mid-way ("mid" state, grey) and top ("up" state, maroon) of an oscillation, demonstrating intersection of curves consistently at approximately −82mV which indicates oscillations involve the repeated opening and closure of one or more K^+ conductances (E_2). Top right in each set of trace sweeps indicates the magnitude of current injection steps and holding current (I_{HOLD}). Re-application of 5.0mM D-glucose had no obvious effect on membrane potential oscillations or firing (E_3), however application of $GABA_A$ receptor antagonist, Gabazine (10μM), reversibly prevented the firing of action potentials during a burst, but did not completely block the underlying oscillations in membrane potential (E_4).

Note that breaks in electrophysiology recordings are denoted with "//" along with the length of time for which recording was broken, to the nearest minute. Breaks in recording of less than two minutes are not denoted further than a gap in the trace. Black, grey and maroon arrows indicate the break in respective recordings where IV relationships were determined.

5.3.2 Adenosine receptor-regulated glucose-sensing in POMC neurons

We examined expression of adenosine receptors in hypothalamic POMC neurons and their association with astrocytes using immunohistochemistry on brain sections from $Pomc^{eGFP}$ mice. We observed that the overwhelming majority of GFP-expressing POMC cell bodies colocalised with A_1R, $A_{2A}R$ and A_3R (**Figures 5.2A-C**). In fact, there was abundant expression of adenosine receptors throughout the arcuate nucleus and retrochiasmatic area in both POMC-expressing and non-POMC neurons, indicating the potential for widespread action of adenosine in these neural circuits. To identify astrocyte processes that may interact with adenosine receptor-expressing POMC neurons, we co-stained sections for the astrocyte marker, glial fibrillary acidic protein (GFAP). We observed numerous POMC neurons expressing A_1R, $A_{2A}R$ or A_3R with close appositions to, or even ensheathed by astrocytic processes (**Figures 5.2A-C,** white arrows). Interestingly, many astrocytic processes colocalised with the A_3R (**Figure 5.2C,** grey arrow) but not A_1R or $A_{2A}R$, indicating that astrocyte activity itself may also be modulated by extracellular adenosine.

We next investigated the role of extracellular adenosine in mediating or regulating glucose-responsive POMC neurons. Using the non-selective adenosine receptor (AR) inhibitor, CGS15943, we observed that AR antagonism reversed or prevented 40% (*n* = 2 of 5) of glucose-induced excitations in POMC neurons (**Figure 5.2D$_2$**). The remaining GE neurons were unaffected by adenosine receptor antagonism, reversing only upon washout of 5.0mM glucose (**Figure 5.2D$_3$**). Similarly, the reversal of a glucose-induced inhibition was seen when CGS15943 was applied at the peak of the response while 5.0mM glucose was still present (*n* = 1 of 3, 33%) (**Figure 5.2E$_2$**), however other GI POMC neurons remained responsive to glucose in the presence of the antagonist (**Figure 5.2E$_3$**). To test for the presence of tonic adenosinergic input to POMC neurons, or whether adenosine specifically signals changes in extracellular glucose, we investigated the effect of adenosine receptor antagonism in POMC neurons from *ad libitum* fed mice bathed in 5.0mM glucose, as relevant for the physiological state (**Figure 5.2F$_1$**). We observed mixed responses to CGS15943 application where most cells did not respond, but 15% (*n* = 2 of 13) were inhibited and 38% (*n* = 5 of 13) were reversibly excited (**Figures 5.2F$_2$ and F$_3$**), confirming the presence of adenosinergic tone moderating neuronal activity in a subset of POMC neurons.

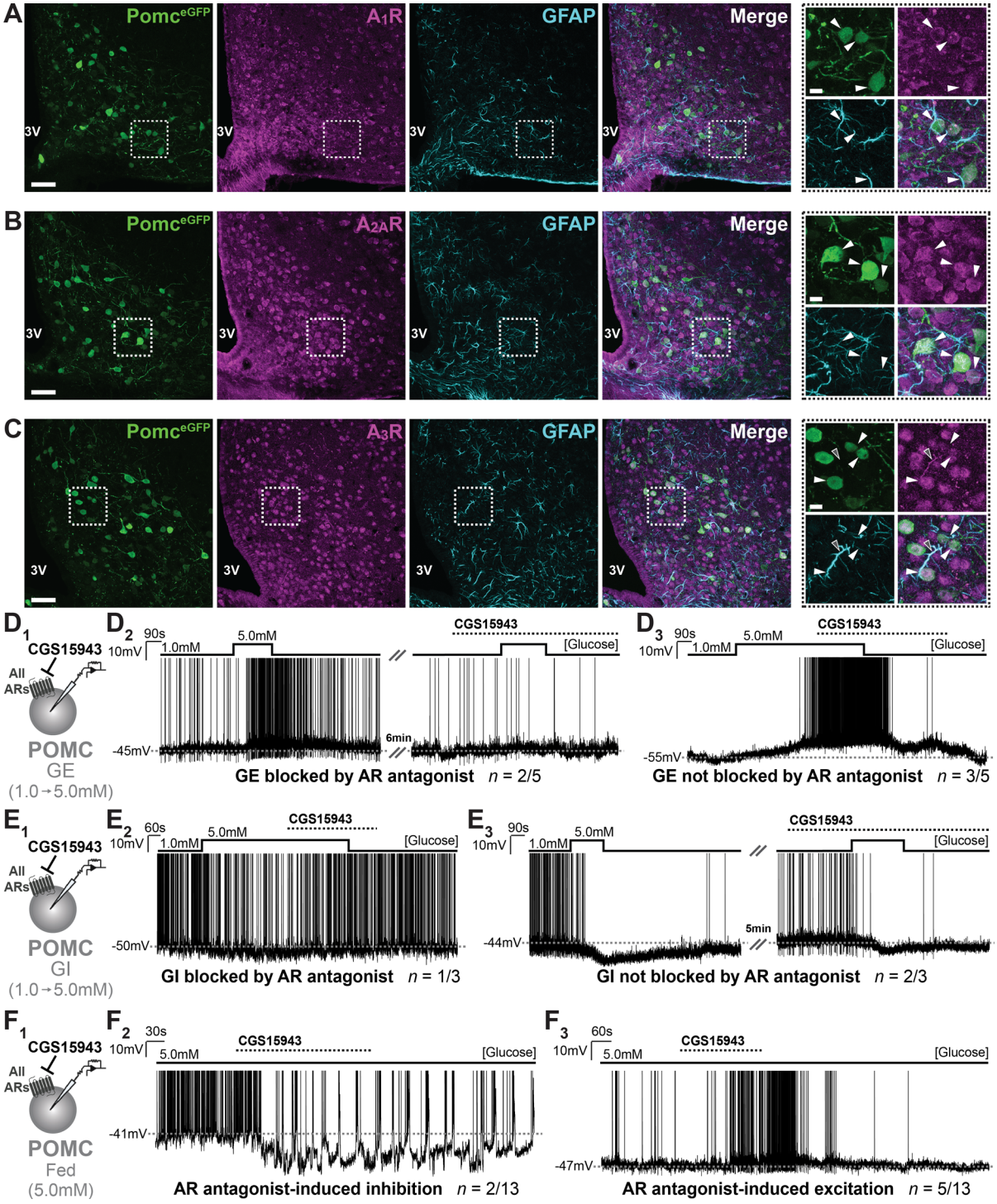

Figure 5.2 | POMC neurons express adenosine receptors which provide excitatory or inhibitory tone

(A-C) Representative confocal microphotographs of coronal sections of the arcuate nucleus from Pomc^{eGFP} mice immunohistochemically stained for GFAP, an astrocyte marker, and A_1R (A), $A_{2A}R$ (B) or A_3R (C). Zoom insets: white arrow heads indicate POMC cells (green) which colocalise with adenosine receptor (magenta) that also have touching or apposing astrocytic processes (cyan). Grey arrowhead with white outline in (C) indicates an astrocyte process that colocalises with A3R. 3V, third ventricle. Scale bars, 50µm (low magnification), 10µm (high magnification). **(D_{1-3})** Testing the involvement of adenosine receptors in GE POMC neurons from overnight-fasted Pomc^{eGFP} mice using non-selective adenosine receptor (AR) antagonist, CGS15943 (1µM). Representative whole-cell current-clamp recording where 5.0mM glucose reversibly excited a POMC neuron, but when high glucose was re-applied in the presence of CGS15943 the response was blocked (D_2). Representative

whole-cell current-clamp recording where a POMC neuron was depolarised and increased firing rate in 5.0mM glucose, and application of CGS15943 had no effect on the glucose-induced response which was only reversed upon washout of high glucose (D_3). **(E_{1-3})** Testing the involvement of adenosine receptors in GI POMC neurons from overnight-fasted $Pomc^{eGFP}$ mice using non-selective AR antagonist, CGS15943 (1μM). Representative whole-cell current-clamp recording of POMC neuron whose action potential firing and membrane potential was inhibited in 5.0mM glucose, but this effect was completely reversed when CGS15943 was bath-applied while 5.0mM glucose was still present (E_2). Representative whole-cell current-clamp recording of a GI POMC neuron sharply hyperpolarised by 5.0mM glucose, an effect which remained when re-applied in the presence of CGS15943 (E_3). **(F_{1-3})** Testing the constitutive activity at adenosine receptors in POMC neurons of *ad libitum* fed $Pomc^{eGFP}$ mice in 5.0mM extracellular glucose using non-selective AR antagonist, CGS15943 (1μM). Representative whole-cell current-clamp recordings of POMC neuron that was inhibited (F_2) or excited (F_3) by application of CGS15943, indicating a tonic excitatory or inhibitory adenosine-mediated tone, respectively.

Note that breaks in electrophysiology recordings are denoted with "//" along with the length of time for which recording was broken, to the nearest minute. Breaks in recording of less than two minutes are not denoted further than a gap in the trace.

5.3.3 Adenosine receptor subtypes involved in POMC neuron glucose-sensing

We next aimed to establish the involvement of specific adenosine receptor subtypes in influencing neuronal activity following elevations in glucose in POMC neurons. In light of reports indicating astrocyte-derived adenosine acts on hypothalamic A_1R to regulate appetite (Yang *et al.*, 2015; Sweeney *et al.*, 2016), we focussed primarily on the role for A_1R-mediated signalling in POMC neuron glucose-sensing. Remarkably, application of the selective A_1R antagonist, DPCPX, completely reversed or prevented glucose-induced excitations in 50% (n = 9 of 18) of neurons (**Figure 5.3A$_2$**). On average, DPCPX-sensitive GE POMC neurons showed a baseline depolarisation of 6.1 ± 1.1mV and increase in AP firing by 0.44 ± 0.12Hz in response to 5.0mM glucose, which were abrogated to 0.4 ± 0.3mV (p=0.0013) and −0.07 ± 0.05Hz (p=0.0109), respectively, when re-applied in the presence of the A_1R antagonist (**Figure 5.3A$_3$**). To confirm that A_1R activation can mimic the effects of elevated glucose and activate POMC neurons, the selective A_1R agonist, SDZ WAG 994, was applied to a subset of POMC neurons that were already determined to be glucose-excited. Indeed, 38% (n = 3 of 8) of GE POMC neurons were reversibly depolarised by A_1R agonism, resulting in an increase in input resistance and change in current-voltage relationship consistent with the closure of one or more potassium conductances (**Figure 5.3B**). Importantly, we found that A_1R antagonism had no effect on glucose-induced inhibitions in all (n = 5 of 5) GI POMC neurons tested (**Figure 5.3C**).

We briefly addressed the role of A_3R in regulating POMC neuron activity. Re-application of 5.0mM glucose with the selective A_3R antagonist, MRS1523, on GE POMC neurons had no effect on glucose-induced excitations in most cases (n = 9 of 11, 82%). However, in a fraction of cells (n = 2 of 11, 18%), A_3R antagonism during the second application of high glucose evoked a “glucose-adapting” response, previously reported in CART- (POMC-) expressing neurons in the ARC in the absence of pharmacological intervention (van den Top *et al.*, 2017). Glucose-adapting responses were characterised by transient membrane hyperpolarisation and inhibition of action potential firing, followed by the establishment of a firing rate at a lower frequency than at basal glucose levels (**Figures 5.3D$_1$ and D$_2$**). Importantly, upon washout of high glucose, the cells returned to the original firing frequency. Furthermore, we observed in a minority of otherwise NR POMC neurons that MRS1523 application induced a transient inhibition that appeared to be mediated by the closure of a potassium conductance (n = 2 of 12, 17%) (**Figure 5.3E$_2$**), but had no effect on the membrane potential of other POMC cells. In both cases, re-application of glucose revealed a glucose-adapting response, even though the cells were not responsive to glucose in the absence of MRS1523. This finding highlights the possibility of plasticity in the glucose-sensitivity of POMC neurons.

We hypothesised that adenosine-mediated modulation of POMC neuron activity would affect food intake and/or energy expenditure *in vivo*. To this end, we acutely injected selective adenosine receptor antagonists into the lateral ventricle of C57Bl/6^{WT} mice just before the onset of the dark cycle, when mice engage in consummatory behaviour. Antagonism of central A_1R had no effect on food consumption in the first three hours of the dark cycle (p>0.05), but caused a 22.9 ± 8.0% increase in overnight food intake (16h, p=0.0009; $p_{interaction}$=0.0174) (**Figure 5.3F$_1$**). In light of these findings, we also tested a role for central A_1R-regulated energy expenditure through indirect calorimetry, and found DPCPX treatment significantly reduced dark cycle energy expenditure ($p_{treatment}$=0.0337) (**Figure 5.3F$_2$**).

Notably, central administration of antagonists for $A_{2A}R$, $A_{2B}R$ and A_3R had no effect on short- or long-term food intake (p>0.05) (**Figures 5.3G-I**).

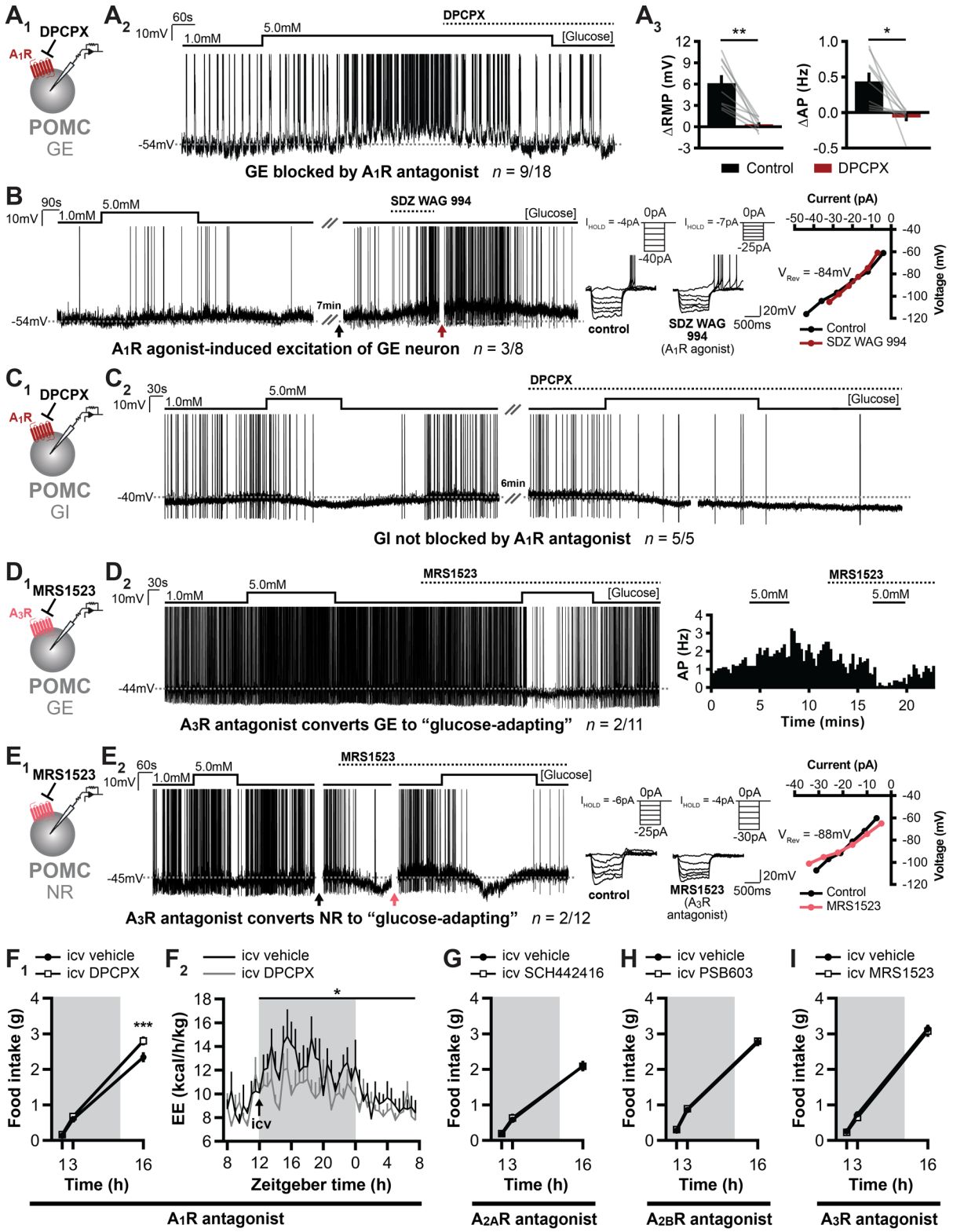

Figure 5.3 | A_1R-dependent glucose-induced activation of POMC neurons mediates satiety and energy expenditure

($A_{1\text{-}3}$) Testing the involvement of A_1R in GE POMC neurons from overnight-fasted $Pomc^{eGFP}$ mice using selective A_1R antagonist, DPCPX (100nM) (A_1). Representative whole-cell current-clamp recording from a POMC neuron that was depolarised and increased firing frequency in response to 5.0mM D-glucose, but concurrent application of DPCPX reversed this effect entirely (A_2). Diagrams depicting the change in resting membrane potential (RMP) and action potential (AP) firing frequency of the POMC neurons whose glucose-induced excitations were abolished by DPCPX (A_3). Changes in

electrophysiological parameters were analysed by paired *t* test (RMP, *n* = 9 cells; *t* = 4.822, *df* = 8, ***p*=0.0013. AP, *n* = 9 cells; *t* = 3.298, *df* = 8, **p*=0.0109). **(B)** Representative whole-cell current-clamp recording of GE POMC neuron that was also reversibly excited by bath-application of selective A_1R agonist, SDZ WAG 994 (500nM). IV relationship curves are plotted for the cell's response to superimposed hyperpolarising current steps just prior to (control, black arrow) and during application of A_1R agonist (maroon arrow), indicating increased resistance (slope) and resting membrane potential for the cell. IV curves intersect at approximately −84mV, which approximates to the reversal potential of K^+ under our recording conditions, indicating agonism of A_1R in POMC neurons induces excitation as a result of closure of one or more K^+ conductances. Top right in each set of trace sweeps indicates the magnitude of current injection steps and holding current (I_{HOLD}). **(C_1 and C_2)** Testing the involvement of A_1R in GI POMC neurons from overnight-fasted $Pomc^{eGFP}$ mice using selective A_1R antagonist, DPCPX (100nM) (C_1). Representative whole-cell current-clamp recording from a POMC neuron that was hyperpolarised and silenced both in the presence and absence of DPCPX, indicating that a mechanism independent of the A_1R mediates glucose-induced inhibition (C_2). **(D_1 and D_2)** Testing the involvement of A_3R in GE POMC neurons from overnight-fasted $Pomc^{eGFP}$ mice using selective A_3R antagonist, MRS1523 (300nM) (D_1). Representative whole-cell current-clamp recording from a POMC neuron that was at first excited by glucose but became "glucose-adapting" when glucose was re-applied in the presence of MRS1523 (D_2). The adaptation response was characterised by a transient inhibition that stabilised at a lower firing frequency than in 1.0mM glucose, but then reversed back to basal firing upon washout of 5.0mM glucose. The diagram indicates the spontaneous AP frequency (measured in 15 second bins) across the entirety of the trace with indications of when 5.0mM glucose and MRS1523 were applied. **(E_1 and E_2)** Testing the involvement of A_3R in NR POMC neurons from overnight-fasted $Pomc^{eGFP}$ mice using selective A_3R antagonist, MRS1523 (300nM) (E_1). Representative whole-cell current-clamp recording from a POMC neuron that was at first not responsive to the elevation in extracellular glucose. However, upon application of MRS1523, the cell exhibited a transient hyperpolarisation that was replicated when 5.0mM glucose was applied in the presence of MRS1523, indicating that glucose-sensing in POMC neurons may be subject to a functional plasticity (E_2). IV relationship curves are plotted for the cell's response to hyperpolarising current steps (shown superimposed) just prior to (control, black arrow) and during the transient inhibition following application of the A_3R antagonist (pink arrow), indicating decreased resistance (slope) and resting membrane potential for the cell. IV curves intersect at approximately −88mV, which approximates to the reversal potential of K^+ under our recording conditions, indicating antagonism of A_3R in POMC neurons induces a transient inhibition as a result of opening of one or more K^+ conductances. Top right in each set of trace sweeps indicates the magnitude of current injection steps and holding current (I_{HOLD}). **(F_1 and F_2)** Cumulative food intake (F_1) and energy expenditure (F_2) in $C57Bl/6^{WT}$ mice that were injected via the lateral ventricle with 2µL of vehicle (20%DMSO in saline) or 300ng DPCPX, A_1R antagonist, just before the onset of the dark cycle. Food intake measurements were made at indicated times, energy expenditure measurements were made every 30 minutes. Grey box indicates hours of dark cycle. Food intake was analysed by repeated measures (both factors) two-way ANOVA followed by Sidak's multiple comparisons test (F_1: *n* = 11 animals; treatment $F(1, 10) = 6.462$, $p=0.0293$; time $F(2, 20) = 346.3$, $p<0.0001$; interaction $F(2, 20) = 4.995$, $p=0.0174$. 1h, $p=0.9873$; 3h, $p=0.8629$; 16h, ***$p=0.0009$. F_2: *n* = 7 animals; treatment $F(1, 6) = 7.506$, *$p=0.0337$; time $F(39, 234) = 3.538$, $p<0.0001$; interaction $F(39, 234) = 0.9126$, $p=0.6220$. All time points, $p>0.05$). **(G)** Cumulative food intake in $C57Bl/6^{WT}$ mice that were injected with 2µL of vehicle (20%DMSO in saline) or 300ng SCH442416, $A_{2A}R$ antagonist, into the lateral ventricle just before the onset of the dark cycle. Food intake measurements were made at indicated times. Grey box indicates hours of dark cycle. Food intake was analysed by repeated measures (time factor only) two-way ANOVA followed by Sidak's multiple comparisons test (*n* = 5 vehicle, *n* = 5 antagonist; treatment $F(1, 8) = 0.02829$, $p=0.8706$; time $F(2, 16) = 326.5$, $p<0.0001$; interaction $F(2, 16) = 0.09092$, $p=0.9136$. 1h, $p=0.9997$ 3h, $p=0.9739$; 16h, $p=0.9997$). **(H)** Cumulative food intake in $C57Bl/6^{WT}$ mice that were injected with 2µL of vehicle (20%DMSO in saline) or 300ng PSB603, $A_{2B}R$ antagonist, into the lateral ventricle just before the onset of the dark cycle. Food intake measurements were made at indicated times. Grey box indicates hours of dark cycle. Food intake was analysed by repeated measures (both factors) two-way ANOVA followed by Sidak's multiple comparisons test (*n* = 11 animals; treatment $F(1, 10) =$

0.2076, p=0.6584; time F(2, 20) = 546.9, p<0.0001; interaction F(2, 20) = 0.0002530, p=0.9997. 1h, p=0.9720 3h, p=0.9699; 16h, p=0.9653). **(I)** Cumulative food intake in C57Bl/6^{WT} mice that were injected with 2µL of vehicle (10%DMSO in saline) or 100ng MRS1523, A_3R antagonist, into the lateral ventricle just before the onset of the dark cycle. Food intake measurements were made at indicated times. Grey box indicates hours of dark cycle. Food intake was analysed by repeated measures (both factors) two-way ANOVA followed by Sidak's multiple comparisons test (n = 10 animals; treatment F(1, 9) = 1.043, p=0.3339; time F(2, 18) = 1065, p<0.0001; interaction F(2, 18) = 0.06737, p=0.9351. 1h, p=0.9935 3h, p=0.8444; 16h, p=0.9237).

Note that breaks in electrophysiology recordings are denoted with "//" along with the length of time for which recording was broken, to the nearest minute. Breaks in recording of less than two minutes are not denoted further than a gap in the trace. Black, maroon and pink arrows indicate the break in respective recordings where IV relationships were determined. Data in A_3 and F-I are represented as mean ± SEM, and grey lines in A_3 represent paired individual values.

5.3.4 Astrocytic Cx43 hemichannel-dependent regulation of POMC glucose-sensing

Having established a role for adenosine in regulating glucose-sensing in POMC neurons, we next sought to explore the source of endogenous adenosine. Numerous studies have previously shown adenosine can act as a neurotransmitter/neuromodulator released from neurons in an activity-dependent manner (Wall & Dale, 2008; Wall & Dale, 2013). However, adenosine can also be released from glia via hemi-channels or converted from ATP following release from glia hemi-channels (Bennett *et al.*, 2003; Kang *et al.*, 2008). Therefore, we investigated the function of the glial hemi-channel Cx43 in the regulation of POMC glucose-sensing by identifying glucose-excited neurons whose response reversed completely upon washout to basal glucose concentration, and then re-applying 5.0mM glucose in the presence of the non-selective gap-junction/hemi-channel blocker, carbenoxolone (**Figure 5.4A$_1$**). Carbenoxolone was applied for at least 10 minutes, allowing for at least inhibition of Cx43 hemi-channels (Kang *et al.*, 2008), but there is also some indication of inhibition of gap-junctions at this incubation time (Verselis & Srinivas, 2013). Application of carbenoxolone alone to GE POMC neurons caused hyperpolarisation in 79% of neurons (n = 19 of 24; ∆−5.4 ± 0.6mV), while 8% were depolarised (n = 2 of 24; ∆+7.2 ± 3.6mV) and 13% were unaffected (n = 3 of 24). Strikingly, re-application of high glucose in the presence of carbenoxolone revealed that only 27% (n = 7 of 26) of formerly glucose-excited POMC neurons remained activated by elevated extracellular glucose (**Figures 5.4A$_2$ and A$_5$**). Instead, the majority of cells (n = 10 of 26, 38%) exhibited hyperpolarisations (∆−4.6 ± 0.6mV, p<0.0001, compared to control) and reductions in firing rate (∆−0.09 ± 0.07Hz, p=0.0200) consistent with a reversal from a glucose-excited to a glucose-inhibited neuron (**Figures 5.4A$_4$ and A$_6$**). In the remaining cells (n = 9 of 26, 35%), glucose-responsiveness was blocked entirely by Cx43 inhibition, with average membrane potential and firing changes significantly blunted from the original response (RMP, p<0.0001; AP, p=0.0200) (**Figures 5.4A$_3$ and A$_6$**).

Considering that carbenoxolone alone exposed plasticity in POMC neuron glucose-responsiveness, we investigated whether Cx43 inhibition could unveil glucose-sensitivity in POMC neurons otherwise identified as glucose-unresponsive (**Figure 5.4B$_1$**). Carbenoxolone application hyperpolarised the majority of NR POMC neurons (54%, n = 21 of 39; ∆−5.5 ± 0.7mV), but depolarised 18% (n = 7 of 39; ∆+12.8 ± 1.8mV) of cells with no effect on the remainder (n = 11 of 39, 28%). While the majority of POMC neurons (n = 19 of 38, 50%) remained non-responsive to fluctuations in extracellular glucose (**Figure 5.4B$_5$**), remarkably, 29% (n = 11 of 38) of formerly unresponsive neurons were excited (∆+7.7 ± 1.0mV, p<0.0001) upon re-application of high glucose in the presence of carbenoxolone (**Figures 5.4B$_2$, B$_3$ and B$_6$**). Furthermore, the remaining 21% (n = 8 of 38) of NR POMC neurons exhibited glucose-induced inhibitions (∆−6.6 ± 0.8mV, p=0.0002) (**Figure 5.4B$_4$**), indicating that carbenoxolone treatment can reveal glucose-sensitivity in POMC neurons that otherwise displayed no obvious changes in membrane potential or firing frequency in 5.0mM glucose.

To investigate the mechanism of carbenoxolone-induced membrane potential changes (independent of glucose-sensing), we determined the IV relationships pre- and post-application of carbenoxolone. Interestingly, carbenoxolone-induced hyperpolarisation occurred primarily through the activation or inhibition of one or more ion pumps, reflected by a shift in the IV curve with no obvious change in input resistance (n = 14 of 27, 52%). However, it is worthy to note that a change in membrane

potential without obvious change in conductance could be explained by co-incident activation/inhibition of separate conductances that give rise to no overall net change in whole-cell conductance. Inhibition was also mediated by the opening of one or more potassium (*n* = 10 of 27, 37%; $V_{Rev} \approx -86 \pm 2mV$) or chloride (*n* = 3 of 27, 11%; $V_{Rev} \approx -63 \pm 2mV$) conductances. Alternatively, the carbenoxolone-induced excitations were primarily mediated by the closure of one or more potassium channels (*n* = 4 of 4, 100%; $V_{Rev} \approx -92 \pm 5mV$).

Carbenoxolone is known to have low specificity for Cx43 (Willebrords *et al.*, 2017), so to clarify the role of Cx43 activity, the experiments were repeated using a highly specific Cx43 inhibitor peptide, Gap26 (**Figure 5.4C$_1$**). Following identification of reversibly glucose-activated POMC neurons, Gap26 was bath-applied for at least 10 minutes, which is sufficient time to specifically inhibit Cx43 hemi-channels (but not gap-junctions) (Desplantez *et al.*, 2012). Gap26 application alone evoked fewer responses than carbenoxolone. The majority of POMC cells displayed no Gap26-induced change in membrane potential or firing (*n* = 7 of 14, 50%), but 29% (*n* = 4 of 14) of cells were depolarised (∆+5.5 ± 0.8mV) and 21% (*n* = 3 of 14) hyperpolarised (∆−4.1 ± 0.4mV) by Cx43 hemi-channel inhibition. Upon subsequent application of 5.0mM glucose, Gap26-mediated inhibition of Cx43 revealed a strikingly similar proportion of changes to glucose responses in otherwise GE neurons as was observed with carbenoxolone (**Figure 5.4C$_2$** compared to **Figure 5.4B$_2$**). Gap26 completely abolished glucose-induced depolarisations (*p*=0.0131, compared to control) in 40% (*n* = 6 of 15) of neurons (**Figures 5.4C$_2$, C$_3$ and C$_6$**). 27% (*n* = 4 of 15) of responses were reversed to glucose-induced hyperpolarisations (∆−7.3 ± 1.0mV, *p*=0.0014) and inhibition of firing (∆−0.51 ± 0.49Hz, *p*=0.0214) (**Figure 5.4C$_4$**). Similar to carbenoxolone, only 33% (*n* = 5 of 15) of GE POMC neurons were activated when 5.0mM glucose was re-applied in the presence of the specific Cx43 inhibitor, Gap26 (**Figure 5.4C$_5$**).

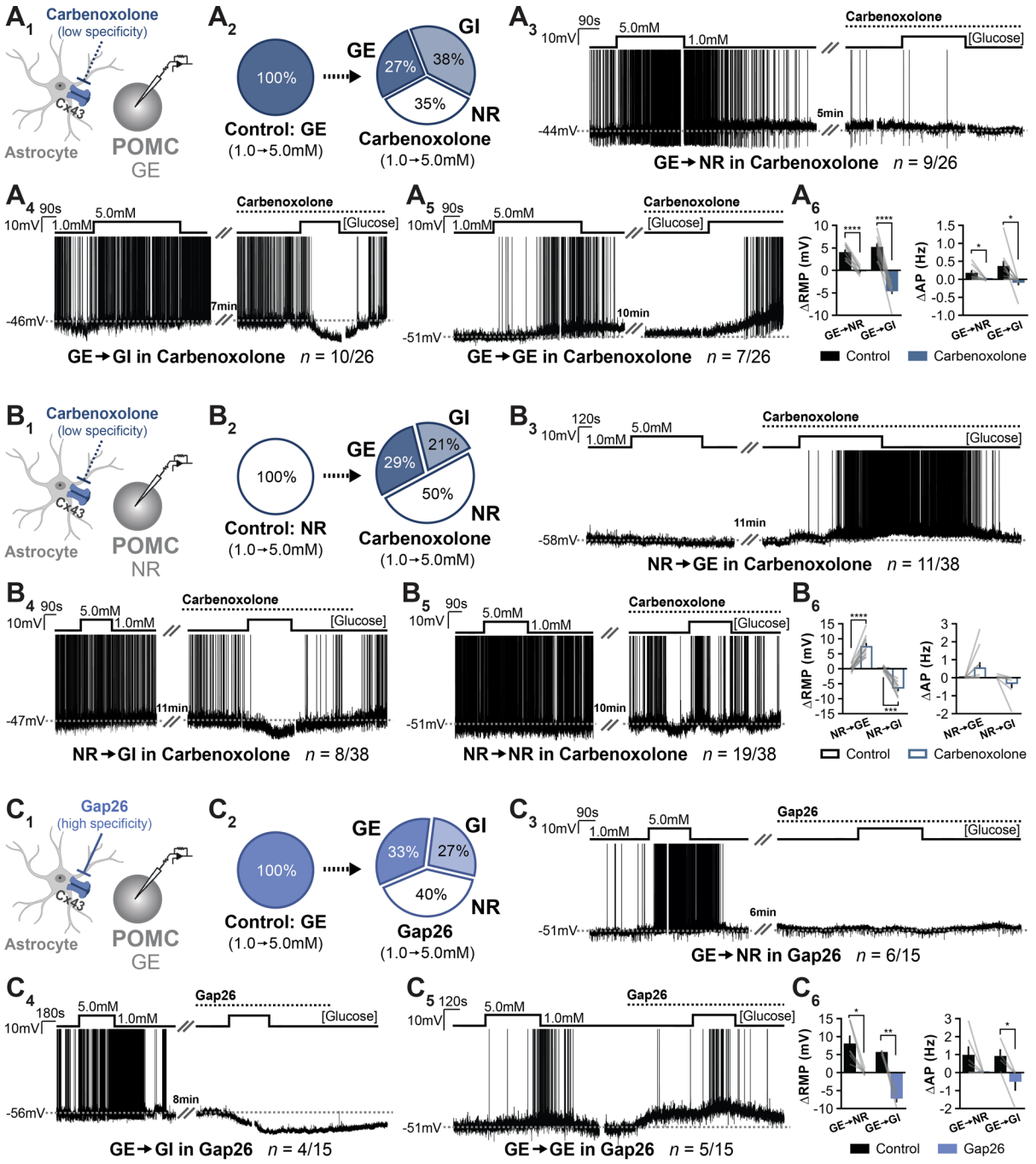

Figure 5.4 | Astrocytic Cx43 hemi-channels contribute to sensing of glucose in POMC neurons

(A$_{1-6}$) Testing the involvement of Cx43 hemi-channels expressed on astrocytes in the regulation of glucose-sensing in GE POMC neurons using the low-specificity inhibitor, carbenoxolone (100μM) (A$_1$). The change in proportion of response types in previously-identified GE POMC neurons following a second exposure to 5.0mM glucose in the presence of carbenoxolone (A$_2$). Representative whole-cell current-clamp recording from a POMC neuron that was originally excited by glucose and then became: non-responsive (A$_3$), glucose-inhibited (A$_4$) or remained glucose-excited (A$_5$) upon subsequent challenge with elevated glucose. Diagrams depicting the RMP and AP firing frequency changes of GE POMC neurons that became NR or GI in the presence of carbenoxolone (A$_6$). Changes in electrophysiological parameters were analysed by paired *t* test (RMP: GE to NR, *n* = 9 cells; *t* = 9.226, *df* = 8, ****p<0.0001; GE to GI, *n* = 10 cells; *t* = 11.39, *df* = 9, ****p<0.0001. AP: GE to NR, *n* = 9 cells; *t* = 2.897, *df* = 8, *p=0.0200; GE to GI, *n* = 10 cells; *t* = 2.821, *df* = 9, *p=0.0200). **(B$_{1-6}$)** Testing the involvement of Cx43 hemi-channels expressed on astrocytes in the regulation of glucose-sensing in non-responsive POMC neurons using the low-specificity inhibitor, carbenoxolone (100μM) (B$_1$). The

change in proportion of response types in previously-identified NR POMC neurons following a second exposure to 5.0mM glucose in the presence of carbenoxolone (B_2). Representative whole-cell current-clamp recording from a POMC neuron that was originally non-responsive to glucose and then became: glucose-excited (B_3), glucose-inhibited (B_4) or remained non-responsive (B_5) upon subsequent challenge with elevated glucose. Diagrams depicting the resting membrane potential (RMP) and firing frequency changes of NR POMC neurons that became GE or GI in the presence of carbenoxolone (B_6). Changes in electrophysiological parameters were analysed by paired *t* test (RMP: NR to GE, *n* = 11 cells; *t* = 7.133, *df* = 10, ****p<0.0001; NR to GI, *n* = 8 cells; *t* = 7.373, *df* = 7, ***p=0.0002. AP: NR to GE, *n* = 11 cells; *t* = 2.124, *df* = 10, p=0.0596; NR to GI, *n* = 8 cells; *t* = 1.666, *df* = 7, p=0.1396). **(C_{1-6})** Testing the involvement of connexin43 (Cx43) hemichannels expressed on astrocytes in the regulation of glucose-sensing in glucose-excited POMC neurons using the high-specificity peptide inhibitor, Gap26 (200μM) (C_1). The change in proportion of response types in previously-identified GE POMC neurons following a second exposure to 5.0mM glucose in the presence of Gap26 (C_2). Representative whole-cell current-clamp recording from a POMC neuron that was originally excited by glucose and then became: non-responsive (C_3), glucose-inhibited (C_4) or remained glucose-excited (C_5) upon subsequent challenge with elevated glucose. Diagrams depicting the RMP and firing frequency changes of GE POMC neurons that became NR or GI in the presence of Gap26 (C_6). Changes in electrophysiological parameters were analysed by paired *t* test (RMP: GE to NR, *n* = 6 cells; *t* = 3.766, *df* = 5, *p=0.0131; GE to GI, *n* = 4 cells; *t* = 11.43, *df* = 3, **p=0.0014. AP: GE to NR, *n* = 6 cells; *t* = 2.109, *df* = 5, p=0.0887; GE to GI, *n* = 4 cells; *t* = 4.425, *df* = 3, *p=0.0214).

Note that breaks in electrophysiology recordings are denoted with "//" along with the length of time for which recording was broken, to the nearest minute. Breaks in recording of less than two minutes are not denoted further than a gap in the trace. Data in A_6, B_6 and C_6 are represented as mean ± SEM and grey lines represent paired individual values.

5.3.5 Ectonucleotidease activity and astrocyte metabolism contribute to POMC neuron glucose-sensing

Local extracellular adenosine concentration can be influenced by the activity of extracellularly-expressed ectonucleotideases which successively dephosphorylate of released nucleotides into adenosine (Latini & Pedata, 2001). The final dephosphorylation step from adenosine monophosphate (AMP) into adenosine is catalysed by the enzyme ecto-5'-nucleotidease (also known as CD73) (Zimmermann, 1992). Using the highly specific CD73 inhibitor, PSB12379, we investigated a role for extracellularly produced adenosine in the regulation of glucose-induced excitations in POMC neurons (**Figure 5.5A$_1$**). CD73 inhibition alone had no effect on the majority of POMC neurons (*n* = 14 of 18, 78%), but in a fraction of cells did induce either inhibition (17%, *n* = 3 of 18) or excitation (5%, *n* = 1 of 18). Strikingly, CD73 inhibition reversed the majority of glucose-induced excitations, where 35% (*n* = 7 of 20) of previously GE POMC cells became unresponsive to 5.0mM glucose (RMP change: *p*=0.0001 compared to control), while another 35% (*n* = 7 of 20) were hyperpolarised and inhibited by increased extracellular glucose (∆−5.4 ± 0.8mV, *p*=0.0007) (**Figures 5.5A$_{2-4}$ and A$_6$**). The remaining 30% (*n* = 6 of 20) of GE POMC neurons remained depolarised upon re-application of high glucose (**Figure 5.5A$_5$**). We also tested whether CD73 inhibition would change the responsiveness of otherwise glucose-insensitive neurons. Intriguingly, while 4 of 7 (57%) neurons remained unresponsive, PSB12379 uncovered glucose-induced inhibitions in 3 of 7 (43%) cells, reinforcing the potential plastic nature of glucose-sensing in POMC neurons.

To emphasize the role specifically of astrocytic glucose metabolism in modulating POMC activity, we utilised the glial-specific metabolic poison, fluorocitrate, to inhibit mitochondrial respiration in astrocytes but not neurons (**Figure 5.5B$_1$**). Application of the glial metabolic toxin hyperpolarised 44% (*n* = 7 of 16; ∆−4.4 ± 1.0mV) of POMC neurons previously identified as glucose-excited, and depolarised and excited 31% (*n* = 5 of 16; ∆+4.8 ± 1.5mV). Fluorocitrate had perhaps the most profound effect on glucose-induced excitations compared to other inhibitors used, preventing or reversing over 80% of responses (**Figure 5.5B$_2$**). Glucose-induced depolarisation (*p*=0.0013) and activation of firing (*p*=0.0130) was abolished completely in 7 of 16 (44%) cells, while the metabolic poison also uncovered a glucose-induced hyperpolarisation (∆−6.1 ± 0.9mV, *p*=0.0010) and suppression of firing (∆−0.11 ± 0.08Hz, *p*=0.0372) in 37% (*n* = 6 of 16) of formerly glucose-excited POMC neurons (**Figures 5.5B$_3$, B$_4$ and B$_6$**). Only 19% (*n* = 3 of 16) of POMC neurons persisted to be excited by the second application of 5.0mM glucose in the presence of fluorocitrate (**Figure 5.5B$_5$**).

To further test the role of astrocyte metabolism on POMC neuron activity, we pharmacologically inactivated the major glucose transporter isoform expressed in astrocytes, GLUT1, with the specific inhibitor BAY876. GLUT1 inhibition blocked 50% (*n* = 2 of 4) of glucose-induced excitations in POMC neurons (not shown). To test whether astrocyte-derived metabolites provide modulatory tone to adjacent POMC neurons, we investigated the effect of GLUT1 inhibition on POMC neurons from *ad libitum* fed mice in 5.0mM glucose (**Figure 5.5C$_1$**). BAY876 alone induced a reversible membrane hyperpolarisation in 38% (*n* = 6 of 16) of POMC neurons, with only a fraction of cells depolarising in response to the GLUT1 inhibitor (13%, *n* = 2 of 16), indicating the presence of a more dominant excitatory paracrine input from astrocytes in the calorically-sated state (**Figures 5.5C$_2$ and C$_3$**).

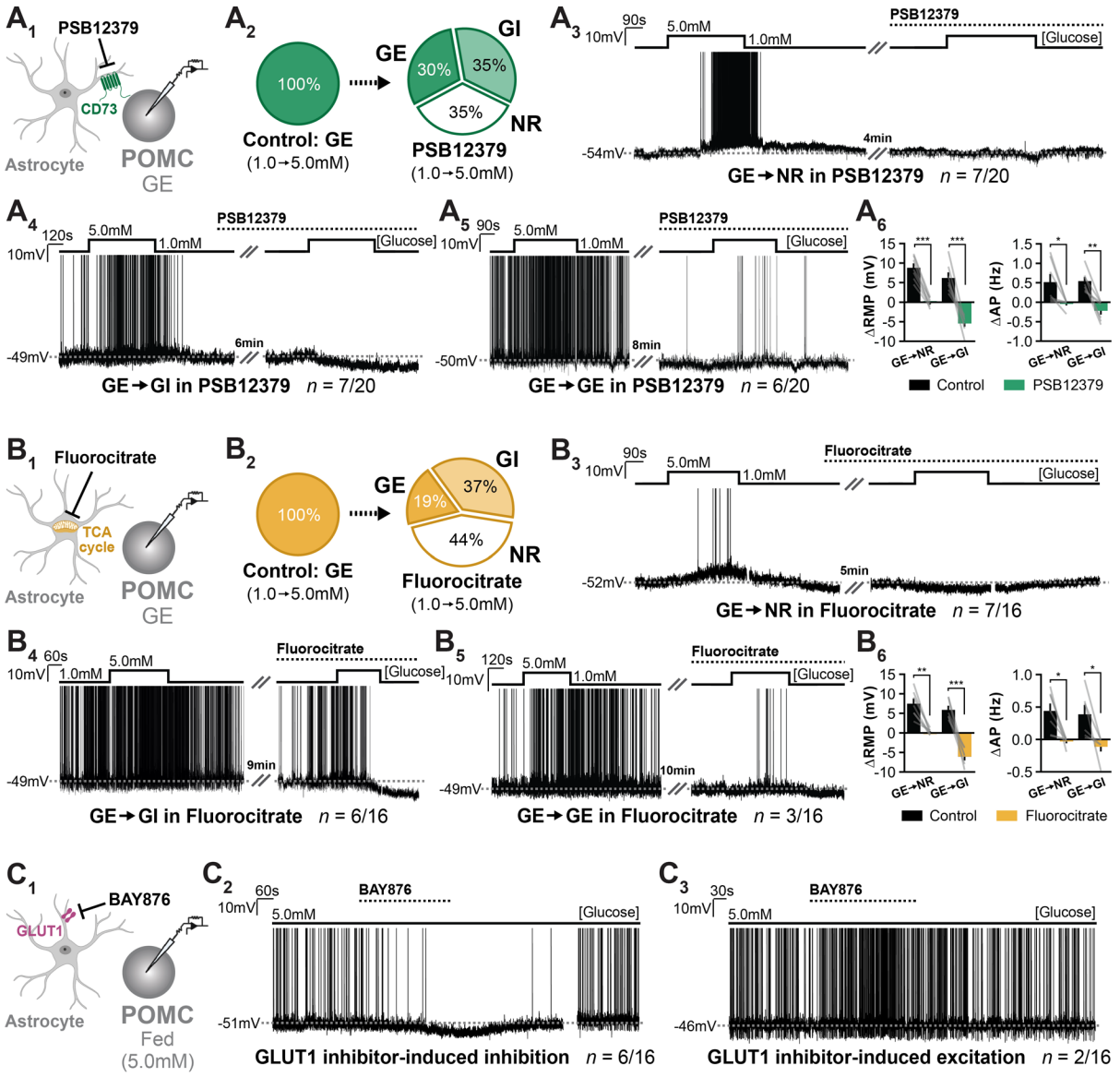

Figure 5.5 | Astrocyte metabolism and extracellular adenosine production regulate POMC neuron glucose-sensing

(A_{1-6}) Testing the involvement of ecto-5'-nucleotidease (CD73), an extracellularly expressed enzyme that degrades AMP to adenosine, in the regulation of glucose-sensing in GE POMC neurons using the inhibitor, PSB12379 (1μM) (A_1). Note that CD73 is on the astrocyte for graphical purposes only; it is unclear where exactly CD73 is expressed extracellularly. The change in proportion of response types in previously-identified GE POMC neurons following a second exposure to 5.0mM glucose in the presence of PSB12379 (A_2). Representative whole-cell current-clamp recording from a POMC neuron that was originally excited by glucose and then became: non-responsive (A_3), glucose-inhibited (A_4) or remained glucose-excited (A_5) upon subsequent challenge with elevated glucose. Diagrams depicting the RMP and firing frequency changes of GE POMC neurons that became NR or GI in the presence of PSB12379 (A_6). Changes in electrophysiological parameters were analysed by paired *t* test (RMP: GE to NR, $n = 7$ cells; $t = 8.646$, $df = 6$, ***p=0.0001; GE to GI, $n = 7$ cells; $t = 6.315$, $df = 6$, ***p=0.0007. AP: GE to NR, $n = 7$ cells; $t = 2.783$, $df = 6$, *p=0.0319; GE to GI, $n = 7$ cells; $t = 5.777$, $df = 6$, **p=0.0012). **(B_{1-6})** Testing the involvement of astrocyte metabolism in the regulation of glucose-sensing in GE POMC neurons using the tri-carboxylic acid (TCA) cycle inhibitor, fluorocitrate (50μM) (B_1). The change in proportion of response types in previously-identified GE POMC neurons following a second exposure to 5.0mM glucose in the presence of fluorocitrate (B_2). Representative whole-cell current-clamp recording from a POMC neuron that was originally excited by glucose and then became: non-responsive (B_3), glucose-inhibited (B_4) or remained glucose-excited (B_5) upon subsequent

challenge with elevated glucose. Diagrams depicting the RMP and firing frequency changes of GE POMC neurons that became NR or GI in the presence of fluorocitrate (B_6). Changes in electrophysiological parameters were analysed by paired *t* test (RMP: GE to NR, $n = 7$ cells; $t = 5.626$, $df = 6$, $^{**}p=0.0013$; GE to GI, $n = 6$ cells; $t = 6.892$, $df = 5$, $^{***}p=0.0010$. AP: GE to NR, $n = 7$ cells; $t = 3.490$, $df = 6$, $^{*}p=0.0130$; GE to GI, $n = 6$ cells; $t = 2.817$, $df = 5$, $^{*}p=0.0372$). **(C_{1-3})** Testing the constitutive function of glucose transporter-1 (GLUT1), expressed primarily in astrocytes, on POMC neuron activity from *ad libitum* fed $Pomc^{eGFP}$ mice in 5.0mM extracellular glucose using the specific inhibitor, BAY876 (1μM). Representative whole-cell current-clamp recordings of POMC neuron that was inhibited (C_2) or excited (C_3) by application of BAY876, indicating the tonic release of excitatory or inhibitory signals from astrocytes, respectively.

Note that breaks in electrophysiology recordings are denoted with "//" along with the length of time for which recording was broken, to the nearest minute. Breaks in recording of less than two minutes are not denoted further than a gap in the trace. Data in A_6 and B_6 are represented as mean ± SEM and grey lines represent paired individual values.

5.3.6 DREADD-mediated stimulation of mediobasal hypothalamus astrocytes activates adjacent POMC neurons

Fluctuations in glucose availability have been reported to evoke calcium waves which spread through interconnected astrocyte networks as a form of excitability, promoting the release of ATP and adenosine to act on neighbouring neurons in the NTS (McDougal *et al.*, 2013; Rogers *et al.*, 2018). A temporally-precise chemogenetic tool to selectively prevent or subdue astrocytic calcium flux would permit optimal testing of the involvement of astrocytes in POMC neuron glucose-sensing, however this technology does not presently exist. As an alternative, the expression and activation of Gq-coupled DREADDs in astrocytes has been shown to *promote* calcium flux and hence the release of neurotransmitters, such as ATP or adenosine (Martin-Fernandez *et al.*, 2017; Durkee *et al.*, 2019). To investigate whether the DREADD-mediated activation of astrocytes regulates POMC neuronal activity, we injected a recombinant AAV viral vector encoding the hM3Dq DREADD with a GFAP promoter to target expression specifically to astrocytes (AAV-GFAP-hM3Dq-mCherry) into the mediobasal hypothalamus of mice (**Figure 5.6A**). Using C57Bl/6^{WT} mice, we optimised injection volume to ensure DREADD (mCherry) labelling that encompassed both the rostro-caudal extent of the ARC and RCA, but with minimal expression in adjacent nuclei (**Figure 5.6B**). Furthermore, by reducing the viral titre (see *Section 5.2.7*), expression of mCherry-tagged DREADDs was restricted specifically to GFAP-expressing astrocytes (>95%), with negligible levels of expression in neurons (NeuN-labelled cells) (**Figures 5.6D$_1$ and D$_2$**). DREADD (mCherry) expression was most abundant at the astrocyte cell body (see arrows in **Figure 5.6D$_1$**), but labelling of fine astrocytic spongiform processes was also evident, manifesting as sparse “cloud”-like mCherry labelling around the more densely-labelled cell body.

To investigate astrocyte-mediated regulation of POMC neuron activity, AAV-GFAP-hM3Dq-mCherry into the mediobasal hypothalamus of Pomc^{eGFP} mice (Pomc^{eGFP}::GFAP^{hM3Dq}) (**Figure 5.6C**). Following vehicle or CNO (1mg/kg) intraperitoneal injection, Pomc^{eGFP}::GFAP^{hM3Dq} mice were perfused and brains collected for processing of the neuronal marker of activation, c-Fos. We found that DREADD-mediated activation of astrocytes *in vivo* significantly elevated the total number of Fos-expressing cells in the MBH ($p_{treatment}$=0.0145), with CNO-treated mice exhibiting greater numbers of activated cells in the retrochiasmatic area (p=0.0105), and rostral (p=0.0337) and mid (p=0.0245) arcuate nucleus (**Figures 5.6E and F**). Importantly, POMC neurons constituted a substantial portion of activated cells, where 36.7 ± 3.7% of all POMC neurons colocalised with Fos in CNO-treated mice compared with 6.6 ± 1.8% in control (unpaired *t* test, t = 6.130, df = 3, p=0.0087). Astrocyte-mediated activation of POMC neurons was consistent along the rostro-caudal extent of the RCA and ARC ($p_{treatment}$=0.0080), where CNO-treated mice showed greater activation of POMC neurons than vehicle in the retrochiasmatic area (p=0.0027), and rostral (p=0.0026), mid (p=0.0204) and caudal (p=0.0068) arcuate nucleus (**Figure 5.6F**). Notably, we observed that all CNO-treated mice showed at least some CNO-induced Fos labelling of cells lining the third ventricle, consistent with the location and elongated morphology of tanycytes (see **Figure 5.6E**). All Fos-expressing (putative) tanycytes also colocalised with mCherry (not shown), suggesting that tanycyte activation is a result of direct stimulation through hM3Dq receptors expressed by the cell, and not as a response secondary to astrocyte activation.

We next performed current-clamp recordings from POMC neurons in acute *ex vivo* brain slices from $Pomc^{eGFP}$::$GFAP^{hM3Dq}$ mice (**Figure 5.6G$_1$**). Consistent with findings from the Fos-activation experiment, 60% (*n* = 9 of 15) of POMC neurons were reversibly depolarised (Δ+6.7 ± 1.3mV) and showed increased firing (Δ+0.70 ± 0.21Hz) in response to bath-application of CNO (**Figures 5.6G$_2$, G$_3$ and G$_5$**). Intriguingly, patch-clamp recordings revealed that a small subset (20%, *n* = 3 of 15) of neurons were in fact hyperpolarised (Δ−7.7 ± 0.5mV) following astrocyte activation, while a further 20% (*n* = 3 of 15) of neurons showed no response, suggesting that there is heterogeneity in responsivity between POMC cells (**Figures 5.6G$_4$ and G$_5$**). Following washout and reversal of the CNO-induced excitation, we investigated the mechanism through which Gq-signalling activation in astrocytes can depolarise neighbouring POMC neurons. Pre-treatment with a non-selective adenosine receptor antagonist and CD73 inhibitor significantly reduced subsequent CNO-induced excitation in 63% (*n* = 5 of 8) cells, attenuating depolarisation (p=0.0330) and action potential firing (p=0.0653) compared to baseline CNO application (**Figures 5.6G$_6$ and G$_7$**), indicating that at least part of the response is mediated by activation of adenosine receptors which promote membrane depolarisation.

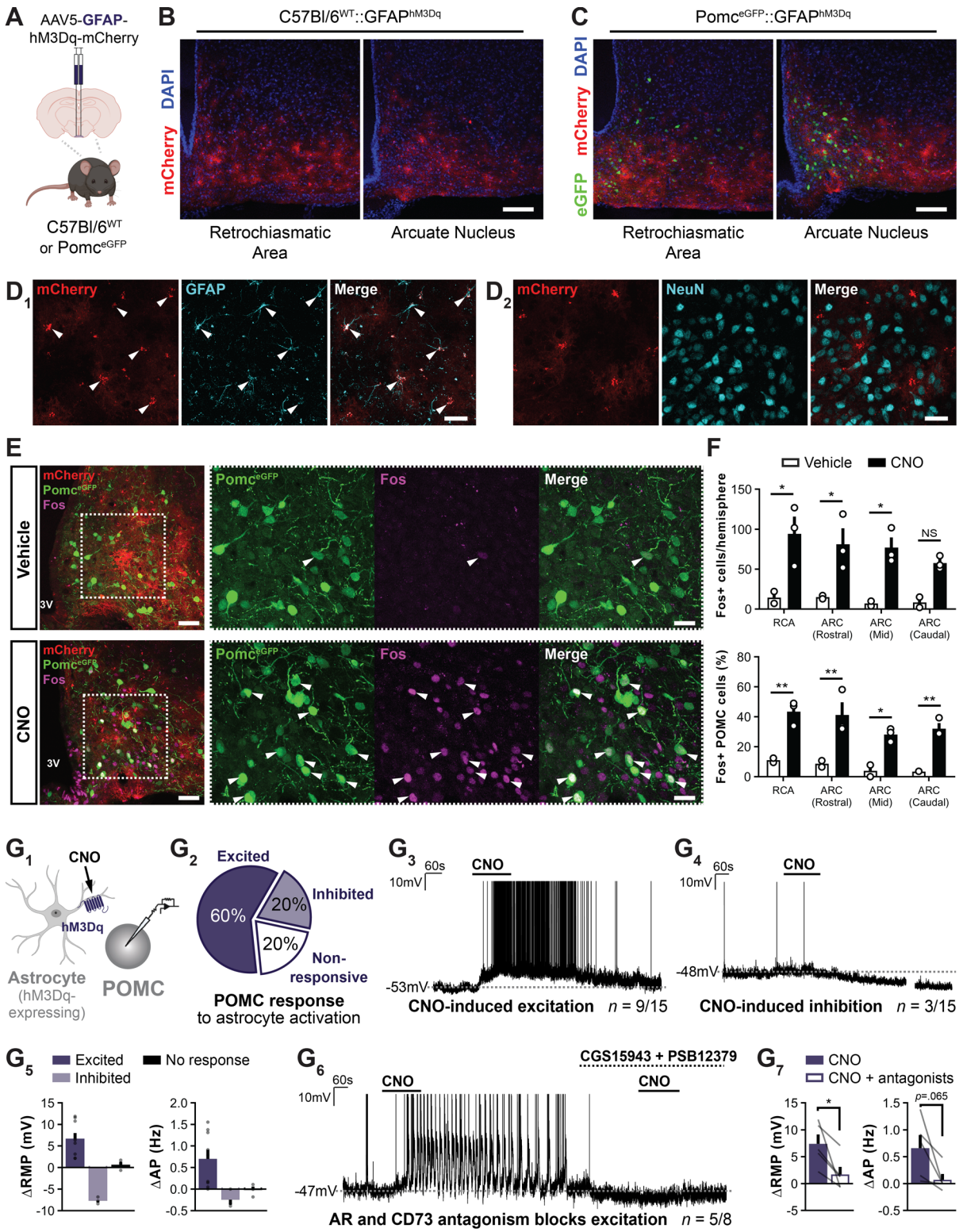

Figure 5.6 | DREADD-mediated activation of MBH astrocytes activates POMC neurons

(A) Astrocyte-activation strategy: C57Bl/6^{WT} or Pomc^{eGFP} mice injected bilaterally with AAV with GFAP promoter to induce expression of excitatory DREADD receptor, hM3Dq, in astrocytes in the mediobasal hypothalamus. **(B)** Representative confocal microphotographs of coronal sections from C57Bl/6^{WT}::GFAP^{hM3Dq} mice revealing expression of mCherry-tagged DREADD expressed in astrocytes restricted to the RCA and ARC, with DAPI counterstain. Scale bar, 100µm. **(C)** Representative confocal microphotographs of coronal sections from Pomc^{eGFP}::GFAP^{hM3Dq} mice revealing expression of mCherry-tagged DREADD expressed in astrocytes restricted to the RCA and ARC encompassing eGFP-labelled POMC neurons, with DAPI counterstain. Scale bar, 100µm. **(D$_1$**

and D_2) Representative confocal microphotographs of coronal sections from C57Bl/6^{WT}::GFAP^{hM3Dq} mice confirming that DREADD (mCherry) expression is restricted to astrocytes (GFAP, D_1), and is not expressed in neurons (NeuN, D_2). Scale bar, 25µm. **(E)** Representative confocal microphotographs of coronal sections from Pomc^{eGFP}::GFAP^{hM3Dq} mice injected with vehicle (top) or CNO (1mg/kg, bottom) intraperitoneally 90 minutes prior to perfusion. Left images show the expression of mCherry-tagged DREADD in arcuate nucleus (red), POMC neurons (green), and Fos protein (magenta). Zoom insets: white arrow heads indicate POMC cells (green) which colocalise with Fos protein (magenta). 3V, third ventricle. Scale bars, 50µm (low magnification), 25µm (high magnification). **(F)** Diagrams depicting the total number of Fos-expressing cells per hemisphere (top) and percentage of POMC cells that colocalise with Fos (bottom) throughout the rostro-caudal extent of the RCA and ARC, following intraperitoneal injection of vehicle or CNO (1mg/kg). Fos expression between treatments were analysed by repeated measures (by brain region only) two-way ANOVA followed by Sidak's multiple comparisons test (Total Fos+, n = 2 (vehicle), n = 3 (CNO) animals; treatment $F(1, 3) = 26.06$, p=0.0145; brain region $F(3, 9) = 0.8955$, p=0.4802; interaction $F(3, 9) = 0.4421$, p=0.7286. RCA, *p=0.0105; ARC (rostral), *p=0.0337; ARC (mid), *p=0.0245; ARC (caudal), p=0.1444 (NS). %POMC Fos+, n = 2 (vehicle), n = 3 (CNO) animals; treatment $F(1, 3) = 40.09$, p=0.0080; brain region $F(3, 9) = 3.010$, p=0.0871; interaction $F(3, 9) = 0.3882$, p=0.7643. RCA, **p=0.0027; ARC (rostral), **p=0.0026; ARC (mid), *p=0.0204; ARC (caudal), **p=0.0068). **($G_{1\text{-}7}$)** Investigating the effect of DREADD-mediated activation of MBH astrocytes on POMC neuron activity, by bath-application of the hM3Dq agonist, CNO (1µM) (G_1). The proportion of POMC neuron responses to CNO-induced activation of MBH astrocytes (G_2). Representative whole-cell current-clamp recording from a POMC neuron that was excited (G_3) or inhibited (G_4) by DREADD-mediated activation of astrocytes. In a subset of POMC neurons excited by astrocyte activation, re-application of CNO in the presence of the non-selective adenosine receptor antagonist, CGS15943, and CD73 inhibitor, PSB12379, blocked or attenuated the excitation (G_6). Diagrams depicting the CNO-induced changes in RMP and firing frequency for: the different POMC neuron responses to astrocyte activation (G_5), and the effect of adenosine receptor and CD73 inhibition on CNO-mediated excitation of POMC neurons (G_7). Changes in electrophysiological parameters were analysed by one sample t test (G_5; RMP: excited, n = 9 cells, t = 5.157, df = 8, ***p=0.0009; inhibited, n = 3 cells, t = 16.67, df = 2, **p=0.0036; non-responsive, n = 3 cells, t = 1.001, df = 2, p=0.4224. AP: excited, n = 9 cells, t = 3.384, df = 8, **p=0.0096; inhibited, n = 3 cells, t = 1.981, df = 2, p=0.1862; non-responsive, n = 3 cells, t = 0.2701, df = 2, p=0.8124) and paired t test (G_7; RMP, n = 5 cells, t = 3.197, df = 4, *p=0.0330; AP, n = 5 cells, t = 2.521, df = 4, p=0.0653).

Data in F, G_5 and G_7 are represented as mean ± SEM. Grey circles in G_5 and grey lines in G_7 represent individual and paired values, respectively.

5.3.7 Astrocyte-mediated activation of both POMC and AgRP neurons

Despite our findings that activation of MBH astrocytes stimulates satiety-promoting POMC neurons, previous studies report marked hyperphagia following *in vivo* chemogenetic stimulation of MBH astrocytes (Chen *et al.*, 2016). The authors found that co-inhibition of orexigenic AgRP neurons abolished the effect entirely, leading to the conclusion that AgRP neuron activity increases following activation of astrocyte gliotransmission. In consideration of this and our findings presented here, we hypothesised that in the context of chemogenetic (non-physiological) activation of astrocytes, there is indiscriminate activation of both AgRP and anorexigenic POMC neuronal populations. To test this hypothesis *in vivo*, we designed an experiment to measure food intake and brown fat temperature, each of which are increased following activation of AgRP or POMC neurons, respectively (Krashes *et al.*, 2011; Fenselau *et al.*, 2017) (see also **Chapter 4**).

To reproduce the experiments performed by Chen *et al.* (2016), which permit concurrent activation of MBH astrocytes and inhibition of AgRP neurons, we injected AAV-GFAP-hM3Dq-mChery into the MBH of $Agrp^{IRES\text{-}Cre}$ mice, in addition to a Cre-dependent AAV with a neuronal promoter to express mCherry (control; $GFAP^{hM3Dq}$::$Agrp^{mCherry}$) or the inhibitory DREADD, hM4Di ($GFAP^{hM3Dq}$::$Agrp^{hM4Di}$), in AgRP neurons (**Figure 5.7A$_1$ and A$_2$**). We included an additional control group in which only AgRP neurons were transfected with the hM4Di DREADD ($Agrp^{hM4Di}$) (**Figure 5.7A$_3$**), to account for effects related to silencing AgRP neurons without MBH astrocyte activation. Hypothalamic sections from experimental mice revealed expression of mCherry-labelled cells with neuronal morphology in the innermost ventromedial portion of the arcuate nucleus and retrochiasmatic area in all mice, consistent with viral expression of mCherry or hM4Di-mCherry (**Figures 5.7A$_{1\text{-}3}$**). In addition, $GFAP^{hM3Dq}$-injected mice showed dispersed mCherry expression in cells of spongiform morphology wholly or predominantly contained within the boundaries of the ARC and RCA, indicative of hM3Dq-mCherry expression in astrocytes (**Figures 5.7A$_1$ and A$_2$**).

Intraperitoneal injection of CNO (3mg/kg) into $GFAP^{hM3Dq}$::$Agrp^{mCherry}$ mice during the early light cycle revealed the expected hyperphagia induced by MBH astrocyte activation ($p_{treatment}$=0.0002, $p_{interaction}$<0.0001) (**Figure 5.7B$_1$**). CNO treatment dramatically increased 4h food intake by an average of 0.66 ± 0.07g compared to vehicle (p<0.0001), but did not appear to stimulate hyperphagia any further than control beyond this time point (8h: ∆0.62 ± 0.06g). Interestingly, by 24h post-injection, CNO-treated mice had consumed the same amount of food as vehicle-treated animals (p=0.9653). Consistent with previous reports (Chen *et al.*, 2016), the hyperphagia induced by MBH astrocyte activation was attributed to stimulation of AgRP neuron activity. This was evidenced by a markedly blunted food intake in $GFAP^{hM3Dq}$::$Agrp^{hM4Di}$ mice, consuming only 0.11 ± 0.06g (p=0.0166) more food 4 hours after CNO administration compared to vehicle (**Figure 5.7B$_2$**). Similarly to $GFAP^{hM3Dq}$::$Agrp^{mCherry}$ mice, there was no effect of CNO treatment in 24h food intake (p=0.3890) in $GFAP^{hM3Dq}$::$Agrp^{hM4Di}$ mice. Importantly, AgRP neuron inhibition in the absence of astrocyte stimulation caused a reduction in 8h (p=0.0111) and 24h (p=0.0317) food intake compared to vehicle-treated $Agrp^{hM4Di}$ animals (**Figure 5.7B$_3$**), consistent with the expected outcome of inhibition of orexigenic AgRP neurons.

We recorded interscapular BAT temperature changes to gauge whether MBH astrocyte activation simultaneously activates POMC neurons. While there was no effect of CNO administration

on BAT temperature in GFAP^{hM3Dq}::Agrp^{mCherry} mice relative to vehicle ($p_{treatment}$=0.5716, $p_{interaction}$=0.2508) (**Figure 5.7C$_1$**), we observed a CNO-induced thermogenic response in GFAP^{hM3Dq}::Agrp^{hM4Di} animals that persisted at least three hours following injection ($p_{interaction}$=0.0334) (**Figure 5.7C$_2$**). Importantly, AgRP neuron inhibition alone had no effect on BAT thermogenesis ($p_{treatment}$=0.7284, $p_{interaction}$=0.9735) (**Figure 5.7C$_3$**). These findings together indicate astrocyte-driven activation of BAT thermogenesis, presumably by promoting POMC neuron activity, is uncovered only under conditions of concurrent AgRP inhibition.

To gain insight on whether metabolic state influences the physiological outcome of DREADD-mediated MBH astrocyte activation, we fasted mice overnight and administered CNO (or vehicle) a half-hour prior to refeeding the next morning. MBH astrocyte activation (alone) did not exacerbate fasting-induced hyperphagia upon refeed, in fact CNO-treated GFAP^{hM3Dq}::Agrp^{mCherry} mice ate modestly less food following 8 hours of refeeding (∆−0.30 ± 0.20g, p=0.0399), but this effect had normalised by 24h (p=0.7010) (**Figure 5.7D$_1$**). Conversely, CNO treatment significantly reduced short-term food intake at 4h (p=0.0444) and 8h (p=0.0347) post-refeed for GFAP^{hM3Dq}::Agrp^{hM4Di} mice, and at all 1-8h (p<0.01) timepoints in Agrp^{hM4Di} mice, but had no impact on overnight food intake in either group (24h: p=0.4796, p=0.3455, respectively) (**Figures 5.7D$_2$ and D$_3$**). These findings reinforce the notion that AgRP-driven hyperphagia resulting from MBH astrocyte activation occurs only in the calorically-sated state. hM4Di-mediated inhibition of AgRP neurons, however, in both the presence and absence of astrocyte activation is sufficient to abrogate fasting-induced hyperphagia. There was no effect of MBH astrocyte activation, AgRP neuron inhibition, or a combination of both on postprandial thermogenesis in overnight fasted mice (all: $p_{treatment}$>0.05, $p_{interaction}$>0.05) (**Figures 5.7D$_{1-3}$**).

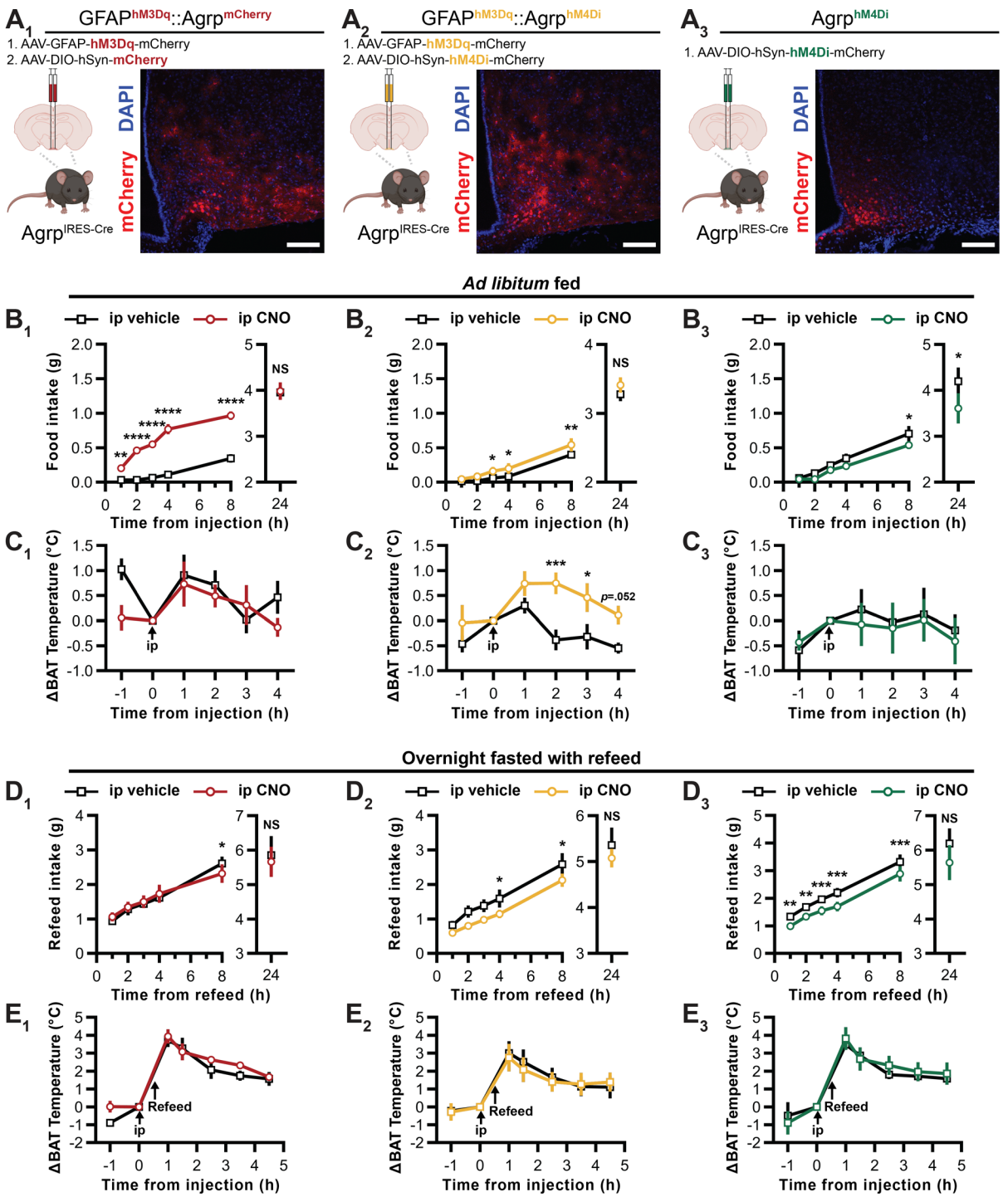

Figure 5.7 | DREADD-mediated activation of MBH astrocytes *in vivo* likely activates both AgRP and POMC neurons

(A1-3) Strategy to deconstruct the potential recruitment of both AgRP and POMC neurons following the DREADD-mediated activation of MBH astrocytes. Two experimental groups enabling MBH astrocyte activation were injected with an AAV encoding for the expression of the excitatory hM3Dq DREADD in astrocytes, and the Cre-dependent expression of either mCherry ($GFAP^{hM3Dq}::Agrp^{mCherry}$, A_1) or the inhibitory DREADD hM4Di ($GFAP^{hM3Dq}::Agrp^{hM4Di}$, A_2) in AgRP neurons (using $Agrp^{IRES\text{-}Cre}$ mice). A third experimental group controlling for AgRP neuron inhibition were injected with only the AAV encoding for the Cre-dependent expression of the inhibitory DREADD hM4Di ($Agrp^{hM4Di}$, A_3). Representative confocal microphotographs of coronal sections from the experimental groups, demonstrating mCherry fluorescence in astrocytes in the arcuate nucleus and AgRP neurons (A_1 and A_2), or just in AgRP neurons (A_3), consistent with expected expression based on viruses injected. DAPI

counterstain. Scale bar, 100µm. **(B_{1-3})** Diagrams depicting food intake in the hours subsequent to intraperitoneal injection of vehicle or CNO (3mg/kg), performed during the early light phase in calorically-sated $GFAP^{hM3Dq}$::$Agrp^{mCherry}$ (B_1), $GFAP^{hM3Dq}$::$Agrp^{hM4Di}$ (B_2) or $Agrp^{hM4Di}$ (B_3) mice. Differences in food intake from 1-8h were analysed by repeated measures (both factors) two-way ANOVA followed by Sidak's multiple comparisons test (B_1, n = 5 animals; treatment $F(1, 4) = 157.0$, p=0.0002; time $F(4, 16) = 70.40$, p<0.0001; interaction $F(4, 16) = 27.38$, p<0.0001. 1h, **p=0.0013; 2h, ****p<0.0001; 3h, ****p<0.0001; 4h, ****p<0.0001; 8h, ****p<0.0001. B_2, n = 5 animals; treatment $F(1, 4) = 3.651$, p=0.1286; time $F(4, 16) = 91.40$, p<0.0001; interaction $F(4, 16) = 1.710$, p=0.1970. 1h, p=0.8645; 2h, p=0.2717; 3h, *p=0.0378; 4h, *p=0.0166; **8h, p=0.0023. B_3, n = 5 animals; treatment $F(1, 4) = 1.864$, p=0.2440; time $F(4, 16) = 39.18$, p<0.0001; interaction $F(4, 16) = 1.458$, p=0.2609. 1h, p=0.9987; 2h, p=0.3453; 3h, p=0.5546; 4h, p=0.1306; 8h, *p=0.0111) and food intake at 24h was analysed by paired t test (B_1, n = 5 animals; t = 0.1128, df = 4, p=0.9157 (NS). B_2, n = 5 animals; t = 0.9653, df = 4, p=0.3890 (NS). B_3, n = 5 animals; t = 3.241, df = 4, *p=0.0317). **(C_{1-3})** Diagrams depicting change in BAT temperature in the four hours subsequent to intraperitoneal injection of vehicle or CNO (3mg/kg), performed during the early light phase in calorically-sated $GFAP^{hM3Dq}$::$Agrp^{mCherry}$ (C_1), $GFAP^{hM3Dq}$::$Agrp^{hM4Di}$ (C_2) or $Agrp^{hM4Di}$ (C_3) mice. Differences in BAT temperature were analysed by repeated measures (both factors) two-way ANOVA followed by Sidak's multiple comparisons test (C_1, n = 5 animals; treatment $F(1, 4) = 0.3788$, p=0.5716; time $F(4, 16) = 4.773$, p=0.0100; interaction $F(4, 16) = 1.494$, p=0.2508. 0h, p>0.9999; 1h, p=0.9708; 2h, p=0.9383; 3h, p=0.8156; 4h, p=0.1827. C_2, n = 5 animals; treatment $F(1, 4) = 5.028$, p=0.0884; time $F(4, 16) = 9.080$, p=0.0005; interaction $F(4, 16) = 3.420$, p=0.0334. 0h, p>0.9999; 1h, p=0.3028; ***2h, p=0.0007; *3h, p=0.0169; 4h, p=0.0519. C_3, n = 5 animals; treatment $F(1, 4) = 0.1388$, p=0.7284; time $F(4, 16) = 0.7938$, p=0.5463; interaction $F(4, 16) = 0.1195$, p=0.9735. 0h, p>0.9999; 1h, p=0.9082; 2h, p=0.9987; 3h, p=0.9986; 4h, p=0.9719). **(D_{1-3})** Diagrams depicting food intake in the hours subsequent to refeeding overnight fasted $GFAP^{hM3Dq}$::$Agrp^{mCherry}$ (D_1), $GFAP^{hM3Dq}$::$Agrp^{hM4Di}$ (D_2) or $Agrp^{hM4Di}$ (D_3) mice, where mice were injected intraperitoneally with vehicle or CNO (3mg/kg) a half-hour prior to refeeding. Differences in food intake from 1-8h were analysed by repeated measures (both factors) two-way ANOVA followed by Sidak's multiple comparisons test (D_1, n = 5 animals; treatment $F(1, 4)$ =0.004151, p=0.9517; time $F(4, 16) = 96.07$, p<0.0001; interaction $F(4, 16) = 3.154$, p=0.0432. 1h, p=0.7686; 2h, p=0.9753; 3h, p=0.9862; 4h, p=0.7686; 8h, *p=0.0399. D_2, n = 5 animals; treatment $F(1, 4) = 4.151$, p=0.1113; time $F(4, 16) = 127.3$, p<0.0001; interaction $F(4, 16) = 0.4207$, p=0.7914. 1h, p=0.5790; 2h, p=0.0631; 3h, p=0.0760; 4h, *p=0.0444; *8h, p=0.0347. D_3, n = 5 animals; treatment $F(1, 4) = 4.824$, p=0.0930; time $F(4, 16) = 78.32$, p<0.0001; interaction $F(4, 16) = 0.6071$, p=0.6633. 1h, **p=0.0044; 2h, **p=0.0046; 3h, ***p=0.0008; 4h, ***p=0.0001; 8h, ***p=0.0005) and food intake at 24h was analysed by paired t test (D_1, n = 5 animals; t = 0.4127, df = 4, p=0.7010 (NS). D_2, n = 5 animals; t = 0.7788, df = 4, p=0.4796 (NS). D_3, n = 5 animals; t = 1.068, df = 4, p=0.3455 (NS)). **(E_{1-3})** Diagrams depicting change in BAT temperature following refeeding of overnight fasted $GFAP^{hM3Dq}$::$Agrp^{mCherry}$ (E_1), $GFAP^{hM3Dq}$::$Agrp^{hM4Di}$ (E_2) or $Agrp^{hM4Di}$ (E_3) mice, where mice were injected intraperitoneally with vehicle or CNO (3mg/kg) a half-hour prior to refeeding. Differences in BAT temperature were analysed by repeated measures (both factors) two-way ANOVA followed by Sidak's multiple comparisons test (E_1, n = 5 animals; treatment $F(1, 4) = 0.2084$, p=0.6717; time $F(5, 20) = 73.85$, p<0.0001; interaction $F(5, 20) = 0.6024$, p=0.6988. 0h, p>0.9999; 1h, p=0.9708; 1.5h, p=0.9980; 2.5h, p=0.6600; 3.5h, p=0.6635; 4.5h, p>0.9999. E_2, n = 5 animals; treatment $F(1, 4) = 0.01094$, p=0.9217; time $F(5, 20) = 31.19$, p<0.0001; interaction $F(5, 20) = 0.3048$, p=0.9042. 0h, p>0.9999; 1h, p=0.9972; 1.5h, p=0.9469; 2.5h, p=0.9962; 3.5h, p>0.9999; 4.5h, p=0.9935. E_3, n = 5 animals; treatment $F(1, 4) = 0.1432$, p=0.7243; time $F(5, 20) = 55.35$, p<0.0001; interaction $F(5, 20) = 0.5353$, p=0.7471. 0h, p>0.9999; 1h, p=0.9059; 1.5h, p=0.9960; 2.5h, p=0.6187; 3.5h, p=0.9802; 4.5h, p=0.9644).

Data in B-E are represented as mean ± SEM.

5.4 Discussion

In this chapter, we aimed to comprehensively profile the glucose-sensitivity of hypothalamic POMC neurons and to delineate the underlying signal transduction mechanisms driving POMC neuronal glucose-sensing. Patch clamp recordings obtained from over 450 POMC-expressing neurons in the mediobasal hypothalamus revealed responses not previously reported in POMC neurons; namely glucose-induced inhibitions and novel glucose-induced burst-firing responses. We also defined the contribution of astrocyte metabolism and adenosine signalling to the mechanistic underpinnings of glucose-responsiveness. Approximately half of glucose-induced excitations were blocked or reversed by a selective A_1R antagonist. Investigation of the nature of glucose-induced changes in adenosine signalling indicated that astrocyte mitochondrial respiration of glucose leads to increased release of ATP through Cx43 hemi-channels. ATP is subsequently degraded extracellularly by ectonucleotideases into adenosine which in turn drives excitation of glucose-excited POMC neurons. These data show for the first time a critical role of glial-derived adenosine in POMC glucose-sensing. Pharmacological manipulation of the adenosine synthesis pathway revealed a remarkable plasticity in POMC neuron glucose-responsiveness, reflective of a multifactorial glucose-sensing mechanism whereby glucose-excited neurons could be switched to glucose-inhibited. Further studies will be required to fully appreciate the functional significance of this potential plasticity. Finally, we substantiate the sufficiency of chemogenetically-stimulated astrocyte signalling to activate adjacent POMC and AgRP neurons, the former via liberation of adenosine, resulting in rapid physiological adaptations to appetite and brown fat thermogenesis.

5.4.1 Novel insights into the heterogeneity of hypothalamic POMC neuron glucose-sensing

Glucose-induced changes in POMC neuron activity are widely believed to underpin two primary physiological functions of the melanocortin system: 1) the detection of caloric sufficiency and resultant promotion of satiety, and 2) the regulation of peripheral glucose homeostasis through modulation of autonomic outflow (Plum *et al.*, 2006; Claret *et al.*, 2007; Parton *et al.*, 2007; Santoro *et al.*, 2017). However, both traditional electrophysiological or indirect calcium imaging-based assessments of glucose-sensitivity have yielded conflicting results regarding POMC neuron glucose-responsiveness. In most studies, POMC neurons are reported to be depolarised and activated by elevated glucose (from 51-100% of sampled cells) (Ibrahim *et al.*, 2003; Claret *et al.*, 2007; Parton *et al.*, 2007), but there are others that suggest a lack of cell-autonomous glucose sensitivity (Fioramonti *et al.*, 2007; Fioramonti *et al.*, 2017).

5.4.1.1 Glucose-induced excitations

In the present study, we found that 33% (ARC) to 39% (RCA) of POMC-eGFP neurons (*n* = 452), investigated using brain slice whole-cell patch clamp electrophysiology, were excited by an extracellular D-glucose transition from 1.0 to 5.0mM. Given that the data presented here clearly

demonstrate differential sensitivity of hypothalamic POMC neurons to elevated glucose, relatively small sample sizes (*n* = 7 to 59 cells in the papers referenced above) and methodological differences (extracellular glucose/intracellular ATP concentrations, mode of measuring neuronal activity) may account for inconsistencies in glucose-sensitivity assessment. Indeed, it was recently shown that recordings made with low (1.0mM) or high (5.0mM) intracellular ATP elicit differing proportions of glucose-sensing responses in ARC neurons (van den Top *et al.*, 2017). The current-voltage relationship changes in most glucose-excited POMC neurons were associated with the closure of one or more potassium conductances, consistent with previous reports that K_{ATP} inactivation mediates glucose-induced depolarisation of POMC cells (Ibrahim *et al.*, 2003; Parton *et al.*, 2007). While examination of conductance changes was not a focus of the present study, we did also observe the glucose-induced activation of non-selective cation conductance(s) in a smaller fraction of POMC neurons. A recent study demonstrated that deletion of transient receptor potential channel (TRPC) 3, a non-selective cation channel, from MBH neurons reduces glucose-induced satiety and the overall proportion of glucose-excited neurons in the MBH (Chrétien *et al.*, 2017). Moreover, it is known that other cues relating to energy status, such as leptin and insulin, activate POMC neurons by coupling to non-selective cation TRPC channels (Qiu *et al.*, 2010; Qiu *et al.*, 2014). The potential for involvement of TRPC channels in POMC neuron glucose-induced excitations requires further investigation.

5.4.1.2 Glucose-induced inhibitions

Remarkably, the glucose-induced inhibition of POMC neurons, observed in 7-8% of cells sampled in this study, has never been reported. The physiological function of POMC cells inhibited by elevations in extracellular glucose remains to be determined, but mechanistically the response appeared to be mediated by activation of a potassium and/or chloride conductance. It could be that, in this subpopulation of POMC neurons, glucose activates PI3K intracellular signalling to activate K_{ATP} conductances and induce hyperpolarisation in a similar manner to insulin receptor activation on POMC neurons (Plum *et al.*, 2006; Hill *et al.*, 2008). Indeed, the fatty acid oleic acid has been demonstrated to hyperpolarise (unidentified) ARC neurons through K_{ATP} activation (Dadak *et al.*, 2017). Moreover, it was recently shown that octanoic acid hyperpolarises a subset of POMC neurons by activation of potassium and/or chloride ion channels (Haynes *et al.*, 2020), similar to glucose-induced hyperpolarisations observed here.

5.4.1.3 Glucose-induced burst-firing

The observed glucose-induced burst-firing response in POMC neurons of the RCA (8%) and rostral/middle ARC (4%) is a novel pattern of glucose-induced neural activity that has not been reported in any neuronal system. The burst-firing pattern of activity appeared to be the result of two co-ordinated bioelectrical events: 1) phasic/oscillatory changes in membrane potential which appear to involve the cyclic opening/closure of voltage-dependent non-selective cation and potassium conductance(s), and 2) $GABA_A$-mediated post-synaptic potentials which instigate or sustain prolonged burst-firing bouts during the “up” state of the oscillation. The nature of the potassium conductance(s) contributing to

glucose-induced oscillations in POMC membrane potential was not clarified. However, IV relationships determined during glucose-induced burst-firing indicated activation of an inwardly-rectifying potassium conductance (K_{IR}). In this vein, K_{ATP} channels, which are made up of $K_{IR}6$ subunits (Inagaki *et al.*, 1995), have been demonstrated to mediate glucose-induced excitations in POMC neurons in a manner comparable to pancreatic β-cell glucose-sensing (Parton *et al.*, 2007). It is tempting to speculate that the oscillations in membrane potential associated with glucose-induced burst-firing cells are mechanistically similar to those which occur in β-cells to promote phasic insulin release (Tengholm & Gylfe, 2009). Indeed, it has been suggested that cyclical changes in pancreatic ATP/ADP cytosolic ratio resulting from the metabolic cost of phasic insulin release underpins membrane potential oscillations by the reciprocal activation/inhibition of K_{ATP} channels (Miwa & Imai, 1999; Rolland *et al.*, 2002; Fridlyand *et al.*, 2010). As an alternative, adenosine receptors (as outlined below) may have contributed to the response, acting via G protein-coupled inwardly-rectifying potassium channels (GIRK; $K_{IR}3$) (Kim & Johnston, 2015; James *et al.*, 2018).

In addition to activation of K_{IR}, a common feature of these cells was the expression of I_H. This conductance has been extensively described in neurons and in the heart, where they contribute to pacemaker-like oscillatory activity (McCormick & Pape, 1990; Brãuer *et al.*, 2001; Herrmann *et al.*, 2015). This non-selective cation conductance is activated by membrane hyperpolarisation, once activated then driving the cell to depolarise to threshold for firing. Other intrinsic conductances can then lead to hyperpolarisation and re-activation of I_H, creating oscillatory pacemaker-like activity. Such state-dependent shifts in activity have been extensively documented, for example in the thalamus (see McCormick and Pape (1990)). Hyperpolarisation is requisite for this pacemaker activity and the data presented here suggest direct involvement of $GABA_A$ synaptic transmission. Indeed, studies in other brain regions have identified that $GABA_A$-mediated inhibitory post-synaptic potentials evoke or contribute to prolonged rebound firing (Alviña *et al.*, 2008; Zheng & Raman, 2011). Of particular interest, glucose-sensing GABAergic and glutamatergic populations in the ARC are synaptically inter-connected (van den Top *et al.*, 2017), suggesting that glucose-induced POMC burst-firing observed here may be orchestrated by other local glucose-sensing GABAergic populations in a pre-synaptic manner.

5.4.2 Adenosine receptor regulation of POMC neuron activity

Chemo- and opto-genetic strategies to activate hypothalamic astrocytes reveal increased local concentrations of extracellular adenosine, which act in an A_1R-dependent manner to regulate satiety (Yang *et al.*, 2015; Sweeney *et al.*, 2016). In addition, elevations in extracellular glucose stimulate astrocyte metabolism-dependent production of adenosine which activate GPCRs expressed on adjacent neurons in both the hindbrain and rostral hypothalamus, implicating astrocyte-derived adenosine in the mediation of neuronal glucose-sensing (McDougal *et al.*, 2013; Rogers *et al.*, 2016; Scharbarg *et al.*, 2016; Rogers *et al.*, 2018). We demonstrate here that a similar adenosine-dependent mechanism of glucose-sensing occurs for some hypothalamic POMC neurons. We show immunohistochemically that the majority of POMC neurons express A_1R, $A_{2A}R$ and A_3R, and, importantly, that GFAP-expressing astrocytic processes and cell bodies were found in close apposition to adenosine receptor-expressing POMC cells. Using a non-selective adenosine receptor antagonist,

we confirm that adenosinergic signalling accounts for ~40% of glucose-induced excitations of POMC neurons. These glucose-induced excitations appear to be dependent on activation of A_1R, as a selective A_1R antagonist blocked a similar (~50%) proportion of GE responses. However, it is unclear how A_1R activation transduces neuronal excitation as post-synaptic A_1R is typically coupled to $G_{i/o}$ protein intracellular signalling pathways, adenylate cyclase and cAMP, and can activate K^+ and inhibit Ca^{2+} conductances to hyperpolarise the neuron (see Dunwiddie and Masino (2001)). Considering that our experiments were not performed in the presence of synaptic blockers, there is the possibility of a pre-synaptically-mediated effect. For example, inhibition of pre-synaptic GABAergic release following A_1R activation mediates the cannabinoid-induced excitation of neurons in the suprachiasmatic nucleus (Acuna-Goycolea *et al.*, 2010; Hablitz *et al.*, 2020), and GABAergic input to POMC neurons is known to be regulated by energy status (Vong *et al.*, 2011; Rau & Hentges, 2019). However, this mode of action seems unlikely given that A_1R agonism depolarised GE POMC neurons through closure of a K^+ conductance. It is tempting to speculate, then, that depolarisation is mediated by inactivation of K_{ATP} channels through a A_1R-dependent G-protein signalling cascade (i.e. closure occurs independently of cytosolic ATP/ADP concentration). Indeed, an ATP-independent mechanism of glucose-induced closure of K_{ATP} has been suggested in hypothalamic neurons co-cultured with glial cells (Ainscow *et al.*, 2002). Furthermore, reduced extracellular glucose is sensed by hippocampal neurons via an A_1R-dependent mechanism which *activates* K_{ATP} channels and leads to neuronal hyperpolarisation (Kawamura *et al.*, 2010), evidence of a plausible link between glucose availability, A_1R signalling and K_{ATP} channels. In any case, we found that *in vivo* i.c.v. administration of DPCPX before the onset of the dark period increased overnight (but not short-term) food intake and decreased dark cycle energy expenditure. Given that POMC/melanocortin-receptor activation promotes slow-onset satiety but rapidly increases BAT thermogenesis and energy expenditure (Monge-Roffarello *et al.*, 2014b; Fenselau *et al.*, 2017), these data support the notion that POMC neurons are activated by an A_1R-dependent mechanism during the feeding phase.

We also found some evidence for adenosine-mediated inhibition of POMC neurons. In the fed state and bathed in 5.0mM extracellular glucose, non-selective adenosine receptor antagonism revealed both tonic excitatory *and* inhibitory adenosine-regulated inputs. Indeed, in the small sample of GI POMC neurons investigated, non-selective adenosine receptor antagonism was able to reverse glucose-induced hyperpolarisation (n = 1 of 3), but A_1R antagonism had no effect (n = 5 of 5). While we are hesitant to draw strong conclusions on the basis of these few observations, it is possible that $A_{2A}R$ and/or $A_{2B}R$ signalling mediate at least part of the adenosine-mediated inhibitory tone considering recent findings that these receptors mediate octanoic acid-induced hyperpolarisation of POMC neurons (Haynes *et al.*, 2020). Interestingly though, central administration of neither $A_{2A}/A_{2B}R$ nor A_3R antagonists had an effect on food intake, suggestive of a dominant role for A_1R signalling in the regulation of appetite. In spite of this finding, A_3R antagonism revealed a “conversion” of a small subset of both GE and NR POMC neurons into a glucose-adapting response type, which has been recently identified in CART-expressing neurons in the ARC (van den Top *et al.*, 2017). It is unclear why we did not observe any glucose-adapting POMC neurons without pharmacological intervention considering that most CART-expressing neurons also express POMC (Vrang *et al.*, 1999). This may be the result of species-related differences in the glucose-responsiveness of POMC neurons (mouse used here, rat

used by van den Top *et al.* (2017)), or alternatively it may reflect the time of exposure to the increase in glucose. Glucose-adaptors were identified based upon prolonged exposure of neurons to glucose changes, and as such the approach used here may not have permitted time for the adaptation to engage. Further studies are required to substantiate the mechanism of the A_3R-mediated effect, but it may involve adenosine signalling on astrocytes considering that we found the A_3R frequently colocalised with GFAP-positive processes adjacent to POMC neurons.

5.4.3 A model for astrocyte-regulated glucose-sensing in POMC neurons

Using an array of pharmacological inhibitors, we demonstrated the involvement of astrocyte activity and signalling in regulating glucose-dependent changes in POMC activity. Astrocytes release adenosine and ATP into the extracellular space through Cx43 hemi-channels (Bennett *et al.*, 2003; Kang *et al.*, 2008). Inactivation of Cx43 produced distinct disturbances to the glucose-sensitivity of POMC neurons, blocking or even reversing the glucose-sensitivity of ~70% of glucose-excited POMC cells when glucose was re-applied in the presence of the Cx43 inhibitors. Considering that we have found POMC neurons reliably reproduce glucose-sensing responses upon washout and re-application (data not shown here; see van den Top *et al.* (2017)), we are confident that the effects observed with Cx43 (and other) inhibitors are robust. We demonstrate that inactivation of astrocyte glucose uptake blocked half of glucose-induced excitations in POMC neurons, as well as revealing both excitatory and inhibitory tone from astrocytes when applied to cells in the calorically-sated state. Similarly, application of fluorocitrate, a selective glial cell metabolic poison, disrupted glucose-induced excitations in greater than 80% of POMC neurons.

The finding that inhibition of ecto-5'-nucleotidease (i.e. CD73), the enzyme which dephosphorylates AMP to adenosine, resulted in similar defects in POMC glucose-sensing suggests that astrocytes release ATP which is subsequently degraded *in situ* into adenosine by extracellularly expressed ectonucleotideases. This is consistent with reports of ectonucleotidease expression and activity in cells from the arcuate nucleus (He *et al.*, 2005; Belcher *et al.*, 2006; Bjelobaba *et al.*, 2006). While we cannot completely discount the possibility that adenosine is also released directly from astrocytes, it was reported that hippocampal astrocytes transition from ATP to adenosine release specifically during metabolic *stress* (hypoxia) (Martín *et al.*, 2007), and therefore adenosine (rather than ATP) release is perhaps unlikely in the environment of metabolic *surplus* that is simulated here (increased glucose).

We sought to reinforce these findings by using a chemogenetic strategy to modulate the activity of astrocytes in the mediobasal hypothalamus. While activation of G_i-coupled DREADDs causes neuronal hyperpolarisation and inhibition (Armbruster *et al.*, 2007), in astrocytes, activation of all presently available G-protein coupled DREADDs (G_q, G_i and G_s) lead to stimulation of Ca^{2+} flux and hence *increase* astrocyte gliotransmission (Durkee *et al.*, 2019). In lieu of appropriate tools to acutely reduce astrocyte activity, we induced expression of hM3Dq specifically in astrocytes of the mediobasal hypothalamus to test instead the *sufficiency* of astrocyte activity to modulate POMC neuron activity. Indeed, bath-application of CNO resulted primarily in depolarisation and increased firing rate (~60%) of

adjacent POMC neurons, but also, in some cases, silencing and hyperpolarisation (~20%). Importantly, re-application of CNO in the presence of a non-selective adenosine receptor antagonist and CD73 inhibitor blocked the majority of CNO-induced excitations of POMC neurons, confirming the involvement of adenosine in astrocyte-POMC neuron intercommunication.

5.4.3.1 A schema for astrocyte-mediated glucose-sensing in POMC neurons

In view of our findings, we propose a novel means for POMC neurons to sense fluctuations in extracellular glucose, presented graphically in the schematic below (**Figure 5.8**). Postprandial elevations in circulating glucose enter the CNS through GLUT1-mediated transporters which are expressed on astrocytic endfeet that ensheath cerebral capillaries. Increased uptake drives astrocytic respiration of glucose into ATP which is released through Cx43 hemi-channels into the extracellular space. ATP is degraded extracellularly by ectonucleotideases, with the final AMP to adenosine dephosphorylation step catalysed by CD73. The resulting elevation in extracellular concentration of adenosine acts in a paracrine fashion on A_1R-expressing POMC neurons to promote neuronal activity. The activation and subsequent function of other adenosine receptor(s) expressed by POMC neurons requires further investigation.

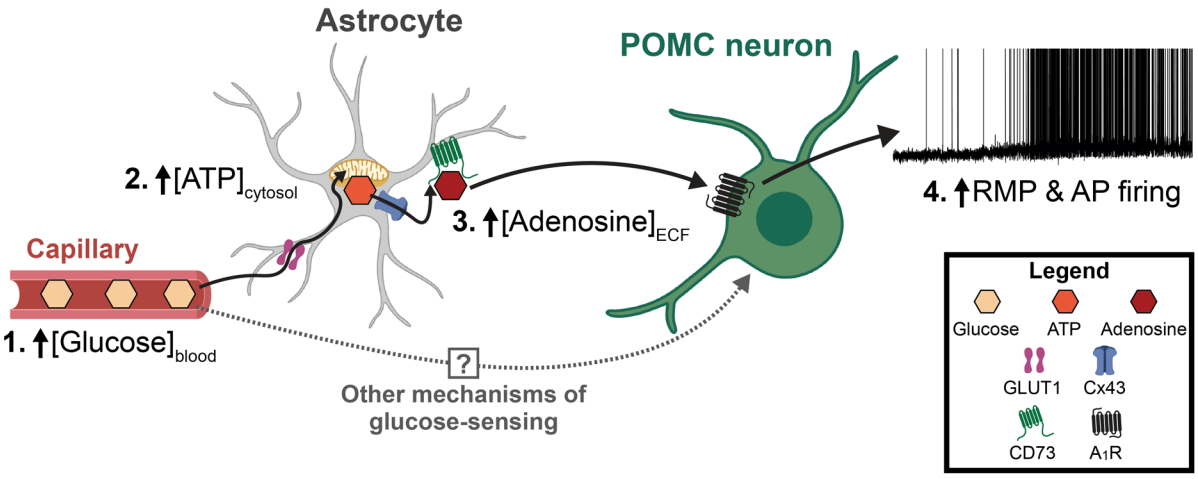

Figure 5.8 | Proposed schema for astrocyte-regulated POMC neuron glucose-sensing

Elevated glucose concentration circulating in the blood (1) undergoes facilitated transport through GLUT1 into astrocytes which ensheath cerebral capillaries. Mitochondrial respiration of glucose within astrocytes increases cytosolic ATP concentration (2) which is released through Cx43 hemi-channels into the extracellular fluid (ECF). ATP undergoes dephosphorylation by extracellularly-expressed ectonucleotideases, including the final step of conversion of AMP to adenosine by CD73 (3). Adenosine binds to A_1R expressed on POMC neurons to increase resting membrane potential (RMP) and action potential (AP) firing (4). Grey dotted line denotes the existence of other POMC glucose-sensing mechanisms that are independent of the described pathway.

5.4.3.2 Evidence for "plasticity" in glucose-sensitivity of POMC neurons?

The schema presented in **Figure 5.8** includes an indication of other glucose-sensing pathways that regulate POMC neuron activity, either in addition to or distinct from the astrocyte-adenosine-A_1R circuit described here. This is an important consideration that is reflected in the present study by the insufficiency of pharmacological inhibition at any step of this pathway to block *all* glucose-induced excitations, also frequently leading to the "uncovering" of glucose-induced *inhibitions* in formerly-identified glucose-excited POMC neurons. Furthermore, Cx43 inhibition (with carbenoxolone) revealed, remarkably, a mixture of glucose-induced excitations (29%) and inhibitions (21%) in POMC neurons that were otherwise demonstrably *insensitive* to glucose. In light of these findings, we propose a model of multiple, competing and/or complementary "inputs" to POMC neurons in response to elevations in extracellular glucose. That is, the observed neuronal "output" (activity) is the result of the summation of the relative magnitudes of each input. For example, the revelation of glucose-induced inhibitions in formerly glucose-excited or glucose-insensitive POMC neurons may be explained by the disruption of excitatory but not inhibitory input.

The concept of several means of signalling the glucose stimulus to POMC neurons may underpin prior observations of energy-status-dependent "plasticity" of glucose-sensing networks in the ARC (van den Top *et al.*, 2017). The authors found that the proportion and polarity of glucose-induced responses in ARC neurons was dependent on intracellular ATP concentration and the energy status of the animal (calorically sated vs. deplete). Observations described in our study suggest that energy-status-dependent tone signalled via glial-derived adenosine may also be a factor in setting glucose-sensitivity in these networks. Adenosine antagonists or inhibitors of the adenosine synthesis pathway alone induced changes in electrical excitability, suggesting that distinct subpopulations are tonically regulated by adenosine in both the fed and fasted state. Therefore, depending on energy status and glucose-dependent adenosine tone, the gain or sensitivity of the glia-neuronal network to subsequent shifts in glucose levels may be subject to an energy-status-dependent plasticity. Indeed, cues associated with metabolic status have been shown to affect astrocyte glucose uptake as well as astroglial coverage of POMC neurons (Fuente-Martín *et al.*, 2012; Kim *et al.*, 2014; Garcia-Caceres *et al.*, 2016; Nuzzaci *et al.*, 2020). In conjunction with gene-expression changes in POMC neurons that accompany alterations in energy status (Henry *et al.*, 2015; Campbell *et al.*, 2017), these adaptations may form the molecular basis of the heterogeneity and plasticity of POMC neuron glucose-sensing, ultimately engaging a co-ordinated neuronal response that is appropriate for the physiological state. The mechanisms that mediate the residual glucose-sensing inputs to POMC neurons remain to be determined. This includes whether POMC neurons are capable of cell-autonomous glucose-induced excitation, produced by closure of K_{ATP} channels as has been previously described (Ibrahim *et al.*, 2003; Parton *et al.*, 2007).

5.4.4 *In vivo* relevance of mediobasal hypothalamus astrocyte activity

In contrast to the satiety-promoting effects reported following activation of astrocytes in the whole hypothalamus (Yang *et al.*, 2015; Sweeney *et al.*, 2016), chemogenetic stimulation of astrocytes

specifically within the ARC is reported to rapidly evoke feeding behaviour in an AgRP-dependent manner (Chen *et al.*, 2016). In addition to the discussed electrophysiological and histological indices of astrocyte-stimulation-induced POMC activity, *in vivo* experiments performed here suggest that ARC/RCA astrocyte activity is sufficient to activate *both* AgRP and POMC neurons. In line with Chen *et al.* (2016), we demonstrate that pronounced hyperphagia upon stimulation of MBH astrocytes was markedly attenuated with concurrent inhibition of AgRP neurons. Importantly, elevated food intake resulting from astrocyte stimulation (alone) was completely normalised 24 hours post-administration of CNO. This contrasts with the hyperphagia induced via *direct* chemogenetic-activation of AgRP neurons which endures at least 24 hours (Krashes *et al.*, 2011; Nakajima *et al.*, 2016). In addition, astrocyte stimulation in overnight-fasted mice, when AgRP neuron activity is already elevated (Liu *et al.*, 2012), did not produce an exacerbated hyperphagic phenotype, rather a mildly *reduced* 8-hour food intake. These findings are suggestive of a counter-balancing, longer-term satiety signal that is consistent with the (concurrent) activation of POMC neurons (Zhan *et al.*, 2013; Fenselau *et al.*, 2017). Indeed, due to the dominant and rapid hyperphagia induced by AgRP neuron activation, optogenetic stimulation of both AgRP and POMC neurons in sated mice is capable of producing similar short-term feeding to AgRP stimulation alone, but effects on long-term food intake were not reported (Atasoy *et al.*, 2012).

We and others have shown that acute activation of POMC neurons is also sufficient to stimulate thermogenic activity in brown fat (see **Chapter 4** and Fenselau *et al.* (2017)). Notably, while astrocyte stimulation alone had no effect on BAT thermogenesis, the concurrent inhibition of AgRP neurons (but not AgRP inhibition alone) revealed a robust thermogenic response. This finding supports the notion that MBH astrocyte activity *in vivo* can modulate BAT thermogenesis via POMC neuron activation, which is only revealed upon elimination of AgRP/NPY-mediated sympathoinhibition (Shi *et al.*, 2013; Burke *et al.*, 2017). Importantly, the concurrent astrocyte-mediated activation of antagonistic POMC and AgRP populations observed here is likely a consequence of the “artificial” or “non-physiological” nature of the chemogenetic intervention. We suggest that this is unlikely to occur in the context of endogenous glia-neuron signalling in the ARC/RCA, however future studies are required to confirm this.

5.4.5 Conclusions

The present study builds upon rapidly-accumulating evidence for heterogeneity amongst hypothalamic POMC neurons, as well as the role that astrocytes play in the relaying of interoceptive signals to these energy-sensing cells. We identify novel subpopulations of POMC neurons that are silenced or undergo rhythmic burst-firing patterns of activity in response to elevations in extracellular glucose, challenging the dogma that all POMC neurons are excited by this meal-derived stimulus. We discovered an astrocyte-mediated A_1R-dependent activation of POMC neurons following increased glucose availability, as well as indications that individual glucose-excited POMC neurons can also receive opposing inhibitory inputs in response to the same stimulus (high glucose). On the basis of these and previously published findings, we propose that POMC glucose-sensing is adaptable according to metabolic status, and therefore that POMC neuron output is finely tuned to engage physiological responses appropriate to the internal state.

Chapter 6

General Discussion

6.1 Brief overview

The primary aim of this thesis was to dissect the central pathways and mechanisms involved in the endogenous recruitment of meal-induced sympathetic outflow to brown fat. Until now, there has been an extensive focus (only) on the central thermoregulatory pathways that initiate and effect cold-induced BAT thermogenesis. Here, we enter largely "uncharted territory" in our efforts to demarcate the hypothalamic circuitry that regulates the postprandial activation of brown fat thermogenesis. A key platform of this study was the implementation of PRV-facilitated mapping of BAT-projecting neurons, permitting the discovery of a multi-nodal **glucose-sensing** system within the hypothalamus, headed by predominantly **glucose-activated POMC neurons** in the ARC and RCA. We provide support for the hypothesis that glucose (meal)-activated hypothalamic POMC neurons contribute to postprandial thermogenesis by combining of POMC loss-of-function models with the measurement of real-time changes in postprandial BAT temperature. Furthermore, we make considerable inroads toward an understanding of the formerly unrecognised breadth and complexity in the nature of POMC neuron glucose-sensing. In particular, we shift the focus away from traditional "neuron-centric" views of glucose-detection, and bring astrocyte-mediated glucose metabolism and paracrine gliotransmission into the spotlight.

6.2 "Food" for thought: more on the regulation of postprandial thermogenesis

Considering much of this thesis has focussed on the detail of the central neural control of diet-induced thermogenesis, and that we have endeavoured to be as broad in our approach and considerations as possible, it is necessarily selective and there are clear gaps. Some of the areas that fall between the gaps in this project, or that we feel warrant future research efforts, are considered briefly in the following sections.

6.2.1 Divergence in circuitry regulating cold- and diet-induced thermogenesis

In consideration of the marked distinction in the physical nature of cold exposure and meal consumption, it is clear that there must be a divergence in the neural "headwaters" regulating cold- and diet-induced thermogenesis. This is a fascinating subject where little progress has been made, largely due to a lack of evidence of the central determinants subserving the latter; a deficiency that the work described in this thesis has aimed to address. The divergence in circuitry regulating each is most likely to occur at brain regions where the afferent sensory signals pertaining to cold or diet are processed, which are either one or two synapses upstream of the sympathetic pre-ganglionic neurons of the spinal cord. Numerous studies highlight neurons of the DMH and the broader region encompassing the POA as critical integrators of temperature-related sensory signals (reviewed by Morrison and Nakamura (2019)); the role played by these regions for diet-induced thermogenesis remains to be clarified.

There is reason to believe that the centrality of the melanocortin system identified in this thesis *uniquely* regulates diet-induced (but not cold-induced) thermogenesis in brown fat. Specifically, *Mc4r* knockout mice maintain the ability to mount a robust BAT thermogenic response to cold-exposure in order to maintain core temperature, while notably lacking apposite high-calorie diet-induced thermogenesis (Ste. Marie *et al.*, 2000; Butler *et al.*, 2001; Voss-Andreae *et al.*, 2007). That being said, there is some evidence that the melanocortin system may provide an energy-status "overlay" to the thermoregulatory circuitry, tempering cold-induced thermogenesis during periods of energy deficit. For example, inactivation of GLUT2 disrupts central glucose-sensing and engenders defective maintenance of body temperature during both cold exposure and prolonged fasting; an effect which could be prevented by administration of a MC3/4R agonist (Mounien *et al.*, 2010). Indeed, melanocortin agonism of the prototypical thermoregulatory POA → DMH circuit is sufficient to activate thermogenesis in brown fat (Monge-Roffarello *et al.*, 2014a).

Nevertheless, the challenge for metabolic neuroscience in relation to the distinction between the processing of cold- and nutrient-based information is to dissect the downstream pathways of POMC neurons *en route* to brown fat in order to confirm their functional relevance (discussed in detail in *Chapter 3: Section 3.4.4*). These studies will enable us to determine where there is confluence, and where there is disparity, pertaining to central circuitry regulating cold- and diet-induced thermogenesis.

6.2.2 Astrocyte-derived adenosine, energy availability and brown fat thermogenesis

The primacy of neurons in the regulation of brain glucose-sensing and brown fat thermogenesis has been brought into question in this thesis. In support of recent indications of a link between astrocyte function and POMC neuron glucose-sensing (Garcia-Caceres *et al.*, 2016; Nuzzaci *et al.*, 2020), we comprehensively demonstrate that appropriate glucose-induced changes in POMC neuron activity, particularly glucose-induced excitations, require in-tact astrocyte metabolism and associated A_1R-mediated signalling. It flows logically, then, that astrocytes may be involved in glucose (meal)-regulated control of BAT-directed SNA via an adenosine-dependent activation of adjacent POMC neurons. Indeed, our data demonstrating that dark phase (i.e. food consummatory phase) energy expenditure is reduced by central A_1R antagonism, and that BAT thermogenesis is increased in response to DREADD-mediated activation of MBH astrocytes, are in support of this view.

Intriguingly, central adenosine signalling also facilitates the transition into energy-*conserving*, torpor-like states (in rodents) (Iliff & Swoap, 2012; Muzzi *et al.*, 2013; Carlin *et al.*, 2017). Studies suggest that this mechanism is mediated via A_1R signalling in the NTS, and involves an *inhibition* of BAT SNA which contributes to the promotion of the torpor-like state (Tupone *et al.*, 2013). Considering that hypoglycaemia has been shown to activate NTS neurons via an astrocyte-derived adenosine-dependent mechanism (Rogers *et al.*, 2016; Rogers *et al.*, 2018), it is possible that astrocytes also play a role in the suppression of energy expenditure during caloric *deficit*. This suggests that astrocyte-derived adenosine has the potential to differentially regulate BAT thermogenesis, depending on the neuronal population through which it signals and the metabolic status of the organism. The implication this has for the role of astrocytes in the regulation of diet-induced thermogenesis remains a challenge.

6.2.3 Other central and peripheral determinants

The studies in **Chapter 3** and **Chapter 5** were focussed on the capability of POMC neurons, particularly those that have a defined multi-synaptic trajectory to brown fat, to sense changes in extracellular glucose. While there is no doubt that glucose is a reasonable surrogate of a meal and that glucose-sensing provides a crucial role in the regulation of energy (and glucose) homeostasis, it would be remiss to discount the potential involvement of other meal-derived nutrients or hormones in the activation of postprandial thermogenesis. Indeed, POMC neuron excitability has been shown to be modulated by circulating amino and fatty acids (Blouet *et al.*, 2009; Heeley *et al.*, 2018; Haynes *et al.*, 2020), and there are convincing lines of evidence that leptin and insulin signal through POMC neurons to modulate energy expenditure (Dodd *et al.*, 2015; Dodd *et al.*, 2019).

Alternatively, the involvement of other neuronal populations requires consideration; for instance, rat insulin-2 promoter-expressing neurons in the arcuate nucleus and glucose-sensing neurons in the locus coeruleus have been implicated in diet-induced thermogenesis in brown fat (Kong *et al.*, 2012; Tovar *et al.*, 2013). Notably, in addition to astrocyte-regulated glucose-sensing, there is emerging evidence indicating a similar role for tanycytes, the glial-like cells that line the third ventricle (Cortes-Campos *et al.*, 2011; Frayling *et al.*, 2011). An explicit connection between hypothalamic tanycytes, POMC neuron glucose-sensing and brown fat thermogenesis is yet to be established.

It is also appropriate to consider drivers of meal-related thermogenesis in brown fat that circumvent neuronal signalling in the hypothalamus. For example, the chemo-detection of nutrients in the gut has been suggested to lead to cholecystokinin-mediated activation of vagal nerves which in turn promote BAT-directed SNA and thermogenesis (Blouet & Schwartz, 2012; Yamazaki *et al.*, 2019). Alternatively, there are also suggestions of peripherally-active hormones that bypass the SNS entirely and signal directly through the brown adipocyte. Most notably of which is the hormone secretin, plasma levels of which rise postprandially and have been demonstrated to have capacity to promote thermogenic gene transcription *in vitro* or thermogenesis *in vivo* (Li *et al.*, 2018). Clearly, there is a long road ahead by way of a complete deconstruction of what is, ostensibly, a multi-factorially-regulated physiological process.

6.3 A unified perspective: POMC-regulated postprandial thermogenesis in BAT

The findings presented in this thesis permit the tentative description of a discrete POMC neural circuit linking glucose-sensing in the hypothalamus with BAT thermogenesis, including a putative role for MBH astrocytes in the contribution to glucose-induced activation of POMC neurons. A synthesis of the key findings of this thesis are presented in **Figure 6.1**, in what could be considered a working hypothesis of the integrated schema of POMC-regulated BAT thermogenesis in the postprandial state.

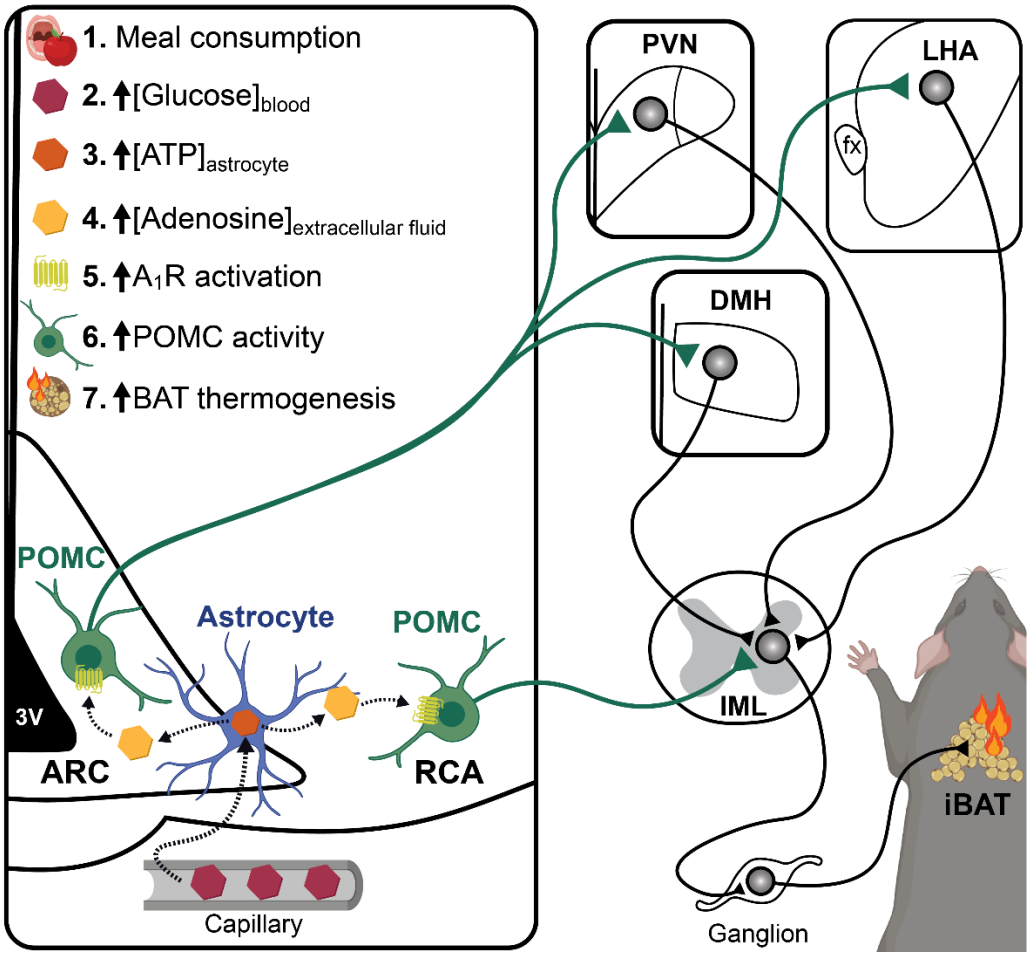

Figure 6.1 | Integrated schema of glucose-regulated astrocyte-POMC-brown fat connection

Meal consumption (1) leads to increased circulating levels of the nutrient, glucose (2). Glucose is taken up by astrocytes and metabolised into ATP (3). Astrocytes then release ATP which is degraded extracellularly (not shown) to increase extracellular fluid concentrations of adenosine (4). Adenosine binds to A_1R expressed by POMC neurons (5), which leads to depolarisation and increased neuronal activity (6). POMC neurons in the ARC project to the PVN, LHA and DMH while POMC neurons in the RCA project directly to the IML; increased melanocortin signalling ultimately leads to increased BAT-directed sympathetic nerve activity and hence BAT thermogenesis (7).

6.4 Concluding remarks

It has been over a decade since the therapeutic prospects for brown fat underwent its (most recent) “renaissance” spurred by evolving metabolic imaging technologies, and now *four* decades since Rothwell and Stock (1979) made their pivotal observations of diet-induced thermogenesis in rodents. The fat-igniting capacity of brown fat has the potential to correct the health and economic burden that is posed by escalating levels of obesity. However, despite extensive research, its touted metabolic benefits are yet to be realised in the current clinical context. What we are in search of, then, is a paradigm shift in the way brown fat thermogenesis is activated.

In this vein, there are essentially two feasible strategies: 1) to expand the reservoir of brown or brown-like fat through a process known as “beiging”, which has not been explored by this thesis, or 2) to consider the best methods by which to activate recruitable brown (or brown-like) fat. In this respect, cold exposure has been harnessed as the primary means to capture maximal brown fat activity, and indeed, this has led to promising clinical data that (at least) supports improvements in glycaemic control. However, perhaps the greatest potential lies within the exploitation of diet-induced thermogenesis by interrogating the differential effect of nutrients acting in the brain to promote thermogenic outcomes; because, at the end of the day, nobody wants to be “left out in the cold”.

The metabolic physiologist Abdul G. Dulloo referred to the quote “Life is a combustion” from Lavoisier, the 18th century chemist and father of the notion of oxygen combustion, with the following commentary: “we must simulate the appropriate dietary conditions under which DIT is recruited in order to understand the physiological and molecular mechanisms that enable the fire of life to burn brighter in some than in others" (Dulloo, 2002). The findings presented in this thesis highlights the activity of hypothalamic POMC neuron activity as one such mechanism.

Chapter 7

List of References

Acheson K, Jequier E & Wahren J. (1983). Influence of beta-adrenergic blockade on glucose-induced thermogenesis in man. *The Journal of clinical investigation* **72,** 981-986.

Acuna-Goycolea C, Obrietan K & van den Pol AN. (2010). Cannabinoids excite circadian clock neurons. *The Journal of neuroscience : the official journal of the Society for Neuroscience* **30,** 10061-10066.

Acuna-Goycolea C, Tamamaki N, Yanagawa Y, Obata K & van den Pol AN. (2005). Mechanisms of neuropeptide Y, peptide YY, and pancreatic polypeptide inhibition of identified green fluorescent protein-expressing GABA neurons in the hypothalamic neuroendocrine arcuate nucleus. *The Journal of neuroscience : the official journal of the Society for Neuroscience* **25,** 7406-7419.

Adam CL, Archer ZA, Findlay PA, Thomas L & Marie M. (2002). Hypothalamic Gene Expression in Sheep for Cocaine- and Amphetamine-Regulated Transcript, Pro-Opiomelanocortin, Neuropeptide Y, Agouti-Related Peptide and Leptin Receptor and Responses to Negative Energy Balance. *Neuroendocrinology* **75,** 250-256.

Adank DN, Lunzer MM, Lensing CJ, Wilber SL, Gancarz AM & Haskell-Luevano C. (2018). Comparative in Vivo Investigation of Intrathecal and Intracerebroventricular Administration with Melanocortin Ligands MTII and AGRP into Mice. *ACS Chem Neurosci* **9,** 320-327.

Ainscow EK, Mirshamsi S, Tang T, Ashford MLJ & Rutter GA. (2002). Dynamic imaging of free cytosolic ATP concentration during fuel sensing by rat hypothalamic neurones: evidence for ATP-independent control of ATP-sensitive K+ channels. *The Journal of physiology* **544,** 429-445.

Albarado DC, McClaine J, Stephens JM, Mynatt RL, Ye J, Bannon AW, Richards WG & Butler AA. (2004). Impaired coordination of nutrient intake and substrate oxidation in melanocortin-4 receptor knockout mice. *Endocrinology* **145,** 243-252.

Almeida MC, Hew-Butler T, Soriano RN, Rao S, Wang W, Wang J, Tamayo N, Oliveira DL, Nucci TB, Aryal P, Garami A, Bautista D, Gavva NR & Romanovsky AA. (2012). Pharmacological blockade of the cold receptor TRPM8 attenuates autonomic and behavioral cold defenses and decreases deep body temperature. *The Journal of neuroscience : the official journal of the Society for Neuroscience* **32,** 2086-2099.

Alviña K, Walter JT, Kohn A, Ellis-Davies G & Khodakhah K. (2008). Questioning the role of rebound firing in the cerebellum. *Nat Neurosci* **11,** 1256-1258.

Anand BK, Chhina GS, Sharma KN, Dua S & Singh B. (1964). Activity of Single Neurons in the Hypothalamic Feeding Centers: Effect of Glucose. *The American journal of physiology* **207,** 1146-1154.

Antunes VR, Brailoiu GC, Kwok EH, Scruggs P & Dun NJ. (2001). Orexins/hypocretins excite rat sympathetic preganglionic neurons in vivo and in vitro. *American journal of physiology Regulatory, integrative and comparative physiology* **281,** R1801-1807.

Anunciado-Koza R, Ukropec J, Koza RA & Kozak LP. (2008). Inactivation of UCP1 and the Glycerol Phosphate Cycle Synergistically Increases Energy Expenditure to Resist Diet-induced Obesity. *Journal of Biological Chemistry* **283,** 27688-27697.

Aponte Y, Atasoy D & Sternson SM. (2011). AGRP neurons are sufficient to orchestrate feeding behavior rapidly and without training. *Nat Neurosci* **14,** 351-355.

Arase K, York DA & Bray GA. (1987). Corticosterone inhibition of the intracerebroventricular effect of 2-deoxy-D-glucose on brown adipose tissue thermogenesis. *Physiology & behavior* **40,** 489-495.

Arluison M, Quignon M, Nguyen P, Thorens B, Leloup C & Penicaud L. (2004). Distribution and anatomical localization of the glucose transporter 2 (GLUT2) in the adult rat brain--an immunohistochemical study. *Journal of chemical neuroanatomy* **28,** 117-136.

Armbruster BN, Li X, Pausch MH, Herlitze S & Roth BL. (2007). Evolving the lock to fit the key to create a family of G protein-coupled receptors potently activated by an inert ligand. *Proceedings of the National Academy of Sciences of the United States of America* **104,** 5163-5168.

Ashford ML, Boden PR & Treherne JM. (1990). Glucose-induced excitation of hypothalamic neurones is mediated by ATP-sensitive K+ channels. *Pflugers Archiv : European journal of physiology* **415,** 479-483.

Atasoy D, Betley JN, Li W-P, Su HH, Sertel SM, Scheffer LK, Simpson JH, Fetter RD & Sternson SM. (2014). A genetically specified connectomics approach applied to long-range feeding regulatory circuits. *Nature Neuroscience* **17,** 1830-1839.

Atasoy D, Betley JN, Su HH & Sternson SM. (2012). Deconstruction of a neural circuit for hunger. *Nature* **488,** 172-177.

Australian Bureau of Statistics. (2015). National Health Survey: First Results 2014-15. http://www.abs.gov.au/ausstats/abs@.nsf/Lookup/by%20Subject/4364.0.55.001~2014-15~Main%20Features~Overweight%20and%20obesity~22.

Australian Bureau of Statistics. (2018). National Health Survey: First Results 2017-18. https://www.abs.gov.au/ausstats/abs@.nsf/Lookup/by%20Subject/4364.0.55.001~2017-18~Main%20Features~Overweight%20and%20obesity~90.

Baffi JS & Palkovits M. (2000). Fine topography of brain areas activated by cold stress. A fos immunohistochemical study in rats. *Neuroendocrinology* **72,** 102-113.

Balthasar N, Dalgaard LT, Lee CE, Yu J, Funahashi H, Williams T, Ferreira M, Tang V, McGovern RA, Kenny CD, Christiansen LM, Edelstein E, Choi B, Boss O, Aschkenasi C, Zhang CY, Mountjoy K, Kishi T, Elmquist JK & Lowell BB. (2005). Divergence of melanocortin pathways in the control of food intake and energy expenditure. *Cell* **123,** 493-505.

Bamshad M, Song CK & Bartness TJ. (1999). CNS origins of the sympathetic nervous system outflow to brown adipose tissue. *The American journal of physiology* **276,** R1569-1578.

Barrington SF & Maisey MN. (1996). Skeletal muscle uptake of fluorine-18-FDG: effect of oral diazepam. *Journal of nuclear medicine : official publication, Society of Nuclear Medicine* **37,** 1127-1129.

Bartelt A, Bruns OT, Reimer R, Hohenberg H, Ittrich H, Peldschus K, Kaul MG, Tromsdorf UI, Weller H, Waurisch C, Eychmuller A, Gordts PLSM, Rinninger F, Bruegelmann K, Freund B, Nielsen P, Merkel M & Heeren J. (2011). Brown adipose tissue activity controls triglyceride clearance. *Nat Med* **17,** 200-205.

Beiroa D, Imbernon M, Gallego R, Senra A, Herranz D, Villarroya F, Serrano M, Fernø J, Salvador J, Escalada J, Dieguez C, Lopez M, Frühbeck G & Nogueiras R. (2014). GLP-1 Agonism Stimulates Brown Adipose Tissue Thermogenesis and Browning Through Hypothalamic AMPK. *Diabetes* **63,** 3346.

Belcher SM, Zsarnovszky A, Crawford PA, Hemani H, Spurling L & Kirley TL. (2006). Immunolocalization of ecto-nucleoside triphosphate diphosphohydrolase 3 in rat brain: implications for modulation of multiple homeostatic systems including feeding and sleep-wake behaviors. *Neuroscience* **137,** 1331-1346.

Bell CG, Walley AJ & Froguel P. (2005). The genetics of human obesity. *Nature reviews Genetics* **6,** 221-234.

Bennett MV, Contreras JE, Bukauskas FF & Sáez JC. (2003). New roles for astrocytes: gap junction hemichannels have something to communicate. *Trends in neurosciences* **26,** 610-617.

Berglund ED, Liu T, Kong X, Sohn JW, Vong L, Deng Z, Lee CE, Lee S, Williams KW, Olson DP, Scherer PE, Lowell BB & Elmquist JK. (2014). Melanocortin 4 receptors in autonomic neurons regulate thermogenesis and glycemia. *Nat Neurosci* **17,** 911-913.

Betley JN, Cao ZFH, Ritola KD & Sternson SM. (2013). Parallel, redundant circuit organization for homeostatic control of feeding behavior. *Cell* **155,** 1337-1350.

Bicknell RJ & Leng G. (1981). Relative efficiency of neural firing patterns for vasopressin release in vitro. *Neuroendocrinology* **33,** 295-299.

Bittar PG, Charnay Y, Pellerin L, Bouras C & Magistretti PJ. (1996). Selective distribution of lactate dehydrogenase isoenzymes in neurons and astrocytes of human brain. *Journal of cerebral blood flow and metabolism : official journal of the International Society of Cerebral Blood Flow and Metabolism* **16,** 1079-1089.

Bjelobaba I, Nedeljkovic N, Subasic S, Lavrnja I, Pekovic S, Stojkov D, Rakic L & Stojiljkovic M. (2006). Immunolocalization of ecto-nucleotide pyrophosphatase/phosphodiesterase 1 (NPP1) in the rat forebrain. *Brain research* **1120,** 54-63.

Blessing WW. (2018). Thermoregulation and the ultradian basic rest-activity cycle. *Handbook of clinical neurology* **156,** 367-375.

Blondin DP, Labbe SM, Christian Tingelstad H, Noll C, Kunach M, Phoenix S, Guerin B, Turcotte EE, Carpentier AC, Richard D & Haman F. (2014). Increased brown adipose tissue oxidative capacity in cold-acclimated humans. *J Clin Endocrinol Metab***,** jc20133901.

Blouet C, Jo YH, Li X & Schwartz GJ. (2009). Mediobasal hypothalamic leucine sensing regulates food intake through activation of a hypothalamus-brainstem circuit. *The Journal of neuroscience : the official journal of the Society for Neuroscience* **29,** 8302-8311.

Blouet C & Schwartz GJ. (2012). Duodenal lipid sensing activates vagal afferents to regulate non-shivering brown fat thermogenesis in rats. *PloS one* **7,** e51898-e51898.

BonDurant LD, Ameka M, Naber MC, Markan KR, Idiga SO, Acevedo MR, Walsh SA, Ornitz DM & Potthoff MJ. (2017). FGF21 Regulates Metabolism Through Adipose-Dependent and -Independent Mechanisms. *Cell metabolism* **25,** 935-+.

Bouillaud F, Combes-George M & Ricquier D. (1983). Mitochondria of adult human brown adipose tissue contain a 32 000-Mr uncoupling protein. *Bioscience reports* **3,** 775-780.

Bouret SG, Draper SJ & Simerly RB. (2004). Formation of Projection Pathways from the Arcuate Nucleus of the Hypothalamus to Hypothalamic Regions Implicated in the Neural Control of Feeding Behavior in Mice. *The Journal of Neuroscience* **24,** 2797.

Bouzier-Sore AK, Voisin P, Bouchaud V, Bezancon E, Franconi JM & Pellerin L. (2006). Competition between glucose and lactate as oxidative energy substrates in both neurons and astrocytes: a comparative NMR study. *The European journal of neuroscience* **24,** 1687-1694.

Brãuer AU, Savaskan NE, Kole MH, Plaschke M, Monteggia LM, Nestler EJ, Simburger E, Deisz RA, Ninnemann O & Nitsch R. (2001). Molecular and functional analysis of hyperpolarization-activated pacemaker channels in the hippocampus after entorhinal cortex lesion. *FASEB journal : official publication of the Federation of American Societies for Experimental Biology* **15,** 2689-2701.

Brito MN, Brito NA, Baro DJ, Song CK & Bartness TJ. (2007). Differential activation of the sympathetic innervation of adipose tissues by melanocortin receptor stimulation. *Endocrinology* **148,** 5339-5347.

Burdakov D, Gerasimenko O & Verkhratsky A. (2005). Physiological changes in glucose differentially modulate the excitability of hypothalamic melanin-concentrating hormone and orexin neurons in situ. *The Journal of neuroscience : the official journal of the Society for Neuroscience* **25,** 2429-2433.

Burdakov D, Jensen LT, Alexopoulos H, Williams RH, Fearon IM, O'Kelly I, Gerasimenko O, Fugger L & Verkhratsky A. (2006). Tandem-Pore K+ Channels Mediate Inhibition of Orexin Neurons by Glucose. *Neuron* **50,** 711-722.

Burke LK, Darwish T, Cavanaugh AR, Virtue S, Roth E, Morro J, Liu S-M, Xia J, Dalley JW, Burling K, Chua S, Vidal-Puig T, Schwartz GJ & Blouet C. (2017). mTORC1 in AGRP neurons integrates exteroceptive and interoceptive food-related cues in the modulation of adaptive energy expenditure in mice. *eLife* **6,** e22848.

Butler AA, Marks DL, Fan W, Kuhn CM, Bartolome M & Cone RD. (2001). Melanocortin-4 receptor is required for acute homeostatic responses to increased dietary fat. *Nat Neurosci* **4,** 605-611.

Calle EE, Rodriguez C, Walker-Thurmond K & Thun MJ. (2003). Overweight, obesity, and mortality from cancer in a prospectively studied cohort of U.S. adults. *The New England journal of medicine* **348,** 1625-1638.

Campbell JN, Macosko EZ, Fenselau H, Pers TH, Lyubetskaya A, Tenen D, Goldman M, Verstegen AMJ, Resch JM, McCarroll SA, Rosen ED, Lowell BB & Tsai LT. (2017). A molecular census of arcuate hypothalamus and median eminence cell types. *Nat Neurosci* **20,** 484-496.

Cannon B & Nedergaard J. (2004). Brown adipose tissue: function and physiological significance. *Physiological reviews* **84,** 277-359.

Cano G, Passerin AM, Schiltz JC, Card JP, Morrison SF & Sved AF. (2003). Anatomical substrates for the central control of sympathetic outflow to interscapular adipose tissue during cold exposure. *The Journal of comparative neurology* **460,** 303-326.

Cao WH, Fan W & Morrison SF. (2004). Medullary pathways mediating specific sympathetic responses to activation of dorsomedial hypothalamus. *Neuroscience* **126,** 229-240.

Carey AL, Formosa MF, Van Every B, Bertovic D, Eikelis N, Lambert GW, Kalff V, Duffy SJ, Cherk MH & Kingwell BA. (2013). Ephedrine activates brown adipose tissue in lean but not obese humans. *Diabetologia* **56,** 147-155.

Carlin JL, Jain S, Gizewski E, Wan TC, Tosh DK, Xiao C, Auchampach JA, Jacobson KA, Gavrilova O & Reitman ML. (2017). Hypothermia in mouse is caused by adenosine A(1) and A(3) receptor agonists and AMP via three distinct mechanisms. *Neuropharmacology* **114,** 101-113.

Cazalis M, Dayanithi G & Nordmann JJ. (1985). The role of patterned burst and interburst interval on the excitation-coupling mechanism in the isolated rat neural lobe. *The Journal of physiology* **369,** 45-60.

Cechetto DF & Saper CB. (1988). Neurochemical organization of the hypothalamic projection to the spinal cord in the rat. *The Journal of comparative neurology* **272,** 579-604.

Challis BG, Coll AP, Yeo GSH, Pinnock SB, Dickson SL, Thresher RR, Dixon J, Zahn D, Rochford JJ, White A, Oliver RL, Millington G, Aparicio SA, Colledge WH, Russ AP, Carlton MB & Rahilly S. (2004). Mice lacking pro-opiomelanocortin are sensitive to high-fat feeding but respond normally to the acute anorectic effects of peptide-YY<sub>3-36</sub&gt. *Proceedings of the National Academy of Sciences of the United States of America* **101,** 4695.

Chaudhry A & Granneman JG. (1999). Differential regulation of functional responses by beta-adrenergic receptor subtypes in brown adipocytes. *The American journal of physiology* **277,** R147-153.

Chen AS, Metzger JM, Trumbauer ME, Guan XM, Yu H, Frazier EG, Marsh DJ, Forrest MJ, Gopal-Truter S, Fisher J, Camacho RE, Strack AM, Mellin TN, MacIntyre DE, Chen HY & Van der Ploeg LH. (2000). Role of the melanocortin-4 receptor in metabolic rate and food intake in mice. *Transgenic Res* **9,** 145-154.

Chen KY, Brychta RJ, Linderman JD, Smith S, Courville A, Dieckmann W, Herscovitch P, Millo CM, Remaley A, Lee P & Celi FS. (2013). Brown fat activation mediates cold-induced thermogenesis in adult humans in response to a mild decrease in ambient temperature. *J Clin Endocrinol Metab* **98,** E1218-1223.

Chen M, Berger A, Kablan A, Zhang J, Gavrilova O & Weinstein LS. (2012). Gsα deficiency in the paraventricular nucleus of the hypothalamus partially contributes to obesity associated with Gsα mutations. *Endocrinology* **153,** 4256-4265.

Chen M, Shrestha YB, Podyma B, Cui Z, Naglieri B, Sun H, Ho T, Wilson EA, Li YQ, Gavrilova O & Weinstein LS. (2017). Gsα deficiency in the dorsomedial hypothalamus underlies obesity associated with Gsα mutations. *The Journal of clinical investigation* **127,** 500-510.

Chen M, Wilson EA, Cui Z, Sun H, Shrestha YB, Podyma B, Le CH, Naglieri B, Pacak K, Gavrilova O & Weinstein LS. (2019). Gsα deficiency in the dorsomedial hypothalamus leads to obesity, hyperphagia, and reduced thermogenesis associated with impaired leptin signaling. *Molecular metabolism* **25,** 142-153.

Chen N, Sugihara H, Kim J, Fu Z, Barak B, Sur M, Feng G & Han W. (2016). Direct modulation of GFAP-expressing glia in the arcuate nucleus bi-directionally regulates feeding. *Elife* **5**.

Cheunsuang O, Stewart AL & Morris R. (2006). Differential uptake of molecules from the circulation and CSF reveals regional and cellular specialisation in CNS detection of homeostatic signals. *Cell and tissue research* **325,** 397-402.

Chhabra KH, Adams JM, Fagel B, Lam DD, Qi N, Rubinstein M & Low MJ. (2016). Hypothalamic POMC Deficiency Improves Glucose Tolerance Despite Insulin Resistance by Increasing Glycosuria. *Diabetes* **65,** 660-672.

Chhabra KH, Morgan DA, Tooke BP, Adams JM, Rahmouni K & Low MJ. (2017). Reduced renal sympathetic nerve activity contributes to elevated glycosuria and improved glucose tolerance in hypothalamus-specific Pomc knockout mice. *Molecular metabolism* **6,** 1274-1285.

Chrétien C, Fenech C, Liénard F, Grall S, Chevalier C, Chaudy S, Brenachot X, Berges R, Louche K, Stark R, Nédélec E, Laderrière A, Andrews ZB, Benani A, Flockerzi V, Gascuel J, Hartmann J, Moro C, Birnbaumer L, Leloup C, Pénicaud L & Fioramonti X. (2017). Transient Receptor Potential Canonical 3 (TRPC3) Channels Are Required for Hypothalamic Glucose Detection and Energy Homeostasis. *Diabetes* **66,** 314-324.

Chu Z, Takagi H & Moenter SM. (2010). Hyperpolarization-activated currents in gonadotropin-releasing hormone (GnRH) neurons contribute to intrinsic excitability and are regulated by gonadal steroid feedback. *The Journal of neuroscience : the official journal of the Society for Neuroscience* **30,** 13373-13383.

Cinti S. (2007). The adipose organ. In *Adipose tissue and adipokines in health and disease*, pp. 3-19. Springer.

Ciofi P. (2011). The arcuate nucleus as a circumventricular organ in the mouse. *Neuroscience letters* **487,** 187-190.

Claret M, Smith MA, Batterham RL, Selman C, Choudhury AI, Fryer LGD, Clements M, Al-Qassab H, Heffron H, Xu AW, Speakman JR, Barsh GS, Viollet B, Vaulont S, Ashford MLJ, Carling D & Withers DJ. (2007). AMPK is essential for energy homeostasis regulation and glucose sensing by POMC and AgRP neurons. *Journal of Clinical Investigation* **117,** 2325-2336.

Clasadonte J, Scemes E, Wang Z, Boison D & Haydon PG. (2017). Connexin 43-Mediated Astroglial Metabolic Networks Contribute to the Regulation of the Sleep-Wake Cycle. *Neuron* **95,** 1365-1380.e1365.

Colagiuri S, Lee CM, Colagiuri R, Magliano D, Shaw JE, Zimmet PZ & Caterson ID. (2010). The cost of overweight and obesity in Australia. *The Medical journal of Australia* **192,** 260-264.

Coll AP & Yeo GS. (2013). The hypothalamus and metabolism: integrating signals to control energy and glucose homeostasis. *Current opinion in pharmacology* **13,** 970-976.

Cone RD. (2005). Anatomy and regulation of the central melanocortin system. *Nature Neuroscience* **8,** 571-578.

Coppola A, Liu Z, Andrews Z, Paradis E, Roy M-C, Friedman JM, Ricquier D, Richard D, Horvath TL, Gao X-B & Diano S. (2007). A Central Thermogenic-like Mechanism in Feeding Regulation: an Interplay Between Arcuate Nucleus T3 and UCP2. *Cell metabolism* **5,** 21-33.

Cortes-Campos C, Elizondo R, Llanos P, Uranga RM, Nualart F & Garcia MA. (2011). MCT expression and lactate influx/efflux in tanycytes involved in glia-neuron metabolic interaction. *PloS one* **6,** e16411.

Cote I, Sakarya Y, Kirichenko N, Morgan D, Carter CS, Tumer N & Scarpace PJ. (2016). Activation of the central melanocortin system chronically reduces body mass without the necessity of long-term caloric restriction. *Canadian journal of physiology and pharmacology***,** 1-9.

Cowley MA, Pronchuk N, Fan W, Dinulescu DM, Colmers WF & Cone RD. (1999). Integration of NPY, AGRP, and melanocortin signals in the hypothalamic paraventricular nucleus: evidence of a cellular basis for the adipostat. *Neuron* **24,** 155-163.

Cowley MA, Smart JL, Rubinstein M, Cerdan MG, Diano S, Horvath TL, Cone RD & Low MJ. (2001). Leptin activates anorexigenic POMC neurons through a neural network in the arcuate nucleus. *Nature* **411,** 480-484.

Creemers JWM, Lee YS, Oliver RL, Bahceci M, Tuzcu A, Gokalp D, Keogh J, Herber S, White A, O'Rahilly S & Farooqi IS. (2008). Mutations in the amino-terminal region of proopiomelanocortin (POMC) in patients with early-onset obesity impair POMC sorting to the regulated secretory pathway. *The Journal of clinical endocrinology and metabolism* **93,** 4494-4499.

Cui H, Sohn J-W, Gautron L, Funahashi H, Williams KW, Elmquist JK & Lutter M. (2012). Neuroanatomy of melanocortin-4 receptor pathway in the lateral hypothalamic area. *The Journal of comparative neurology* **520,** 4168-4183.

Cypess AM, Chen Y-C, Sze C, Wang K, English J, Chan O, Holman AR, Tal I, Palmer MR, Kolodny GM & Kahn CR. (2012). Cold but not sympathomimetics activates human brown adipose tissue in vivo. *Proceedings of the National Academy of Sciences*.

Cypess AM, Lehman S, Williams G, Tal I, Rodman D, Goldfine AB, Kuo FC, Palmer EL, Tseng Y-H, Doria A, Kolodny GM & Kahn CR. (2009). Identification and Importance of Brown Adipose Tissue in Adult Humans. *New England Journal of Medicine* **360,** 1509-1517.

Cypess Aaron M, Weiner Lauren S, Roberts-Toler C, Elía Elisa F, Kessler Skyler H, Kahn Peter A, English J, Chatman K, Trauger Sunia A, Doria A & Kolodny Gerald M. (2015). Activation of Human Brown Adipose Tissue by a β3-Adrenergic Receptor Agonist. *Cell metabolism* **21,** 33-38.

Dadak S, Beall C, Vlachaki Walker JM, Soutar MPM, McCrimmon RJ & Ashford MLJ. (2017). Oleate induces KATP channel-dependent hyperpolarization in mouse hypothalamic glucose-excited neurons without altering cellular energy charge. *Neuroscience* **346,** 29-42.

de Jesus LA, Carvalho SD, Ribeiro MO, Schneider M, Kim S-W, Harney JW, Larsen PR & Bianco AC. (2001). The type 2 iodothyronine deiodinase is essential for adaptive thermogenesis in brown adipose tissue. *The Journal of clinical investigation* **108,** 1379-1385.

De Jonge L & Garrel DR. (1997). Role of the autonomic nervous system in the thermogenic response to food in lean individuals. *The American journal of physiology* **272,** E775-780.

de Vries MG, Arseneau LM, Lawson ME & Beverly JL. (2003). Extracellular glucose in rat ventromedial hypothalamus during acute and recurrent hypoglycemia. *Diabetes* **52,** 2767-2773.

Deisseroth K. (2011). Optogenetics. *Nat Meth* **8,** 26-29.

Desautels M, Dulos RA & Mozaffari B. (1986). Selective loss of uncoupling protein from mitochondria of surgically denervated brown adipose tissue of cold-acclimated mice. *Biochemistry and cell biology = Biochimie et biologie cellulaire* **64,** 1125-1134.

Desplantez T, Verma V, Leybaert L, Evans WH & Weingart R. (2012). Gap26, a connexin mimetic peptide, inhibits currents carried by connexin43 hemichannels and gap junction channels. *Pharmacological Research* **65,** 546-552.

Devraj K, Klinger ME, Myers RL, Mokashi A, Hawkins RA & Simpson IA. (2011). GLUT-1 glucose transporters in the blood-brain barrier: differential phosphorylation. *Journal of neuroscience research* **89,** 1913-1925.

Dicken MS, Tooker RE & Hentges ST. (2012). Regulation of GABA and glutamate release from proopiomelanocortin neuron terminals in intact hypothalamic networks. *The Journal of neuroscience : the official journal of the Society for Neuroscience* **32,** 4042-4048.

Dietrich MO & Horvath TL. (2012). Limitations in anti-obesity drug development: the critical role of hunger-promoting neurons. *Nature reviews Drug discovery* **11,** 675-691.

Dodd GT, Decherf S, Loh K, Simonds SE, Wiede F, Balland E, Merry TL, Munzberg H, Zhang ZY, Kahn BB, Neel BG, Bence KK, Andrews ZB, Cowley MA & Tiganis T. (2015). Leptin and insulin act on POMC neurons to promote the browning of white fat. *Cell* **160,** 88-104.

Dodd GT, Michael NJ, Lee-Young RS, Mangiafico SP, Pryor JT, Munder AC, Simonds SE, Brüning JC, Zhang ZY, Cowley MA, Andrikopoulos S, Horvath TL, Spanswick D & Tiganis T. (2018). Insulin regulates POMC neuronal plasticity to control glucose metabolism. *Elife* **7**.

Dodd GT, Xirouchaki CE, Eramo M, Mitchell CA, Andrews ZB, Henry BA, Cowley MA & Tiganis T. (2019). Intranasal Targeting of Hypothalamic PTP1B and TCPTP Reinstates Leptin and Insulin Sensitivity and Promotes Weight Loss in Obesity. *Cell Rep* **28,** 2905-2922.e2905.

Dulloo AG. (2002). Biomedicine. A sympathetic defense against obesity. *Science (New York, NY)* **297,** 780-781.

Dunwiddie TV, Diao L & Proctor WR. (1997). Adenine nucleotides undergo rapid, quantitative conversion to adenosine in the extracellular space in rat hippocampus. *The Journal of neuroscience : the official journal of the Society for Neuroscience* **17,** 7673-7682.

Dunwiddie TV & Masino SA. (2001). The role and regulation of adenosine in the central nervous system. *Annu Rev Neurosci* **24,** 31-55.

Durkee CA, Covelo A, Lines J, Kofuji P, Aguilar J & Araque A. (2019). Gi/o protein-coupled receptors inhibit neurons but activate astrocytes and stimulate gliotransmission. *Glia* **67,** 1076-1093.

Dutton A & Dyball RE. (1979). Phasic firing enhances vasopressin release from the rat neurohypophysis. *The Journal of physiology* **290,** 433-440.

Egawa M, Yoshimatsu H & Bray GA. (1989a). Effects of 2-deoxy-D-glucose on sympathetic nerve activity to interscapular brown adipose tissue. *The American journal of physiology* **257,** R1377-1385.

Egawa M, Yoshimatsu H & Bray GA. (1989b). Lateral hypothalamic injection of 2-deoxy-D-glucose suppresses sympathetic activity. *The American journal of physiology* **257,** R1386-1392.

Egawa M, Yoshimatsu H & Bray GA. (1991). Neuropeptide Y suppresses sympathetic activity to interscapular brown adipose tissue in rats. *The American journal of physiology* **260,** R328-334.

Elias CF, Aschkenasi C, Lee C, Kelly J, Ahima RS, Bjorbaek C, Flier JS, Saper CB & Elmquist JK. (1999). Leptin differentially regulates NPY and POMC neurons projecting to the lateral hypothalamic area. *Neuron* **23,** 775-786.

Elias CF, Lee C, Kelly J, Aschkenasi C, Ahima RS, Couceyro PR, Kuhar MJ, Saper CB & Elmquist JK. (1998). Leptin Activates Hypothalamic CART Neurons Projecting to the Spinal Cord. *Neuron* **21,** 1375-1385.

Elizondo-Vega R, Cortes-Campos C, Barahona MJ, Carril C, Ordenes P, Salgado M, Oyarce K & Garcia-Robles ML. (2016). Inhibition of hypothalamic MCT1 expression increases food intake and alters orexigenic and anorexigenic neuropeptide expression. *Scientific reports* **6,** 33606.

Enerback S, Jacobsson A, Simpson EM, Guerra C, Yamashita H, Harper ME & Kozak LP. (1997). Mice lacking mitochondrial uncoupling protein are cold-sensitive but not obese. *Nature* **387,** 90-94.

Engel H, Steinert H, Buck A, Berthold T, Huch Boni RA & von Schulthess GK. (1996). Whole-body PET: physiological and artifactual fluorodeoxyglucose accumulations. *Journal of nuclear medicine : official publication, Society of Nuclear Medicine* **37,** 441-446.

Enriori PJ, Sinnayah P, Simonds SE, Garcia Rudaz C & Cowley MA. (2011). Leptin action in the dorsomedial hypothalamus increases sympathetic tone to brown adipose tissue in spite of systemic leptin resistance. *The Journal of neuroscience : the official journal of the Society for Neuroscience* **31,** 12189-12197.

Fabbiano S, Suarez-Zamorano N, Rigo D, Veyrat-Durebex C, Stevanovic Dokic A, Colin DJ & Trajkovski M. (2016). Caloric Restriction Leads to Browning of White Adipose Tissue through Type 2 Immune Signaling. *Cell metabolism* **24,** 434-446.

Farooqi IS, Yeo GS, Keogh JM, Aminian S, Jebb SA, Butler G, Cheetham T & O'Rahilly S. (2000). Dominant and recessive inheritance of morbid obesity associated with melanocortin 4 receptor deficiency. *The Journal of clinical investigation* **106,** 271-279.

Fedorenko A, Lishko PV & Kirichok Y. (2012). Mechanism of fatty-acid-dependent UCP1 uncoupling in brown fat mitochondria. *Cell* **151,** 400-413.

Feldmann HM, Golozoubova V, Cannon B & Nedergaard J. (2009). UCP1 ablation induces obesity and abolishes diet-induced thermogenesis in mice exempt from thermal stress by living at thermoneutrality. *Cell metabolism* **9,** 203-209.

Fenselau H, Campbell JN, Verstegen AM, Madara JC, Xu J, Shah BP, Resch JM, Yang Z, Mandelblat-Cerf Y, Livneh Y & Lowell BB. (2017). A rapidly acting glutamatergic ARC-->PVH satiety circuit postsynaptically regulated by alpha-MSH. *Nat Neurosci* **20,** 42-51.

Ferguson AV & Samson WK. (2003). The orexin/hypocretin system: a critical regulator of neuroendocrine and autonomic function. *Frontiers in neuroendocrinology* **24,** 141-150.

Ferrari LL, Park D, Zhu L, Palmer MR, Broadhurst RY & Arrigoni E. (2018). Regulation of Lateral Hypothalamic Orexin Activity by Local GABAergic Neurons. *The Journal of neuroscience : the official journal of the Society for Neuroscience* **38,** 1588-1599.

Fields RD & Burnstock G. (2006). Purinergic signalling in neuron–glia interactions. *Nature Reviews Neuroscience* **7,** 423-436.

Fioramonti X, Chretien C, Leloup C & Penicaud L. (2017). Recent Advances in the Cellular and Molecular Mechanisms of Hypothalamic Neuronal Glucose Detection. *Front Physiol* **8,** 875.

Fioramonti X, Contie S, Song Z, Routh VH, Lorsignol A & Penicaud L. (2007). Characterization of glucosensing neuron subpopulations in the arcuate nucleus: integration in neuropeptide Y and pro-opio melanocortin networks? *Diabetes* **56,** 1219-1227.

Fioramonti X, Lorsignol A, Taupignon A & Pénicaud L. (2004). A New ATP-Sensitive K+ Channel–Independent Mechanism Is Involved in Glucose-Excited Neurons of Mouse Arcuate Nucleus. *Diabetes* **53,** 2767-2775.

Fischer AW, Hoefig CS, Abreu-Vieira G, de Jong JMA, Petrovic N, Mittag J, Cannon B & Nedergaard J. (2016). Leptin Raises Defended Body Temperature without Activating Thermogenesis. *Cell Rep* **14,** 1621-1631.

Fischer AW, Schlein C, Cannon B, Heeren J & Nedergaard J. (2019). Intact innervation is essential for diet-induced recruitment of brown adipose tissue. *American journal of physiology Endocrinology and metabolism* **316,** E487-e503.

Fischer K, Ruiz HH, Jhun K, Finan B, Oberlin DJ, van der Heide V, Kalinovich AV, Petrovic N, Wolf Y, Clemmensen C, Shin AC, Divanovic S, Brombacher F, Glasmacher E, Keipert S, Jastroch M, Nagler J, Schramm K-W, Medrikova D, Collden G, Woods SC, Herzig S, Homann D, Jung S, Nedergaard J, Cannon B, Tschop MH, Muller TD & Buettner C. (2017). Alternatively activated macrophages do not synthesize catecholamines or contribute to adipose tissue adaptive thermogenesis. *Nat Med* **23**.

Fletcher LA, Kim K, Leitner BP, Cassimatis TM, O'Mara AE, Johnson JW, Halprin MS, McGehee SM, Brychta RJ, Cypess AM & Chen KY. (2020). Sexual Dimorphisms in Adult Human Brown Adipose Tissue. *Obesity (Silver Spring, Md)* **28,** 241-246.

François M, Torres H, Huesing C, Zhang R, Saurage C, Lee N, Qualls-Creekmore E, Yu S, Morrison CD, Burk D, Berthoud HR & Münzberg H. (2019). Sympathetic innervation of the interscapular brown adipose tissue in mouse. *Annals of the New York Academy of Sciences* **1454,** 3-13.

Frayling C, Britton R & Dale N. (2011). ATP-mediated glucosensing by hypothalamic tanycytes. *The Journal of physiology* **589,** 2275-2286.

Freinkel N, Metzger BE, Harris E, Robinson S & Mager M. (1972). The Hypothermia of Hypoglycemia. *New England Journal of Medicine* **287,** 841-845.

Fridlyand LE, Tamarina N & Philipson LH. (2010). Bursting and calcium oscillations in pancreatic beta-cells: specific pacemakers for specific mechanisms. *American journal of physiology Endocrinology and metabolism* **299,** E517-E532.

Fu O, Iwai Y, Narukawa M, Ishikawa AW, Ishii KK, Murata K, Yoshimura Y, Touhara K, Misaka T, Minokoshi Y & Nakajima K-i. (2019). Hypothalamic neuronal circuits regulating hunger-induced taste modification. *Nature communications* **10,** 4560.

Fuente-Martín E, García-Cáceres C, Granado M, de Ceballos ML, Sánchez-Garrido M, Sarman B, Liu ZW, Dietrich MO, Tena-Sempere M, Argente-Arizón P, Díaz F, Argente J, Horvath TL & Chowen JA. (2012). Leptin regulates glutamate and glucose transporters in hypothalamic astrocytes. *The Journal of clinical investigation* **122,** 3900-3913.

Garcia-Caceres C, Quarta C, Varela L, Gao Y, Gruber T, Legutko B, Jastroch M, Johansson P, Ninkovic J, Yi CX, Le Thuc O, Szigeti-Buck K, Cai W, Meyer CW, Pfluger PT, Fernandez AM, Luquet S, Woods SC, Torres-Aleman I, Kahn CR, Gotz M, Horvath TL & Tschop MH. (2016). Astrocytic Insulin Signaling Couples Brain Glucose Uptake with Nutrient Availability. *Cell* **166,** 867-880.

Garfield AS, Li C, Madara JC, Shah BP, Webber E, Steger JS, Campbell JN, Gavrilova O, Lee CE, Olson DP, Elmquist JK, Tannous BA, Krashes MJ & Lowell BB. (2015). A neural basis for melanocortin-4 receptor-regulated appetite. *Nat Neurosci* **18,** 863-871.

Garré JM, Retamal MA, Cassina P, Barbeito L, Bukauskas FF, Sáez JC, Bennett MV & Abudara V. (2010). FGF-1 induces ATP release from spinal astrocytes in culture and opens pannexin and connexin hemichannels. *Proceedings of the National Academy of Sciences of the United States of America* **107,** 22659-22664.

Geloen A, Collet AJ & Bukowiecki LJ. (1992). Role of sympathetic innervation in brown adipocyte proliferation. *American Journal of Physiology-Regulatory, Integrative and Comparative Physiology* **263,** R1176-R1181.

Geracioti TD, Loosen PT, Ebert MH, Schmidt D & Ekhator NN. (1995). Fasting and postprandial cerebrospinal fluid glucose concentrations in healthy women and in an obese binge eater. *The International journal of eating disorders* **18,** 365-369.

Ghamari-Langroudi M, Digby GJ, Sebag JA, Millhauser GL, Palomino R, Matthews R, Gillyard T, Panaro BL, Tough IR, Cox HM, Denton JS & Cone RD. (2015). G-protein-independent coupling of MC4R to Kir7.1 in hypothalamic neurons. *Nature* **520,** 94-98.

Ghamari-Langroudi M, Srisai D & Cone RD. (2011). Multinodal regulation of the arcuate/paraventricular nucleus circuit by leptin. *Proceedings of the National Academy of Sciences of the United States of America* **108,** 355-360.

Giaume C, Koulakoff A, Roux L, Holcman D & Rouach N. (2010). Astroglial networks: a step further in neuroglial and gliovascular interactions. *Nature Reviews Neuroscience* **11,** 87-99.

Goetze O, Steingoetter A, Menne D, van der Voort IR, Kwiatek MA, Boesiger P, Weishaupt D, Thumshirn M, Fried M & Schwizer W. (2007). The effect of macronutrients on gastric volume responses and gastric emptying in humans: A magnetic resonance imaging study. *American journal of physiology Gastrointestinal and liver physiology* **292,** G11-17.

Golozoubova V, Hohtola E, Matthias A, Jacobsson A, Cannon B & Nedergaard J. (2001). Only UCP1 can mediate adaptive nonshivering thermogenesis in the cold. *FASEB journal : official publication of the Federation of American Societies for Experimental Biology* **15,** 2048-2050.

Gong TW, Horwitz BA & Stern JS. (1990). The effects of 2-deoxy-D-glucose and sympathetic denervation of brown fat GDP binding in Sprague-Dawley rats. *Life sciences* **46,** 1037-1044.

Gordon GR, Iremonger KJ, Kantevari S, Ellis-Davies GC, MacVicar BA & Bains JS. (2009). Astrocyte-mediated distributed plasticity at hypothalamic glutamate synapses. *Neuron* **64,** 391-403.

Gourine AV, Kasymov V, Marina N, Tang F, Figueiredo MF, Lane S, Teschemacher AG, Spyer KM, Deisseroth K & Kasparov S. (2010). Astrocytes control breathing through pH-dependent release of ATP. *Science (New York, NY)* **329,** 571-575.

Greenway FL, Whitehouse MJ, Guttadauria M, Anderson JW, Atkinson RL, Fujioka K, Gadde KM, Gupta AK, O'Neil P, Schumacher D, Smith D, Dunayevich E, Tollefson GD, Weber E & Cowley MA. (2009). Rational design of a combination medication for the treatment of obesity. *Obesity (Silver Spring)* **17,** 30-39.

Guan HZ, Dong J, Jiang ZY & Chen X. (2017). alpha-MSH Influences the Excitability of Feeding-Related Neurons in the Hypothalamus and Dorsal Vagal Complex of Rats. *Biomed Res Int* **2017,** 2034691.

Guillod-Maximin E, Lorsignol A, Alquier T & Penicaud L. (2004). Acute intracarotid glucose injection towards the brain induces specific c-fos activation in hypothalamic nuclei: involvement of astrocytes in cerebral glucose-sensing in rats. *J Neuroendocrinol* **16,** 464-471.

Hablitz LM, Gunesch AN, Cravetchi O, Moldavan M & Allen CN. (2020). Cannabinoid Signaling Recruits Astrocytes to Modulate Presynaptic Function in the Suprachiasmatic Nucleus. *eneuro* **7,** ENEURO.0081-0019.2020.

Haery L, Deverman BE, Matho KS, Cetin A, Woodard K, Cepko C, Guerin KI, Rego MA, Ersing I, Bachle SM, Kamens J & Fan M. (2019). Adeno-Associated Virus Technologies and Methods for Targeted Neuronal Manipulation. *Frontiers in Neuroanatomy* **13**.

Hanssen MJ, van der Lans AA, Brans B, Hoeks J, Jardon KM, Schaart G, Mottaghy FM, Schrauwen P & van Marken Lichtenbelt WD. (2016). Short-term Cold Acclimation Recruits Brown Adipose Tissue in Obese Humans. *Diabetes* **65,** 1179-1189.

Hanssen MJW, Hoeks J, Brans B, van der Lans AAJJ, Schaart G, van den Driessche JJ, Jörgensen JA, Boekschoten MV, Hesselink MKC, Havekes B, Kersten S, Mottaghy FM, van Marken Lichtenbelt WD & Schrauwen P. (2015). Short-term cold acclimation improves insulin sensitivity in patients with type 2 diabetes mellitus. *Nature Medicine* **21,** 863-865.

Hany TF, Gharehpapagh E, Kamel EM, Buck A, Himms-Hagen J & von Schulthess GK. (2002). Brown adipose tissue: a factor to consider in symmetrical tracer uptake in the neck and upper chest region. *European journal of nuclear medicine and molecular imaging* **29,** 1393-1398.

Haskell-Luevano C & Monck EK. (2001). Agouti-related protein functions as an inverse agonist at a constitutively active brain melanocortin-4 receptor. *Regulatory peptides* **99,** 1-7.

Hayes AJ, Lung TW, Bauman A & Howard K. (2017). Modelling obesity trends in Australia: unravelling the past and predicting the future. *International journal of obesity (2005)* **41,** 178-185.

Haynes VR, Michael NJ, van den Top M, Zhao F-Y, Brown RD, De Souza D, Dodd GT, Spanswick D & Watt MJ. (2020). A Neural basis for Octanoic acid regulation of energy balance. *Molecular metabolism* **34,** 54-71.

Haynes WG, Morgan DA, Djalali A, Sivitz WI & Mark AL. (1999). Interactions between the melanocortin system and leptin in control of sympathetic nerve traffic. *Hypertension (Dallas, Tex : 1979)* **33,** 542-547.

He M-L, Gonzalez-Iglesias AE, Tomic M & Stojilkovic SS. (2005). Release and extracellular metabolism of ATP by ecto-nucleotidase eNTPDase 1–2 in hypothalamic and pituitary cells. *Purinergic Signalling* **1,** 135.

He Z, Gao Y, Alhadeff AL, Castorena CM, Huang Y, Lieu L, Afrin S, Sun J, Betley JN, Guo H & Williams KW. (2018). Cellular and synaptic reorganization of arcuate NPY/AgRP and POMC neurons after exercise. *Molecular metabolism* **18,** 107-119.

Heeley N, Kirwan P, Darwish T, Arnaud M, Evans ML, Merkle FT, Reimann F, Gribble FM & Blouet C. (2018). Rapid sensing of l-leucine by human and murine hypothalamic neurons: Neurochemical and mechanistic insights. *Molecular metabolism* **10,** 14-27.

Henneberger C, Papouin T, Oliet SH & Rusakov DA. (2010). Long-term potentiation depends on release of D-serine from astrocytes. *Nature* **463,** 232-236.

Henry BA, Blache D, Rao A, Clarke IJ & Maloney SK. (2010). Disparate effects of feeding on core body and adipose tissue temperatures in animals selectively bred for Nervous or Calm temperament. *American journal of physiology Regulatory, integrative and comparative physiology* **299,** R907-917.

Henry FE, Sugino K, Tozer A, Branco T & Sternson SM. (2015). Cell type-specific transcriptomics of hypothalamic energy-sensing neuron responses to weight-loss. *eLife* **4,** e09800.

Herrero-Mendez A, Almeida A, Fernandez E, Maestre C, Moncada S & Bolanos JP. (2009). The bioenergetic and antioxidant status of neurons is controlled by continuous degradation of a key glycolytic enzyme by APC/C-Cdh1. *Nature cell biology* **11,** 747-752.

Herrmann S, Schnorr S & Ludwig A. (2015). HCN channels--modulators of cardiac and neuronal excitability. *Int J Mol Sci* **16,** 1429-1447.

Hibi M, Oishi S, Matsushita M, Yoneshiro T, Yamaguchi T, Usui C, Yasunaga K, Katsuragi Y, Kubota K, Tanaka S & Saito M. (2016). Brown adipose tissue is involved in diet-induced thermogenesis and whole-body fat utilization in healthy humans. *International journal of obesity* **40,** 1655-1661.

Hill JW, Williams KW, Ye C, Luo J, Balthasar N, Coppari R, Cowley MA, Cantley LC, Lowell BB & Elmquist JK. (2008). Acute effects of leptin require PI3K signaling in hypothalamic proopiomelanocortin neurons in mice. *The Journal of clinical investigation* **118,** 1796-1805.

Himms-Hagen J. (1989). Role of thermogenesis in the regulation of energy balance in relation to obesity. *Canadian journal of physiology and pharmacology* **67,** 394-401.

Holt SJ & York DA. (1989). Interaction of intracerebroventricular insulin and glucose in the regulation of the activity of sympathetic efferent nerves to brown adipose tissue in lean and obese Zucker rats. *Brain research* **500,** 384-388.

Hui X, Gu P, Zhang J, Nie T, Pan Y, Wu D, Feng T, Zhong C, Wang Y, Lam KS & Xu A. (2015). Adiponectin Enhances Cold-Induced Browning of Subcutaneous Adipose Tissue via Promoting M2 Macrophage Proliferation. *Cell metabolism* **22,** 279-290.

Huszar D, Lynch CA, Fairchild-Huntress V, Dunmore JH, Fang Q, Berkemeier LR, Gu W, Kesterson RA, Boston BA, Cone RD, Smith FJ, Campfield LA, Burn P & Lee F. (1997). Targeted disruption of the melanocortin-4 receptor results in obesity in mice. *Cell* **88,** 131-141.

Hwa JJ, Ghibaudi L, Gao J & Parker EM. (2001). Central melanocortin system modulates energy intake and expenditure of obese and lean Zucker rats. *American Journal of Physiology-Regulatory, Integrative and Comparative Physiology* **281,** R444-R451.

Ibrahim N, Bosch MA, Smart JL, Qiu J, Rubinstein M, Ronnekleiv OK, Low MJ & Kelly MJ. (2003). Hypothalamic proopiomelanocortin neurons are glucose responsive and express K(ATP) channels. *Endocrinology* **144,** 1331-1340.

Iliff BW & Swoap SJ. (2012). Central adenosine receptor signaling is necessary for daily torpor in mice. *American Journal of Physiology-Regulatory, Integrative and Comparative Physiology* **303,** R477-R484.

Inagaki N, Gonoi T, Clement JP, Namba N, Inazawa J, Gonzalez G, Aguilar-Bryan L, Seino S & Bryan J. (1995). Reconstitution of I_{KATP}: An Inward Rectifier Subunit Plus the Sulfonylurea Receptor. *Science (New York, NY)* **270,** 1166.

Itoh Y, Esaki T, Shimoji K, Cook M, Law MJ, Kaufman E & Sokoloff L. (2003). Dichloroacetate effects on glucose and lactate oxidation by neurons and astroglia in vitro and on glucose utilization by brain in vivo. *Proceedings of the National Academy of Sciences* **100,** 4879-4884.

Jais A, Paeger L, Sotelo-Hitschfeld T, Bremser S, Prinzensteiner M, Klemm P, Mykytiuk V, Widdershooven PJM, Vesting AJ, Grzelka K, Minère M, Cremer AL, Xu J, Korotkova T, Lowell BB, Zeilhofer HU, Backes H, Fenselau H, Wunderlich FT, Kloppenburg P & Brüning JC. (2020). PNOCARC Neurons Promote Hyperphagia and Obesity upon High-Fat-Diet Feeding. *Neuron*.

James SD, Hawkins VE, Falquetto B, Ruskin DN, Masino SA, Moreira TS, Olsen ML & Mulkey DK. (2018). Adenosine Signaling through A1 Receptors Inhibits Chemosensitive Neurons in the Retrotrapezoid Nucleus. *eneuro* **5,** ENEURO.0404-0418.2018.

Jarvie BC & Hentges ST. (2012). Expression of GABAergic and glutamatergic phenotypic markers in hypothalamic proopiomelanocortin neurons. *The Journal of comparative neurology* **520,** 3863-3876.

Johnson DR & Kida MY. (1995). Development of the spinous process of the second thoracic vertebra of the mouse in the late fetal and early postnatal period. *Okajimas Folia Anat Jpn* **72,** 45-49.

Johnson DR, McAndrew TJ & Oguz O. (1999). Shape differences in the cervical and upper thoracic vertebrae in rats (Rattus norvegicus) and bats (Pteropus poiocephalus): can we see shape patterns derived from position in column and species membership? *Journal of anatomy* **194 (Pt 2),** 249-253.

Kacem K, Lacombe P, Seylaz J & Bonvento G. (1998). Structural organization of the perivascular astrocyte endfeet and their relationship with the endothelial glucose transporter: a confocal microscopy study. *Glia* **23,** 1-10.

Kaiyala KJ, Ogimoto K, Nelson JT, Muta K & Morton GJ. (2016). Physiological role for leptin in the control of thermal conductance. *Molecular metabolism* **5,** 892-902.

Kajimura S & Saito M. (2014). A new era in brown adipose tissue biology: molecular control of brown fat development and energy homeostasis. *Annual review of physiology* **76,** 225-249.

Kang J, Kang N, Lovatt D, Torres A, Zhao Z, Lin J & Nedergaard M. (2008). Connexin 43 Hemichannels Are Permeable to ATP. *The Journal of Neuroscience* **28,** 4702.

Kataoka N, Hioki H, Kaneko T & Nakamura K. (2014). Psychological stress activates a dorsomedial hypothalamus-medullary raphe circuit driving brown adipose tissue thermogenesis and hyperthermia. *Cell metabolism* **20,** 346-358.

Kataoka N, Shima Y, Nakajima K & Nakamura K. (2020). A central master driver of psychosocial stress responses in the rat. *Science (New York, NY)* **367,** 1105.

Kawamura M, Ruskin DN & Masino SA. (2010). Metabolic Autocrine Regulation of Neurons Involves Cooperation among Pannexin Hemichannels, Adenosine Receptors, and K_{ATP} Channels. *The Journal of Neuroscience* **30,** 3886.

Khaodhiar L, McCowen KC & Blackburn GL. (1999). Obesity and its comorbid conditions. *Clinical cornerstone* **2,** 17-31.

Khera R, Murad M, Chandar AK & et al. (2016). Association of pharmacological treatments for obesity with weight loss and adverse events: A systematic review and meta-analysis. *JAMA* **315,** 2424-2434.

Kim CS & Johnston D. (2015). A1 adenosine receptor-mediated GIRK channels contribute to the resting conductance of CA1 neurons in the dorsal hippocampus. *J Neurophysiol* **113,** 2511-2523.

Kim JG, Suyama S, Koch M, Jin S, Argente-Arizon P, Argente J, Liu ZW, Zimmer MR, Jeong JK, Szigeti-Buck K, Gao Y, Garcia-Caceres C, Yi CX, Salmaso N, Vaccarino FM, Chowen J, Diano S, Dietrich MO, Tschöp MH & Horvath TL. (2014). Leptin signaling in astrocytes regulates hypothalamic neuronal circuits and feeding. *Nat Neurosci* **17,** 908-910.

Klingenberg M. (2010). Wanderings in bioenergetics and biomembranes. *Biochimica et biophysica acta* **1797,** 579-594.

Koizumi S, Fujishita K, Tsuda M, Shigemoto-Mogami Y & Inoue K. (2003). Dynamic inhibition of excitatory synaptic transmission by astrocyte-derived ATP in hippocampal cultures. *Proceedings of the National Academy of Sciences of the United States of America* **100,** 11023-11028.

Kong D, Tong Q, Ye C, Koda S, Fuller PM, Krashes MJ, Vong L, Ray RS, Olson DP & Lowell BB. (2012). GABAergic RIP-Cre neurons in the arcuate nucleus selectively regulate energy expenditure. *Cell* **151,** 645-657.

Kong D, Vong L, Parton LE, Ye C, Tong Q, Hu X, Choi B, Bruning JC & Lowell BB. (2010). Glucose stimulation of hypothalamic MCH neurons involves K(ATP) channels, is modulated by UCP2, and regulates peripheral glucose homeostasis. *Cell metabolism* **12,** 545-552.

Könner AC, Janoschek R, Plum L, Jordan SD, Rother E, Ma X, Xu C, Enriori P, Hampel B, Barsh GS, Kahn CR, Cowley MA, Ashcroft FM & Brüning JC. (2007). Insulin action in AgRP-expressing neurons is required for suppression of hepatic glucose production. *Cell metabolism* **5,** 438-449.

Kooijman S, Boon MR, Parlevliet ET, Geerling JJ, van de Pol V, Romijn JA, Havekes LM, Meurs I & Rensen PC. (2014). Inhibition of the central melanocortin system decreases brown adipose tissue activity. *Journal of lipid research* **55,** 2022-2032.

Kozak LP. (2010). Brown fat and the myth of diet-induced thermogenesis. *Cell metabolism* **11,** 263-267.

Krashes MJ, Koda S, Ye C, Rogan SC, Adams AC, Cusher DS, Maratos-Flier E, Roth BL & Lowell BB. (2011). Rapid, reversible activation of AgRP neurons drives feeding behavior in mice. *The Journal of clinical investigation* **121,** 1424-1428.

Krashes MJ, Lowell BB & Garfield AS. (2016). Melanocortin-4 receptor-regulated energy homeostasis. *Nat Neurosci* **19,** 206-219.

Krude H, Biebermann H, Luck W, Horn R, Brabant G & Grüters A. (1998). Severe early-onset obesity, adrenal insufficiency and red hair pigmentation caused by POMC mutations in humans. *Nat Genet* **19,** 155-157.

Kublaoui BM, Holder JL, Jr., Gemelli T & Zinn AR. (2006). Sim1 haploinsufficiency impairs melanocortin-mediated anorexia and activation of paraventricular nucleus neurons. *Molecular endocrinology (Baltimore, Md)* **20,** 2483-2492.

Labbé SM, Caron A, Lanfray D, Monge-Rofarello B, Bartness TJ & Richard D. (2015). Hypothalamic control of brown adipose tissue thermogenesis. *Front Syst Neurosci* **9,** 150-150.

Lam BYH, Cimino I, Polex-Wolf J, Nicole Kohnke S, Rimmington D, Iyemere V, Heeley N, Cossetti C, Schulte R, Saraiva LR, Logan DW, Blouet C, O'Rahilly S, Coll AP & Yeo GSH. (2017). Heterogeneity of hypothalamic pro-opiomelanocortin-expressing neurons revealed by single-cell RNA sequencing. *Molecular metabolism* **6,** 383-392.

Lam CK, Chari M, Wang PY & Lam TK. (2008). Central lactate metabolism regulates food intake. *American journal of physiology Endocrinology and metabolism* **295,** E491-496.

Lam DD, Attard CA, Mercer AJ, Myers MG, Jr., Rubinstein M & Low MJ. (2015). Conditional expression of Pomc in the Lepr-positive subpopulation of POMC neurons is sufficient for normal energy homeostasis and metabolism. *Endocrinology* **156,** 1292-1302.

Lamy Christophe M, Sanno H, Labouèbe G, Picard A, Magnan C, Chatton J-Y & Thorens B. (2014). Hypoglycemia-Activated GLUT2 Neurons of the Nucleus Tractus Solitarius Stimulate Vagal Activity and Glucagon Secretion. *Cell metabolism* **19,** 527-538.

Latini S & Pedata F. (2001). Adenosine in the central nervous system: release mechanisms and extracellular concentrations. *J Neurochem* **79,** 463-484.

Laughton JD, Bittar P, Charnay Y, Pellerin L, Kovari E, Magistretti PJ & Bouras C. (2007). Metabolic compartmentalization in the human cortex and hippocampus: evidence for a cell- and region-specific localization of lactate dehydrogenase 5 and pyruvate dehydrogenase. *BMC neuroscience* **8,** 35.

LeBlanc J & Cabanac M. (1989). Cephalic postprandial thermogenesis in human subjects. *Physiology & behavior* **46,** 479-482.

LeBlanc J, Cabanac M & Samson P. (1984). Reduced postprandial heat production with gavage as compared with meal feeding in human subjects. *The American journal of physiology* **246,** E95-101.

Lee P, Smith S, Linderman J, Courville AB, Brychta RJ, Dieckmann W, Werner CD, Chen KY & Celi FS. (2014). Temperature-acclimated brown adipose tissue modulates insulin sensitivity in humans. *Diabetes* **63,** 3686-3698.

Leitner BP, Huang S, Brychta RJ, Duckworth CJ, Baskin AS, McGehee S, Tal I, Dieckmann W, Gupta G, Kolodny GM, Pacak K, Herscovitch P, Cypess AM & Chen KY. (2017). Mapping of human brown adipose tissue in lean and obese young men. *Proceedings of the National Academy of Sciences* **114,** 8649-8654.

Lever JD, Jung RT, Nnodim JO, Leslie PJ & Symons D. (1986). Demonstration of a catecholaminergic innervation in human perirenal brown adipose tissue at various ages in the adult. *The Anatomical record* **215,** 251-255, 227-259.

Levin BE. (2002). Metabolic sensors: Viewing glucosensing neurons from a broader perspective. *Physiology & behavior* **76,** 397-401.

Li MF & Cheung BM. (2011). Rise and fall of anti-obesity drugs. *World journal of diabetes* **2,** 19-23.

Li Y, Gao XB, Sakurai T & van den Pol AN. (2002). Hypocretin/Orexin excites hypocretin neurons via a local glutamate neuron-A potential mechanism for orchestrating the hypothalamic arousal system. *Neuron* **36,** 1169-1181.

Li Y, Schnabl K, Gabler S-M, Willershäuser M, Reber J, Karlas A, Laurila S, Lahesmaa M, u Din M, Bast-Habersbrunner A, Virtanen KA, Fromme T, Bolze F, O'Farrell LS, Alsina-Fernandez J, Coskun T, Ntziachristos V, Nuutila P & Klingenspor M. (2018). Secretin-Activated Brown Fat Mediates Prandial Thermogenesis to Induce Satiation. *Cell* **175,** 1561-1574.e1512.

Limberg JK, Malterer KR, Matzek LJ, Levine JA, Charkoudian N, Miles JM, Joyner MJ & Curry TB. (2017). Resting sympathetic activity is associated with the sympathetically mediated component of energy expenditure following a meal. *Physiological reports* **5,** e13389.

Liu H, Kishi T, Roseberry AG, Cai X, Lee CE, Montez JM, Friedman JM & Elmquist JK. (2003a). Transgenic Mice Expressing Green Fluorescent Protein under the Control of the Melanocortin-4 Receptor Promoter. *The Journal of Neuroscience* **23,** 7143.

Liu T, Kong D, Shah BP, Ye C, Koda S, Saunders A, Ding JB, Yang Z, Sabatini BL & Lowell BB. (2012). Fasting activation of AgRP neurons requires NMDA receptors and involves spinogenesis and increased excitatory tone. *Neuron* **73,** 511-522.

Liu X, Rossmeisl M, McClaine J, Riachi M, Harper ME & Kozak LP. (2003b). Paradoxical resistance to diet-induced obesity in UCP1-deficient mice. *The Journal of clinical investigation* **111,** 399-407.

Llewellyn-Smith IJ, Martin CL, Marcus JN, Yanagisawa M, Minson JB & Scammell TE. (2003). Orexin-immunoreactive inputs to rat sympathetic preganglionic neurons. *Neuroscience letters* **351,** 115-119.

Lockie SH, Heppner KM, Chaudhary N, Chabenne JR, Morgan DA, Veyrat-Durebex C, Ananthakrishnan G, Rohner-Jeanrenaud F, Drucker DJ, DiMarchi R, Rahmouni K, Oldfield BJ,

Tschop MH & Perez-Tilve D. (2012). Direct control of brown adipose tissue thermogenesis by central nervous system glucagon-like peptide-1 receptor signaling. *Diabetes* **61,** 2753-2762.

López-Gambero AJ, Martínez F, Salazar K, Cifuentes M & Nualart F. (2019). Brain Glucose-Sensing Mechanism and Energy Homeostasis. *Molecular Neurobiology* **56,** 769-796.

López M, Lage R, Tung YCL, Challis BG, Varela L, Virtue S, O'Rahilly S, Vidal-Puig A, Diéguez C & Coll AP. (2007). Orexin expression is regulated by alpha-melanocyte-stimulating hormone. *Journal of neuroendocrinology* **19,** 703-707.

Lopez M, Varela L, Vazquez MJ, Rodriguez-Cuenca S, Gonzalez CR, Velagapudi VR, Morgan DA, Schoenmakers E, Agassandian K, Lage R, de Morentin PBM, Tovar S, Nogueiras R, Carling D, Lelliott C, Gallego R, Oresic M, Chatterjee K, Saha AK, Rahmouni K, Dieguez C & Vidal-Puig A. (2010). Hypothalamic AMPK and fatty acid metabolism mediate thyroid regulation of energy balance. *Nat Med* **16,** 1001-1008.

Lowell BB & Spiegelman BM. (2000). Towards a molecular understanding of adaptive thermogenesis. *Nature* **404,** 652-660.

Ma SWY, Foster DO, Nadeau BE & Triandafillou J. (1988). Absence of increased oxygen consumption in brown adipose tissue of rats exhibiting "cafeteria" diet-induced thermogenesis. *Canadian journal of physiology and pharmacology* **66,** 1347-1354.

Madden CJ & Morrison SF. (2006). Serotonin potentiates sympathetic responses evoked by spinal NMDA. *The Journal of physiology* **577,** 525-537.

Madden CJ & Morrison SF. (2009). Neurons in the paraventricular nucleus of the hypothalamus inhibit sympathetic outflow to brown adipose tissue. *American journal of physiology Regulatory, integrative and comparative physiology* **296,** R831-843.

Madden CJ & Morrison SF. (2010). Endogenous activation of spinal 5-hydroxytryptamine (5-HT) receptors contributes to the thermoregulatory activation of brown adipose tissue. *American journal of physiology Regulatory, integrative and comparative physiology* **298,** R776-783.

Madden CJ, Tupone D, Cano G & Morrison SF. (2013). alpha2 Adrenergic receptor-mediated inhibition of thermogenesis. *The Journal of neuroscience : the official journal of the Society for Neuroscience* **33,** 2017-2028.

Madden CJ, Tupone D & Morrison SF. (2012). Orexin modulates brown adipose tissue thermogenesis. *Biomol Concepts* **3,** 381-386.

Madisen L, Zwingman TA, Sunkin SM, Oh SW, Zariwala HA, Gu H, Ng LL, Palmiter RD, Hawrylycz MJ, Jones AR, Lein ES & Zeng H. (2010). A robust and high-throughput Cre reporting and characterization system for the whole mouse brain. *Nat Neurosci* **13,** 133-140.

Mandelblat-Cerf Y, Ramesh RN, Burgess CR, Patella P, Yang Z, Lowell BB & Andermann ML. (2015). Arcuate hypothalamic AgRP and putative POMC neurons show opposite changes in spiking across multiple timescales. *Elife* **4**.

Martin-Fernandez M, Jamison S, Robin LM, Zhao Z, Martin ED, Aguilar J, Benneyworth MA, Marsicano G & Araque A. (2017). Synapse-specific astrocyte gating of amygdala-related behavior. *Nature Neuroscience* **20,** 1540-1548.

Martín ED, Fernández M, Perea G, Pascual O, Haydon PG, Araque A & Ceña V. (2007). Adenosine released by astrocytes contributes to hypoxia-induced modulation of synaptic transmission. *Glia* **55,** 36-45.

Marty N, Dallaporta M, Foretz M, Emery M, Tarussio D, Bady I, Binnert C, Beermann F & Thorens B. (2005). Regulation of glucagon secretion by glucose transporter type 2 (glut2) and astrocyte-dependent glucose sensors. *The Journal of clinical investigation* **115,** 3545-3553.

Maxwell GM, Nobbs S & Bates DJ. (1987). Diet-induced thermogenesis in cafeteria-fed rats: a myth? *American Journal of Physiology - Endocrinology and Metabolism* **253,** E264-E270.

McCarthy KM, Tank DW & Enquist LW. (2009). Pseudorabies virus infection alters neuronal activity and connectivity in vitro. *PLoS pathogens* **5,** e1000640.

McCormick DA & Pape HC. (1990). Properties of a hyperpolarization-activated cation current and its role in rhythmic oscillation in thalamic relay neurones. *The Journal of physiology* **431,** 291-318.

McDougal D, Hermann G & Rogers R. (2013). Astrocytes in the nucleus of the solitary tract are activated by low glucose or glucoprivation: evidence for glial involvement in glucose homeostasis. *Frontiers in neuroscience* **7**.

Melnick IV, Price CJ & Colmers WF. (2011). Glucosensing in parvocellular neurons of the rat hypothalamic paraventricular nucleus. *The European journal of neuroscience* **34,** 272-282.

Melnikova I & Wages D. (2006). Anti-obesity therapies. *Nature reviews Drug discovery* **5,** 369-370.

Meyer CW, Ootsuka Y & Romanovsky AA. (2017). Body Temperature Measurements for Metabolic Phenotyping in Mice. *Front Physiol* **8,** 520.

Mickelsen LE, Kolling FW, Chimileski BR, Fujita A, Norris C, Chen K, Nelson CE & Jackson AC. (2017). Neurochemical Heterogeneity Among Lateral Hypothalamic Hypocretin/Orexin and Melanin-Concentrating Hormone Neurons Identified Through Single-Cell Gene Expression Analysis. *eneuro* **4,** ENEURO.0013-0017.2017.

Millan C, Martinez F, Cortes-Campos C, Lizama I, Yanez MJ, Llanos P, Reinicke K, Rodriguez F, Peruzzo B, Nualart F & Garcia MA. (2010). Glial glucokinase expression in adult and post-natal development of the hypothalamic region. *ASN neuro* **2,** e00035.

Miwa Y & Imai Y. (1999). Simulation of spike-burst generation and Ca(2+) oscillation in pancreatic beta-cells. *Jpn J Physiol* **49,** 353-364.

Mohammed M, Ootsuka Y, Yanagisawa M & Blessing W. (2014). Reduced brown adipose tissue thermogenesis during environmental interactions in transgenic rats with ataxin-3-mediated ablation of hypothalamic orexin neurons. *American journal of physiology Regulatory, integrative and comparative physiology* **307,** R978-989.

Monda M, Viggiano A & De Luca V. (2003). Parodoxical effect of orexin A: hypophagia induced by hyperthermia. *Brain Research* **961,** 220-228.

Monge-Roffarello B, Labbe SM, Lenglos C, Caron A, Lanfray D, Samson P & Richard D. (2014a). The medial preoptic nucleus as a site of the thermogenic and metabolic actions of melanotan II in male rats. *American journal of physiology Regulatory, integrative and comparative physiology* **307,** R158-166.

Monge-Roffarello B, Labbe SM, Roy MC, Lemay ML, Coneggo E, Samson P, Lanfray D & Richard D. (2014b). The PVH as a site of CB1-mediated stimulation of thermogenesis by MC4R agonism in male rats. *Endocrinology* **155,** 3448-3458.

Morgan DA, McDaniel LN, Yin T, Khan M, Jiang J, Acevedo MR, Walsh SA, Ponto LL, Norris AW, Lutter M, Rahmouni K & Cui H. (2015). Regulation of glucose tolerance and sympathetic activity by MC4R signaling in the lateral hypothalamus. *Diabetes* **64,** 1976-1987.

Morrison SF. (2016). Central control of body temperature. *F1000Res* **5**.

Morrison SF, Madden CJ & Tupone D. (2012). Central control of brown adipose tissue thermogenesis. *Frontiers in endocrinology* **3**.

Morrison Shaun F, Madden Christopher J & Tupone D. (2014). Central Neural Regulation of Brown Adipose Tissue Thermogenesis and Energy Expenditure. *Cell metabolism* **19,** 741-756.

Morrison SF & Nakamura K. (2019). Central Mechanisms for Thermoregulation. *Annual review of physiology* **81,** 285-308.

Morton GJ, Cummings DE, Baskin DG, Barsh GS & Schwartz MW. (2006). Central nervous system control of food intake and body weight. *Nature* **443,** 289-295.

Mounien L, Marty N, Tarussio D, Metref S, Genoux D, Preitner F, Foretz M & Thorens B. (2010). Glut2-dependent glucose-sensing controls thermoregulation by enhancing the leptin sensitivity of NPY and POMC neurons. *FASEB journal : official publication of the Federation of American Societies for Experimental Biology* **24,** 1747-1758.

Mountjoy KG, Mortrud MT, Low MJ, Simerly RB & Cone RD. (1994). Localization of the melanocortin-4 receptor (MC4-R) in neuroendocrine and autonomic control circuits in the brain. *Molecular endocrinology (Baltimore, Md)* **8,** 1298-1308.

Mountjoy PD, Bailey SJ & Rutter GA. (2007). Inhibition by glucose or leptin of hypothalamic neurons expressing neuropeptide Y requires changes in AMP-activated protein kinase activity. *Diabetologia* **50,** 168-177.

Mukherjee S, Lever JD, Norman D, Symons D, Spriggs TL & Jung RT. (1989). A comparison of the effects of 6-hydroxydopamine and reserpine on noradrenergic and peptidergic nerves in rat brown adipose tissue. *Journal of anatomy* **167,** 189-193.

Muller C, Voirol MJ, Stefanoni N, Surmely JF, Jequier E, Gaillard RC & Tappy L. (1997). Effect of chronic intracerebroventricular infusion of insulin on brown adipose tissue activity in fed and fasted rats. *Int J Obes Relat Metab Disord* **21,** 562-566.

Münzberg H, Huo L, Nillni EA, Hollenberg AN & Bjørbæk C. (2003). Role of Signal Transducer and Activator of Transcription 3 in Regulation of Hypothalamic Proopiomelanocortin Gene Expression by Leptin. *Endocrinology* **144,** 2121-2131.

Murphy BA, Fakira KA, Song Z, Beuve A & Routh VH. (2009). AMP-activated protein kinase and nitric oxide regulate the glucose sensitivity of ventromedial hypothalamic glucose-inhibited neurons. *American journal of physiology Cell physiology* **297,** C750-758.

Muzzi M, Blasi F, Masi A, Coppi E, Traini C, Felici R, Pittelli M, Cavone L, Pugliese AM, Moroni F & Chiarugi A. (2013). Neurological Basis of AMP-Dependent Thermoregulation and its Relevance to Central and Peripheral Hyperthermia. *Journal of Cerebral Blood Flow & Metabolism* **33,** 183-190.

Nagai N, Sakane N, Ueno LM, Hamada T & Moritani T. (2003). The -3826 A-->G variant of the uncoupling protein-1 gene diminishes postprandial thermogenesis after a high fat meal in healthy boys. *J Clin Endocrinol Metab* **88,** 5661-5667.

Nakajima K, Cui Z, Li C, Meister J, Cui Y, Fu O, Smith AS, Jain S, Lowell BB, Krashes MJ & Wess J. (2016). Gs-coupled GPCR signalling in AgRP neurons triggers sustained increase in food intake. *Nature communications* **7,** 10268.

Nakamura Y, Yanagawa Y, Morrison SF & Nakamura K. (2017). Medullary Reticular Neurons Mediate Neuropeptide Y-Induced Metabolic Inhibition and Mastication. *Cell metabolism* **25,** 322-334.

Nedergaard J, Bengtsson T & Cannon B. (2007). Unexpected evidence for active brown adipose tissue in adult humans. *American journal of physiology Endocrinology and metabolism* **293,** E444-452.

Nedergaard J, Bengtsson T & Cannon B. (2011). New powers of brown fat: fighting the metabolic syndrome. *Cell metabolism* **13,** 238-240.

Nguyen KD, Qiu Y, Cui X, Goh YP, Mwangi J, David T, Mukundan L, Brombacher F, Locksley RM & Chawla A. (2011). Alternatively activated macrophages produce catecholamines to sustain adaptive thermogenesis. *Nature* **480,** 104-108.

Nicholls DG & Locke RM. (1984). Thermogenic mechanisms in brown fat. *Physiological reviews* **64,** 1-64.

Nogueira MI, de Rezende BD, Ribeiro do Vale LE & Bittencourt JC. (2000). Afferent connections of the caudal raphe pallidus nucleus in rats: a study using the fluorescent retrograde tracers fluorogold and true-blue. *Annals of Anatomy - Anatomischer Anzeiger* **182,** 35-45.

NPS MedicineWise. (2017a). Saxenda Solution for injection. www.nps.org.au/medical-info/medicine-finder/saxenda-solution-for-injection.

NPS MedicineWise. (2017b). Victoza Solution for injection. www.nps.org.au/medical-info/medicine-finder/victoza-solution-for-injection.

Nuzzaci D, Cansell C, Liénard F, Nédélec E, Ben Fradj S, Castel J, Foppen E, Denis R, Grouselle D, Laderrière A, Lemoine A, Mathou A, Tolle V, Heurtaux T, Fioramonti X, Audinat E, Pénicaud L, Nahon J-L, Rovère C & Benani A. (2020). Postprandial Hyperglycemia Stimulates Neuroglial Plasticity in Hypothalamic POMC Neurons after a Balanced Meal. *Cell Reports* **30,** 3067-3078.e3065.

O'Brien J, Kla KM, Hopkins IB, Malecki EA & McKenna MC. (2007). Kinetic parameters and lactate dehydrogenase isozyme activities support possible lactate utilization by neurons. *Neurochemical research* **32,** 597-607.

O'Brien PE, Brown WA & Dixon JB. (2005). Obesity, weight loss and bariatric surgery. *The Medical journal of Australia* **183,** 310-314.

O'Malley D, Reimann F, Simpson AK & Gribble FM. (2006). Sodium-Coupled Glucose Cotransporters Contribute to Hypothalamic Glucose Sensing. *Diabetes* **55,** 3381.

Oldfield BJ, Giles ME, Watson A, Anderson C, Colvill LM & McKinley MJ. (2002). The neurochemical characterisation of hypothalamic pathways projecting polysynaptically to brown adipose tissue in the rat. *Neuroscience* **110,** 515-526.

Ollmann MM, Wilson BD, Yang YK, Kerns JA, Chen Y, Gantz I & Barsh GS. (1997). Antagonism of central melanocortin receptors in vitro and in vivo by agouti-related protein. *Science (New York, NY)* **278,** 135-138.

Onakpoya IJ, Heneghan CJ & Aronson JK. (2016). Post-marketing withdrawal of anti-obesity medicinal products because of adverse drug reactions: a systematic review. *BMC Medicine* **14,** 191.

Ono K, Tsukamoto-Yasui M, Hara-Kimura Y, Inoue N, Nogusa Y, Okabe Y, Nagashima K & Kato F. (2011). Intragastric administration of capsiate, a transient receptor potential channel agonist, triggers thermogenic sympathetic responses. *Journal of applied physiology* **110,** 789-798.

Oomura Y, Ono T, Ooyama H & Wayner MJ. (1969). Glucose and osmosensitive neurones of the rat hypothalamus. *Nature* **222,** 282-284.

Oomura Y & Yoshimatsu H. (1984). Neural network of glucose monitoring system. *Journal of the autonomic nervous system* **10,** 359-372.

Ouellet V, Labbe SM, Blondin DP, Phoenix S, Guerin B, Haman F, Turcotte EE, Richard D & Carpentier AC. (2012). Brown adipose tissue oxidative metabolism contributes to energy expenditure during acute cold exposure in humans. *The Journal of clinical investigation* **122,** 545-552.

Owen BM, Ding X, Morgan DA, Coate KC, Bookout AL, Rahmouni K, Kliewer SA & Mangelsdorf DJ. (2014). FGF21 acts centrally to induce sympathetic nerve activity, energy expenditure, and weight loss. *Cell metabolism* **20,** 670-677.

Padilla SL, Reef D & Zeltser LM. (2012). Defining POMC neurons using transgenic reagents: impact of transient Pomc expression in diverse immature neuronal populations. *Endocrinology* **153,** 1219-1231.

Parsons MP & Hirasawa M. (2010). ATP-Sensitive Potassium Channel-Mediated Lactate Effect on Orexin Neurons: Implications for Brain Energetics during Arousal. *The Journal of Neuroscience* **30,** 8061.

Parton LE, Ye CP, Coppari R, Enriori PJ, Choi B, Zhang CY, Xu C, Vianna CR, Balthasar N, Lee CE, Elmquist JK, Cowley MA & Lowell BB. (2007). Glucose sensing by POMC neurons regulates glucose homeostasis and is impaired in obesity. *Nature* **449,** 228-232.

Paxinos G & Watson C. (1998). *The Rat Brain in Stereotaxic Coordinates*. Academic Press.

Pei H, Patterson CM, Sutton AK, Burnett KH, Myers MG, Jr. & Olson DP. (2019). Lateral Hypothalamic Mc3R-Expressing Neurons Modulate Locomotor Activity, Energy Expenditure, and Adiposity in Male Mice. *Endocrinology* **160,** 343-358.

Penicaud L, Thompson DA & Le Magnen J. (1986). Effects of 2-deoxy-D-glucose on food and water intake and body temperature in rats. *Physiology & behavior* **36,** 431-435.

Perry RJ, Lyu K, Rabin-Court A, Dong J, Li X, Yang Y, Qing H, Wang A, Yang X & Shulman GI. (2020). Leptin mediates postprandial increases in body temperature through hypothalamus–adrenal medulla–adipose tissue crosstalk. *The Journal of clinical investigation* **130**.

Pezeshki A, Zapata R, Singh A, Yee N & Chelikani P. (2016). Low protein diets produce divergent effects on energy balance. *Scientific reports* **6,** 25145.

Pickard GE, Smeraski CA, Tomlinson CC, Banfield BW, Kaufman J, Wilcox CL, Enquist LW & Sollars PJ. (2002). Intravitreal Injection of the Attenuated Pseudorabies Virus PRV Bartha Results in Infection of the Hamster Suprachiasmatic Nucleus Only by Retrograde Transsynaptic Transport via Autonomic Circuits. *The Journal of Neuroscience* **22,** 2701.

Plum L, Ma X, Hampel B, Balthasar N, Coppari R, Münzberg H, Shanabrough M, Burdakov D, Rother E, Janoschek R, Alber J, Belgardt BF, Koch L, Seibler J, Schwenk F, Fekete C, Suzuki A, Mak TW, Krone W, Horvath TL, Ashcroft FM & Brüning JC. (2006). Enhanced PIP3 signaling in POMC neurons causes KATP channel activation and leads to diet-sensitive obesity. *The Journal of clinical investigation* **116,** 1886-1901.

Pomeranz LE, Ekstrand MI, Latcha KN, Smith GA, Enquist LW & Friedman JM. (2017). Gene Expression Profiling with Cre-Conditional Pseudorabies Virus Reveals a Subset of Midbrain Neurons That Participate in Reward Circuitry. *The Journal of neuroscience : the official journal of the Society for Neuroscience* **37,** 4128-4144.

Pronchuk N, Beck-Sickinger AG & Colmers WF. (2002). Multiple NPY Receptors Inhibit GABAA Synaptic Responses of Rat Medial Parvocellular Effector Neurons in the Hypothalamic Paraventricular Nucleus. *Endocrinology* **143,** 535-543.

Qiu J, Fang Y, Rønnekleiv OK & Kelly MJ. (2010). Leptin excites proopiomelanocortin neurons via activation of TRPC channels. *The Journal of neuroscience : the official journal of the Society for Neuroscience* **30,** 1560-1565.

Qiu J, Zhang C, Borgquist A, Nestor CC, Smith AW, Bosch MA, Ku S, Wagner EJ, Rønnekleiv OK & Kelly MJ. (2014). Insulin Excites Anorexigenic Proopiomelanocortin Neurons via Activation of Canonical Transient Receptor Potential Channels. *Cell metabolism* **19,** 682-693.

Rao RR, Long JZ, White JP, Svensson KJ, Lou J, Lokurkar I, Jedrychowski MP, Ruas JL, Wrann CD, Lo JC, Camera DM, Lachey J, Gygi S, Seehra J, Hawley JA & Spiegelman BM. (2014). Meteorin-like is a hormone that regulates immune-adipose interactions to increase beige fat thermogenesis. *Cell* **157,** 1279-1291.

Rau AR & Hentges ST. (2019). GABAergic Inputs to POMC Neurons Originating from the Dorsomedial Hypothalamus Are Regulated by Energy State. *The Journal of Neuroscience* **39,** 6449.

Rezai-Zadeh K, Yu S, Jiang Y, Laque A, Schwartzenburg C, Morrison CD, Derbenev AV, Zsombok A & Munzberg H. (2014). Leptin receptor neurons in the dorsomedial hypothalamus are key regulators of energy expenditure and body weight, but not food intake. *Molecular metabolism* **3,** 681-693.

Ribeiro-Barbosa ÉR, Skorupa AL, Cipolla-Neto J & Canteras NS. (1999). Projections of the basal retrochiasmatic area: a neural site involved in the photic control of pineal metabolism. *Brain Research* **839,** 35-40.

Roberts ZS, Wolden-Hanson T, Matsen ME, Ryu V, Vaughan CH, Graham JL, Havel PJ, Chukri DW, Schwartz MW, Morton GJ & Blevins JE. (2017). Chronic hindbrain administration of oxytocin is sufficient to elicit weight loss in diet-induced obese rats. *American Journal of Physiology-Regulatory, Integrative and Comparative Physiology* **313,** R357-R371.

Rogers RC, McDougal DH, Ritter S, Qualls-Creekmore E & Hermann GE. (2018). Response of catecholaminergic neurons in the mouse hindbrain to glucoprivic stimuli is astrocyte dependent. *American Journal of Physiology-Regulatory, Integrative and Comparative Physiology* **315,** R153-R164.

Rogers RC, Ritter S & Hermann GE. (2016). Hindbrain cytoglucopenia-induced increases in systemic blood glucose levels by 2-deoxyglucose depend on intact astrocytes and adenosine release. *American Journal of Physiology-Regulatory, Integrative and Comparative Physiology* **310,** R1102-R1108.

Rolland JF, Henquin JC & Gilon P. (2002). Feedback control of the ATP-sensitive K(+) current by cytosolic Ca(2+) contributes to oscillations of the membrane potential in pancreatic beta-cells. *Diabetes* **51,** 376-384.

Rossi J, Balthasar N, Olson D, Scott M, Berglund E, Lee CE, Choi MJ, Lauzon D, Lowell BB & Elmquist JK. (2011). Melanocortin-4 Receptors Expressed by Cholinergic Neurons Regulate Energy Balance and Glucose Homeostasis. *Cell metabolism* **13,** 195-204.

Rothwell NJ & Stock MJ. (1979). A role for brown adipose tissue in diet-induced thermogenesis. *Nature* **281,** 31-35.

Rothwell NJ & Stock MJ. (1984a). Effects of denervating brown adipose tissue on the responses to cold, hyperphagia and noradrenaline treatment in the rat. *The Journal of physiology* **355,** 457-463.

Rothwell NJ & Stock MJ. (1984b). Energy balance, thermogenesis and brown adipose tissue activity in tube-fed rats. *The Journal of nutrition* **114,** 1965-1970.

Rousset S, Alves-Guerra MC, Mozo J, Miroux B, Cassard-Doulcier AM, Bouillaud F & Ricquier D. (2004). The biology of mitochondrial uncoupling proteins. *Diabetes* **53 Suppl 1,** S130-135.

Routh VH, Hao L, Santiago AM, Sheng Z & Zhou C. (2014). Hypothalamic glucose sensing: making ends meet. *Front Syst Neurosci* **8**.

Rowland LA, Maurya SK, Bal NC, Kozak L & Periasamy M. (2016). Sarcolipin and uncoupling protein 1 play distinct roles in diet-induced thermogenesis and do not compensate for one another. *Obesity (Silver Spring)* **24,** 1430-1433.

Sakaguchi T & Bray GA. (1987). The effect of intrahypothalamic injections of glucose on sympathetic efferent firing rate. *Brain research bulletin* **18,** 591-595.

Sakaguchi T & Bray GA. (1988). Sympathetic activity following paraventricular injections of glucose and insulin. *Brain research bulletin* **21,** 25-29.

Santoro A, Campolo M, Liu C, Sesaki H, Meli R, Liu Z-W, Kim JD & Diano S. (2017). DRP1 Suppresses Leptin and Glucose Sensing of POMC Neurons. *Cell metabolism* **25,** 647-660.

Savtchouk I & Volterra A. (2018). Gliotransmission: Beyond Black-and-White. *The Journal of neuroscience : the official journal of the Society for Neuroscience* **38,** 14-25.

Scemes E & Giaume C. (2006). Astrocyte calcium waves: what they are and what they do. *Glia* **54,** 716-725.

Scharbarg E, Daenens M, Lemaître F, Geoffroy H, Guille-Collignon M, Gallopin T & Rancillac A. (2016). Astrocyte-derived adenosine is central to the hypnogenic effect of glucose. *Scientific reports* **6,** 19107.

Schuit FC, Huypens P, Heimberg H & Pipeleers DG. (2001). Glucose Sensing in Pancreatic β-Cells A Model for the Study of Other Glucose-Regulated Cells in Gut, Pancreas, and Hypothalamus. *Diabetes* **50,** 1-11.

Schwartz RS, Jaeger LF & Veith RC. (1988). Effect of clonidine on the thermic effect of feeding in humans. *The American journal of physiology* **254,** R90-94.

Secher A, Jelsing J, Baquero AF, Hecksher-Sorensen J, Cowley MA, Dalboge LS, Hansen G, Grove KL, Pyke C, Raun K, Schaffer L, Tang-Christensen M, Verma S, Witgen BM, Vrang N & Bjerre Knudsen L. (2014). The arcuate nucleus mediates GLP-1 receptor agonist liraglutide-dependent weight loss. *The Journal of clinical investigation* **124,** 4473-4488.

Shah BP, Vong L, Olson DP, Koda S, Krashes MJ, Ye C, Yang Z, Fuller PM, Elmquist JK & Lowell BB. (2014). MC4R-expressing glutamatergic neurons in the paraventricular hypothalamus regulate feeding and are synaptically connected to the parabrachial nucleus. *Proceedings of the National Academy of Sciences of the United States of America* **111,** 13193-13198.

Shan T, Liang X, Bi P, Zhang P, Liu W & Kuang S. (2013). Distinct populations of adipogenic and myogenic Myf5-lineage progenitors in white adipose tissues. *Journal of lipid research* **54,** 2214-2224.

Sherman MM, Ungureanu S & Rey JA. (2016). Naltrexone/Bupropion ER (Contrave): Newly Approved Treatment Option for Chronic Weight Management in Obese Adults. *P t* **41,** 164-172.

Shi YC, Lau J, Lin Z, Zhang H, Zhai L, Sperk G, Heilbronn R, Mietzsch M, Weger S, Huang XF, Enriquez RF, Baldock PA, Zhang L, Sainsbury A, Herzog H & Lin S. (2013). Arcuate NPY controls sympathetic output and BAT function via a relay of tyrosine hydroxylase neurons in the PVN. *Cell metabolism* **17,** 236-248.

Shiraishi T & Mager M. (1980). Hypothermia following injection of 2-deoxy-D-glucose into selected hypothalamic sites. *The American journal of physiology* **239,** R265-269.

Silva JE & Larsen PR. (1983). Adrenergic activation of triiodothyronine production in brown adipose tissue. *Nature* **305,** 712-713.

Silver IA & Erecinska M. (1994). Extracellular glucose concentration in mammalian brain: continuous monitoring of changes during increased neuronal activity and upon limitation in oxygen supply in normo-, hypo-, and hyperglycemic animals. *The Journal of neuroscience : the official journal of the Society for Neuroscience* **14,** 5068-5076.

Silver IA & Erecinska M. (1998). Glucose-induced intracellular ion changes in sugar-sensitive hypothalamic neurons. *J Neurophysiol* **79,** 1733-1745.

Sim LJ & Joseph SA. (1991). Arcuate nucleus projections to brainstem regions which modulate nociception. *Journal of Chemical Neuroanatomy* **4,** 97-109.

Smeets PA, Erkner A & de Graaf C. (2010). Cephalic phase responses and appetite. *Nutrition reviews* **68,** 643-655.

Smith BN, Banfield BW, Smeraski CA, Wilcox CL, Dudek FE, Enquist LW & Pickard GE. (2000). Pseudorabies virus expressing enhanced green fluorescent protein: A tool for in vitro electrophysiological analysis of transsynaptically labeled neurons in identified central nervous system circuits. *Proceedings of the National Academy of Sciences of the United States of America* **97,** 9264-9269.

Smith MA, Hisadome K, Al-Qassab H, Heffron H, Withers DJ & Ashford MLJ. (2007). Melanocortins and agouti-related protein modulate the excitability of two arcuate nucleus neuron populations by alteration of resting potassium conductances. *The Journal of physiology* **578,** 425-438.

Sohn J-W, Harris LE, Berglund ED, Liu T, Vong L, Lowell BB, Balthasar N, Williams KW & Elmquist JK. (2013). Melanocortin 4 Receptors Reciprocally Regulate Sympathetic and Parasympathetic - Preganglionic Neurons. *Cell* **152,** 612-619.

Song CK, Vaughan CH, Keen-Rhinehart E, Harris RB, Richard D & Bartness TJ. (2008). Melanocortin-4 receptor mRNA expressed in sympathetic outflow neurons to brown adipose tissue: neuroanatomical and functional evidence. *American journal of physiology Regulatory, integrative and comparative physiology* **295,** R417-428.

Stachniak TJ, Ghosh A & Sternson SM. (2014). Chemogenetic synaptic silencing of neural circuits localizes a hypothalamus→midbrain pathway for feeding behavior. *Neuron* **82,** 797-808.

Stagkourakis S, Kim H, Lyons DJ & Broberger C. (2016). Dopamine Autoreceptor Regulation of a Hypothalamic Dopaminergic Network. *Cell Rep* **15,** 735-747.

Stanley S, Domingos Ana I, Kelly L, Garfield A, Damanpour S, Heisler L & Friedman J. (2013). Profiling of Glucose-Sensing Neurons Reveals that GHRH Neurons Are Activated by Hypoglycemia. *Cell metabolism* **18,** 596-607.

Ste. Marie L, Miura GI, Marsh DJ, Yagaloff K & Palmiter RD. (2000). A metabolic defect promotes obesity in mice lacking melanocortin-4 receptors. *Proceedings of the National Academy of Sciences* **97,** 12339.

Steculorum SM, Ruud J, Karakasilioti I, Backes H, Engström Ruud L, Timper K, Hess ME, Tsaousidou E, Mauer J, Vogt MC, Paeger L, Bremser S, Klein AC, Morgan DA, Frommolt P, Brinkkötter PT, Hammerschmidt P, Benzing T, Rahmouni K, Wunderlich FT, Kloppenburg P & Brüning JC. (2016). AgRP Neurons Control Systemic Insulin Sensitivity via Myostatin Expression in Brown Adipose Tissue. *Cell* **165,** 125-138.

Steffens AB, Scheurink AJ, Porte D, Jr. & Woods SC. (1988). Penetration of peripheral glucose and insulin into cerebrospinal fluid in rats. *The American journal of physiology* **255,** R200-204.

Steiner AA, Turek VF, Almeida MC, Burmeister JJ, Oliveira DL, Roberts JL, Bannon AW, Norman MH, Louis JC, Treanor JJ, Gavva NR & Romanovsky AA. (2007). Nonthermal activation of transient receptor potential vanilloid-1 channels in abdominal viscera tonically inhibits autonomic cold-defense effectors. *The Journal of neuroscience : the official journal of the Society for Neuroscience* **27,** 7459-7468.

Stern JE. (2001). Electrophysiological and morphological properties of pre-autonomic neurones in the rat hypothalamic paraventricular nucleus. *The Journal of physiology* **537,** 161-177.

Stobart JL & Anderson CM. (2013). Multifunctional role of astrocytes as gatekeepers of neuronal energy supply. *Front Cell Neurosci* **7,** 38-38.

Sun CL, Thoa NB & Kopin IJ. (1979). Comparison of the effects of 2-deoxyglucose and immobilization on plasma levels of catecholamines and corticosterone in awake rats. *Endocrinology* **105,** 306-311.

Sutton AK, Pei H, Burnett KH, Myers MG, Rhodes CJ & Olson DP. (2014). Control of Food Intake and Energy Expenditure by Nos1 Neurons of the Paraventricular Hypothalamus. *The Journal of Neuroscience* **34,** 15306-15318.

Swanson LW & Kuypers HG. (1980a). A direct projection from the ventromedial nucleus and retrochiasmatic area of the hypothalamus to the medulla and spinal cord of the rat. *Neuroscience letters* **17,** 307-312.

Swanson LW & Kuypers HGJM. (1980b). A direct projection from the ventromedial nucleus and retrochiasmatic area of the hypothalamus to the medulla and spinal cord of the rat. *Neuroscience letters* **17,** 307-312.

Sweeney P, Qi Y, Xu Z & Yang Y. (2016). Activation of hypothalamic astrocytes suppresses feeding without altering emotional states. *Glia* **64,** 2263-2273.

Tan Chan L, Cooke Elizabeth K, Leib David E, Lin Y-C, Daly Gwendolyn E, Zimmerman Christopher A & Knight Zachary A. (2016). Warm-Sensitive Neurons that Control Body Temperature. *Cell* **167,** 47-59.e15.

Tan Z, Liu Y, Xi W, Lou H-f, Zhu L, Guo Z, Mei L & Duan S. (2017). Glia-derived ATP inversely regulates excitability of pyramidal and CCK-positive neurons. *Nature communications* **8,** 13772.

Tengholm A & Gylfe E. (2009). Oscillatory control of insulin secretion. *Mol Cell Endocrinol* **297,** 58-72.

Tong Q, Ye CP, Jones JE, Elmquist JK & Lowell BB. (2008). Synaptic release of GABA by AgRP neurons is required for normal regulation of energy balance. *Nat Neurosci* **11,** 998-1000.

Tovar S, Paeger L, Hess S, Morgan DA, Hausen AC, Bronneke HS, Hampel B, Ackermann PJ, Evers N, Buning H, Wunderlich FT, Rahmouni K, Kloppenburg P & Bruning JC. (2013). K(ATP)-channel-dependent regulation of catecholaminergic neurons controls BAT sympathetic nerve activity and energy homeostasis. *Cell metabolism* **18,** 445-455.

Trout DL, Conway ES & Putney JD. (1977). Dietary influences on gastric emptying of carbohydrate versus fat in the rat. *The Journal of nutrition* **107,** 104-111.

Tsien JZ. (2016). Cre-Lox Neurogenetics: 20 Years of Versatile Applications in Brain Research and Counting…. *Frontiers in genetics* **7,** 19.

Tupone D, Madden CJ, Cano G & Morrison SF. (2011). An orexinergic projection from perifornical hypothalamus to raphe pallidus increases rat brown adipose tissue thermogenesis. *The Journal of neuroscience : the official journal of the Society for Neuroscience* **31,** 15944-15955.

Tupone D, Madden CJ & Morrison SF. (2013). Central Activation of the A1 Adenosine Receptor (A1AR) Induces a Hypothermic, Torpor-Like State in the Rat. *The Journal of Neuroscience* **33,** 14512-14525.

U Din M, Saari T, Raiko J, Kudomi N, Maurer SF, Lahesmaa M, Fromme T, Amri E-Z, Klingenspor M, Solin O, Nuutila P & Virtanen KA. (2018). Postprandial Oxidative Metabolism of Human Brown Fat Indicates Thermogenesis. *Cell metabolism*.

Ueta CB, Fernandes GW, Capelo LP, Fonseca TL, Maculan FD, Gouveia CH, Brum PC, Christoffolete MA, Aoki MS, Lancellotti CL, Kim B, Bianco AC & Ribeiro MO. (2012). β(1) Adrenergic receptor is key to cold- and diet-induced thermogenesis in mice. *J Endocrinol* **214,** 359-365.

Üner AG, Keçik O, Quaresma PGF, De Araujo TM, Lee H, Li W, Kim HJ, Chung M, Bjørbæk C & Kim Y-B. (2019). Role of POMC and AgRP neuronal activities on glycaemia in mice. *Scientific reports* **9,** 13068.

Vaisse C, Clement K, Guy-Grand B & Froguel P. (1998). A frameshift mutation in human MC4R is associated with a dominant form of obesity. *Nat Genet* **20,** 113-114.

van den Pol AN, Acuna-Goycolea C, Clark KR & Ghosh PK. (2004). Physiological Properties of Hypothalamic MCH Neurons Identified with Selective Expression of Reporter Gene after Recombinant Virus Infection. *Neuron* **42,** 635-652.

van den Top M, Lee K, Whyment AD, Blanks AM & Spanswick D. (2004). Orexigen-sensitive NPY/AgRP pacemaker neurons in the hypothalamic arcuate nucleus. *Nat Neurosci* **7,** 493-494.

van den Top M, Nolan MF, Lee K, Richardson PJ, Buijs RM, Davies CH & Spanswick D. (2003). Orexins induce increased excitability and synchronisation of rat sympathetic preganglionic neurones. *The Journal of physiology* **549,** 809-821.

van den Top M, Zhao FY, Viriyapong R, Michael NJ, Munder AC, Pryor JT, Renaud LP & Spanswick D. (2017). The impact of ageing, fasting and high-fat diet on central and peripheral glucose tolerance and glucose-sensing neural networks in the arcuate nucleus. *Journal of neuroendocrinology* **29,** 10.1111/jne.12528.

van der Lans AA, Hoeks J, Brans B, Vijgen GH, Visser MG, Vosselman MJ, Hansen J, Jorgensen JA, Wu J, Mottaghy FM, Schrauwen P & van Marken Lichtenbelt WD. (2013). Cold acclimation recruits human brown fat and increases nonshivering thermogenesis. *The Journal of clinical investigation* **123,** 3395-3403.

van Marken Lichtenbelt WD, Vanhommerig JW, Smulders NM, Drossaerts JM, Kemerink GJ, Bouvy ND, Schrauwen P & Teule GJ. (2009). Cold-activated brown adipose tissue in healthy men. *The New England journal of medicine* **360,** 1500-1508.

Verselis VK & Srinivas M. (2013). Connexin channel modulators and their mechanisms of action. *Neuropharmacology* **75,** 517-524.

Verty AN, Allen AM & Oldfield BJ. (2010). The endogenous actions of hypothalamic peptides on brown adipose tissue thermogenesis in the rat. *Endocrinology* **151,** 4236-4246.

Verty ANA, Allen AM & Oldfield BJ. (2009). The Effects of Rimonabant on Brown Adipose Tissue in Rat: Implications for Energy Expenditure. *Obesity* **17,** 254-261.

Virtanen KA, Lidell ME, Orava J, Heglind M, Westergren R, Niemi T, Taittonen M, Laine J, Savisto NJ, Enerback S & Nuutila P. (2009). Functional brown adipose tissue in healthy adults. *The New England journal of medicine* **360,** 1518-1525.

Vitali A, Murano I, Zingaretti MC, Frontini A, Ricquier D & Cinti S. (2012). The adipose organ of obesity-prone C57BL/6J mice is composed of mixed white and brown adipocytes. *Journal of lipid research* **53,** 619-629.

von Essen G, Lindsund E, Cannon B & Nedergaard J. (2017). Adaptive facultative diet-induced thermogenesis in wild-type but not in UCP1-ablated mice. *American journal of physiology Endocrinology and metabolism* **313,** E515-e527.

Vong L, Ye C, Yang Z, Choi B, Chua S, Jr. & Lowell BB. (2011). Leptin action on GABAergic neurons prevents obesity and reduces inhibitory tone to POMC neurons. *Neuron* **71,** 142-154.

Voss-Andreae A, Murphy JG, Ellacott KL, Stuart RC, Nillni EA, Cone RD & Fan W. (2007). Role of the central melanocortin circuitry in adaptive thermogenesis of brown adipose tissue. *Endocrinology* **148,** 1550-1560.

Vrang N, Larsen PJ, Clausen JT & Kristensen P. (1999). Neurochemical characterization of hypothalamic cocaine- amphetamine-regulated transcript neurons. *The Journal of neuroscience : the official journal of the Society for Neuroscience* **19,** Rc5.

Waagepetersen HS, Bakken IJ, Larsson OM, Sonnewald U & Schousboe A. (1998). Comparison of lactate and glucose metabolism in cultured neocortical neurons and astrocytes using 13C-NMR spectroscopy. *Developmental neuroscience* **20,** 310-320.

Wagner EJ, Reyes-Vazquez C, Rønnekleiv OK & Kelly MJ. (2000). The role of intrinsic and agonist-activated conductances in determining the firing patterns of preoptic area neurons in the guinea pig. *Brain Research* **879,** 29-41.

Wall M & Dale N. (2008). Activity-dependent release of adenosine: a critical re-evaluation of mechanism. *Curr Neuropharmacol* **6,** 329-337.

Wall MJ & Dale N. (2013). Neuronal transporter and astrocytic ATP exocytosis underlie activity-dependent adenosine release in the hippocampus. *The Journal of physiology* **591,** 3853-3871.

Wang D, He X, Zhao Z, Feng Q, Lin R, Sun Y, Ding T, Xu F, Luo M & Zhan C. (2015). Whole-brain mapping of the direct inputs and axonal projections of POMC and AgRP neurons. *Frontiers in Neuroanatomy* **9,** 40.

Willebrords J, Maes M, Crespo Yanguas S & Vinken M. (2017). Inhibitors of connexin and pannexin channels as potential therapeutics. *Pharmacol Ther* **180,** 144-160.

Williams DL, Bowers RR, Bartness TJ, Kaplan JM & Grill HJ. (2003). Brainstem melanocortin 3/4 receptor stimulation increases uncoupling protein gene expression in brown fat. *Endocrinology* **144,** 4692-4697.

Williams KW, Margatho LO, Lee CE, Choi M, Lee S, Scott MM, Elias CF & Elmquist JK. (2010). Segregation of acute leptin and insulin effects in distinct populations of arcuate proopiomelanocortin neurons. *The Journal of neuroscience : the official journal of the Society for Neuroscience* **30,** 2472-2479.

Williams KW & Smith BN. (2006). Rapid inhibition of neural excitability in the nucleus tractus solitarii by leptin: implications for ingestive behaviour. *The Journal of physiology* **573,** 395-412.

Williams KW, Zsombok A & Smith BN. (2007). Rapid inhibition of neurons in the dorsal motor nucleus of the vagus by leptin. *Endocrinology* **148,** 1868-1881.

Wittmann G, Hrabovszky E & Lechan RM. (2013). Distinct glutamatergic and GABAergic subsets of hypothalamic pro-opiomelanocortin neurons revealed by in situ hybridization in male rats and mice. *The Journal of comparative neurology* **521,** 3287-3302.

Wu J, Bostrom P, Sparks LM, Ye L, Choi JH, Giang AH, Khandekar M, Virtanen KA, Nuutila P, Schaart G, Huang K, Tu H, van Marken Lichtenbelt WD, Hoeks J, Enerback S, Schrauwen P & Spiegelman BM. (2012). Beige adipocytes are a distinct type of thermogenic fat cell in mouse and human. *Cell* **150,** 366-376.

Wu Q, Lemus MB, Stark R, Bayliss JA, Reichenbach A, Lockie SH & Andrews ZB. (2014). The temporal pattern of cfos activation in hypothalamic, cortical, and brainstem nuclei in response to fasting and refeeding in male mice. *Endocrinology* **155,** 840-853.

Xu AW, Kaelin CB, Morton GJ, Ogimoto K, Stanhope K, Graham J, Baskin DG, Havel P, Schwartz MW & Barsh GS. (2005). Effects of Hypothalamic Neurodegeneration on Energy Balance. *PLOS Biology* **3,** e415.

Xu Y, Wu Z, Sun H, Zhu Y, Kim ER, Lowell BB, Arenkiel BR, Xu Y & Tong Q. (2013). Glutamate mediates the function of melanocortin receptor 4 on Sim1 neurons in body weight regulation. *Cell metabolism* **18,** 860-870.

Yamazaki T, Morimoto-Kobayashi Y, Koizumi K, Takahashi C, Nakajima S, Kitao S, Taniguchi Y, Katayama M & Ogawa Y. (2019). Secretion of a gastrointestinal hormone, cholecystokinin, by hop-derived bitter components activates sympathetic nerves in brown adipose tissue. *The Journal of Nutritional Biochemistry* **64,** 80-87.

Yang CF, Chiang MC, Gray DC, Prabhakaran M, Alvarado M, Juntti SA, Unger EK, Wells JA & Shah NM. (2013). Sexually dimorphic neurons in the ventromedial hypothalamus govern mating in both sexes and aggression in males. *Cell* **153,** 896-909.

Yang L, Qi Y & Yang Y. (2015). Astrocytes control food intake by inhibiting AGRP neuron activity via adenosine A1 receptors. *Cell Rep* **11,** 798-807.

Yasuda T, Masaki T, Kakuma T, Hara M, Nawata T, Katsuragi I & Yoshimatsu H. (2005). Dual Regulatory Effects of Orexins on Sympathetic Nerve Activity Innervating Brown Adipose Tissue in Rats. *Endocrinology* **146,** 2744-2748.

Yasuda T, Masaki T, Kakuma T & Yoshimatsu H. (2004). Hypothalamic melanocortin system regulates sympathetic nerve activity in brown adipose tissue. *Experimental biology and medicine (Maywood, NJ)* **229,** 235-239.

Yaswen L, Diehl N, Brennan MB & Hochgeschwender U. (1999). Obesity in the mouse model of pro-opiomelanocortin deficiency responds to peripheral melanocortin. *Nature Medicine* **5,** 1066-1070.

Yeo GS, Farooqi IS, Aminian S, Halsall DJ, Stanhope RG & O'Rahilly S. (1998). A frameshift mutation in MC4R associated with dominantly inherited human obesity. *Nat Genet* **20,** 111-112.

Yeo SH & Herbison AE. (2011). Projections of arcuate nucleus and rostral periventricular kisspeptin neurons in the adult female mouse brain. *Endocrinology* **152,** 2387-2399.

Yoneshiro T, Aita S, Matsushita M, Kayahara T, Kameya T, Kawai Y, Iwanaga T & Saito M. (2013). Recruited brown adipose tissue as an antiobesity agent in humans. *The Journal of clinical investigation* **123,** 3404-3408.

Yoshimatsu H, Egawa M & Bray GA. (1992). Effects of cholecystokinin on sympathetic activity to interscapular brown adipose tissue. *Brain research* **597,** 298-303.

Yoshimichi G, Yoshimatsu H, Masaki T & Sakata T. (2001). Orexin-A regulates body temperature in coordination with arousal status. *Experimental biology and medicine (Maywood, NJ)* **226,** 468-476.

Yu S, Cheng H, François M, Qualls-Creekmore E, Huesing C, He Y, Jiang Y, Gao H, Xu Y, Zsombok A, Derbenev AV, Nillni EA, Burk DH, Morrison CD, Berthoud H-R & Münzberg H. (2018). Preoptic leptin signaling modulates energy balance independent of body temperature regulation. *eLife* **7,** e33505.

Yu S, Qualls-Creekmore E, Rezai-Zadeh K, Jiang Y, Berthoud H-R, Morrison CD, Derbenev AV, Zsombok A & Münzberg H. (2016). Glutamatergic Preoptic Area Neurons That Express Leptin Receptors Drive Temperature-Dependent Body Weight Homeostasis. *The Journal of Neuroscience* **36,** 5034-5046.

Zaretskaia MV, Zaretsky DV, Shekhar A & DiMicco JA. (2002). Chemical stimulation of the dorsomedial hypothalamus evokes non-shivering thermogenesis in anesthetized rats. *Brain research* **928,** 113-125.

Zhan C, Zhou J, Feng Q, Zhang JE, Lin S, Bao J, Wu P & Luo M. (2013). Acute and long-term suppression of feeding behavior by POMC neurons in the brainstem and hypothalamus, respectively. *The Journal of neuroscience : the official journal of the Society for Neuroscience* **33,** 3624-3632.

Zhang Y, Kerman IA, Laque A, Nguyen P, Faouzi M, Louis GW, Jones JC, Rhodes C & Munzberg H. (2011). Leptin-receptor-expressing neurons in the dorsomedial hypothalamus and median preoptic area regulate sympathetic brown adipose tissue circuits. *The Journal of neuroscience : the official journal of the Society for Neuroscience* **31,** 1873-1884.

Zhao Z-D, Yang WZ, Gao C, Fu X, Zhang W, Zhou Q, Chen W, Ni X, Lin J-K, Yang J, Xu X-H & Shen WL. (2017). A hypothalamic circuit that controls body temperature. *Proceedings of the National Academy of Sciences* **114,** 2042-2047.

Zheng H, Patterson LM, Phifer CB & Berthoud H-R. (2005). Brain stem melanocortinergic modulation of meal size and identification of hypothalamic POMC projections. *American Journal of Physiology-Regulatory, Integrative and Comparative Physiology* **289,** R247-R258.

Zheng N & Raman IM. (2011). Prolonged Postinhibitory Rebound Firing in the Cerebellar Nuclei Mediated by Group I Metabotropic Glutamate Receptor Potentiation of L-Type Calcium Currents. *The Journal of Neuroscience* **31,** 10283.

Zimmermann H. (1992). 5'-Nucleotidase: molecular structure and functional aspects. *Biochem J* **285 (Pt 2),** 345-365.